

**Nuclear Pressurised Water Reactor Transformer
Individual Rod Position Indicator**

A thesis submitted to

The University of Manchester

for the degree of

Doctor of Philosophy

in the

Faculty of Science and Engineering

2017

Angelo Sigona

School of Electrical and Electronic Engineering

Table of Contents

1	Introduction	16
1.1	Background	16
1.2	Aim and Objective	19
1.3	System requirements	19
1.4	Control Rod Drive Mechanism Environment	22
1.5	Key research contributions	25
2	Literature Review	26
2.1	Review of existing technologies	27
2.2	Electromagnetic Sensors	37
2.3	Non Electromagnetic Sensors	61
3	Future Rod Position Sensing Technologies	66
3.1	General Sensing Techniques	66
3.2	Inductance	69
3.3	Transformer principle	72
3.4	Modified Transformer	74
3.5	Reed Switches	77
3.6	Magnetostrictive principle	79
3.7	Ultrasonic	81
3.8	Radar	83
3.9	Resonant Pucks	85
3.10	Hall Effect	87
3.11	Magnetoresistance	89
3.12	Summary	92
4	Finite Element Analysis	93
4.1	Background	93
4.2	Finite Element Method Magnetic (FEMM)	94
5	Techniques to Improve Control Rod Position Accuracy	96
5.1	Option 1: Inductor principle	96
5.2	Option 2: Transformer rod position indicator principle	102
6	Advanced Sensor Design and Analysis	105
6.1	Finite Element Model Approach	105
6.2	Design approach	108
7	Design Optimisation Process	131
8	Magnetic Sensitivity Analyses	141
8.1	Core Matching Sensitivity	141
8.2	Core permeability sensitivity	142
8.3	Core conductivity sensitivity	143
9	Octave/FEMM Expert-Based TIRPI Optimisation	146
9.1	Octave	146
9.2	Approach to expert-based optimisation	147
9.3	Spacing optimisation	148
9.4	Primary bobbin optimisation	150
9.5	Secondary bobbin optimisation	151
9.6	Expert-based optimised TIRPI design	151

10	TIRPI Prototype 1 Build	156
10.1	Introduction	156
10.2	Design Concept	156
10.3	Electrical Connector	157
10.4	Coil former	158
10.5	Coil varnish impregnation	160
10.6	Winding coil wire	161
10.7	Lead-out wire connection	161
10.8	Rod core insulation	162
10.9	Seal of TIRPI to probe tube	163
10.10	Failure Modes and Effects Analysis (FMEA)	163
10.11	Mean Time before Failure (MTBF)	163
10.12	Demonstration mini unit development for manufacture	163
10.13	Assembly of connector-flange to the core former	164
10.14	TIRPI Prototype 2 Build	166
10.15	DFMEA and PFMEA	168
11	Experimental Testing and Model Validation	173
11.1	Bench test at room ambient temperature	173
11.2	Thermal environmental test	175
11.3	Harmonics Test	176
11.4	Secondary output voltage and primary voltage during warm-up	178
11.5	Frequency response test	179
11.6	Secondary voltage and primary current test	181
11.7	Secondary sensitivity sweep test at 400Hz	182
11.8	TIRPI cable capacitance test	184
11.9	Mini TIRPI with manganin wire	185
11.10	Probe tube electrical conductivity effect	202
11.11	CRDM Hot and Pressurised Water Testing Results	206
11.12	CRDM current test	210
11.13	Channel alignment test	212
11.14	CRDM frequency sweep test	214
11.15	SCRAM engagement repeatability test	215
11.16	Rod drop test	217
11.17	Rod motion measurement accuracy	218
11.18	CRDM to CRDM interference	219
11.19	Conclusion	222
11.20	Post CRDM testing inspection	223
12	Thermal Induced Stress	225
12.1	Introduction	225
12.2	Mechanical and thermal properties	225
12.3	TIRPI variant thermal stress model	227
13	Conclusion and Future Work	231
13.1	Conclusion	231
13.2	Future Work – Design optimisation	232
13.3	Future work – TIRPI CRDM stator immunity	234
13.4	Random optimisation	235
13.5	Future Work - Electromagnetic Compatibility (EMC) Environmental Withstand	240
14	Additional Work	241
15	References	244
16	Appendix A TIRPI variant	247

17	Appendix B – DFMEA	250
18	Appendix C – PFMEA	256
19	Appendix D – Bespoke winding machine	261
20	Appendix E – TRL Assessment tool	262
21	Appendix F – Mean time before failure	265
22	Appendix G – Octave random optimisation source software	267
23	Appendix H – Random optimisation output	275

Word count: 49815

Tables

Table 1	Advanced Individual Rod Position Requirements	21
Table 2	Application suitability of various sensors [1]	27
Table 3	Attribute comparison chart of the main linear position technologies [1]	28
Table 1	TIRPI analyses key attributes	95
Table 2	List of TIRPI core materials	112
Table 3	Power efficiency of TIRPI	130
Table 4	Power efficiency of TIRPI within an CRDM	130
Table 5	Variables and constraints	146
Table 6	Variables and constraints initial and end conditions	148
Table 7	Expert-based optimisation parameters	151
Table 8	Comparison of optimisation parameters	153
Table 9	Thermal linear expression compensation equation	209
Table 10	Thermal stress material properties	226
Table 11	TIRPI comparison of optimisation techniques	238
Table 12	CRDM/TIRPI comparison of optimisation techniques	240

Illustrations

Figure 1	Driveshaft external circumference design	18
Figure 2	Control rod indicator transducer system errors	20
Figure 3	Ballscrew engagement	20
Figure 4	Circuit Diagram for a basic potentiometer [2]	29
Figure 5	Capacitive linear position transducer [1]	30
Figure 6	LVDT winding and core configuration [2]	32
Figure 7	Typical power plant LVDT [2]	32
Figure 8	Hall effect [1]	33
Figure 9	Concentration of current carriers [1]	33
Figure 10	Magnetoresistor charge carriers [1]	34
Figure 11	Magnetoresistor – alignment of magnetic domains [1]	35
Figure 12	Magnetostrictive sensor	36
Figure 13	Magnetic encoder	37
Figure 14	Position Indicator Principle [2]	38
Figure 15	Bespoke pattern configuration to determine signal phase shifts [3]	40
Figure 16	Electromagnetic delay line [4]	41
Figure 17	Serial transformer principle [5]	42
Figure 18	Position indication system [6]	44
Figure 19	E-Type Magnetic Sensor [7]	45
Figure 20	Position encoder [8]	47
Figure 21	Position indicating device [9]	48
Figure 22	Magnetic position indicator [10]	50
Figure 23	Electromagnetic position indicator [11]	52
Figure 24	Nuclear control rod indication system [12]	53
Figure 25	Position sensor of linearity moving bodies [13]	55
Figure 26	Control rod position indication system [14]	56
Figure 27	Nuclear reactor control rod drive with rod position indicating means [15]	57
Figure 28	Phase encoded digital position probe assembly [16]	59
Figure 29	Position Indicator [17]	60
Figure 30	Magnetostrictive position indicator [18]	62
Figure 31	Linear position sensor using a strain gauge [18]	63
Figure 32	Position indicator [20]	64
Figure 33	Ultrasonic Position Indicator System [21]	65
Figure 34	Rod Position Techniques	67

Figure 35 TRL assessment tool	68
Figure 36 Inductive electrical topology concept	69
Figure 37 Inductive Concept	70
Figure 38 Transformer Concept	72
Figure 39 Modified Transformer Concept	74
Figure 40 Reed switches concept	77
Figure 41 Magnetostrictive Concept	79
Figure 42 Ultrasonic Concept	82
Figure 43 Radar Concept	84
Figure 44 Resonant Puck Concept	86
Figure 45 Hall Effect Concept	88
Figure 46 Magnetoresistance Concept	90
Figure 47 Finite element	94
Figure 48 B-H curve of driveshaft material	97
Figure 49 Inductive sensor principle	98
Figure 50 Inductor configurations	100
Figure 51 Multi-directional inductor	101
Figure 52 FLUX 2D magnetic model geometry of a multi-directional inductor	102
Figure 53 Transformer rod position indicator principle	103
Figure 54 TIRPI terms	106
Figure 55 TIRPI magnetic fields	110
Figure 56 Span of the TIRPI with optimised bobbin size	115
Figure 57 SoR of the TIRPI with optimised bobbin size	115
Figure 58 Span of the TIRPI with un-optimised bobbin size	116
Figure 59 SoR of the TIRPI with un-optimised Bobbin Size	117
Figure 60 2D axisymmetric finite element model of TIRPI, probe tube and driveshaft in the minimum position and maximum position	119
Figure 61 Bench analysis frequency sweep secondary output	119
Figure 62 Bench analyses frequency sweep secondary span	120
Figure 63 CRDM stator 2D planar finite element model	122
Figure 64 CRDM analyses frequency sweep 2D axisymmetric finite element model	124
Figure 65 CRDM analyses frequency sweep 2D axisymmetric finite element model	125
Figure 66 CRDM analyses frequency sweep secondary output	126
Figure 67 CRDM analyses frequency sweep secondary span	127
Figure 68 TIRPI cable	129
Figure 69 TIRPI power phase diagram	129
Figure 70 Design optimisation sequence diagram	131
Figure 71 Comparison of driveshaft increment size	134
Figure 72 Spacing optimisation	135
Figure 73 Spacing optimisation	136
Figure 74 Span spacing optimisation characteristics	137
Figure 75 Linearity spacing optimisation characteristics	137
Figure 76 Linearity optimisation	138
Figure 77 Bobbin optimisation of TIRPI Selected Regions	138
Figure 78 Span bobbin optimisation characteristics	139
Figure 79 Linearity bobbin optimisation characteristics	139
Figure 80 17.4PH H1100 TIRPI core material permeability variation	142
Figure 81 Secondary voltage Vs core material permeability variation	143
Figure 82 Secondary voltage Vs core material permeability variation error	143
Figure 83 Secondary Voltage Vs Core Material Conductivity Variation	144
Figure 84 Secondary voltage Vs core material conductivity variation error	145
Figure 85 Spacing optimisation using Octave and FEMM	149
Figure 86 Primary Bobbin optimisation using Octave and FEMM	150
Figure 87 Primary Bobbin optimisation using Octave and FEMM	152
Figure 88 Comparison of expert-based optimisation and linear optimisation for 10mm increments	154
Figure 89 Comparison of expert-based optimisation and linear optimisation for 1mm increments	155
Figure 90 Upper arrangement assembly	157

Figure 91 Upper arrangement assembly bolting location	157
Figure 92 Connector-flange PEEK sealing	158
Figure 93 Connector-flange arrangement	158
Figure 94 TIRPI windings (courtesy from Centronics Ltd)	160
Figure 95 TIRPI lead-out wire (courtesy from Centronics Ltd)	161
Figure 96 Polyimide and glass tape insulation (courtesy from Centronics Ltd)	162
Figure 97 Demonstration for manufacture TIRPI (courtesy from Centronics Ltd)	164
Figure 98 Connector to core former connection (courtesy from Centronics Ltd)	165
Figure 99 TIRPI prototype 2 schematic	167
Figure 100 Bench test facility	173
Figure 101 TIRPI Bench test – secondary voltage output	174
Figure 102 TIRPI Bench test – primary voltage output	175
Figure 103 TIRPI environmental thermal Test	176
Figure 104 Cold harmonic testing at 400Hz	177
Figure 105 Hot harmonic testing at 400Hz	177
Figure 106 Hot harmonic testing at 99Hz, 502Hz and 2kHz	178
Figure 107 Secondary voltage as a function of primary voltage output	179
Figure 108 Bench hot frequency sweep test	180
Figure 109 Bench cold frequency sweep test	180
Figure 110 Hot primary current sweep	181
Figure 111 Cold primary current sweep	182
Figure 112 Sensitivity sweep test at 400Hz, 100mA	183
Figure 113 Linearity test	184
Figure 114 TIRPI and cable capacitance test	185
Figure 115 Mini TIRPI thermal effects	188
Figure 116 Mini TIRPI temperature sense wire results	189
Figure 117 Probe tube hot plate testing PC and data logger	190
Figure 118 Probe tube hot plate testing setup	191
Figure 119 Probe tube hot plate testing positions	191
Figure 120 Electrical conductivity meter	192
Figure 121 Probe tube hot plate testing reading position	192
Figure 122 Magnetic permeability meter	193
Figure 123 Digital low resistance ohm meter	194
Figure 124 Mini TIRPI hot plate testing positions	195
Figure 125 Probe tube electrical conductivity at ambient temperature	196
Figure 126 Probe tube point 12 electrical conductivity at temperature	197
Figure 127 Probe tube electrical conductivity at temperature	198
Figure 128 Probe tube magnetic permeability at ambient temperature	199
Figure 129 Probe tube relative magnetic permeability at temperature	200
Figure 130 Core former electrical resistivity temperature	201
Figure 131 Core former electrical conductivity at temperature	202
Figure 132 TIRPI system without probe tube	203
Figure 133 TIRPI without probe tube	203
Figure 134 TIRPI system with probe tube	204
Figure 135 TIRPI with probe tube	205
Figure 136 TIRPI core former DC resistance test	205
Figure 137 Hot and pressurised CRDM test facility	206
Figure 138 TIRPI thermal regions	207
Figure 139 TIRPI warm-up test	208
Figure 140 TIRPI thermal compensation	208
Figure 141 TIRPI thermal compensation technique	209
Figure 142 Thermal compensation characteristics @ 30 % driveshaft withdrawal	210
Figure 143 CRDM stator	211
Figure 144 CRDM current test	212
Figure 145 TIRPI cold alignment test	213
Figure 146 TIRPI cold alignment test normalised	213
Figure 147 TIRPI frequency sweep normalised	214
Figure 148 TIRPI frequency sweep span normalised	215
Figure 149 SCRAM to engagement repeatability	216

Figure 150	Rod drop test	218
Figure 151	CRDM adjacent interference	220
Figure 152	TIRPI secondary output of two adjacent CRDMs	221
Figure 153	Error of TIRPI output with two adjacent CRDM	221
Figure 154	TIRPI post testing thermal inspection discolouration of hot region	223
Figure 155	TIRPI post testing thermal inspection discolouration of cold region	223
Figure 156	TIRPI temperature distribution	226
Figure 157	TIRPI thermal induced stress distribution within the x-direction	227
Figure 158	TIRPI thermal induced stress distribution within the y-direction	228
Figure 159	TIRPI thermal induced stress distribution within the y-direction	228
Figure 160	PT thermal induced stress distribution within the x-direction	228
Figure 161	PT thermal induced stress distribution within the y-direction	229
Figure 162	PT thermal induced stress distribution within the z-direction	229
Figure 163	PT thermal induced stress amplification distribution within mid-section	230
Figure 164	An overview of engineering design optimisation methods [23]	233
Figure 165	Engineering design approach Vs class of optimisation [23]	234
Figure 166	TIRPI Random optimisation flow sequence chart	236
Figure 167	TIRPI secondary Output using Random Optimisation	237
Figure 168	TIRPI secondary voltage output at 10mm incremental driveshaft positions	237
Figure 169	TIRPI within CRDM using Expert-based and Random Optimisation	239
Figure 170	TIRPI sensitivity within CRDM using Expert-based and Random Optimisation	239
Figure 171	TIRPI Variant secondary output characteristics at 21°C, 65°C, 100°C and 200°C full sweep	242
Figure 172	TIRPI Variant secondary output characteristics at 21°C, 65°C, 100°C and 200°C partial sweep	242
Figure 173	TIRPI Variant secondary output voltage change with respect to environment temperature	243
Figure 174	TIRPI variant CAD (Centronics Ltd)	247
Figure 175	TIRPI variant CAD (Centronics Ltd)	248
Figure 176	TIRPI variant (Centronics Ltd)	249
Figure 177	TIRPI bespoke winding machine	261

List of Notations

+Ve	Positive voltage
μ_0	Permeability of free space ($4\pi \times 10^{-7}$ (N/A ²))
H	Magnetic field strength
-Ve	Negative voltage
β	Magnetic flux density
μ_r	Relative permeability
<i>H</i>	Magnetic Field

List of Acronyms

AC	Alternating Current
Am	Ampere-meters
CRDM	Control Rod Drive Mechanism
DFMEA	Design Failure Mode and Effect Analysis
DoE	Design of experiments
EMF	Electromotive force
FE	Finite element
FEMM	Finite element methods magnetics
FLUX2D	Finite element software called Flux 2D
FS	Full scale
LDT	Linear differential transformer
Ni-Fe	Nickel iron
PCB	Printed circuit board
PFMEA	Process Failure Mode Effects Analysis
SCRAM	Safety Control Rod Axe Man
SIPRIC	Synchronous Individual Rod Position Counter
SoR	Signal to offset ratio
TIRPI	Transformer Individual Rod Position Indicator

Abstract

An important function of the control and instrumentation for a nuclear reactor is the ability to display and control all the rod positions within the reactor core. This is an important function as the reactor operators use the control rods to control the nuclear chain reaction throughout the life of the reactor: from initial cold condition start-up, through periods of sustained long-term reactions and finally when the reactor has completed its life cycle. Specific functions of the control rods position indication system include showing the positions of individual control rods in a control rod group, the position of each rod group and the required control rod position versus the actual control rod position.

As well as being important to the operation of a nuclear reactor, the control rod position indication system is important to its efficiency. The associated costs for a nuclear power plant are relatively high, but the efficiency of the reactor can be increased either by increasing the life of the reactor core or using less fuel for the same period of use by managing the positions of the reactor control rods. Control rod position is therefore directly related to the efficiency of the reactor through life and considered an area of where improvements can be made.

The control rod position is determined using two methodologies, known as direct measurement and inferred measurement. The inferred measurement uses a digital counter which increments and decrements as the control rod moves up and down, and which displays a high-resolution position measurement. However, the counter is reset every time the control rod is released during a scram condition. On engagement of the control rod following a scram condition, the counter has no previous position knowledge and restarts counting from the zero position of the control rod. Hence the inferred method does not provide a repeatable rod position measurement. The direct measurement method determines the actual position of the control rod by detecting the position of the driveshaft which is mechanically fixed to the upper section of the control rod. By detecting the driveshaft position, the control rod position can be accurately determined, and the

nuclear reactor controlled to increase overall through-life efficiency reducing cost of operation.

The direct measurement control rod position is achieved by using three system components: the indicator (also known as a transducer), the instrumentation to indicator cable and the instrumentation electronics. Generally, the indicator and the cable are exposed to a harsh environment: mostly high radiation, temperatures and pressures. In addition, within the nuclear reactor the highly radioactive water known as the primary coolant is encapsulated within the metallic boundaries of the reactor to shield the surrounding atmosphere from it.

For a Pressurised Water Reactor (PWR) plant the indicator is placed within a metallic boundary known as a Probe Tube (PT). The driveshaft of the control rod envelops the PT as it rises and exposes the PT as it declines. The PT is designed into a reactor system so a measurement of the driveshaft can be obtained thus measuring the control rod position. Without such a breach of reactor boundary there is no other current methods to measure the control rod position.

Detecting the driveshaft position accurately is difficult as the detecting technology has to penetrate the material of the PT. The technology most widely used is a form of magnetic sensing that has a long term pedigree of use within many worldwide applications. In particular, the use of electro-magnetic sensing leads itself to nuclear applications. Electro-magnetic sensing has been used reliably for many years in nuclear reactors, especially for control rod position detection. However, improving the accuracy of determining the position of a driveshaft has been an ongoing challenge that has been met with limited success.

This thesis investigates a novel method of increasing the detection accuracy of the control rod position, and providing an increased immunity to external Control Rod Drive Mechanism (CRDM) interferences which exist in operation. The transducer has also

shown to offer additional capability such as accurate measurement of the control rod while in motion and a rod drop sensor during a shutdown condition. The philosophy of the novel method is to balance the magnetic flux produced within the core of the transducer and the driveshaft using an optimised transducer design, thus producing a low as possible electrical output signal when the driveshaft fully envelops the PT. This methodology has been named “core matching”. Core matching also provides an additional important benefit as it develops a high concentration of magnetic flux within the transducer core material. This enables the transducer to have a high external magnetic noise tolerance.

In addition to explaining the principle of core matching, the thesis explains the added benefits to the transducer driveshaft sensor detection sensitivity when used at a particular frequency. The research results show that the maximum sensitivity of the transducer is achieved the transducer is optimised for the geometry, core material and frequency value.

The design for an optimised core matched transducer was investigated using finite element analysis, and a number of prototype optimised designs developed for use in a PWR nuclear reactor. The resulting design for the transducer is named the “Transformer Individual Rod Position Indicator” (TIRPI).

The results for bench and CRDM environmental testing of the TIRPI prototype resulted in a fully operational high accuracy measurement transducer. This outcome led to a final manufactured validated design for use in a submarine nuclear reactor. The final design TIRPI can detect the driveshaft enveloping the PT much more accurately than the current control rod position indicator transducer design meeting all the design requirement of the project.

Declaration

No portion of the work referred to in this thesis has been submitted in support of an application for another degree or qualification from this or any other university, or any other institute of learning.

Copyright Statement

The copyright of the content within this thesis is owned by the Author and Rolls-Royce plc.

Copies of this thesis, either in full or in extracts and whether in hard or electronic copy, may be made only with the approval of the Author and/or Rolls-Royce plc.

The ownership of any intellectual property rights which may be described in this thesis is with Rolls-Royce plc, subject to any prior agreement to the contrary, and may not be made available for use by third parties without the written permission from Rolls-Royce plc, which will prescribe the terms and conditions of any such agreement.

Acknowledgement

I would like to thank the Electrical, Controls and Instrumentation and the Research and Development Operational Business Units within Rolls-Royce plc for making this research possible. Special thanks go to John Wilson who proof read the thesis and gave guidance and support. Additional special thanks also go to my immediate organisational leads and colleagues.

I would like to give a special thanks to Professor Sandy Smith and Dr Paul Tuohy from the University of Manchester for their endless guidance and help from the outset and to Mr Robert Gregory from Rolls-Royce plc for supporting me throughout the past seven years.

Finally I would like to thank my family who encouraged and supported me throughout the academic period.

Chapter 1

1 Introduction

1.1 Background

A nuclear reactor is a device which controls a sustained nuclear reaction by splitting fissile atoms to produce high levels of heat. This process is known as fission. Different types of nuclear reactors exist and the type of nuclear reactor chosen is application specific and suited to the operational environment. Typical types of nuclear reactors are Pressurised Water Reactors (PWRs), Boiling Water Reactors (BWRs), Pressurised Heavy Water Reactors (PHWRs), Gas-cooled Reactors (GCRs), Advanced gas-cooled reactors (AGRs), Liquid-metal fast-breeder reactor (LMFBRs) and Light Water Graphite Reactors (RBMK). This thesis considers only the application of control rod position detection within PWRs.

Nuclear energy is an important part of our everyday life as it provides a significant part of our energy requirements. The worldwide demand for energy is expected to double by 2030 and there is an inadequate supply of fossil fuels to sustain the future demand. Currently, nuclear power in the U.S generates 75% of non-emitting power generation. In addition to generation of power to supply commercial energy demands, smaller nuclear reactors are used in research and military applications. Worldwide, approximately 140 military vessels are powered by more than 180 small nuclear reactors. Most of these vessels are submarines.

The Pressurised Water Reactor (PWR) was originally designed for nuclear propulsion on-board nuclear submarines. One of the advantages of PWRs are that a fuel leak would not pass radioactive contaminants into the turbine and condenser however the main advantage is that PWR reactors are smaller in size for the same power output density. In addition PWRs operate at higher pressures and temperatures, providing a higher Carnot efficiency. However, the PWR reactor is more complicated and costly to construct than alternative reactors.

A Control Rod Drive Mechanism (CRDM) is an electrically driven linear drive motor which controls a mechanism to control and position the movement of a driveshaft which is connected to the reactor control rods. The CRDM is a linear drive electric-stepping motor which actuates a set of rotor arms when engaged. The rotor arms are suspended on a pivot and held using mechanical springs. When the CRDM actuates the rotor arms the magnetic field of the motor produces a radial force moving the rotor arms onto the driveshaft. The rotor arms also house a ball screw system which mechanically interfaces between the driveshaft and rotor arms. The ball screws allow the rotor arms to move in a circular motion while still applying the radial force keeping the driveshaft in the desired position and ensuring the control rods (which are attached to neutron absorbers) can be inserted, withdrawn and suspended in a position for lengthy time periods while the reactor is active. As the ball screw system is engaged onto the hollow driveshaft and the Probe Tube (PT) is suspended within the centre of the driveshaft, the driveshaft overlaps and exposes the probe tube when the control rod is moved up and down. This mechanical arrangement enables a sensing device to be inserted within the probe tube to monitor the position of the driveshaft.

The CRDM is installed inside the reactor vessel, enabling the reactor to be compact and simpler in design. In addition, housing the CRDM inside the vessel eliminates the possibility of a rod ejection accident occurring; thus increasing safety.

CRDM's which are housed within the reactor vessel such as this system without a mechanical arrangement to detect the driveshaft has a disadvantage. This is because the control rod driveshaft does not lead itself to being detected by a sensor due to its location. The driveshaft is a threaded tube without an internal centred support rod; thus it cannot be wrapped within an electro-magnetic coil. This makes transducers difficult to design, and causes poor magnetic coupling between the transducer and the driveshaft. The detection of the driveshaft can only be achieved by sensing its external circumference due to its location. To enable detection of the driveshaft a metallic welded tube is inserted inside the driveshaft bore illustrated in Figure 1. The PT provides the driveshaft position transducer housing and becomes enveloped as the driveshaft moves in a linear motion illustrated in Figure 1.

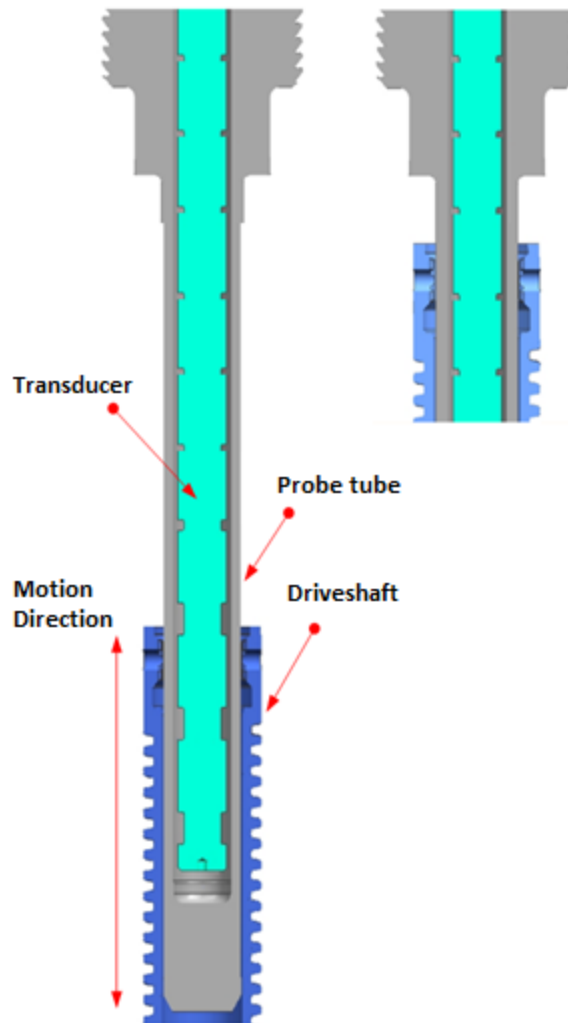


Figure 1 Driveshaft external circumference design

A Rod Position Indication System (RPIS) is used to measure and display the actual positions of the control rods in a nuclear reactor. It delivers information which is used to monitor the consistency of individual rod positions, their positions within each group of rods, and the difference between the rod positions requested and the actual position reached.

The control rods are monitored by two independent systems: a Rod Position Indication System (RPIS) and a Monitor Count System (MCS). The rod position sensor, which is part of the RPIS, detects the physical displacement of the driveshaft connected to the control rod. The MCS monitors the rotation of the CRDM and assumes the control rod is moving synchronously.

The RPIS provides information on the control rod positions to the In-core Instrumentation System which is used to derive information on reactor power and fuel burn-up, as well as providing information on the control rods (eg, scram, stuck rods). Increasing the accuracy

of the Rod position Indicator (RPI) allows the reactor to be operated at higher powers. It is possible to increase the accuracy of the RPI to allow the reactor to operate with an increase of efficiency of approximately 2%. This improvement can be translated into an extended core life as the reactor core is able to function for 2% longer, at the same cost. This can be equated to a cost saving of approximately £400 M, assuming an initial nuclear reactor plant life cost of £20 B.

1.2 Aim and Objective

The aim of this study is to investigate a novel method for improving linear position accuracy of a nuclear reactor control rod and achieve a high accuracy rod position indication.

The main objectives of the project are;

- To review current rod control measuring methodologies
- To review environment limitations affecting technologies for use
- Identify potential technology for use
- Using identified technology to develop an high accuracy measurement system
- Using analyses, to develop an prototype rod position sensor unit
- Test prototype unit within a typical environment

1.3 System requirements

Direct Measurement and Inferred Measurement

Initially it is prudent to identify the sources of errors within the measurement of the control rod system and to establish the contribution of error which is produced by the rod position detection transducer or sensor and how this would relate to the improvement in the systems total measurement accuracy. The system error stack up of the measured control rod position is made up of mechanical errors, transducer limitations, cable limitations and instrumentation errors. Figure 2 illustrates the errors associated with the displayed rod position measurement.

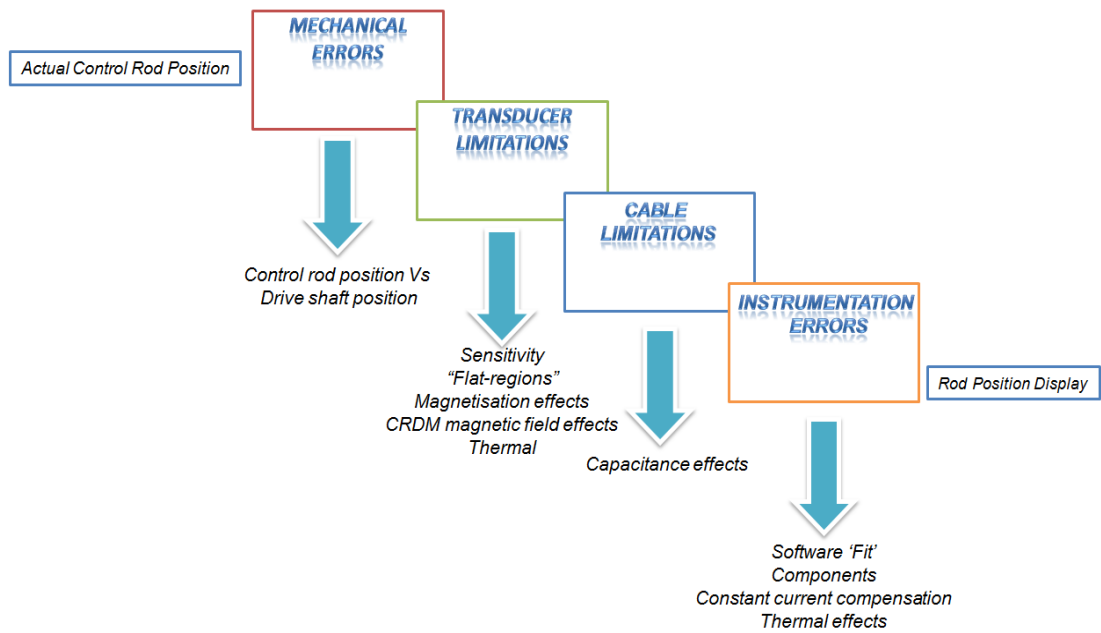


Figure 2 Control rod indicator transducer system errors

When the control rod is in the “scram” condition known as a Safety Control Rod Axe Man, the ball screws are disengaged from the driveshaft. When the CRDM is energised, the ball screws are propelled against a mechanical stop which enables them to engage with the driveshaft thread in a fully engaged position or a critically engaged position, as illustrated in Figure 3. This action causes the driveshaft to move upwards. When the ball screws are critically engaged the resultant position measurement will incur an error because moving the ball screws around the driveshaft will not cause the driveshaft to move the full distance of the required thread pitch. However, when the control rod is moved, the ball screws will eventually engage with the driveshaft, which will further increase the positional error using the Monitor Count System (MCS). The MCS indication will accumulate an increasing or decreasing error following each scram of the nuclear reactor.



Figure 3 Ballscrew engagement

The functional requirements for the project were defined by the industrial sponsor shown in Table 1.

Table 1 Advanced Individual Rod Position Requirements

Functional Requirement	Parameter Limitation	TIRPI Requirement
The system will have a cable with a maximum signal frequency capability of 1.2khz	Maximum frequency is defined by the cable capacitance	Frequency of operation will be less than 1.2khz
The system will have an instrumentation card capable of providing a constant current sinusoidal waveform	Maximum constant current is defined by instrumentation card design and wire resistance causing heating effects	Maximum constant current value will be 100mA
The system will have an instrumentation card capable of providing a maximum peak voltage	Maximum source peak voltage is defined by instrumentation card design	Maximum source peak voltage value will be 4V
The system will have an instrumentation card capable of detecting a maximum peak voltage	Maximum detection peak voltage is defined by instrumentation card design	Maximum detecting peak voltage value will be 4V
The Probe Tube will house a sensor which is capable of detecting 1200mm	Sensor detection range must be greater than 1200mm	Approximate detection length is 1200mm

Functional Requirement	Parameter Limitation	TIRPI Requirement
The Probe Tube will house a sensor which has a diameter no greater than 18mm +0.5mm	Sensor diameter limit is 18mm +0.5mm	Diameter of sensor must be less than 18.5mm
The sensor will comply with the Rolls-Royce metallic and non-metallic database	All materials must be fit for use according to Rolls-Royce process	Use only materials proven-in service defined by the Rolls-Royce processes

1.4 Control Rod Drive Mechanism Environment

The Control Rod Drive Mechanism (CRDM) is exposed to a harsh environment and is expected to operate for many years without maintenance. The TIRPI is collocated with the CRDM, and will be exposed to almost the same environmental harsh surroundings although it will physically not be contaminated with radioactive water. The operating environment of the reactor governs the materials used and limits the technologies for detecting control rod position. The materials used for a nuclear reactor are controlled for their intended location and use. When considering a material for use in a nuclear application such as the TIRPI within the CRDM, the following attributes are considered:

- a) Composition
- b) Condition
- c) Magnetic properties
- d) Form available
- e) Mechanical and physical properties
- f) Material characteristics

- g) Manufacturing considerations
- h) Ease of welding
- i) Machinability
- j) Wear resistance
- k) Resistance to decontamination fluids
- l) Effects of radiation
- m) Corrosion resistance
- n) Stress-corrosion cracking resistance and heat treatment.

As the TIRPI is housed within a probe tube, many of these attributes will not need to be considered.

The CRDM is located in a wet and hot environment; however, any sensing components within the immediate area such as the TIRPI need to be protected as reasonably as practically possible from the harsh environment. In addition, the components fitted on the CRDM are fitted for life, defined as approximately 40 years without maintenance. In practice, maintenance periods are justified but kept to a minimum to avoid radioactive exposure to personnel.

The TIRPI is located on the upper part of the CRDM in its centre and is protected from humidity by the probe tube, which is dried out prior to the TIRPI being inserted. The temperatures to which the TIRPI is exposed too are in the region of 40°C to 200 °C, thus the materials selected for the design should be suitable for use at these temperatures. The vibration and shock withstand of the TIRPI is dependent upon the location where it is used. Unlike commercial reactors, naval reactors need to be much more resilient as they must withstand rigorous operations at sea and possible threats from enemy attack. Thus, the components used in naval reactors must be made to far more stringent standards than

those used in civil reactors. The TIRPI is housed within a qualified probe tube, however, as the sensor is long and thin, it must be designed to withstand possible whiplash from installation and commissioning within the probe tube and significant impact should a shock event affect the submarine.

Electro-magnetic interference is the disturbance caused by electro-magnetic induction or electro-magnetic radiation. The TIRPI is housed within a motor which produces a large electro-magnetic field to move the control rod. The magnetic field produced by the motor will cause electro-magnetic induction on the TIRPI and induce a measurement error. The TIRPI will need to account for this error within the design.

Within the core of a nuclear reactor, the structures used are displaced by the heat being generated many times through-life, resulting in component shape and volume deviations. Due to the nature of the environment and the consequences of failure, it is important to control the materials used. In the case of submarine reactors, the materials used for the components such as the TIRPI are defined by suitability qualified and experienced personnel (SQEP) within Rolls-Royce.

The space envelope for the TIRPI is defined by the nuclear reactor mechanical design and an allocated position for the sensors such as TIRPI is identified as part of the reactor pressure vessel design. Our design is a long thin tube and the space envelope needs to consider for through life support issues, sensor failure in operation and ease of installation and maintenance.

Many designs are suitable from a theoretical approach, but in practice are very difficult to manufacture. To minimise the potential for error and risk, the nuclear industry operate an ALARP (As Low As Reasonably Practical) methodology, to meet the safety regulator standards it is essential that new engineering designs are kept simple as possible in principle for manufacture.

Products used in the nuclear industry often need to meet a life span of approximately 40+ years and in addition might be in storage for a long period prior to operation. Thus, the materials selected must be suitable for the total time from manufacture to the end of life to minimise the potential risk of breakdown in operation.

1.5 Key research contributions

The key contribution to the project was the discovery of the core material characteristics, the optimum frequency, geometry effects and how these would enable an optimised sensor solution. As a result two UK patents have been granted as a result of the work carried out during the course of this thesis. These patents are based on matching the core material of the transducer to the driveshaft being detected and selecting the optimum source signal frequency to enhance the sensor sensitivity and span. In addition, results from the testing of the TIRPI sensor showed it could be used to sense a control rod dropping when a rod drop is initiated known as a SCRAM (Safety Control Rod Axe Man). To date it has never been possible to measure the speed of a dropped control rod within a closed reactor pressure vessel and the rod drop profile has only been inferred using accelerometers. In addition the detection of the control rod gives an indication of the health of the CRDM operation by measuring the speed of a SCRAM. A further additional benefit of the TIRPI is that it can detect single CRDM stepper motor increments as it moves enabling the instrumentation electronics to compare the actual control rod position to the inferred control rod position by counting the steps the CRDM motor has moved. Should the TIRPI output position not equal the CRDM stepper motor count then it is assumed that the CRDM motor has slipped a pole. This is known as detecting pole slipping of the CRDM. To achieve this function the instrumentation electronics will need to measure the TIRPI position and the digital CRDM counter and compare the expected results due to the counter and to the actual results due to the TIRPI position detected. A paper has been published on the health monitoring and the CRDM pole-slipping capability of the TIRPI.

Chapter 2

2 Literature Review

There is an ever-increasing need for accurate measurement techniques, with a requirement for ever-increasing levels of accuracy. A variety of technologies are used to undertake specific sensing tasks that meet these requirements.

Sensors are used in many everyday applications: in the home, at work and even in our cars. It is not possible to operate or survive without biological sensors in our bodies although we probably never think of sensors in this way. Sensors are also used in safety applications and performance-related applications. A typical example would be a train, where safety is the primary concern, followed by performance and the need to meet functional requirements such as train speed and comfort and non-functional parameters such as cost and time taken to design and initial manufacture of train.

There is often confusion what is meant by a sensor or transducer. Different industries and engineers develop individual reasoning why a product is called either a sensor or transducer. To provide a clear definition for this thesis a transducer is a device which converts a signal from one physical form to a corresponding signal having a different physical form [1]. An example would be mechanical energy being converted into electrical energy by devices such as a microphone or a loudspeaker. A sensor is defined as a device that produces a usable output in response to a physical input from a transducer. The physical measured value, known as the measurand, affects the sensor, causing a response on the output which can be used to gain knowledge about the measurand. In some instances a transducer can be a sensor, however the output from a transducer usually requires a form of data processing to be understood. To summarise the term transducer is defined as: *an output which represents an input measurand ready for data processing* and a sensor is defined as: *an output which represents a useable input measurand without further processing for use.*

Many technologies are available for use with transducers and sensors. The preferred technology depends on the measurand, the environment where the device will be used

and the preferred processing method. Although many technologies can be utilised, a general suitability of different measurement technologies is shown in Table 2.

Table 2 Application suitability of various sensors [1]

Technology	Absolute	Noncontact	Lifetime	Resolution	Range	Stability
Resistive	Yes	No	Low	Medium	Medium	Medium
Capacitive	Yes	Some	High	Low to high	Low	Low
Inductive	Yes	Yes	High	Medium	Medium	Low
LVDT	Yes	Yes	High	High	Medium	Medium
Hall effect	Yes	Yes	High	High	Low	Low
Magneto-resistive	Yes	Yes	High	High	Low	Low
Magnetostrictive	Yes	Yes	High	High	High	High
Encoder	Some	Some	Medium	Low to high	Medium	High

The CRDM and probe tube system requires a linear position sensor to determine the position of the driveshaft where a transducer detects the driveshaft motion and its stationary position, and converts this data to an electrical output signal. The technologies shown in Table 2 could be suitable for the TIRPI design however a preferred technology requires further review of the technologies.

2.1 Review of existing technologies

A number of technologies are available for measuring linear position of an object through a metallic structure. However the performance of them will vary and must be considered when choosing which one to select for your application. Table 3 shows how the performance of different technologies varies using a low, fair, moderate, good, very good and excellent selection criteria. The temperature resistance, or thermal characteristics of a technology are very important to a sensor operating in a nuclear reactor as the temperatures of operation are very high. The differences in performances will act as an initial indicator of which technologies would be suitable for use within our application. The technologies further being considered within this section are resistive, capacitive,

inductive, LVDT, Hall effect, Magneto-resistive, Magnetostrictive and encoder to establish the benefits of the technology selected for the TIRPI.

Table 3 Attribute comparison chart of the main linear position technologies [1]

Characteristics	Potentiometers	AC operated LVDTs	DC operated LVDTs	LVRTs	Magneto-resistive	Optical Encoders	Magnetic Encoders
Range	2.5-500mm	0.5-500mm	2.5-500mm	0.25mm-10mm	0.15-1.5m	0.15-1.5m	0.15-3.0m
Accuracy	Moderate	Very good	Very good	Very good	Excellent	Excellent	Very good
Resolution	Moderate	Excellent	Excellent	Excellent	Excellent	Excellent	Very good
Repeatability	Fair	Excellent	Excellent	Excellent	Excellent	Very good	Very good
Temperature Resistance	Fair	Excellent	Moderate	Excellent	Good	Excellent	Good
Linearity	Moderate	Good	Good	Good	Very good	Very good	Very good
Cost	Low	Moderate	High	Moderate	High	Moderate	Moderate
Complexity of support electronics	Low	Moderate	Low	Moderate	Low	High	High

2.1.1 Resistive sensing or potentiometers

A potentiometer is a three-terminal voltage divider which can be powered by a DC or an AC voltage source. Two of the terminals are fixed, while the third terminal can be moved along a resistive strip between the first two terminals. A typical potentiometer would have a mechanical moving object connected to the moving terminal, causing the potential voltage measured at the moving terminal to change as the object moves illustrated in Figure 4. Potentiometers are low- cost devices and easy to implement; however, they rely on mechanical contacts to provide position measurement. This means that potentiometers have poor repeatability and large hysteresis. The mean time between failures (MTBF) for a potentiometer is typically less than 1000 hours. These devices are not suited to high-reliability applications where periodic replacement of the transducer is neither desired nor possible.

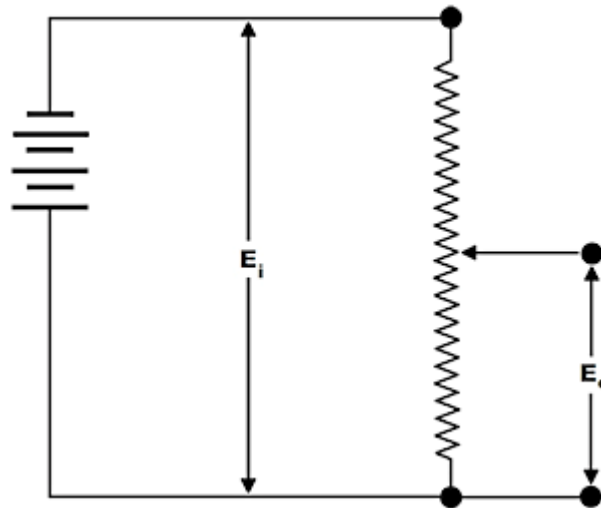


Figure 4 Circuit Diagram for a basic potentiometer [2]

2.1.2 Capacitive sensing

Capacitive sensors are popular in industry as they provide a sensing technique that does not require the use of physical contacts like resistive sensing. The electronics which drive the capacitance transducers are complex as the measured values have to be processed to provide useable output data. The capacitance of a system is the ability to store electrostatic energy. An example of a simple capacitor is two parallel conductive plates on the outer edges of a dielectric (insulator) material. The capacitance value can be changed by changing the dielectric material or dielectric constant of the material, and thus changing the value of capacitance for the device. A typical linear position capacitance sensor would detect the presence of a metal target with respect to the sensing element and produce a change in capacitance which is proportional to the target distance. An example is shown in Figure 5.

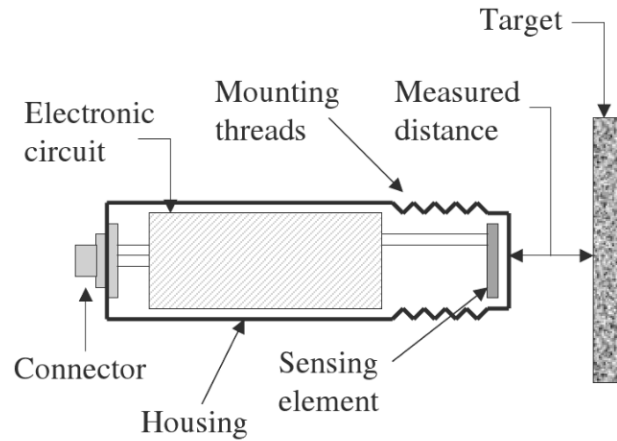


Figure 5 Capacitive linear position transducer [1]

2.1.3 Inductive sensing

A low-cost position transducer can be designed using an inductive type of element which consists of a number of coils wound around a movable core. The inductance of the inductor is determined by the turns, dimensions and the material of the core it is wound upon. If the core is made of a low permeability material, the inductance of the inductor will be less than that for a core made of a high permeability material. In addition to the core material the influence of the inductance of the device is changed by the number of turns in the wire coils and the frequency of the current being applied to the inductor due to eddy current effects of the induced secondary current carrying circuit. Eddy currents are produced in conductive materials where an alternating current drive is used to power them.

The inductance of the coil is a measure of the electromagnetic energy stored within the inductor. The unit for inductance is the Henry, which is named after the American scientist Joseph Henry. Core materials are usually nickel-alloy materials due to their good mechanical and magnetic properties. It is important to note that a final annealing process is desired versus cold working of the core materials to relieve mechanical stress from machining and to make the entire core magnetically uniform.

2.1.4 Linear Variable Differential Transformer (LVDT)

LVDTs consist of three windings and a ferromagnetic core within an enclosed housing. The primary winding has a voltage applied from an AC current or voltage source. The two secondary windings experience an induced electromotive force (emf) and produce a representative voltage on the outputs. LVDTs are non-contacting and robust with long term reliability in harsh environments. They are generally used in applications where high reliability is required such as subsea applications, power plants and high temperature environments. The induced emf is determined by the position of the ferromagnetic core which can be moved freely within the housing. The core is usually attached to the moving object that is being measured. If the core is between the secondary coils, the output voltages will be equal and opposite illustrated in Figure 6. If these outputs are connected in series they will produce a null voltage. To obtain a position from the LVDT, the primary coil should be driven by an alternating current source and the voltages from the secondary coils processed to give the required data. As the LVDT works in a manner similar to a transformer, the output voltage is proportional to the ratio of the number of turns of wire in the secondary coils relative to the number of turns of wire in the primary coil providing the core is not magnetically saturated. When the core is moved in either direction, a differential voltage will be generated across both secondary coils thus detecting position of the core. The LVDT can also be wired to provide a zero secondary output voltage when the core is exactly mid-way between the coils, and an output voltage is then produced when the core is moved either direction. A typical power plant LVDT is shown in Figure 7.

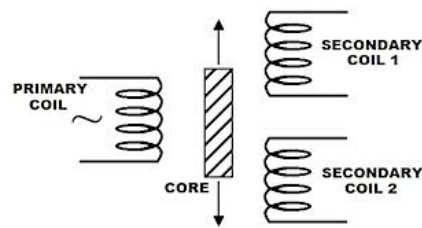
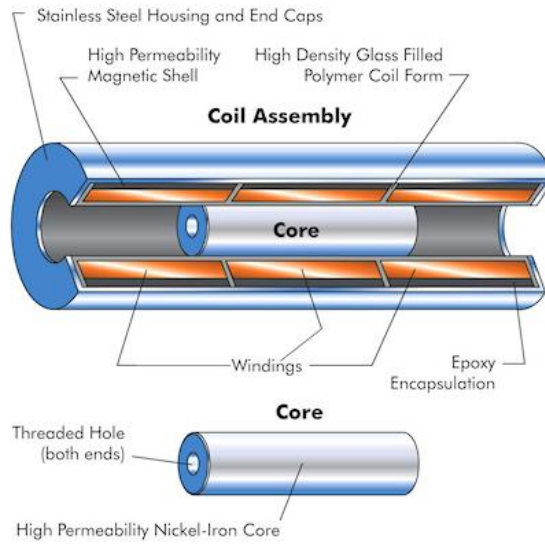


Figure 6 LVDT winding and core configuration [2]



Figure 7 Typical power plant LVDT [2]

2.1.5 Hall Effect transducers

Hall Effect transducers are used mostly in automotive and industrial products due to their long life expectancy and low cost. The sensitivity of the Hall Effect transducer is defined as the measurement of the magnetic field at a certain position within the device package.

These are usually used for relatively small lengths of measurement no greater than 25mm. The Hall Effect transducer measures the polarity and strength of the magnetic field which is produced by a source: usually a magnet connected to the moving object being measured. As the position of the magnet changes, the Hall Effect device produces an electrical output which represents the change of position as shown in Figure 8. The output voltage is very small, but its amplitude is proportional to the magnetic field strength. The Hall Effect or hall device has an electric current passed through a conductive material in addition to the perpendicular magnetic field produced by the position magnet.

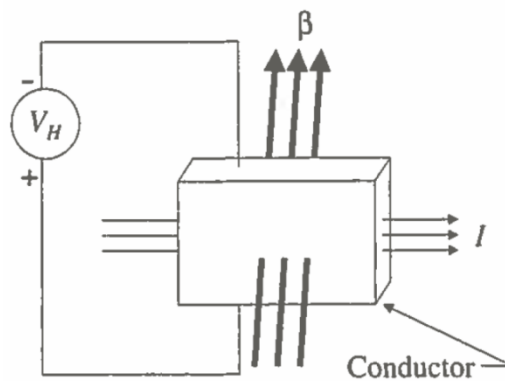


Figure 8 Hall effect [1]

The magnetic field causes the current polarities to move to the opposing sides of the conductor causing a voltage potential. Figure 9 shows an n-type semiconductor where the electrons are concentrated towards the upper edge of the conductor. The upper surface now becomes negatively charged due to the greater number of the electrons there. The difference in potential voltage is the Hall voltage, which varies depending on the magnetic field strength and magnitude of current flow.

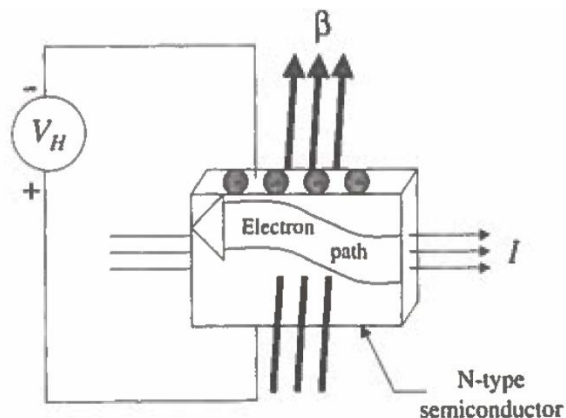


Figure 9 Concentration of current carriers [1]

2.1.6 Magnetoresistive

A magnetoresistive transducer provides a changing electrical resistance in the presence of an external magnetic field. The resistance of the conductor used within the magnetoresistive device changes following a non-linear characteristic. The change is a direct ratio of the magnetic field density, similar to the Hall Effect transducer. Although these devices are used for relatively small length measurement (in the order of 25mm), a number of these devices can be attached in series to provide a longer length measurement. The moving object whose object is being measured will usually have a magnetic field source, like a magnet, connected to it. The magnetic field couples between the moving object and the transducer. The magnetic field density varies as the position of the object changes, thus changing the resistivity of the transducer. In most magnetic materials the electrical resistance actually decreases with an increase in magnetic field strength as the magnetic field direction is perpendicular to the current flow in the magnetoresistor. Due to the effects of Lorentz force, the moving charge carriers are aligned with the magnetic field forcing the charge carriers to one location of the device. This effect causes an increase in resistance due to the unavailability of charge carriers illustrated in Figure 10.

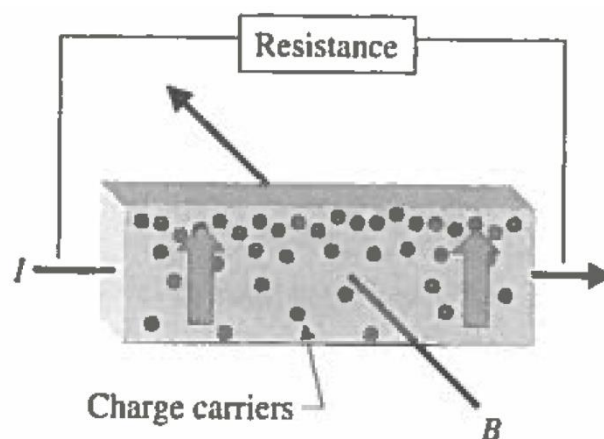


Figure 10 Magnetoresistor charge carriers [1]

In addition to the charge carriers locating in a particular region causing a resistive change, the cross-sectional area of the conductor is also reduced, thus causing an additional change to the resistance of the material. Although any conductor exhibits these effects, they are more prominent in ferromagnetic materials-particular in nickel-iron alloys.

The properties of the conductor can also be changed by manufacturing processes used in its construction. For example the magnetic domains within a wire tend to align parallel with the linear axis as shown in Figure 11. During the manufacturing process, deformation occurs and the grains within the wire material rotate and elongate, which causes crystallographic directions and planes to become aligned. This effect causes anisotropic behaviour in the material, thus it develops an orientation of magnetisation along its axis. To enable a magnetic axis to be changed, a magnetic field can be applied to the material which causes the magnetic axis to be perpendicular to the current flow and causing the electrical resistance to change.

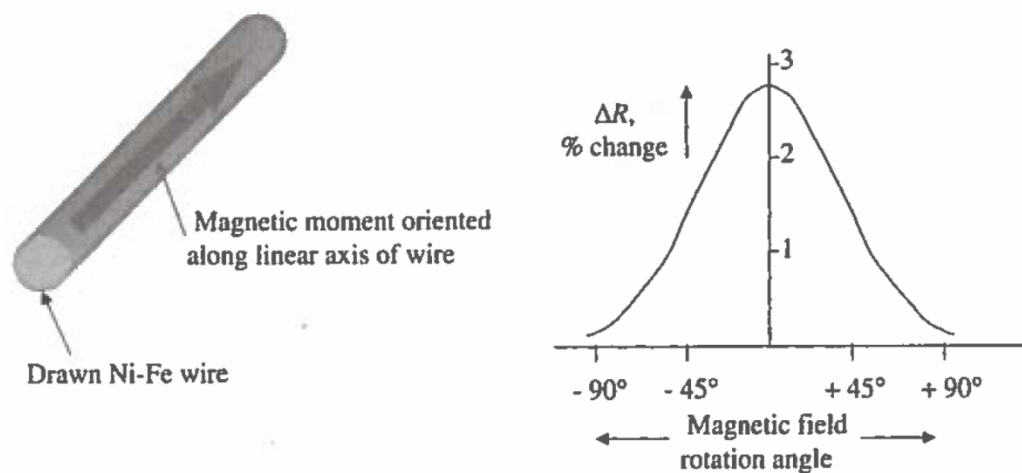


Figure 11 Magnetoresistor – alignment of magnetic domains [1]

2.1.7 Magnetostrictive

Magnetostrictive transducers use a sensing magnet, a wave guide and a pick-up coil to measure a position of the moving object. The magnet is attached to the moving object and its position is measured by applying a current pulse to the waveguide. The current pulse generates a sonic wave in accordance with the Wiedemann Effect. The sonic wave travels along the waveguide and is detected by the pick-up coil. The current pulse transmission and pick-up coil detection is timed, and the elapsed time represents the distance between the magnet and the pickup coil as illustrated in Figure 12. This technology is very accurate, but expensive, and is usually limited to applications where there are no extreme

levels of shock, vibration or temperatures. Typical MTBF values for these sensors are 100,000 to 250000 hours.

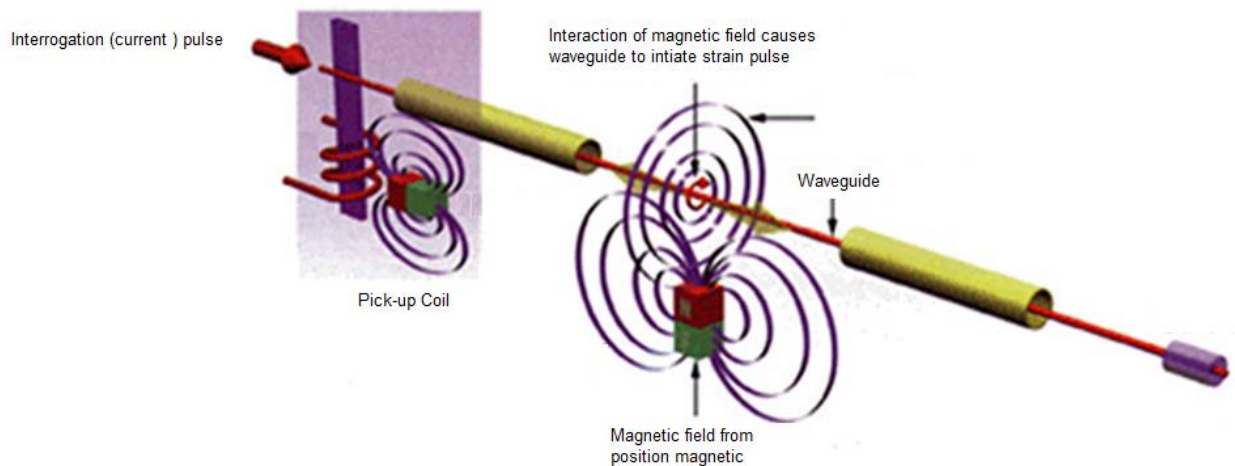


Figure 12 Magnetostrictive sensor

2.1.8 Encoders

Encoders either have optical or magnetic gratings which provide digital signals that can be decoded to give an absolute or relative linear position. Incremental encoders read linear graduations on a glass scale or sense the magnetic poles on a ferromagnetic material. These sensors are better suited for measuring objects which are slow moving; however, they require complex instrumentation to operate. These sensors are used in areas which require high precision and where operation in a harsh environment is not required. The MTBF of encoders is between 100,000 to 1,000,000 hours. An example of an encoder suitable for our application is an magnetic encoder using Hall effects or magnetostrictive pick-up elements. This uses a magnetic tape onto which alternate north and south regions are formed as illustrated in Figure 13. Using moving pickup elements, the variation in the regions is detected by the magnetostrictive pickups and the linear position is obtained of the pickup position. The resolution of the position is determined by the magnetic field region sizes and spacing.

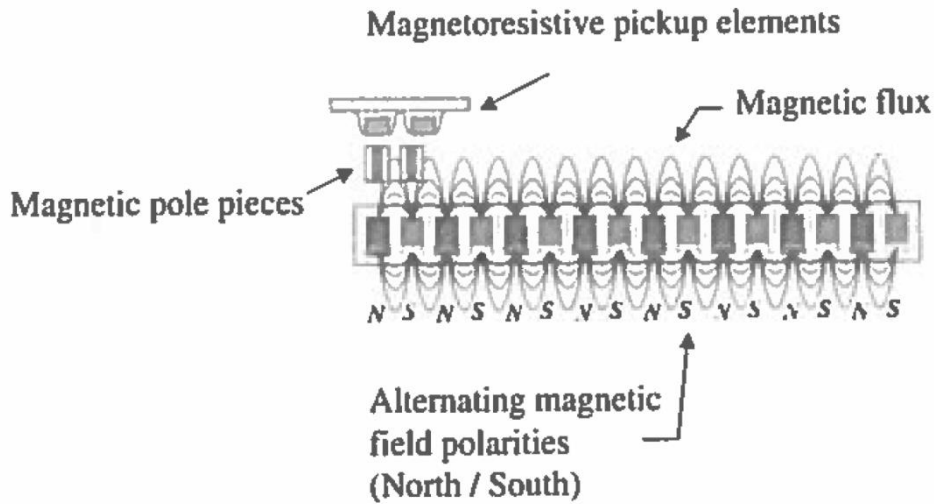


Figure 13 Magnetic encoder

2.1.9 Conclusion

Where reliability and safety are of primary concern within a harsh environment, the LVDT is the most suitable technology for use within our environment. The LVDT has a higher MTBF and can be easily packaged to suit a range of housing. The LVDT is the technology of choice for high temperature, high shock and high vibration environments and especially for use on nuclear plant applications [2].

2.2 Electromagnetic Sensors

This section reviews a number of existing sensors which could be used to measure the control rod position within a reactor plant. These use electromagnetic technology similar to the LVDT principle to indicate linear position of an object.

2.2.1 A position indicator employing magnetic circuits to monitor the position of a magnetically permeable member movable along an axis having one degree of freedom

This position sensor comprises a series of open and closed magnetic loops determined by the position of a hard magnetic polarised core. The magnetic core provides a change in magnetic flux as it moves, closing the flux path between tandem positioned indicators.

The operation is based upon a magnetic flip-flop principle that utilises the narrow hysteresis loop of soft magnetic materials.

Each indicator has a soft magnetic core, having a closed or open magnetic loop with a common magnetic flux path. The magnetic principle for this sensor is usable and proven; however the physical geometry cannot be implemented within the TIRPI design. This is because the moving hard magnetic core moves internally to the indicators, whereas our CRDM design requires circumferential detection of the driveshaft. In addition the space envelope allocated for the TIRPI is long and thin which limits the sensor size. The physical form of the sensor design is illustrated in Figure 14.

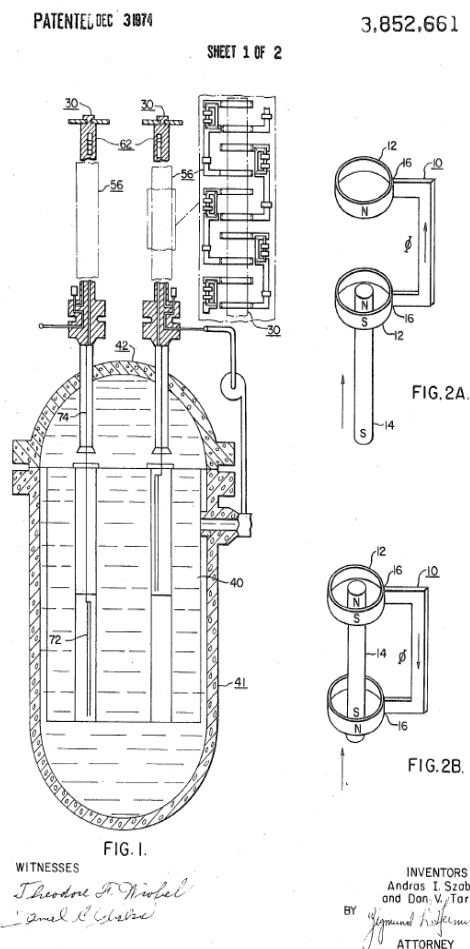


Figure 14 Position Indicator Principle [2]

2.2.2 Inductive position sensor having plural phase windings on a support and a displaceable phase sensing element returning a phase indication signal by electromagnetic induction to eliminate wire connections

The proposed sensor principle uses the detection of signal phase changes supplied by a microcomputer. The changes in signal phases are provided by inductive coupling between a multiplicity of windings and a set of offset pitch windings. A phase signal is detected either by a moving pickup device or a stationary device linked by a ferromagnetic core. A bespoke array of winding arrays enables a distinctive phase pattern to be coded with respect to position. An example of the bespoke pattern is shown in Figure 15. The fundamental systems to derive position from a phase pattern require complex computational techniques. The software complexity overhead is deemed a very high risk area when applying for nuclear licensing. In addition, the sensor would be very complex to manufacture and very difficult to assemble within the limited space envelope available within the probe tube. This sensor would be deemed as having too many associated risks to be deployed by the submarine programme.

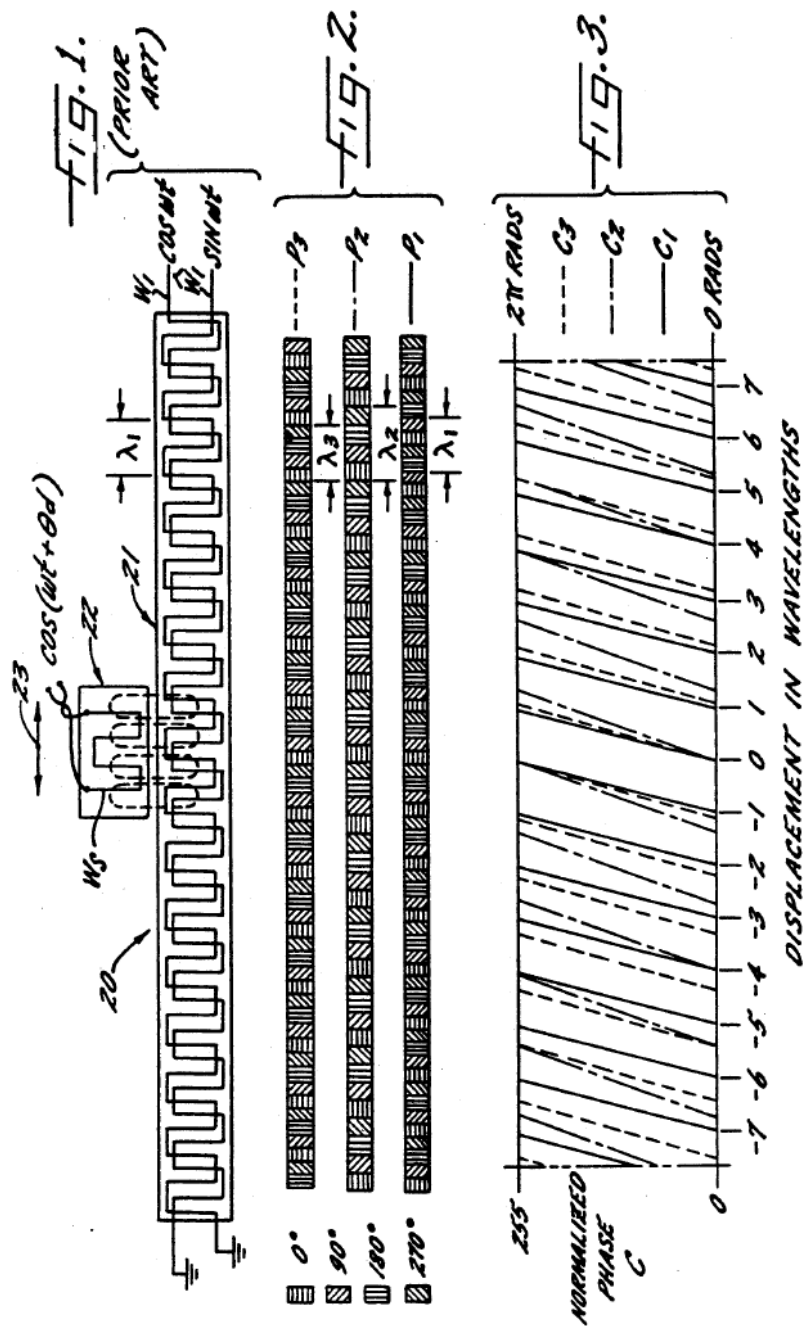


Figure 15 Bespoke pattern configuration to determine signal phase shifts [3]

2.2.3 Electromagnetic delay line incorporated in a position detector for a movable nuclear reactor control rod

This unit comprises a position detector which does not use a mechanical contact. A permanent magnet is attached to the moving object and a sensor determines the position of the magnet.

The sensor core is required to be magnetically saturated while propagating a high frequency pulse onto it. The magnet on the moving object produces a magnetic field where by the pulse is reflected. This principle can be used in an enclosed primary

containment application and has a high accuracy. However, the source of the magnetic field is required to be attached to the moving object. The moving object would have to be manufactured as part of the CRDM and this is not deemed practical or cost effective. This method is not suitable as our driveshaft has not been designed to house a magnet. However, a change to the driveshaft design would enable the principle described to be applied. The principle of operation is illustrated in Figure 16.

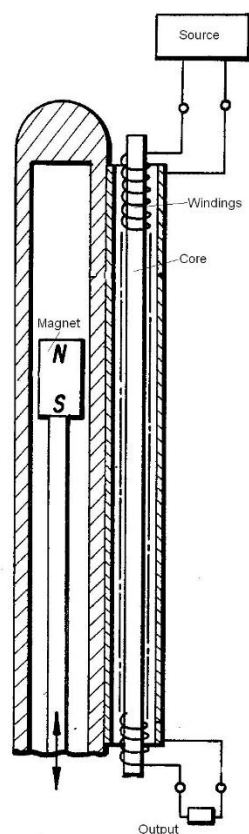


Figure 16 Electromagnetic delay line [4]

2.2.4 Method and System for Indicating the Position of Control Rods of a Nuclear Reactor

This method and system relies on a nuclear reactor control rod shaft sliding vertically inside an internal housing guiding a movable shaft, as illustrated in Figure 17. The vertical shaft has a suspended control rod. Primary and secondary coils are wound around the housing. An AC current is passed through the primary coils, which induces a secondary voltage across the secondary coils. The primary and secondary voltages are put through a low-pass filter and rectified into DC voltages. An algorithm is used to derive the control rod position based on the output voltage value from a secondary coil arrangement.

This design of sensor is very suited to our application as it has minimal software complexity and the design lends itself to our restricted space envelope. However, the moving driveshaft must be within the centre of the sensor to give the maximum electromagnetic sensitivity and to provide greater signal output sensitivity. Our application requires the driveshaft to be detected circumferentially, and this greatly reduces the sensitivity of the sensor. Figure 1 shows the driveshaft position as it moves circumferentially over the probe tube. As the magnetic field is weaker on the circumference than within the centre of the TIRPI the voltage output sensitivity will be greatly reduced. The signal power supply for this sensor is a constant current source which needs to be kept stable in order not to give errors on the output from the secondary coils. In addition, temperature effects can change the secondary output signal. The TIRPI temperature effects are compensated for by reading the primary coil signal drive voltage. This primary coil voltage changes in relation to the temperature due to the thermal coefficient of copper and the primary voltage is used to compensate for thermal effects on the sensor or transducer. This sensor and temperature compensation method should be used in our design. Figure 17 illustrates the primary and secondary coil configurations.

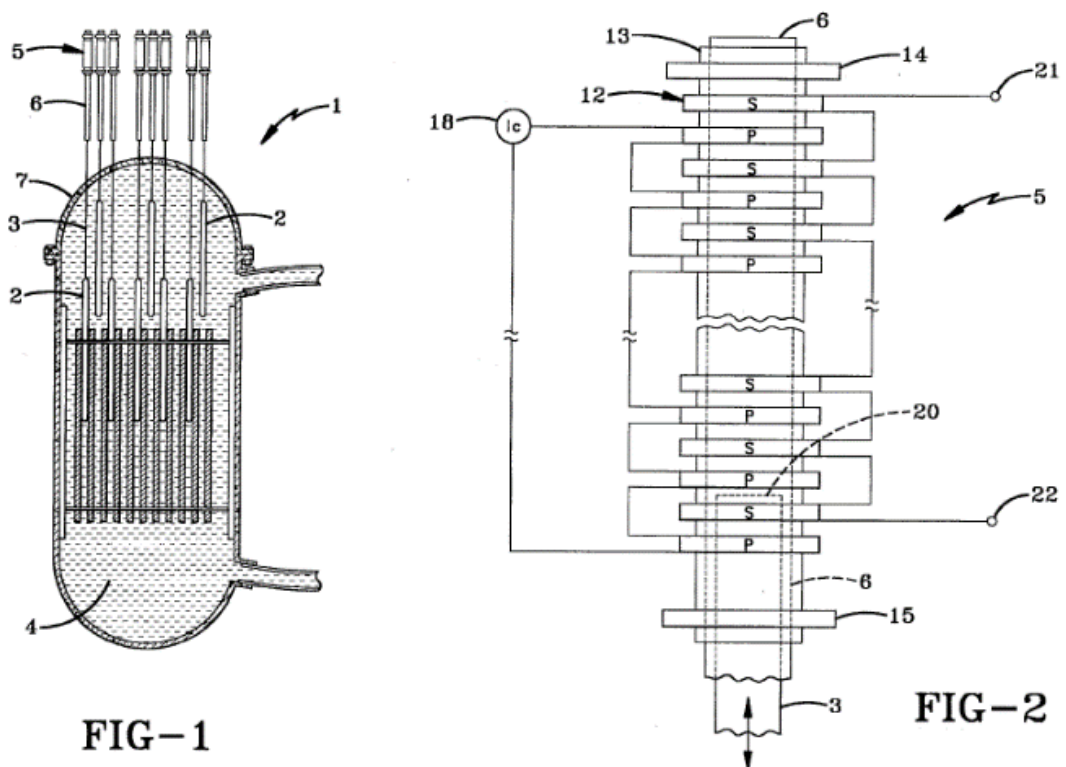


Figure 17 Serial transformer principle [5]

2.2.5 Position indication system

The position indication system comprises a sensor formed from discrete electrical coils. The coils are individually wound around the rod travel housing in a tandem formation along the control rod driveshaft length. An AC current is generated at the coils with a low frequency which enables the magnetic field to penetrate the metallic rod housing. A change of impedance occurs in the coils when the rod driveshaft passes through the flux generated by the coils. The change of impedance determines the position of the control rod.

The principle of operation behind this sensor is suitable use for use in our application. However, due to the requirement for circumferential detection, the coils cannot be placed on the probe tube as shown in Figure 18. The fundamental principle can be adopted for uses in a core former which resembles the previously explained design of the serial transformer within Figure 17.

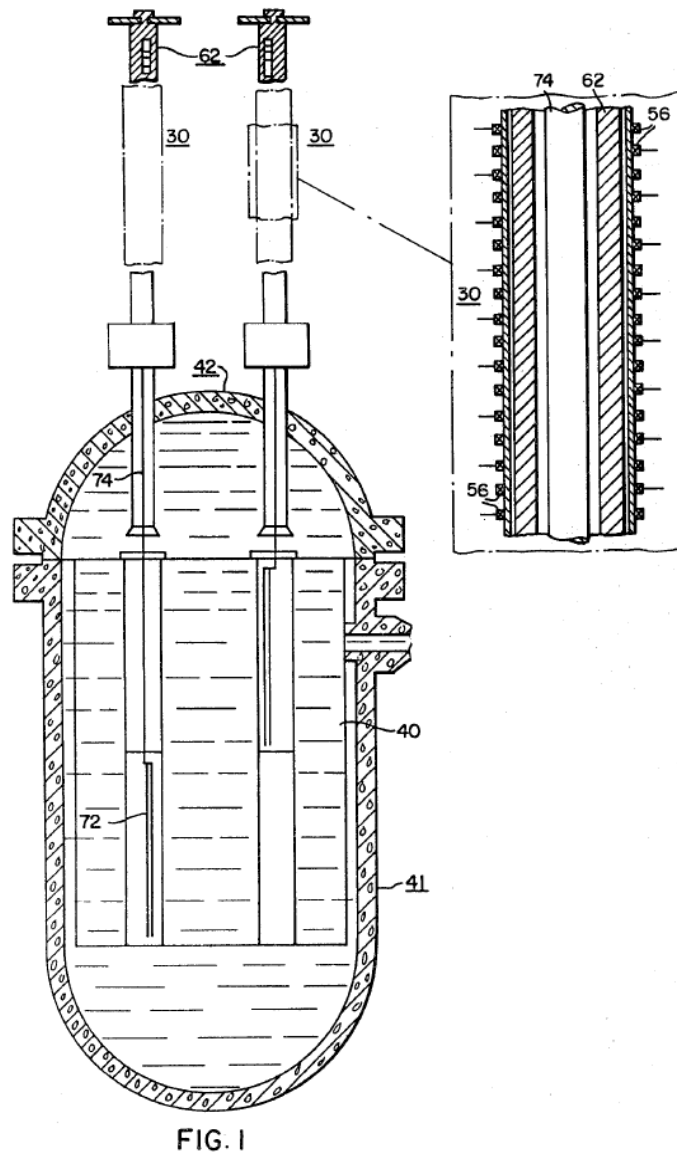


Figure 18 Position indication system [6]

2.2.6 Magnetic position indicator

A closed-loop E-type transformer can be used to detect the presence of a magnetic material by saturating the transformer. The magnetic flux is generated by an AC excitation current source coil and a DC excitation current source coil. The DC coil generates a DC flux, which enables saturation control of the transformer and forms either an open or closed DC magnetic circuit. The AC coil flux, driven by a sinusoidal signal, detects the flux change and changes the secondary voltage output signal accordingly. This sensor would not be suitable for our application as there is insufficient space around the probe tube due to the size of the transformer as shown in Figure 19. However the principle could be applied internally to the probe tube to allow detection of the driveshaft radially.

Although this is a viable option, the manufacture of such a system is deemed too high a risk due to the number of individual piece parts required and the miniaturisation of the components needed to achieve the accurate resolution.

PATENTED JUN 26 1973

3,742,409

SHEET 1 OF 3

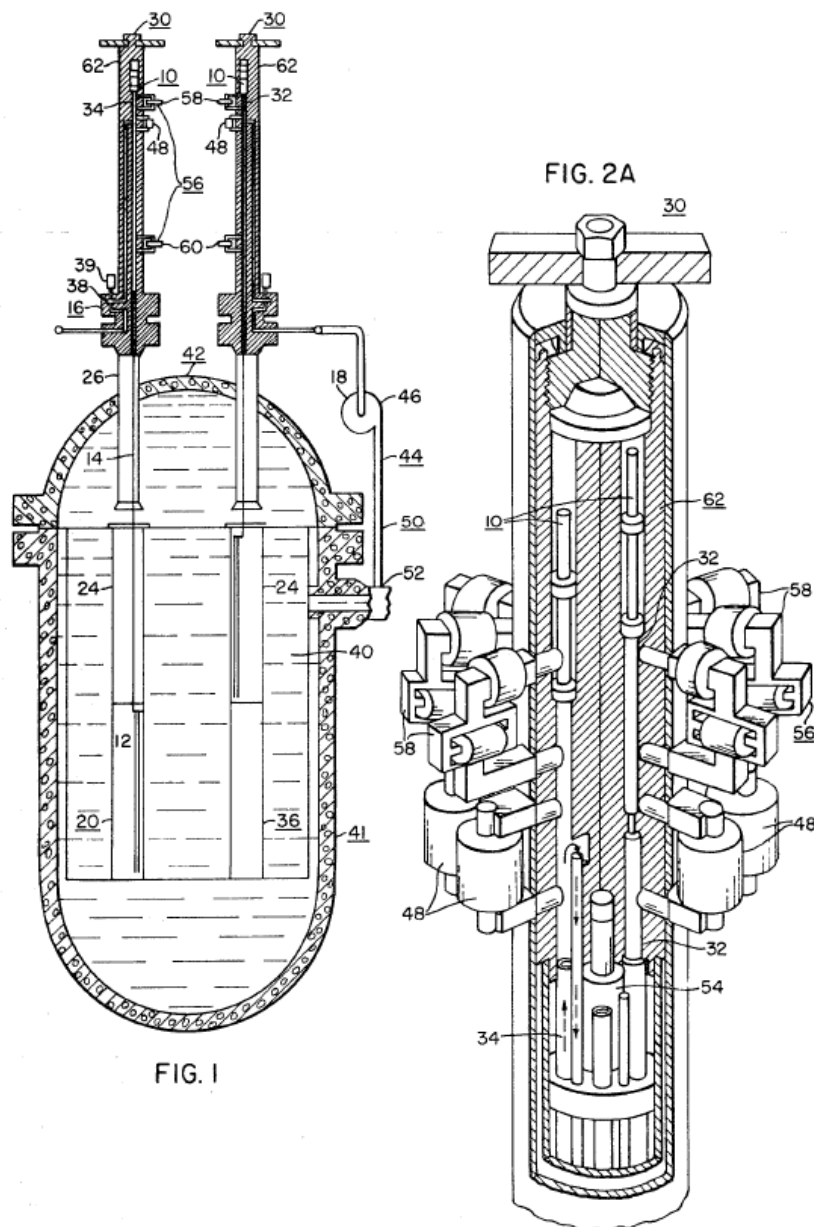


Figure 19 E-Type Magnetic Sensor [7]

2.2.7 Position encoder

A linear position sensor can be produced using a pair of phase quadrature windings on a support. The windings are arranged such that a sinusoidal signal can be measured along the length of the windings when they are magnetically coupled with a pair of additional

movable source windings as shown in Figure 20. To ensure sensitive coupling, the source windings are in series with a capacitor which forms a resonant circuit. As the source windings move along the support, the current induced on the phase quadrature windings is dependent upon their position.

The advantage of this sensor is that it can be manufactured very easily with the minimum of components. However, the sensor relies on moving source windings, which cannot be implemented on our driveshaft. An adaptation of the principle can be utilised where the source is constant and the driveshaft affects the induced magnetic field on the phase quadrature winding. However, this would require additional research before implementation and deemed feasible for this study. In addition, the instrumentation would require complex algorithms to determine the position of the driveshaft due to the complex quadrature relationships. This sensor is deemed too complex to be implemented within a nuclear reactor safety system and will also require many electrical inputs/outputs.

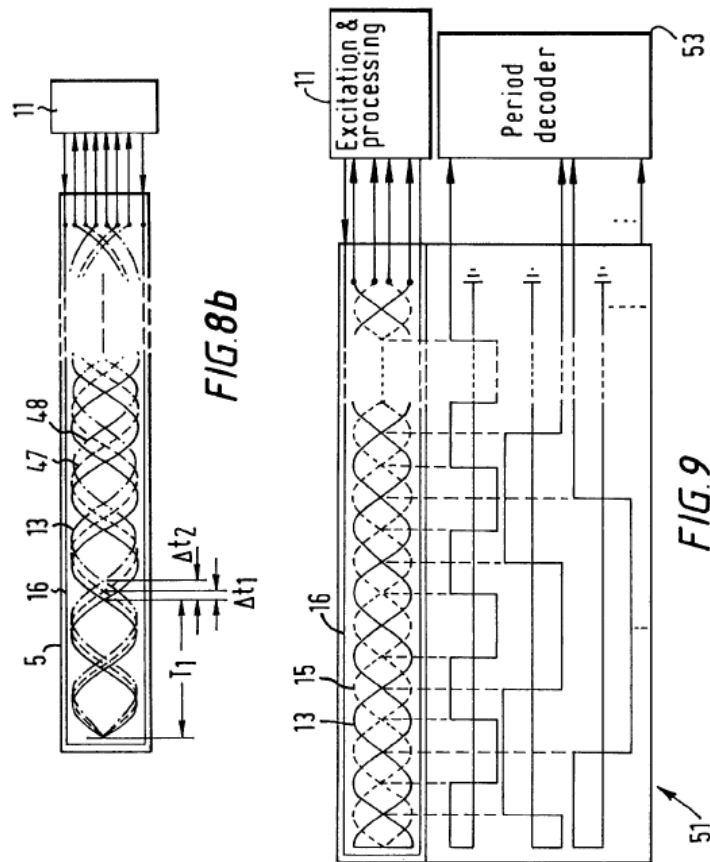


Figure 20 Position encoder [8]

2.2.8 Position indicating device

This particular sensor comprises a number of paired inductors that generate a magnetic field around a specific region. The paired inductors are placed along the length being measured, and connected to an array of electronic comparators to evaluate the voltages across the paired inductors. The inductors are arranged such that each inductor will change inductance with respect to the rod position as it travels along the length being measured.

The principle behind the sensor is suitable for use in our application; however, the sensitivity of the sensor is reduced if we detect the driveshaft on the circumference of the probe tube rather than the centre of the inductors, as illustrated in Figure 21 . In addition the sensor will require multiple connections (one per pair of inductors), thus decreasing its

reliability due to manufacturing complexity. The processing electronics required for the sensor will need to determine the position of the driveshaft by comparing many number of circuit inputs which increases the complexity of the instrumentation electronics. The principles of operation can be considered further; however, the sensor is not deemed sufficiently viable to be considered for implementation within our system.

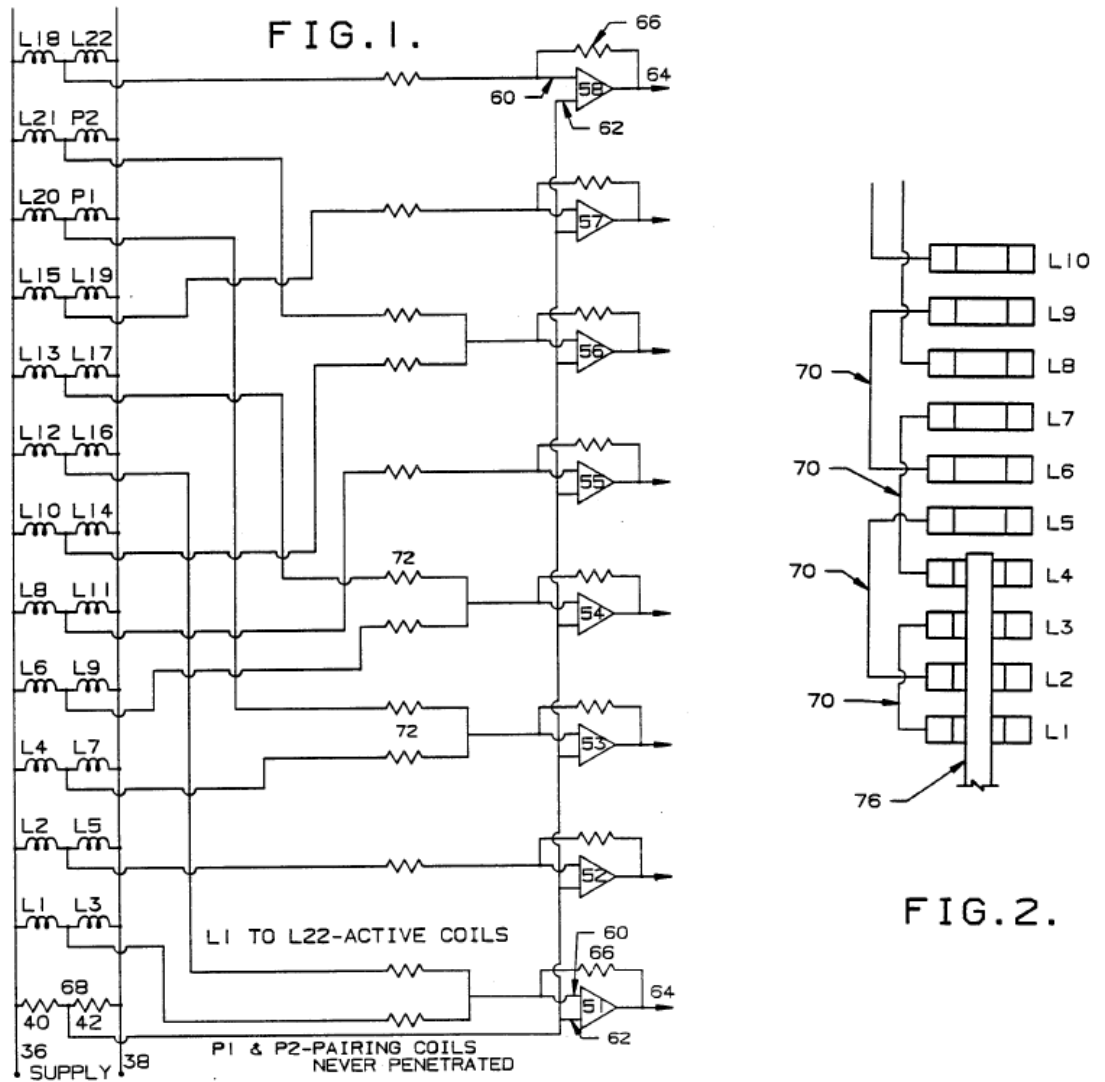


Figure 21 Position indicating device [9]

2.2.9 Magnetic position indicator

A ferromagnetic shaft is detected by a position indicating system comprising magnetic transducers placed longitudinally apart. The transducers are positioned with a fixed spacing, externally to a chamber. Each transducer is a magnetic coil excited by different signal phases. As the ferromagnetic shaft moves inside the chamber, the output from the transducers changes phase; thus providing a means to detect motion. Figure 22 shows the chamber and magnetic transducers. The advantage of this system is that it is temperature-independent. However, a complex system is required to analyse the signal being detected.

The transducer is made up of an 'H'-shaped core, with primary and secondary coils arranged such that the source signal phase becomes the reference phase and the secondary coils detects the position of the ferromagnetic shaft. The fundamental disadvantage of this technique is that the shaft is required to be in the centre of the chamber. In our Control Rod Drive Mechanism (CRDM), the requirement is for an external shaft enveloping the chamber.

This technique of position detection, although useful due to the lack of temperature compensation, will be difficult to implement in the probe tube internal geometry. The complexity of the associated electronics makes this sensor an unsuitable solution for our application.

FIG. 3

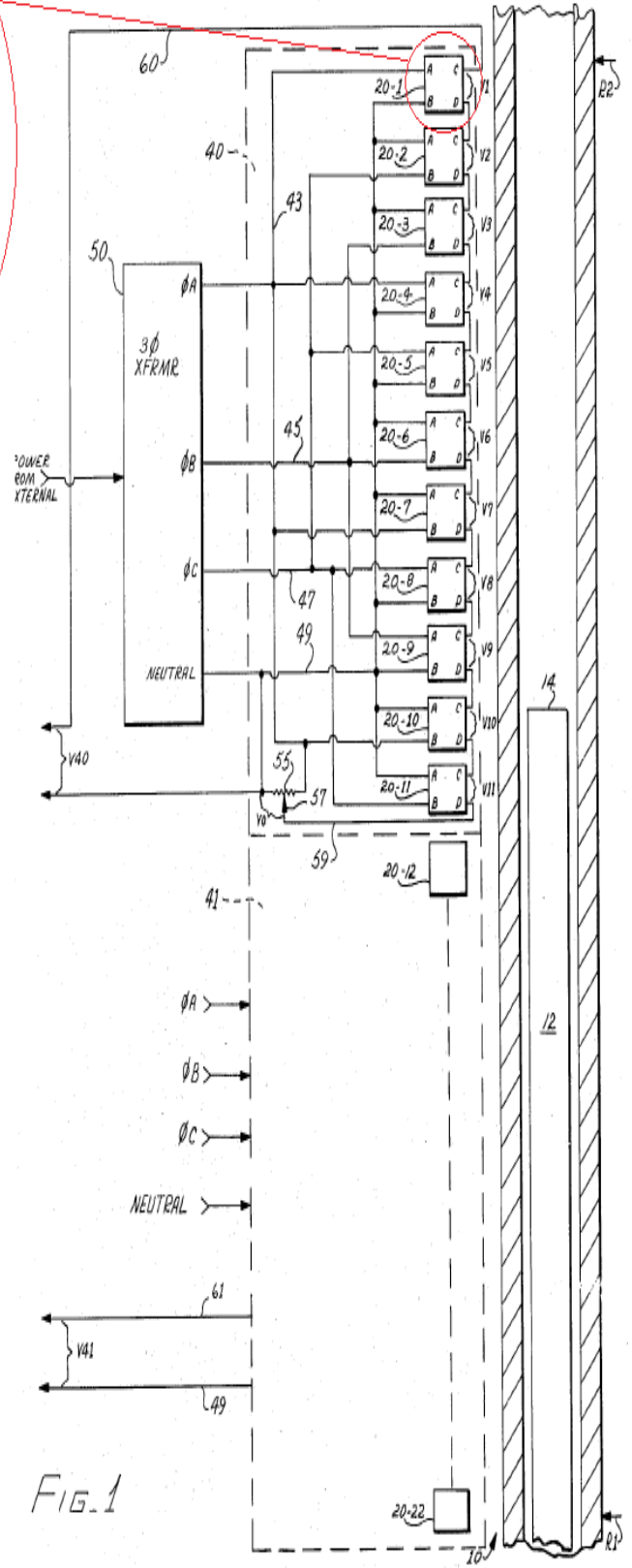
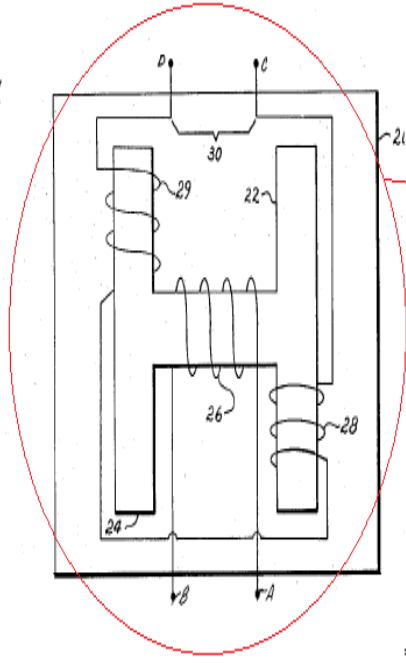


FIG. 1

Figure 22 Magnetic position indicator [10]

2.2.10 Electromagnetic position indicator

A continuously indicating position linear sensor is illustrated in Figure 23. This sensor uses inductive coupling between primary and secondary coils to detect a moving object. The secondary winding has oppositely connected coils spaced in such a way as to increase measurement precision however reducing the amplitude of the secondary output signal. Similarly to previous solutions, the shaft is detected within the centre of the coils as this location has the greatest magnetic flux density and produces the maximum voltage signal displacement on the secondary coils.

This solution suggests the spacing between the coils has an effect on the measurement accuracy of the sensor. In addition, the secondary coils are oppositely connected, which suggests accuracy improvements as a result of this specific configuration.

The fundamental principles of this solution should be investigated to determine whether it is suitable for use in our application. However, because the shaft whose position is being measured moves within the coil centres and not on the circumference of the coils, a direct implementation of this solution is not suitable.

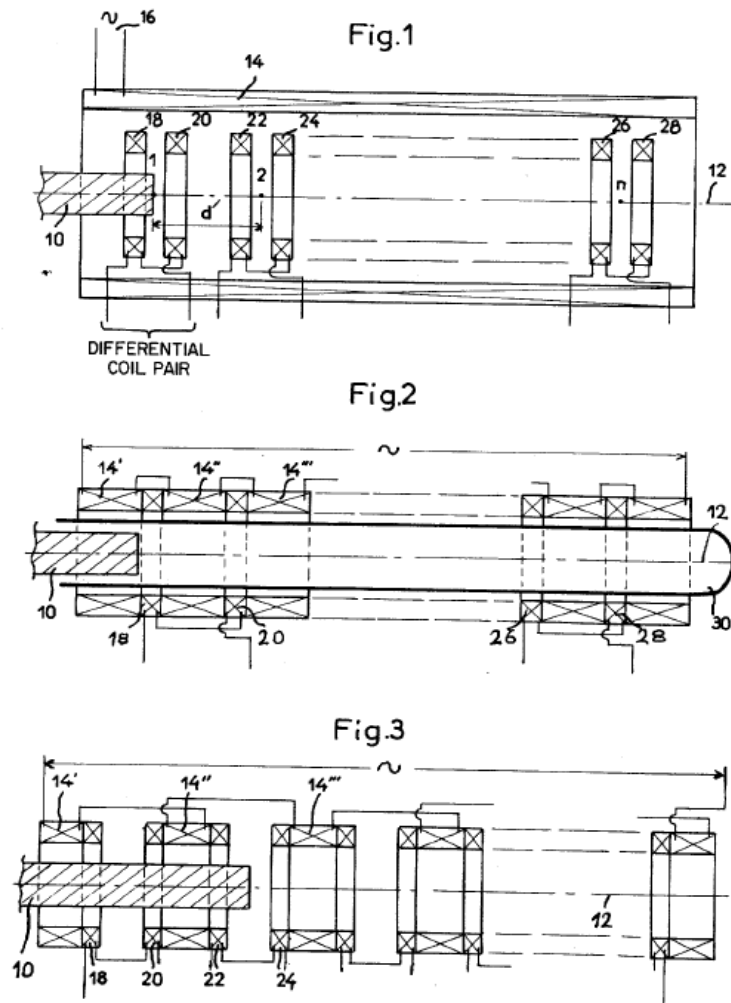


Figure 23 Electromagnetic position indicator [11]

2.2.11 Nuclear Control Rod Position Indication System

This sensor comprises an array of magnetic reed switches, enclosed within an outer housing which protects against damage by the primary coolant such as our probe tube. The reed switches are positioned such that a magnet moving close to them causes the switches to close when it is in close proximity, as illustrated in Figure 24. The reed switches are connected in a resistive circuit, thus causing a detectable resistance change when they close. This principle is very reliable and easy to implement with an

instrumentation channel; however it would be very difficult to manufacture and there are more potential points of failure than for a wire-wound product. In addition, the accuracy of the sensor is governed by the reed switch size. As the reed switch size decreases, thus increasing the sensors accuracy, the potential fault points increase. This is due to the greater number of reed switches required for a specific length of travel. This design also requires the driveshaft to have a magnet attached which operates the reed assembly. Rolls-Royce has considered a magnetic driveshaft design for use however it was declined by the mechanical design team as it was deemed too high risk to use. This principle is worth considering as a potential solution for use in the future, but it does not meet our current design requirements shown in Table 1.

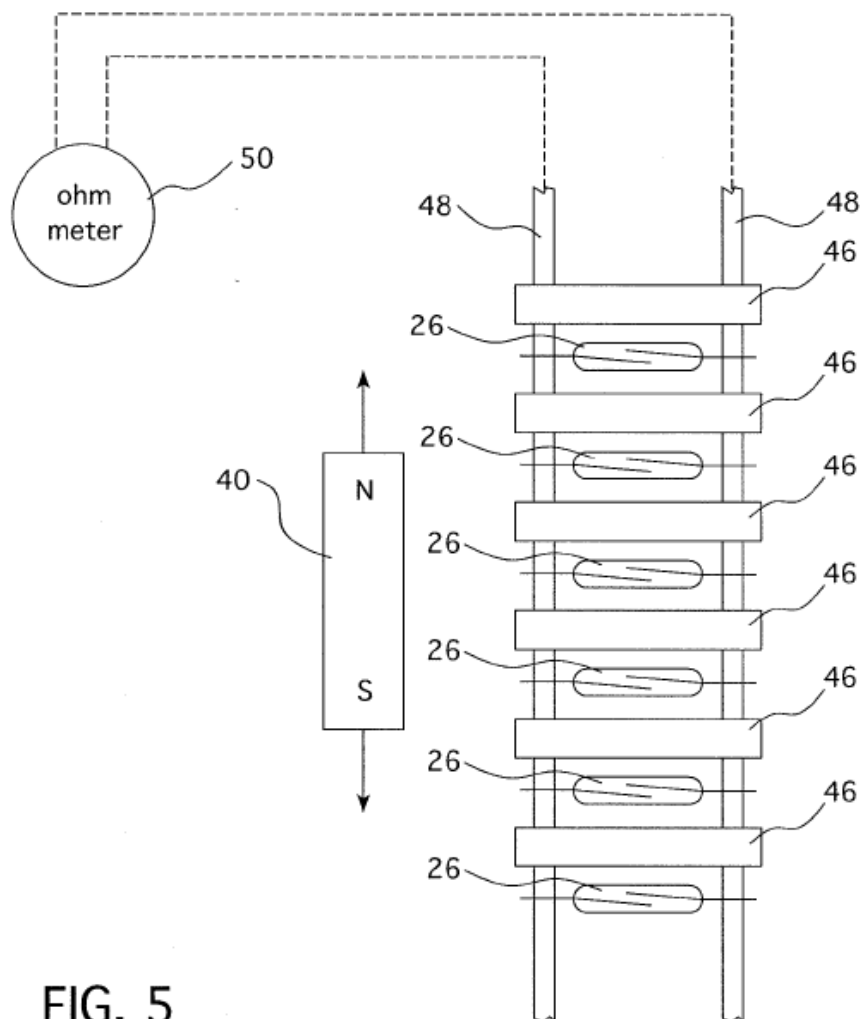


FIG. 5

Figure 24 Nuclear control rod indication system [12]

2.2.12 Position Sensor of Linearity Moving Bodies

This sensor uses a number of inductance coils with open magnetic circuits coaxially arranged one after another. The sensor includes a shunt element which is designed to move along the coil axis. This produces a signal on the circuit output of the inductance coils. The shunt element is connected to the object whose location is being monitored, and the output signal of the coils represents the object position.

The shunt element is designed to produce the maximum accuracy by changing the diameter of the holes and the inter-hole spacing as illustrated in Figure 25. This principle can be easily applied; although the mechanical arrangement and build is extremely complicated, especially in a limited-space probe tube envelope such as is used in our application. In addition, the shunt will have to be connected to the driveshaft, which is deemed to be a high risk solution.

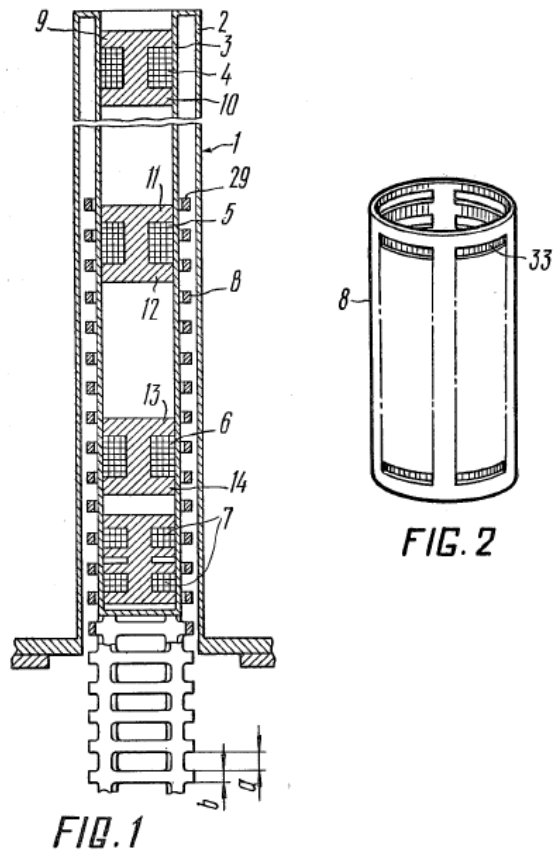


Figure 25 Position sensor of linearity moving bodies [13]

2.2.13 Control Rod Position Indication System

This particular sensing technique relies on a dual sensor system which detects either a magnetic material or a non-magnetic material. The sensors are aligned with an offset to one another, which enables the magnetically-induced output signal to vary as the object being detected moves. The moving object within the sensors requires a grooved housing with magnetic and non-magnetic layers of material, as illustrated in Figure 26. The sensor location is not suitable for use within our system, as the sensor is located on the outer perimeter of the object being detected. In addition, the sensors rely on electronic memory to store historical occurrence of pulse counts. This would not be suitable for the Rolls-

Royce safety case as our sensor must provide a continuous real-time reading of position without the use of electronic memory.

March 14, 1972

D. R. BARTON

3,649,450

CONTROL ROD POSITION INDICATION SYSTEM

Filed March 4, 1970

2 Sheets-Sheet 1

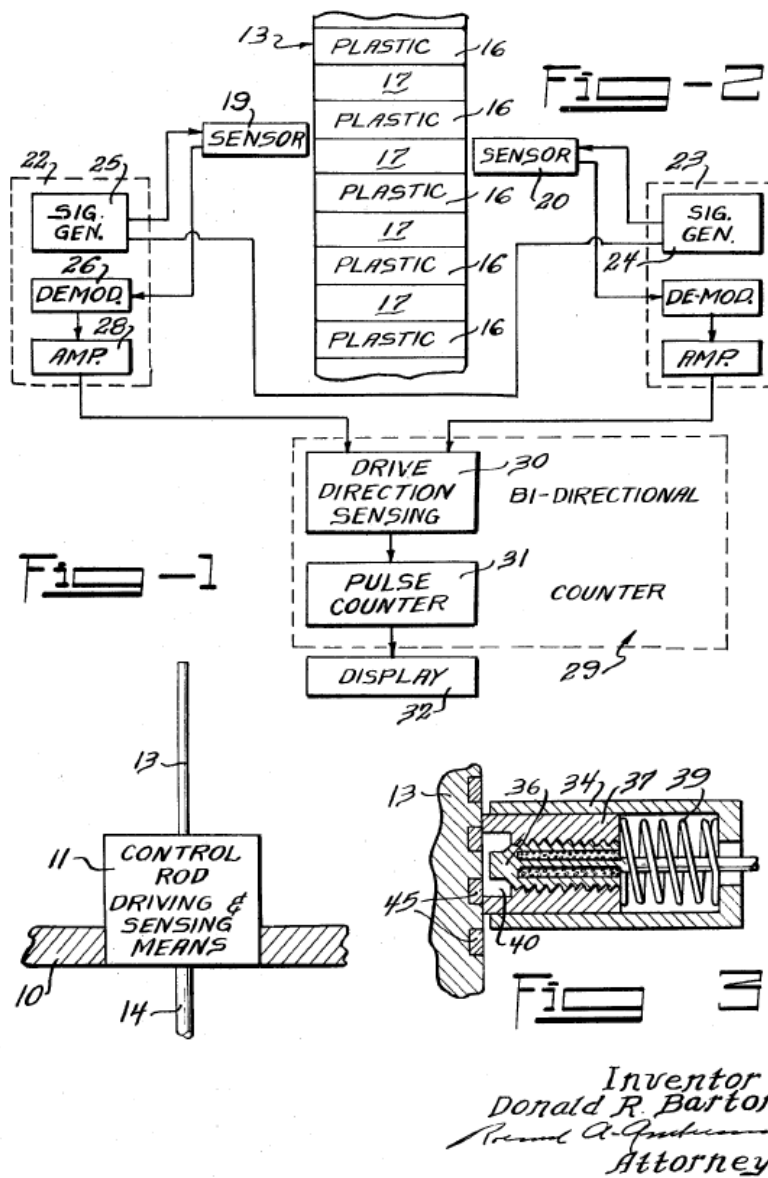


Figure 26 Control rod position indication system [14]

2.2.14 Nuclear Reactor Control Rod Drive with Rod Position Indicating Means

This particular novel sensing method comprises a tube housing a beaded chain. A magnet is located within the lower piston of the driveshaft bearing. The beaded chain is attracted to the magnet as illustrated in Figure 27. The beads are connected to a pair of resistance coils which change resistance as the piston moves. The beaded chain magnet

attraction causes an electrical circuit to be formed, which can then be detected. This sensor requires a means of adding a magnet to the moving driveshaft and a means of supporting the bead chain. Although this sensor is very reliable and simple from an electronic detection circuit perspective, it is not deemed suitable or practical for use given our vibration and shock operation requirements.

May 22, 1973

C. C. RIPLEY
 NUCLEAR REACTOR CONTROL ROD DRIVE WITH ROD
 POSITION INDICATING MEANS

3,734,824

Filed April 14, 1969

4 Sheets-Sheet 4

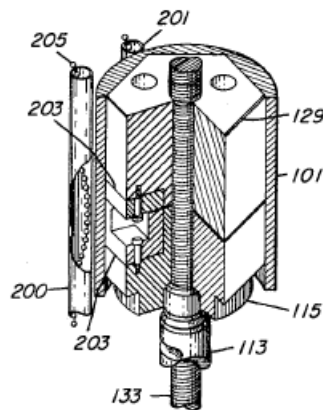


Fig. 6

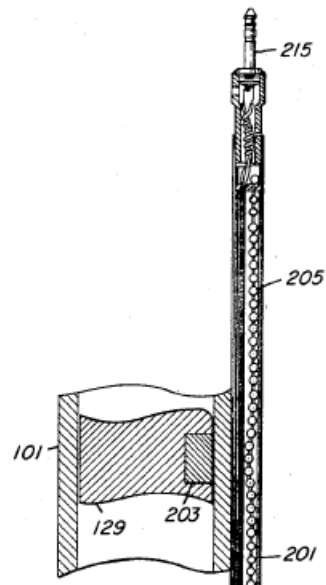


Fig. 7

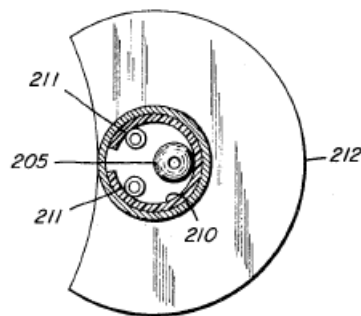


Fig. 8

Figure 27 Nuclear reactor control rod drive with rod position indicating means [15]

2.2.15 Phase Encoded Digital Position Probe Assembly

An array of differential transformers is connected so they generate a phase-encoded signal, dependent upon the position of a piece of permeable magnetic material. The sensor is formed from a primary source winding and four arrays of secondary windings placed along the length to be measured. The arrangement is illustrated in Figure 28. As the driveshaft position changes, the output from each array will generate a binary grey code. This principle is adaptable to our application as it will fit into our space envelope and it can detect the driveshaft as it envelops the probe tube. However, the fundamental disadvantage of this sensor is that the resolution of the output is determined by the number of discrete binary states that can be produced. This, in turn, is governed by the size of the coils used. The example shown in Figure 28 has a resolution of 16 positions. An alternative secondary coil combination is also shown, where a single coil is wound in individual bobbins giving an opposite magnetic field to one another. This configuration has the advantage of reflecting the magnetic field towards the driveshaft due to opposing magnetic fields repelling and increasing the output signal sensitivity. However, using this method results in the sensor having a flat non-responsive region, limiting the accuracy that can be achieved.

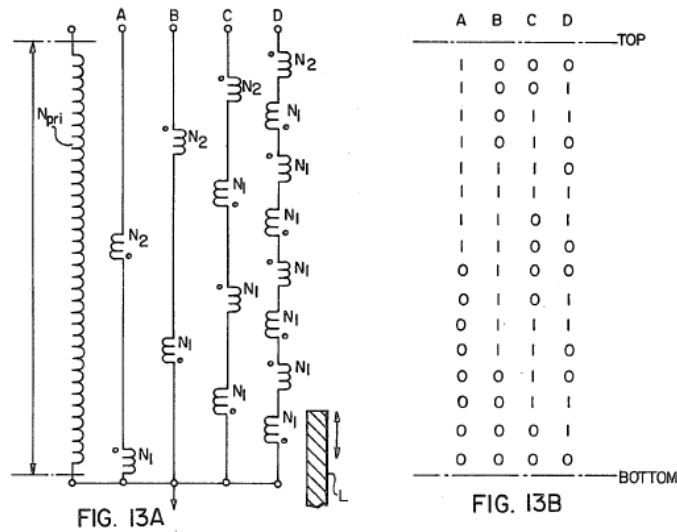
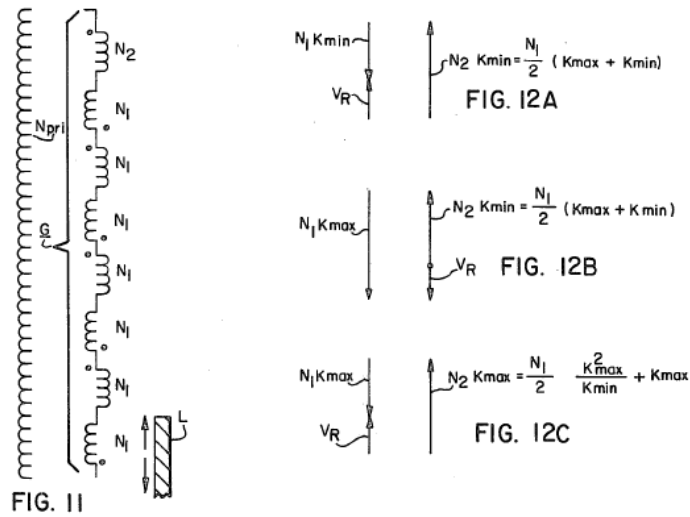


Figure 28 Phase encoded digital position probe assembly [16]

2.2.16 Position Indicator

This particular configuration of sensor relies on an electro-mechanical actuation system. It comprises two coaxial mating cavities forming a casing section. One of the coaxial mating cavities is connected to the control rod, and the other is connected to a Linear Differential Transformer (LDT) armature. The LDT is arranged such that the output voltage signal is nullified when the armature is in the centre of the winding, as illustrated in Figure 29. As the armature moves, the two output voltages of the LDT change in magnitude: one output will increase while the other output will decrease. The difference between the two outputs

constitutes the output signal. This system has the advantage of having a sensitive output voltage. However, changes would be required to the Control Rod Drive Mechanism design which would not be deemed practical in our application.

Jan. 27, 1970

J. C. SINGLETON ET AL

3,492,616

POSITION INDICATOR

Filed Sept. 15, 1966

2 Sheets-Sheet 1

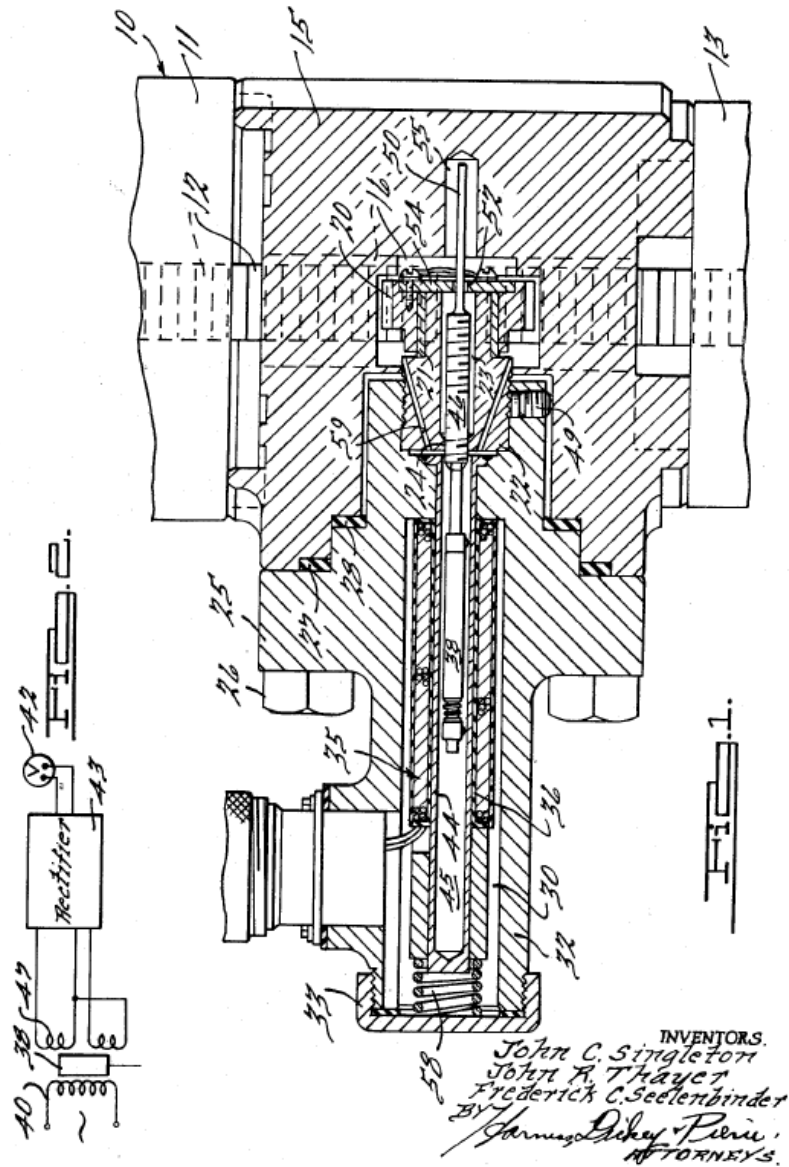


Figure 29 Position Indicator [17]

2.3 Non Electromagnetic Sensors

2.3.1 Magnetostrictive Position Indicator

This sensor uses a magnetic field generator mounted on a moveable object. An elongated ferromagnetic bar or member is positioned adjacent and parallel to the path of movement of the object. The magnetic field will produce a change in the Young's Modulus of Elasticity in an adjacent region of the bar, thus reflecting any strain pulses sent along its length. The time taken is then compared to a given reference which determines the position of the magnetic field generator along the elongated ferromagnetic bar. The position of the driveshaft can be measured without physical contact using this technique. This technique enables the sensor to be housed in a primary containment, such as a probe tube, and still detect the linear position of the moveable object. However, the source of the magnetic field is required to be attached to the moving object. This sensor would have to be manufactured as part of the CRDM driveshaft, and this is deemed neither practical nor cost effective for our reactor design. The principle of operation of this sensor is illustrated in Figure 30. Use of this sensor principle is worth considering, should the driveshaft be designed with a magnetic field source as explained above.

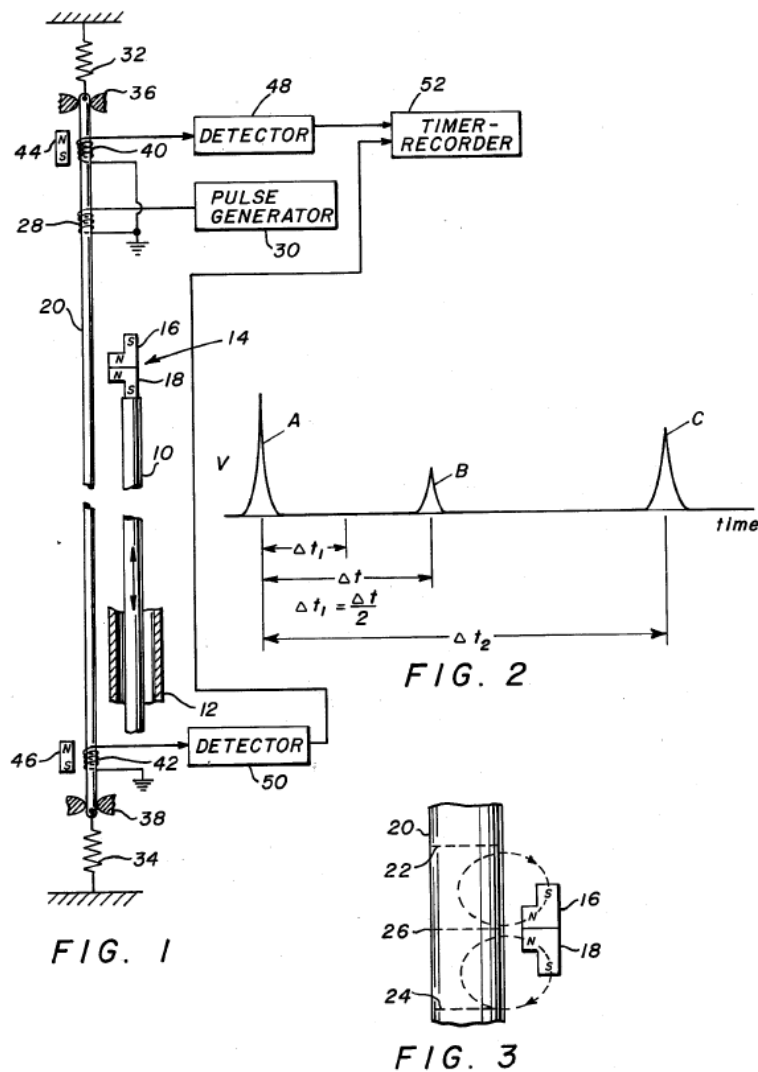


Figure 30 Magnetostrictive position indicator [18]

2.3.2 Linear Sensor Using a Strain Gauge

This concept uses a strain gauge as a transducer to detect linear position. The sensor housing includes a ramp shaped actuator which is attached to the object being measured. The actuator applies a strain to the strain gauge as the object is moved. The strain gauge converts the strain into an electrical signal that is proportional to the objects position. Figure 31 shows a housing with a strain gauge and actuator arrangement. It is clear to see from the mechanical construction that this principle could not be used in a nuclear reactor as many primary containment penetrations would be required.

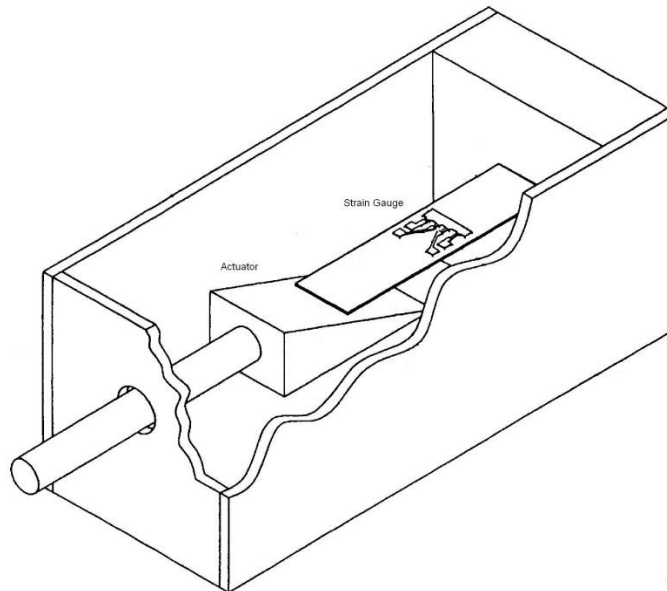


Figure 31 Linear position sensor using a strain gauge [18]

2.3.3 Position Indicator

This sensor can detect any moveable object within the reactor, providing there is a line of sight to the object. Light is radiated from an external source outside the reactor pressure vessel onto a prism which is aligned to the object being detected. The light is then re-directed by the prism onto an array of sensors. The amount of light being reflected is a measure of the object being displaced. A typical arrangement is illustrated in Figure 32. This method of measurement is very accurate and can be adapted to any mechanical moving object; however, it requires an optical window into the pressure vessel. A separate work package could be considered for sapphire windows within the reactor, which would allow this method to be utilised. Currently this solution is not considered as practical for our application.

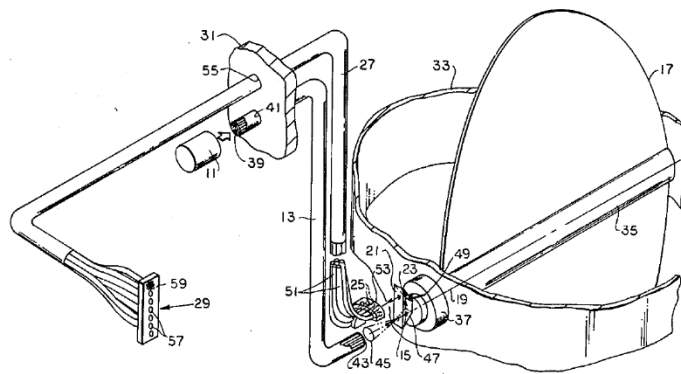


Figure 32 Position indicator [20]

2.3.4 Ultrasonic Position Indicator System

Ultrasonic sensing is used for many applications, including position detection. It measures the time of flight of a pulse between a fixed point and an object at an unknown distance. If the velocity of the pulse is known, the distance of the object can be determined. A typical electronic system for a ultrasonic sensor is shown in Figure 33. The advantage of ultrasonic technology is that it can penetrate metallic barriers. This is fundamental to our requirements. In addition, the sensor can be calibrated to give high measurement accuracies. This method would suit our application, especially for detecting metallic objects such as the driveshaft. The disadvantage of this technology is the complexity in the electronic instrumentation required to produce and detect the ultrasonic pulse. As a result ultrasonic technology is deemed too complex for use within a high-integrity safety system, such as a system for detecting the position of a reactor control rod.

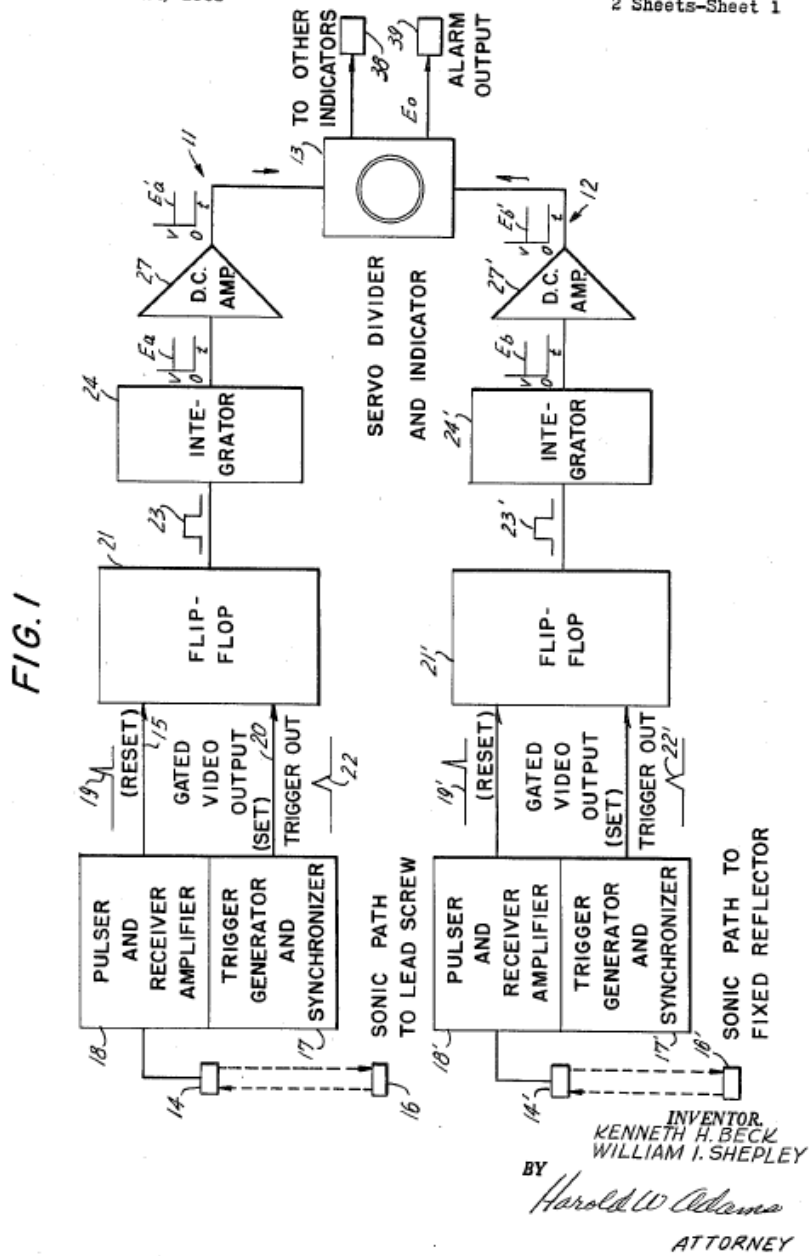


Figure 33 Ultrasonic Position Indicator System [21]

Chapter 3

3 Future Rod Position Sensing Technologies

This following section investigates the use of potential technologies which can be adopted to our application and developed into a practical solution. Each potential solution is explained with the advantages and disadvantages associated with the design and how it is rated against the technology readiness level criteria. Each solution is also considered from a cost perspective and the ability to interface with the mechanical parts and the electrical instrumentation card complexity required to operate the solution.

3.1 General Sensing Techniques

The appropriate rod position technique for use in a given application is determined by application suitability, cost and operating environment. The most common solutions and types of rod position techniques which could be used within the Control Rod Drive Mechanism (CRDM) space envelope are referred to within Figure 34.

Magneto-resistance
Reed Switches
Modified Transformer
Transformer

Inductive
Magnetostrictive
Ultrasonic
Resonant Puck
Hall Effect

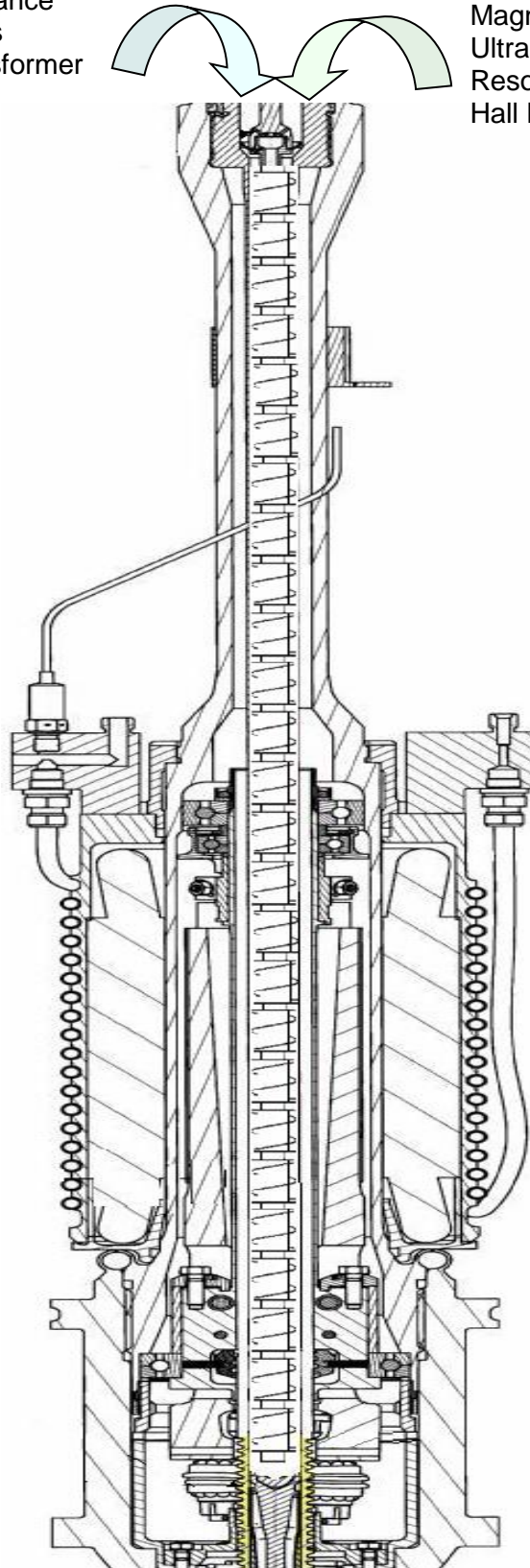


Figure 34 Rod Position Techniques

Figure 34 illustrates a sensor housed by the probe tube and CRDM containment boundary. The rod position sensor will be inserted into a welded probe tube and be at ambient pressure and temperature, and sealed with a rubber o-ring to prevent reactor compartment environment ingress.

The sensors that are suitable for this type of environment will be capable of sensing the driveshaft through air, probe tube material and water primary barrier.

The following section refers to the Technology readiness level (TRL) of a sensor. The TRL is an estimate of technology readiness and confidence of the product for use. A scale of 1 (Scientific research begins translation to applied R&D) to 9 (Actual application of technology is in its final form) is usually used to determine where the technology readiness is at any particular phase within a development program. The TRL method enables different technologies and concepts to be assessed against each other to meet the project requirements. This is a widely known and used methodology within all different types of industries. A TRL tool was developed to help identify the correct TRL level for the TIRPI as the technology used has a proven history of use however the method of technology used is novel and requires assessment for reassurance before development and use. Figure 35 shows a blank assessment window of the tool and Appendix 20 shows the criteria used to carry out an assessment.

Using TRLs to Control Risk of Technology Transition		Technology Readiness Level Calculator For the NPCT workstreams									
		Assumptions Made Prior to TRL Analysis: TRL A - Initial Assessment									
		Main background documents for this analysis <input type="checkbox"/> TRL A White Paper April 6, 1995 John C. Mankins Advanced Concepts Office, Office of Space Access and Technology, NASA <input type="checkbox"/> TECHNOLOGY READINESS LEVELS (TRLs) GUIDANCE, ISSUE 3.0 - Rolls-Royce		Risk Level	TRL 1	TRL 2	TRL 3	TRL 4	TRL 5	TRL 6	TRL 7
		Low									
		Medium									
		High									
		Result	FAIL	FAIL	FAIL	FAIL	FAIL	FAIL	FAIL	FAIL	FAIL
Title of Assessment											
Date of Assessment											
Mandatory Stakeholders											
Sensor Lead		<input type="checkbox"/> Signoff Complete									
Signoff Authority		<input type="checkbox"/> Signoff Complete									
Stakeholders											
Stake 1											
Stake 2											
CLASSIFICATION - NOT PROTECTIVELY MARKED											

Figure 35 TRL assessment tool

3.2 Inductance

Currently a typical solution to measure the rod position is by measuring the number of the control rod drive mechanism revolutions (hence giving an inferred measurement of the rod position) and taking an inductive sensor reading. The changing inductance and signal phase of the control rod drive motor is used to derive the rod position indication.

A constant-current sine wave drive is applied to the sensor by means of an analogue switch, and the voltage across the series combination of switch and transducer is sampled and digitised. The method accomplishes phase-sensitive detection of the output signal by measuring the average value in each of 4 time periods corresponding to quadrants of the excitation sinusoid. If the measured voltages are V_1 to V_4 for the 4 quadrants, the average voltage across the total resistive component (switch plus wiring plus transducer) is $V_1+V_2-V_3-V_4$, while the quadrature component, dominated by transducer inductance, is $V_1-V_2-V_3+V_4$. The system configuration is shown in Figure 36.

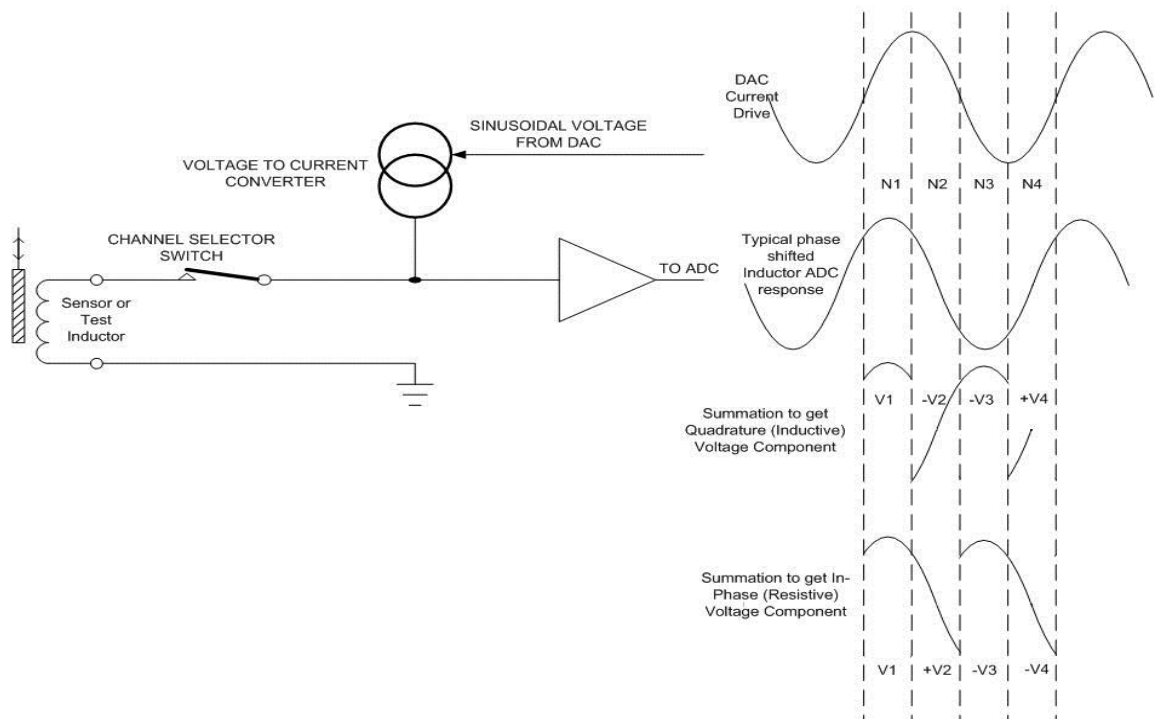


Figure 36 Inductive electrical topology concept

The sensor configuration is a number of inductive coils arranged in a serial connection to produce discrete inductive steps. The coils are arranged around a central former.

The inductive sensor measures linear position of the control rod as the rod is raised or lowered, with the associated driveshaft passing over the probe tube either revealing or enveloping the sensor, affecting the inductance of the coil. This is shown in Figure 37.

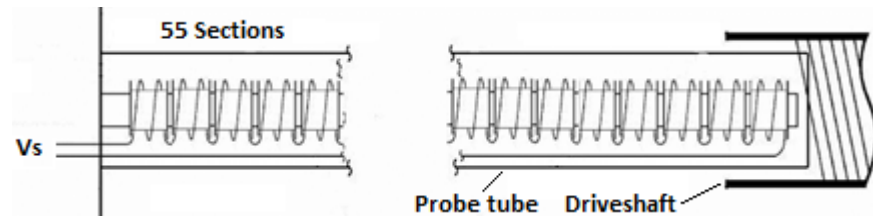


Figure 37 Inductive Concept

The actual relationship between rod position and sensor inductance is fundamentally linear, but with a superimposed ripple due to the sensor coil being wound in discrete sections. Deviations from the 'ideal' driveshaft and probe geometries (and any magnetic non-uniformity) will introduce further linearity errors, some of which will be systematic to a particular driveshaft material.

3.2.1 Inductance advantages

Technology readiness level - The Technology readiness level for the inductance probe is nine. This is a proven and tested technology and is used on current fleet boats. There will be no requirement for additional qualification of the sensor.

Sensor cost – This technology has a low component cost as inductive rods have been used commercially and are readily available.

Reliability –The sensor technology relies on magnetic flux to change the inductance characteristics of the probe, with no mechanical moving parts within the sensor. This makes the sensor very reliable.

Development costs – Only minimal sensor development costs are required as the sensor has pedigree of use.

3.2.2 Inductance disadvantages

Production costs – Currently a specialised manufacturer is required to produce the inductive sensor. The construction of the inductive sensor is difficult and requires specialised manufacturing process.

Transducer complexity – Currently the instrumentation associated with the inductance sensor has low accuracy and suffers from regions where it cannot detect motion of the driveshaft.

3.2.3 Submarine specific advantages

Interface cabling – Only requires two electrical connections per sensor, as the same cable applies the source and sense signal. This reduces cable size, connector size and the potential for electrical connection faults.

3.2.4 Submarine specific disadvantages

Accuracy – Currently has a low accuracy capability within current class boats, which is limited by the instrumentation design for detecting the signal.

Size – Inductance bobbins require a robust core the same length as the probe tube. This will result in space constraints affecting the location and removal of the sensor as the long probe cannot be flexible.

Low insulation resistance – Possible failure due to low insulation resistance of inductance sensing technology as moisture ingress can change the inductance reading. An 'O' ring is used to provide a primary containment barrier against the reactor compartment environment.

Calibration – Due to variation of the signal output amplitude as a result of temperature change of sensors, the resistive component is used to provide temperature compensation for the output signal.

3.3 Transformer principle

The transformer employs the principle of magnetic coupling via a common magnetic path where the distance between the primary and secondary coils can affect the strength of the coupling. The operation of a transformer-based sensor uses this principle.

A transformer contained within the probe tube monitors the position of the control rod as the rod is raised or lowered and the associated driveshaft passes over the probe tube, changing the flux linkage of the individual bobbins shown in Figure 38. The induced signal in the secondary winding represents the driveshaft linear position.

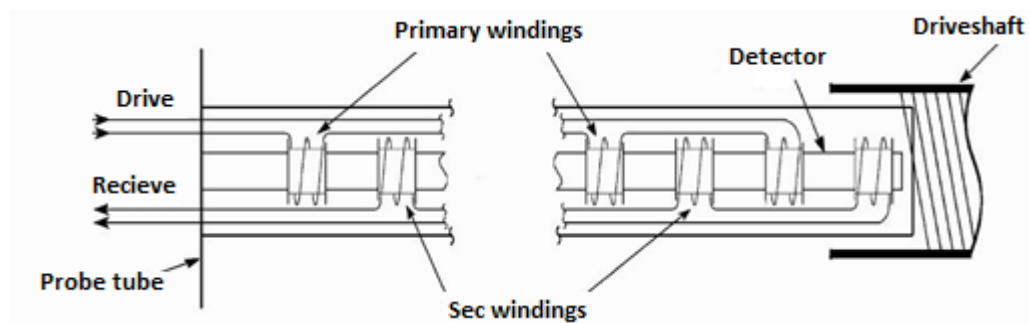


Figure 38 Transformer Concept

Temperature compensation of the sensor is achieved through measurement of the voltage drop across the primary winding when a constant current is applied to the primary coils. Each winding is made up of multiple sections wound on an array of bobbins. These bobbins are evenly spaced on a metallic core at even spaced intervals throughout the length of the core former. The primary bobbin windings are electrically connected in series and are physically interleaved with the secondary bobbin windings, which are also electrically connected in series.

The sensor is mounted inside the probe tube, which is a hollow non-magnetic cylinder closed at the bottom and functioning as the primary containment boundary. The probe tube is totally enclosed by the driveshaft when the control rod within the reactor is withdrawn.

3.3.1 Transformer advantages

Technology readiness level - The Technology readiness level for the transformer is nine. This is a proven and tested technology. There will be minimal requirement for additional qualification of the sensor.

Sensor cost – This technology has a low component cost as transformer components and are readily available commercially.

Reliability –The sensor technology relies on magnetic flux to change the induced voltage of the sensor. There are no mechanical moving parts within the sensor. This makes the sensor very reliable.

Development costs –This solution is currently in use and will be viable to be manufactured.

3.3.2 Submarine specific advantages

Track record – The submarine has experience of using the transformer sensor, and it has proven to be extremely reliable and robust.

Accuracy – The transformer sensor has a potential to achieve high accuracy capability.

3.3.3 Submarine specific disadvantages

Size – The transformer design requires a robust core centre shaft to support the transformer bobbins. This shaft must be approximately the same length as the primary containment probe tube. This will require space above the reactor for installing and removing the sensor for maintenance.

Calibration – The transformer principle is based on the ability to induce a voltage signal from a primary source coil to a secondary sense coil. Both coils have a resistive component which is affected by temperature. Compensation for temperature effects is achieved by calibrating each sensor over its operating temperature band and zeroing the thermal effect within the software algorithm of the instrumentation card.

Interface cabling – The transformer induction principle requires four electrical connections per sensor. This increases the cable size, connector size and potential for electrical connection faults.

3.4 Modified Transformer

The current transformer technology can be used within a modified housing which gives a greater coupling surface area. The change to the housing requires hollow bobbins and a pierced hollow tubing to accommodate an additional driveshaft inner rod inserted into the core of the transformer sensor.

Each winding is made up of multiple sections wound on bobbins that are evenly spaced. The primary bobbin windings are electrically connected in series and are physically interleaved with the secondary bobbin windings, which are also electrically connected in series. The driveshaft will be modified with a magnetic inner-core. The magnetic inner-core could produce better magnetic coupling of the flux density as the maximum flux is produced at the center of a primary and secondary windings core. An illustration of the concept design is shown in Figure 39

The winding will be held together by the pierced hollow tubing which can be placed onto the “pip” shown on Figure 39. The pip will provide mechanical strength and alignment for the sensor windings, and could also be part of the primary containment barrier.

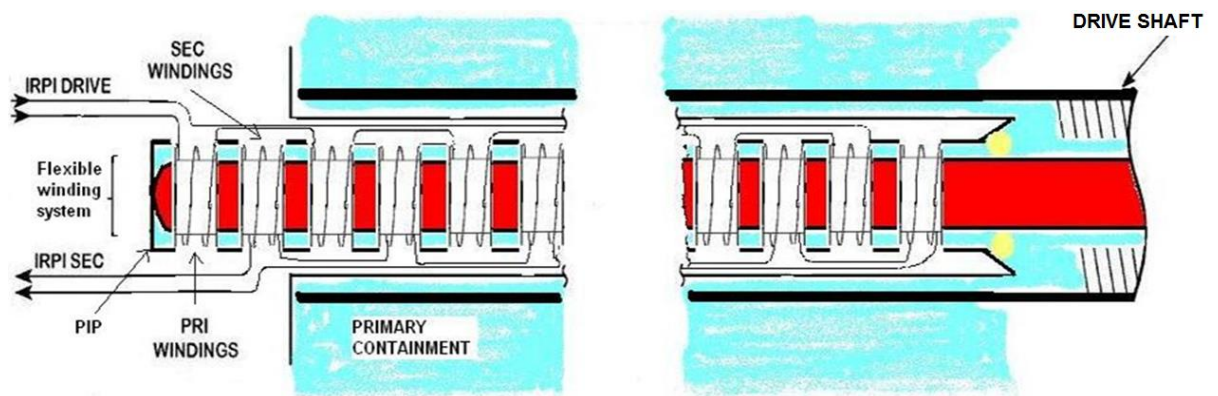


Figure 39 Modified Transformer Concept

3.4.1 Modified transformer advantages

Technology readiness level of Sensor - The Technology readiness level for the transformer is nine. This is a proven and tested technology. There will be minimal requirement for additional qualification of the sensor however the driveshaft design will be novel.

Cost of sensor – This technology has a low component cost as transformers are readily commercially available.

Reliability of sensor–The sensor technology relies on magnetic flux to change the voltage induced in the probe. There are no mechanical moving parts within the sensor making the sensor very reliable.

Accuracy – The modified probe tube, driveshaft and sensor will enable the driveshaft inner rod to penetrate within the core of the coil assembly, providing a better flux absorber and hence increasing the secondary signal output sensitivity.

3.4.2 Modified transformer disadvantages

Technology readiness level of modified probe tube and driveshaft- The Technology readiness level of the modified probe tube and driveshaft is very low. These items are still at the theoretical concept stage and require evaluation.

Development costs of probe tube and driveshaft –The probe tube is a lengthy, relatively thin component and will require very accurate machinery to manufacture. The driveshaft will require a centralised rod to be inserted with very tight tolerances to ensure no mechanical failure during operation such as bending or distortion. Any failure could have a safety implication and the risk of failure needs to be quantified.

Production costs –The production capability for the transformer sensor has been proven. However, the probe tube and driveshaft will be expensive to produce as it differs in design from the existing concept and manufacturing will be difficult.

Instrumentation complexity – Currently the operation of the instrumentation Generic Interface Card (GIC) is feasible. This will need to be accepted by the nuclear regulator before use.

3.4.3 Submarine specific advantages

Track record – The submarine programme is currently using the transformer sensor principle, and it has proven to be extremely reliable and robust.

Accuracy – The signal strength of the modified transformer would increase using the modified transformer principle resulting in a system with better noise immunity of the system.

3.4.4 Submarine specific disadvantages

Size – The transformer design requires a robust core center shaft to support the transformer bobbins. This shaft must be approximately the same length as the primary containment probe tube. This will require space above the reactor for installing and removing the sensor for maintenance.

Calibration – The transformer principle of operation relies on ability to induce a voltage signal between a primary source coil and a secondary sense coil. Both coils have a resistive component which is affected by temperature. Compensation for temperature is achieved by calibrating each sensor over the operational temperature band and zeroing the thermal effect within the software algorithm of the instrumentation card.

Interface cabling – The transformer induction principle requires four electrical connections per sensor. These increase the cable size, connector size and potential for electrical connection faults.

3.4.5 Mechanical analyses of the modified transformer principle

Currently the transformer design concept lends itself to a relatively small output signal throughout rod position length. Typically, the output signal has a magnitude of less than 20mV over the range. The sensitivity of the output signal can be improved by increasing the flux coupling within the centre of the coils.

This principle, although ideal electrically, needs mechanical analysis for potential driveshaft buckling when being used and when a scram condition is initiated.

The analysis of the mechanical concept of changing the driveshaft design to maximise the sensitivity of the transformer electrical signal concluded that it is not viable as the scram condition could be compromised. The modified transformer principle will not be considered for further evaluation as this option is not viable.

3.5 Reed Switches

The reed switching principle relies on the driveshaft magnetic ring field to mechanically change the position of an electrical contact.

As the driveshaft passes over the reed switches, the reed switches close, an electrical short circuit is caused and a new electrical circuit configuration is achieved.

The switching arrangement of the reed switches is designed to output different circuit resistance values to the electrical circuit via the resistive components. The change in resistance causes the voltage output signal reading to change and reflect the position of the Ball screw. See Figure 40.

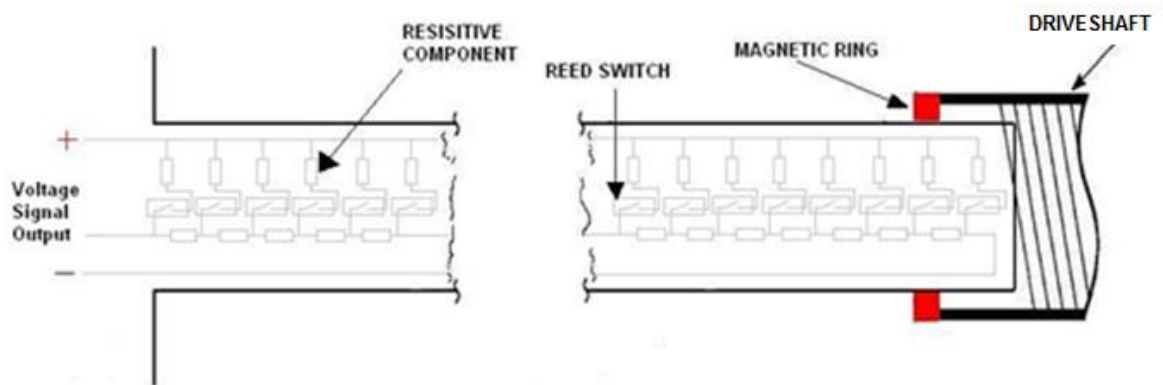


Figure 40 Reed switches concept

3.5.1 Reed switches advantages

Technology readiness level of sensor - The Technology readiness level for the reed switches is nine. This is a proven and tested technology and will only require minimal requirements for additional qualification of the sensor.

Cost of sensor – This technology has a low component cost as reed switches have been used commercially and are readily available.

Instrumentation complexity – This solution requires very simple instrumentation to detect the signal as the resistance is proportional to the control rod position and the voltage read is proportional to resistance, providing the source is a constant current.

3.5.2 Reed switches disadvantages

Moving parts – Every reed switch is a moving part and has the potential to mechanically fail. There are many reed switches within the sensor.

Development costs –Currently the reed switch sensor can be manufactured with a proven record of use.

3.5.3 Submarine specific advantages

Track record – Current programmes have used the reed switch sensor.

Interface cabling – Only two electrical connections are required per sensor as the same cables are used to connect the source to the sensor and to sense the position of the rod. This reduces cable size, connector size and the potential for electrical connection faults.

3.5.4 Submarine specific disadvantages

Driveshaft modification–The driveshaft will require a magnetic ring to energise the reed switches. The magnetic properties of the magnetic ring could be affected by the Control Rod Drive Mechanism (CRDM) and lead to sensor errors.

Accuracy – The accuracy of the sensor is determined by the number of switches that can be fitted within the limited space constraints of the probe tube.

Size – The reed switches design requires a robust core centre shaft to support the individual switches and resistances. This must be approximately the same length as the primary containment probe tube. This will require space above the reactor for installing and removing the sensor for maintenance.

Position calibration – The reed switches will need to be calibrated for the position of the driveshaft, preferably with every reed switch individually energised to ensure its operation and maximum accuracy capability.

Temperature compensation – The effect of temperature on the overall resistance and voltage of the sensor will require compensation. This is a long process as each reed switch resistance value at the selected operating temperature will need to be stored within the instrumentation card.

3.6 Magnetostrictive principle

The magnetostrictive principle is based on changes in the size and shape of a material when it is placed in a magnetic field.

Rearranging the alignment of magnetic dipoles in a material causes changes to occur within the material. Normally these dipoles are arranged in a random pattern within a non energised material. If the material is exposed to a magnetic field, the dipoles re-arrange themselves in a uniform pattern, causing the material to lengthen and thin out.

When the magnetic field is removed, the dipoles return to their original position causing an ultrasonic sound wave in the process.

A transducer can be used to detect the ultrasonic sound wave via a detector rod. The measured time of flight can be calculated to indicate the position of the rod illustrated on Figure 41.

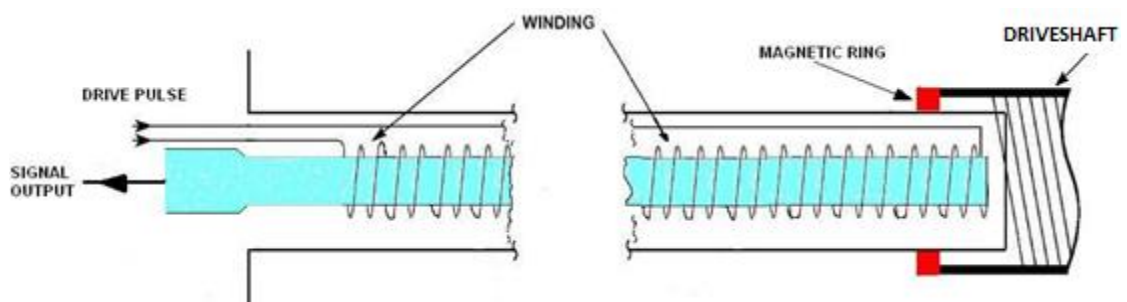


Figure 41 Magnetostrictive Concept

3.6.1 Magnetostrictive advantages

Technology readiness level of sensor - The Technology readiness level for the transformer is nine. This is a proven and tested technology. There will be only minimal requirements for additional qualification of the sensor.

3.6.2 Magnetostrictive disadvantages

Instrumentation complexity – This solution requires very complex instrumentation to detect the signal. The technology relies on detection of ultrasonic waves and a drive pulse source signal to energise the coil of the sensor.

Cost of sensor – This technology has very high component costs as there are three primary components to the sensor: the drive pulse transmitter, ultrasonic wave detector and the magnetic ring on the driveshaft.

Reliability –The sensor technology relies on electrical and magnetic principles, and has no mechanical moving parts. This makes the sensor very reliable.

Development costs –Currently there is the capability to manufacture the magnetostrictive sensors, and it is currently being considered for use within third party submarines.

Production costs –Currently production capability for the magnetostrictive sensor is proven. However, the driveshaft will be expensive to produce as this will be a new design and require qualification.

3.6.3 Submarine specific advantages

Track record – There is known use of the magneto-strictive sensors used within naval vessels.

Temperature calibration – Temperature change will not affect the sensor as the system topology is driven by a drive pulse and ultrasonic wave time calculation. The material thermal characteristics of the core will have a negligible effect on the time of flight for the ultrasonic wave.

3.6.4 Submarine specific disadvantages

Interface cabling – The magnetostrictive principle requires four electrical connections per sensor. This increases the cable size, connector size and the potential for electrical connection faults.

Driveshaft modification–The driveshaft will require a magnetic ring. The magnetic properties of the magnetic ring could be affected by the Control Rod drive Mechanism (CRDM) and results in sensor errors.

Accuracy – The accuracy capability of the magnetostrictive sensor is very high as this is determined by the position of the magnetic ring.

Size – The coil former of the sensor requires a robust core to support the pulse coil. This must be approximately the same length as the primary containment probe tube. This will require space above the reactor for installation and removing the sensor for maintenance.

Position calibration – The magnetostrictive technique will require a calibration of the driveshaft position relative to the magnetic ring position. This needs to be done at only a few selected positions as the detected signal will have a linear response that can be calculated within the software of the instrumentation card to derive a total rod position length.

3.7 Ultrasonic

Ultrasonic ranging and detection devices use high-frequency sound waves to detect the presence of an object and its distance from the sensor. The systems either measure the echo reflection of the sound from objects or detect the interruption of the sound beam as the objects pass between the transmitter and receiver.

A transmitter sends out a pulse of sound that is detected by a receiver. In this application, ultrasonic energy from the transmitter is reflected by the end of the probe tube and the echo is detected. This system measures the elapsed time from when the sound pulse is transmitted to when the echo is detected to determine the exact range of the object from the transducers. The transducer illustrated in Figure 42 sends and receive an ultrasonic signal. The nature of the surface the ultrasonic signal is reflected from introduces a significant difference in the received signal signature.

In this application the driveshaft overlapping the ultrasonic signal path will cause a change in the signal characteristics. The signal signature can be processed and converted into a driveshaft location.

A narrow ultrasonic beam will not detect unwanted objects that are not in the insonified path of the transducer ("insonify" means to fill a specific volume with sound from a transducer). A narrow ultrasonic beam is also less susceptible to background ultrasonic noise, and the systems will also operate over a greater range.

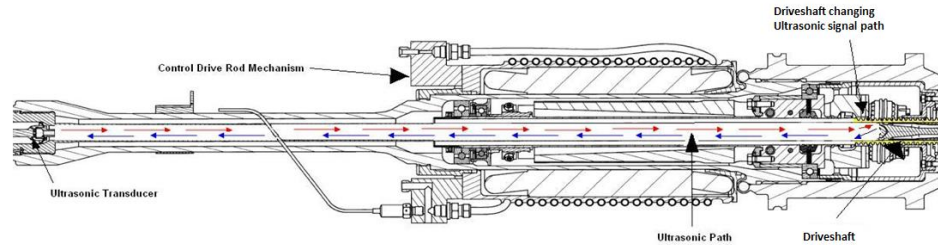


Figure 42 Ultrasonic Concept

3.7.1 Ultrasonic disadvantages

Cost of sensor –There is a very high probability that the sensor will require major design changes to meet the radiation requirements of its operating environment.

Instrumentation complexity – This solution requires very complex instrumentation to detect a signal, as the technology relies on detection of ultrasonic waves to identify signal signatures at different rod positions.

Technology readiness level of Sensor - The Technology readiness level for the ultrasonic sensor is less than five. Although this sensor is used widely within the commercial market it will need to be qualified for use in the submarine radiation environment. Selecting appropriate materials to in the design of use the ultrasonic concept will prove to be difficult as the probe tube provides a primary containment barrier.

Reliability –The sensor technology relies on measuring the time of flight of an ultrasonic signal. This technology has not been proven within this application and has a potential to be unreliable.

Development costs –The sensor will require very high development costs as the sensing principle is very complex and requires significant qualification.

Production costs – The Production costs for this sensor will be very high as a bespoke design with new radiation hard materials will be required for our application.

3.7.2 Submarine specific advantages

Temperature calibration – Temperature will not affect the sensor as the system topology is driven by an ultrasonic wave signature calculation.

Size – The ultrasonic sensor is very small and does not require a large space above the reactor for installation and maintenance.

3.7.3 Submarine specific disadvantages

Interface cabling – The ultrasonic sensor requires four electrical connections per sensor. This increases the cable size, connector size and the potential for electrical connection faults.

Accuracy – The accuracy capability of ultrasonic sensor could be very high, providing it is possible to get a repeatable signal when the rod is stationary.

Position calibration – Use of the ultrasonic technique will require the position of the driveshaft to be calibrated relative to the ultrasonic signature of the signal. This requires a lengthy calibration period as the driveshaft calibration increments need to be less than 0.5 % FS to ensure an operational capability of 1%FS.

Probe tube environment effects – Ultrasonic waves can be affected by air bubbles and vapours. During the first time filling of the Reactor Pressure Vessel with water, the rod position indication system could display erroneous position values. Additional means of confirming the rod position could be required.

3.8 Radar

Radar uses high-frequency microwaves to detect the presence of an object and its distance from the sensor. The system measures the echo reflection from objects.

A transmitter sends out a microwave pulse that is detected by a receiver. In this application, energy from the transmitter is reflected by the end of the probe tube and the echo is detected. This system measures the elapsed time from when the microwave pulse is transmitted to when the echo is detected to determine the exact range of the object from the transducers. The transducer, as illustrated in Figure 43, can be used to send and receive a signal. The nature of the surface the signal is reflected from introduces a significant difference in the received signal's signature.

In this application the driveshaft overlapping the microwave path will cause a change in the signal characteristics. The signal signature can be processed and converted into driveshaft location.

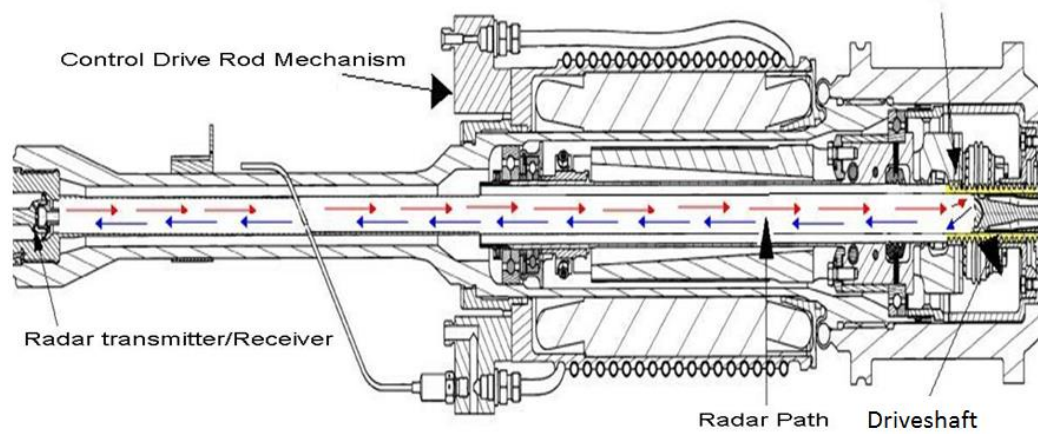


Figure 43 Radar Concept

3.8.1 Radar disadvantages

Technology readiness level of sensor - The Technology readiness level for the radar sensor is less than five. Although this sensing technique is used widely within the commercial market, the sensor used will need to be qualified for the submarine radiation environment. Selecting appropriate materials to use in the design of the radar concept will prove to be difficult as the probe tube provides a primary containment barrier.

Cost of sensor –There is a very high probability that the sensor will require major design changes due to the radiation requirements of its operating environment.

Instrumentation complexity – As the technology relies on detection of radar waves to identify signal signatures for different rod positions this solution requires very complex instrumentation to detect the signal.

Reliability –The sensor technology relies on a principle that has no previous use within this application and could be unreliable in practice.

Development costs –The sensor will require very high development costs as the sensing principle is very complex and will require significant effort to qualify its use.

Production costs – The Production costs for this sensor will be very high as a bespoke design with new radiation-hard materials will be required for our application.

3.8.2 Submarine specific advantages

Temperature calibration – Temperature will not affect the sensor as the system topology is determined by a radar wave signature.

Size – The radar sensor is very small and does not require a large space above the reactor for installation and maintenance.

Probe tube environment effects – Radar waves will not be affected by any air bubbles or vapours that may be present in the Reactor Pressure Vessel (RPV).

3.8.3 Submarine specific disadvantages

Interface Cabling – The radar sensor requires four electrical connections per sensor. This increases the cable size, connector size and the potential for electrical connection faults.

Accuracy – The accuracy capability of radar sensor could be very high, providing it is possible to get a repeatable signal when the rod is stationary.

Position Calibration – The radar technique will require the position of the driveshaft to be calibrated relative to the radar signature of the signal. This requires a lengthy calibration period as the driveshaft calibration increments need to be less than 0.5 % FS to ensure an operational capability of 1%FS.

3.9 Resonant Pucks

This principle is based on the mutual inductance between a transmission aerial constructed on a printed circuit board (PCB) and a detector constructed on a moveable rod known as a “puck”.

A set of transmitters are placed on the PCB, each capable of producing an alternating magnetic field. When the puck is within the electro-magnetic field, a current flow is induced in the pucks, which produce an electro-magnetic field. The puck’s electromagnetic is detected by the receiver on the PCB shown in Figure 44. The signal from the transmitters is emitted at a frequency of approx. 1 to 3 MHz.

The transmitter and receiver circuits are placed on the same PCB, but are electrically isolated. The puck has an inductance coil and capacitor arrangement and can detect positions from distances of 1mm to 10m.

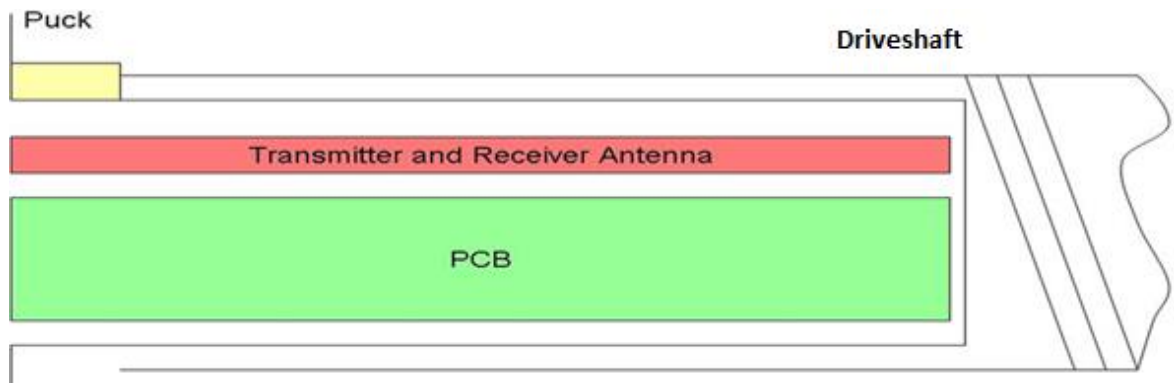


Figure 44 Resonant Puck Concept

3.9.1 Resonant puck advantages

Production costs – The cost for production will be small as the circuits can be etched onto a PCB and easily reproducible.

3.9.2 Resonant puck disadvantages

Cost of sensor – This technology has very high component costs as there are three primary components to the sensor: the drive pulse transmitter, ultrasonic wave detector and the magnetic ring on the driveshaft.

Instrumentation complexity – This solution requires very complex instrumentation to detect a signal which could prove difficult to justify to the nuclear safety regulator.

Technology readiness level of Sensor - The Technology readiness level for the resonant puck is less than five. The solution will require qualification for use within the submarine.

Development costs – The resonant puck principle will require large development costs for submarine use.

3.9.3 Submarine specific advantages

Reliability – The sensor technology relies on an electrical transmitter and receiver with no mechanical moving parts. This makes the sensor very reliable.

Temperature calibration – Temperature will not affect the sensor as the system topology is independent of temperature effects.

3.9.4 Submarine specific disadvantages

Interface cabling – The resonant puck principle requires four or more electrical connections per sensor. This increases the cable size, connector size and the potential for electrical connection faults.

Driveshaft modification–The driveshaft must be modified to incorporate a puck consisting of silicon material components. The environment around the driveshaft in service is not suitable for silicon technology.

Accuracy – The accuracy capability of the resonant puck sensor is very high as this is determined by the magnetic ring directly mounted on the driveshaft.

Size – The PCB requires robust material to support the etched copper tracks. It must be approximately the same length as the primary containment probe tube. This will require space above the reactor for installing and removing the sensor for maintenance.

Position calibration – The resonant puck technique will require the position of the driveshaft to be calibrated relative to the puck position. This needs to be done at only a few selected positions as the detected signal will have a linear response that can be calculated within the software of the instrumentation card to derive the rod position.

3.10 Hall Effect

The Hall Effect is a result of the nature of current in a conductor. Moving charges experience a force, called the Lorentz Force, when they are in a magnetic field that is not parallel to their motion. When such a magnetic field is absent, the charges follow an approximately straight, 'line of sight' path. However, when a perpendicular magnetic field is applied, the path of the charge is changed so that moving charges accumulate on one

face of the conductor. This results in an equal but opposite charge exposed on the other face of the conductor, where there is a scarcity of mobile charges.

The result is an asymmetric distribution of charge density across the material or Hall Element that is perpendicular to both the 'line of sight' path and the applied magnetic field.

The separation of charge establishes an electric field that opposes the migration of further charge, so a steady electrical potential builds up for as long as the charge is flowing.

A magnet will be required on the driveshaft for a sensor based on this principle shown in Figure 45.

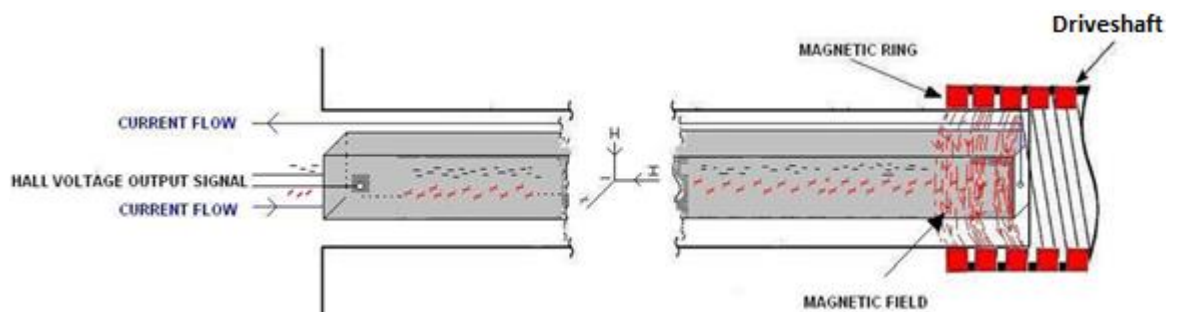


Figure 45 Hall Effect Concept

3.10.1 Hall effect advantages

Instrumentation complexity – This solution requires low complexity instrumentation to detect the voltage signal from the sensor. The output amplitude of the sensor is assumed to be detectable by a voltmeter.

Reliability – The sensor technology relies on electrical and magnetic principles that require no mechanical moving parts. This makes the sensor very reliable.

3.10.2 Hall effect disadvantages

Cost of sensor – This technology has a very high component cost as the materials used on the sensor require qualification for the submarine environment.

Technology readiness level of sensor - The Technology readiness level for the Hall Effect sensor is less than five. Although this sensor is used widely within the commercial market, it will need to be qualified for use in the submarine radiation environment.

Development costs – The development cost of the sensor will be high, due to the current immaturity of the technology.

Production costs –The cost of production of the sensor will be determined by the complexity of the sensor and materials selected during the development phase. It is currently believed that the production cost will be high.

3.10.3 Submarine specific advantages

Temperature calibration – The effect of temperature on the operation of the sensor will be determined by the nature of the materials used. To date, it is presumed the materials used will not be affected by the temperatures the sensor will be exposed to.

3.10.4 Submarine specific disadvantages

Interface cabling – The Hall Effect principle requires four electrical connections per sensor. This increases the cable size, connector size and the potential for electrical connection faults.

Driveshaft modification–The driveshaft will require magnetic rings. The magnetic properties of the magnetic rings could be affected by the Control Rod Drive Mechanism (CRDM) which could lead to sensor errors.

Accuracy – The accuracy capability of the Hall Effect sensor is very high as this is determined by the magnetic ring directly mounted on the driveshaft.

Size – The coil former of the sensor requires a robust core to support the material. This must be approximately the same length as the primary containment probe tube. This will require space above the reactor for installing and removing the sensor for maintenance.

Position calibration – The Hall Effect technique will require the position of the driveshaft to be calibrated relative to the magnetic ring's position. As the calibration response is assumed to be linear, three points of calibration will be sufficient.

3.11 Magnetoresistance

The magnetoresistance principle relies on a change in the material resistance as a current carrying-conductor is exposed to a magnetic field. This is a common effect which occurs within the Hall Effect.

As the magnetic rings illustrated on Figure 46 travel up the driveshaft, the area covered by the magnetic field increases, thereby increasing the magnetoresistance of the sensor. This magnetoresistance principle operates better within large structures where the resistance is greater.

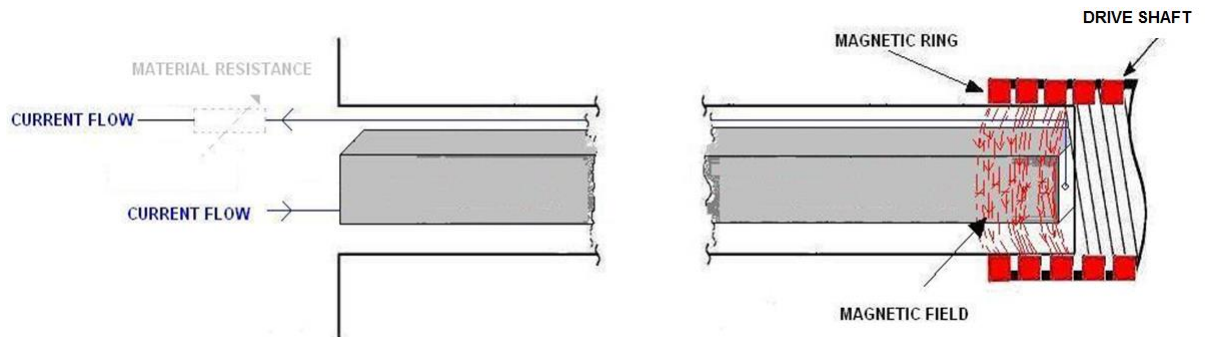


Figure 46 Magnetoresistance Concept

3.11.1 Magnetoresistance advantages

Instrumentation complexity – This solution requires low complexity instrumentation to detect sensor resistance. The output amplitude of the sensor is assumed to be detectable by a voltmeter.

Reliability –The sensor technology relies on electrical and magnetic principles and uses no mechanical moving parts. This makes the sensor very reliable.

3.11.2 Magnetoresistance disadvantages

Cost of sensor – This technology has a very high component cost as the material will require qualification for the submarine environment.

Technology readiness level of sensor - The Technology readiness level for the magnetoresistive sensor is less than five. Although this sensor is used widely within the commercial market, it will need to be qualified for use in the submarine radiation environment.

Development costs – The development cost of the sensor will be high, due to the current immaturity of the technology.

Production costs –The cost of production will be determined by the complexity of the sensor and the materials selected for use during the development phase. To date, it is believed that the production cost of the sensor will be high.

3.11.3 Submarine specific advantages

Temperature calibration – The effect of temperature on the sensor will be determined by the materials used. To date, it is presumed the materials used will not be affected by temperature.

3.11.4 Submarine specific disadvantages

Interface cabling – The magnetoresistance principle requires four electrical connections per sensor. This increases the cable size, connector size and the potential for electrical connection faults.

Driveshaft modification–The driveshaft will require a magnetic ring. The magnetic properties of the magnetic rings could be affected by the Control Rod Drive Mechanism (CRDM), and lead to sensor errors.

Accuracy – The accuracy capability of the magnetoresistance sensor is very high. This is a result of the magnetic ring being directly mounted on the driveshaft and the ability to control the constant current flow through the core material.

Size –A robust core material is required to support the material throughout approximately the same length as the primary containment probe tube. This will also require space above the reactor for installing and removing the sensor for maintenance.

Position calibration – The magnetoresistance technique will require the position of the driveshaft to be calibrated relative to the magnetic ring position. This needs to be done at only a few selected positions as the detected signal will have a ratiometric response that can be calculated within the software of the instrumentation card to derive the rod position.

3.12 Summary

The range of rod position technologies explained above are diverse and have a range of advantages and disadvantages associated with them. However the selected solution is required to be robust with large output signal sensitivity. In addition it needs to be easy to manufacture to ensure repeatable products are produced with a high yield rate and also be capable of withstanding harsh environments with vigorous manual handling. The solution deemed suitable for the project was the transformer principle as it satisfies the electrical, mechanical and manufacturing requirements and can be produced to be robust.

Chapter 4

4 Finite Element Analysis

4.1 Background

A numerical method (the finite element method) of analysing engineering systems has been developed by deriving differential equations which relate the variables in a system through basic principles, such as conservation of energy. These methods are useful when simple analytical solutions are difficult. The finite element method was initially developed in structural engineering sector where structures were considered to be in a stable equilibrium when the total potential energy reached a minimum. Today the finite element analysis is used in many areas as well as the field of electromagnetics.

Using the finite element method, the physical geometry of the system or component is simplified into non-overlapping elements of simple geometry called finite elements. The response of a finite element within the finite element analysis is expressed in terms of finite degrees of freedom at a set of nodal points. The method used to determine the nodal potentials in each finite element is the energy functional. When a number of the finite elements are combined and connected to each other they become known as a finite element mesh.

Many different modelling tools can use different finite element shapes, the most commonly used 3D shape is the tetrahedron. Generally tetrahedron shapes resolve better using 2nd order quadratic interpolation between nodes, thus improving the fidelity of the output result. Using a tetrahedron mesh, the equation for each finite element are assembled into a large global equation for the whole problem and solved using standard techniques such as Sparse Gaussian Elimination. The required mesh density of an arbitrary geometry is governed by the accuracy of the resultant output required and the solution time. Normally there should be no less than three meshed elements around any structure. A pictorial view of an element is given in Figure 47.

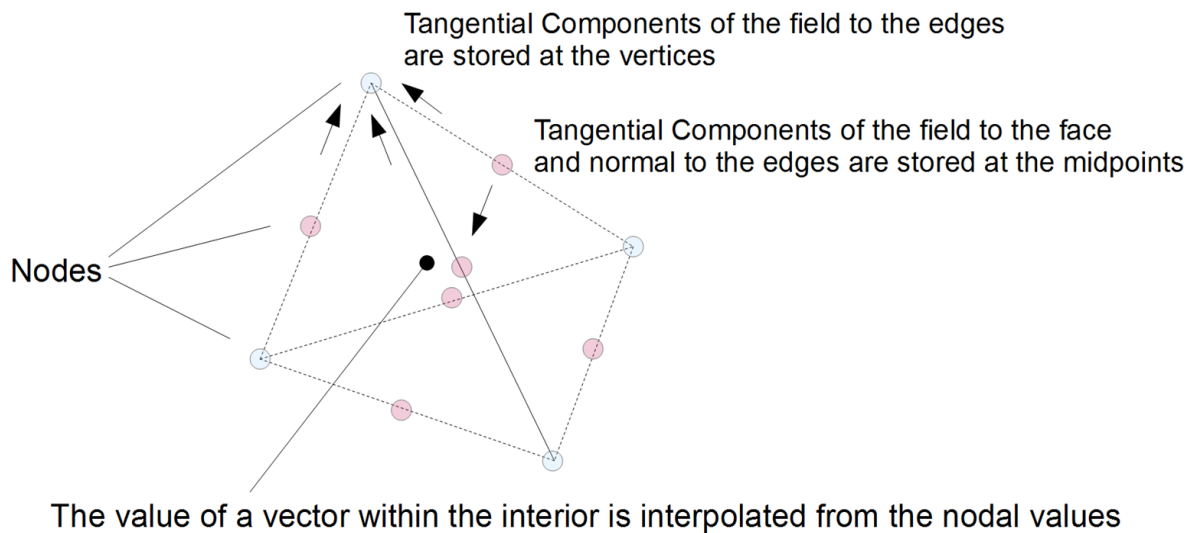


Figure 47 Finite element

Finite element analysis can be considered as three individual functions. The “finite” refers to the countable number of elements used to represent the geometry of the shape being modelled. The “element” refers to a small section of the problem being modelled which can be governed by a set of equations as this is bound by the surrounding parts. The “analysis” refers to the controlled conditions which are imposed to calculate the numerical solution of each element. Each element acts on its neighbouring element.

The finite element analysis assembles the equations from all the elements into one large global system matrix and used to determine the numerical solution. A key and important part of the finite element analyses is that the elements are made small enough and spread across the geometry appropriately such that the numerical solution can closely represent the true magnetic solution.

4.2 Finite Element Method Magnetic (FEMM)

For the TIRPI development the finite element modelling tool called Finite Element Method Magnetics (FEMM) was used. FEMM is a low frequency two-dimensional solver for planar and axisymmetric non-linear time harmonic electromagnetic problems. This tool was suitable for the TIRPI analyses as the driveshaft would only move very slowly in a stepped motion without transient conditions. FEMM can also provide the user to input constant current sources within the windings of the design reducing the complexity of the

user interface. In addition FEMM allows additional interfacing interactive shells such as Octave to be used to control the simulations and carry out mathematical operations to and from the FEMM environment. An important feature of FEMM is the ability to solve the induced eddy currents in materials due to the time-varying magnetic fields incorporated within the supplied solutions. For the TIRPI a number of 2D axisymmetric non-linear time harmonic analyses were carried out to develop the solution. The average BH curve was calculated from tested materials for the FEMM model however no permeability correction was used. The mesh size for the analyses was 1mm as this would be better than the minimum requirement of 3 times the skin depth of the materials used at the particular frequency of the analyses. Table 1 shows the parameters used for the TIRPI analyses. The skin depth of the Inconel 625 material and copper requires a mesh size of approximately 0.01mm and 0.001mm however this would cost a lot of time for the analyses to be carried out and was not practical. A mesh size of 1 mm was used for the TIRPI, probe tube and driveshaft. This was considered to be a good trade-off between accuracy of the design and time taken to complete the simulations.

Table 1 TIRPI analyses key attributes

Attribute	Parameters
<i>Analysis type</i>	<i>2D axisymmetric non-linear time harmonic analyses</i>
<i>Excitation</i>	<i>Constant current source of 100mA r.m.s</i>
<i>Mesh size</i>	<i>1mm</i>
<i>Number of nodes</i>	<i>139427</i>
<i>Skin depth of 17.4PH H1100</i>	<i>Min value = 2.38mm, Max value = 12.53mm</i>
<i>Skin depth of Inconel 625 mesh size</i>	<i>0.04mm (used 1mm)</i>
<i>Skin depth of copper mesh size</i>	<i>0.004mm (used 1mm)</i>
<i>Permeability correction</i>	<i>Not applied</i>
<i>Boundary condition</i>	<i>Dirichlet (A=0) @ outer boundary</i>

Chapter 5

5 Techniques to Improve Control Rod Position Accuracy

This chapter will describe the different areas and techniques investigated to improve the accuracy of the control rod position sensor through improving the transducer. The research to increase the accuracy of the rod position detection was carried out in parallel with a submarine development programme. The requirements to enable the research to be used in a practical application evolved as the system requirements changed throughout the programme.

The initial aim of the research was to improve the sensitivity of the sensor by adhering to the programme requirements. As the submarine development programme matured the requirements changed and increased constraints on the transducer design. In addition, the electronics used to detect the transducer signals were constrained to a bespoke in-house design. This limited the sensor drive currents and voltage amplitudes which could be used.

As the electronics instrumentation and cable requirements evolved, the research on the improved accuracy transducer concentrated on various methods to find a solution which could be used on the submarine programme. A number of methods were investigated, and prototypes based on these methods were built and tested. These are described in the sections below. The principle that was finally selected for use was the Transformer Individual Rod Position Indicator (TIRPI) as it met all the requirements of the instrumentation electronics and cable limitations, while meeting the accuracy requirements of the system.

5.1 Option 1: Inductor principle

The inductor principle depends upon the change of inductance when a magnetic material is placed within the inductor's magnetic flux. The optimum inductance variation occurs when a ferromagnetic material is used, as the magnetic flux is attracted towards it.

The relative permeability (μ_r) of a material within a magnetic field changes the inductance of the electromagnetic coil generating the magnetic field. The changes in inductance of the sensor can be used to infer the driveshaft motion and the transducer inductance value to infer the driveshaft position. A magnetic field generated by an electromagnetic coil can be used to detect the driveshaft, which is made of a martensitic stainless steel, and in addition to penetrate a probe tube made of Inconel 625 or 316L stainless steel. The relative permeability (μ_r) of the driveshaft and probe tube material is affected by the physical properties of the material and the machining processes and heat treatments used on the materials.

The two materials which were used for the development unit testing were stainless steel 316L and HAS4104 Condition A. The relative permeability (μ_r) of the stainless steel used was 1.02. However, the driveshaft material had a greater relative permeability (μ_r) due to its physical properties, machining process and heat treatment used on it. Due to the variation of relative permeability (μ_r) the material was tested to determine its B-H curve. The results of the B-H test of the driveshaft material (presented in Figure 48) show the magnetic response of the driveshaft in terms of magnetic flux density (B) and magnetic field strength (H).

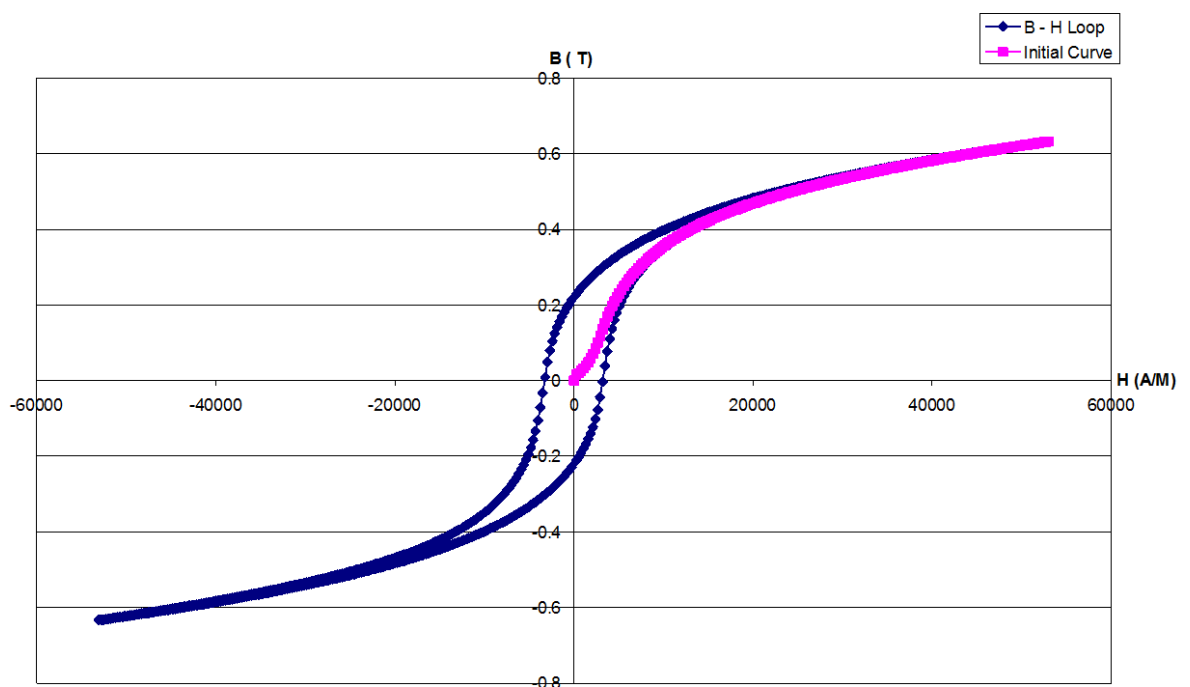


Figure 48 B-H curve of driveshaft material

Within this application (illustrated in Figure 49), the driveshaft material will interact with the magnetic field of the inductor, changing the inductance value of the sensor, when the driveshaft envelops the probe tube.

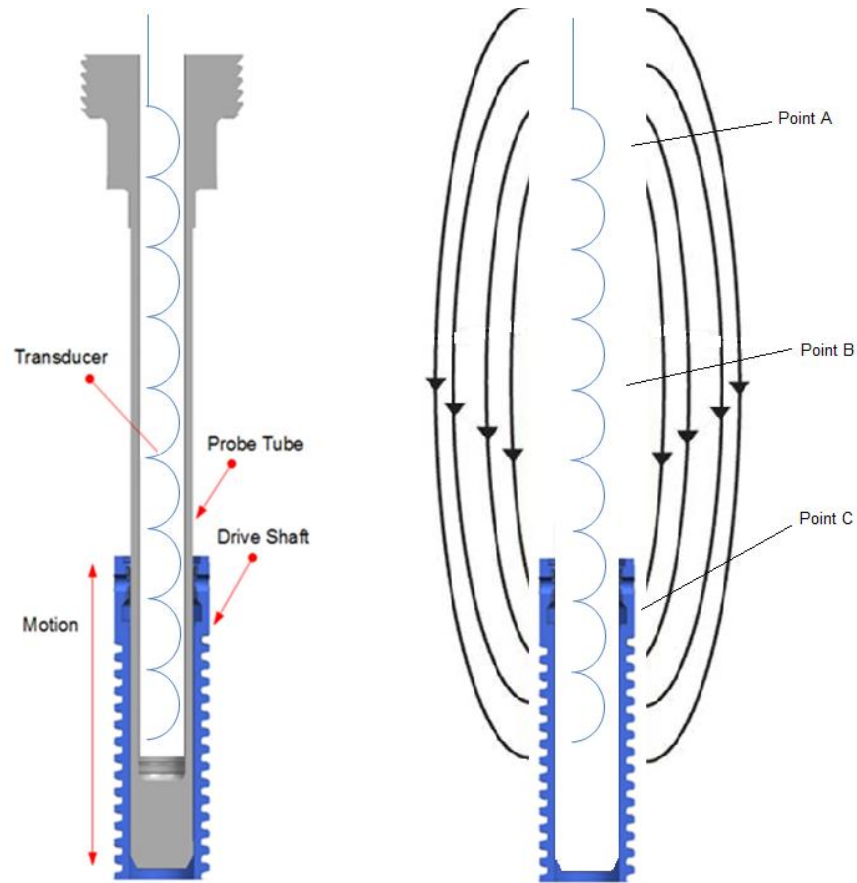


Figure 49 Inductive sensor principle

An important observation is that the geometry of the driveshaft relative to the magnetic flux determines how effectively the inductor can detect the driveshaft location. As shown in Figure 49, points 'a', 'b' and 'c' show the density of the magnetic flux in particular locations where the driveshaft will travel and "cut" the magnetic flux. Points 'a' and 'c' show a high density of magnetic flux, whereas point b shows little to no flux. The shape of the magnetic flux produced by the inductor is not uniform throughout the probe tube length; thus the change in inductance measured by the sensor will not be uniform either. In addition, the driveshaft will not be detected within the mid-region (point b) as virtually no magnetic flux is present in this location.

Although the inductor principle did not meet the accuracy requirements, the principle of operation was investigated further using finite element modelling tools. This enabled an optimum inductor configuration to be determined.

A single inductor, spaced inductor and multi-directional inductor configurations as shown in Figure 50 were analysed to investigate the sensitivity of the output signal.

The single inductor configuration will allow the driveshaft to “cut” the flux field at two locations: the top and bottom of the inductor. The magnetic field is concentrated within the centre of the inductor, thus reducing the amount of flux being absorbed by the driveshaft as it moves over the outer surface of the coil. This has been identified as driveshaft “cut” locations in Figure 50.

The spaced inductor gives more flux field locations for the driveshaft to “cut”, thus increasing the inductance change. However, the majority of the magnetic field is concentrated within the centre of the spaced inductors, thereby reducing the driveshaft effect on the output signal sensitivity. The optimum solution, the one that gives the greatest inductance change, is the multi-directional inductor. This configuration will allow a greater number of inductors to be produced closely together, by reversing the winding at each bobbin. In addition, this configuration produces an anti-phase magnetic field with no spaces between each bobbin. The multi-directional inductor configuration creates an equal and opposite magnetic field within the centre core of the inductor when each bobbin is connected together. This results in an increased field around the driveshaft region and a cancellation effect within the centre core. The increased field around the driveshaft enables a larger deviation in inductance value when the driveshaft overlaps the probe tube.

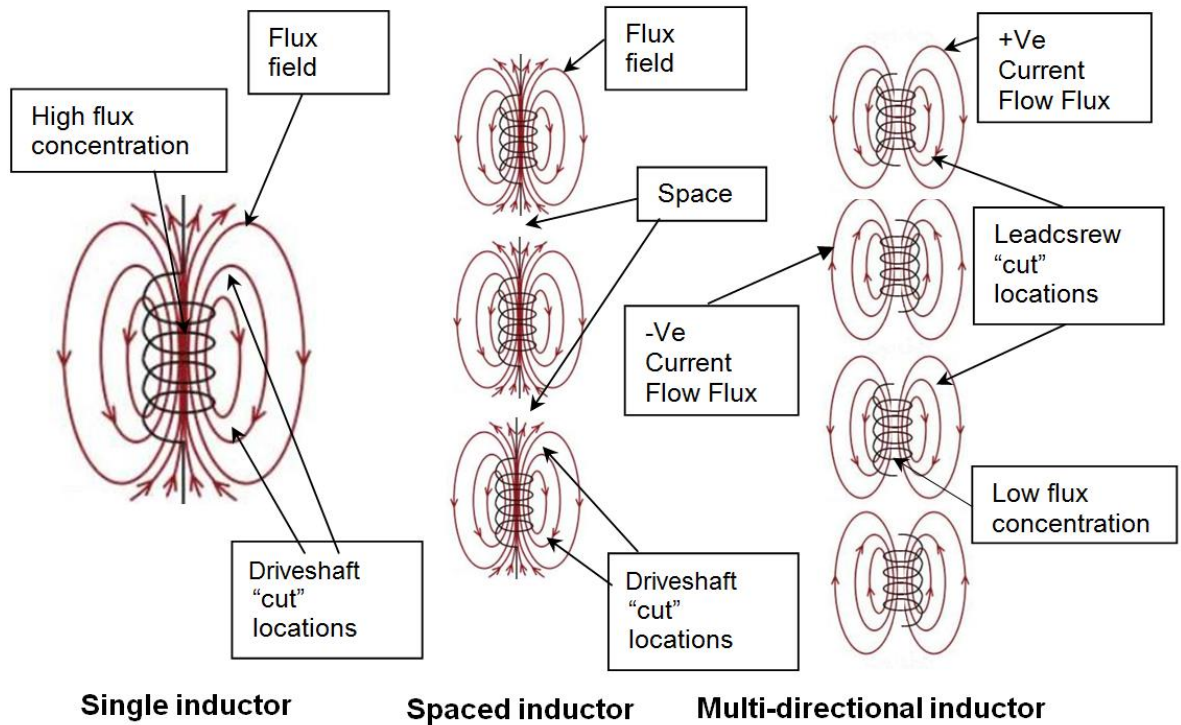


Figure 50 Inductor configurations

The multi-directional inductor principle illustrated in Figure 51 significantly increases the inductance detection sensitivity of the driveshaft as the magnetic flux is concentrated within the coil circumference rather than the core region. This enables the driveshaft to interact with it as it moves up the probe tube. By connecting a number of coils in series, greater output signal sensitivity can be achieved from the transducer as the driveshaft envelops the probe tube. In addition to achieving a high-accuracy sensing sensor it is also important to consider the resolution of the sensor and whether this changes. The multi-directional principle uses the opposing magnetic field polarities to cancel the fields between successive coils, thus creating a “dead zone” where the driveshaft cannot be detected. The “dead zone” occurs between each inductor coil and produces a constant inductance value on the output inductance value as the driveshaft passes through it. This effect is not desirable and therefore results in solutions which cannot be used for high accuracy detection. The error the “dead zone” causes is approximately 2% at every region where the coils are connected together.

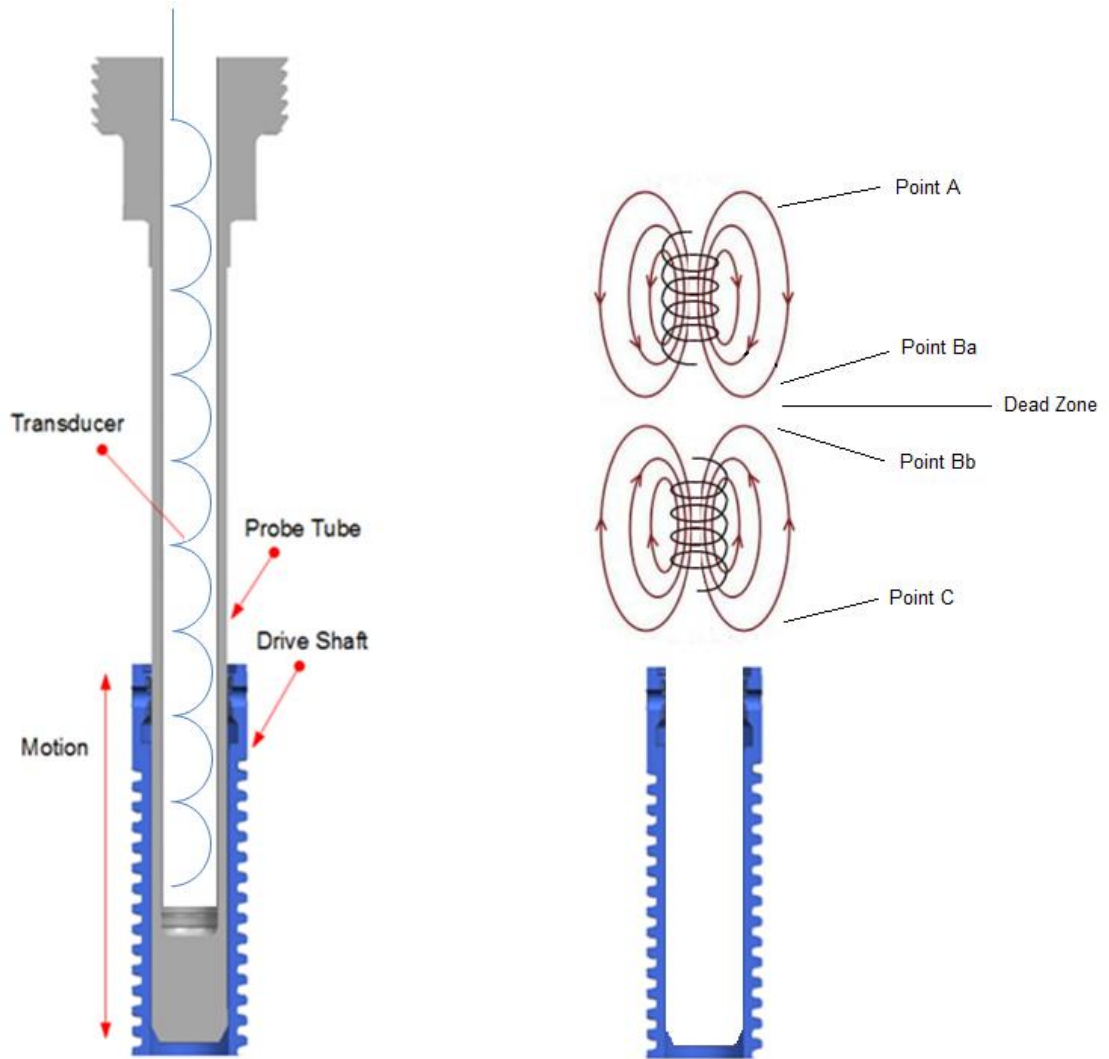


Figure 51 Multi-directional inductor

A magnetic simulation using a FLUX 2D model was developed to show the magnetic flux variation with respect to the driveshaft. The magnetic model also predicted the inductance change of a manufactured practical sensor. Figure 52 shows a half mid-section cut-out of the sensor. The current flow labelled “+ Current flow” shows the direction of the current flow is a clockwise motion around the core. The current flow labelled “- Current flow” shows the direction is anti-clockwise motion around the core, on consecutive bobbins. The magnetic model confirmed the operating principle of the multi-directional inductor and also that the ‘dead zones’ would deem this solution not viable for the design of the TIRPI.

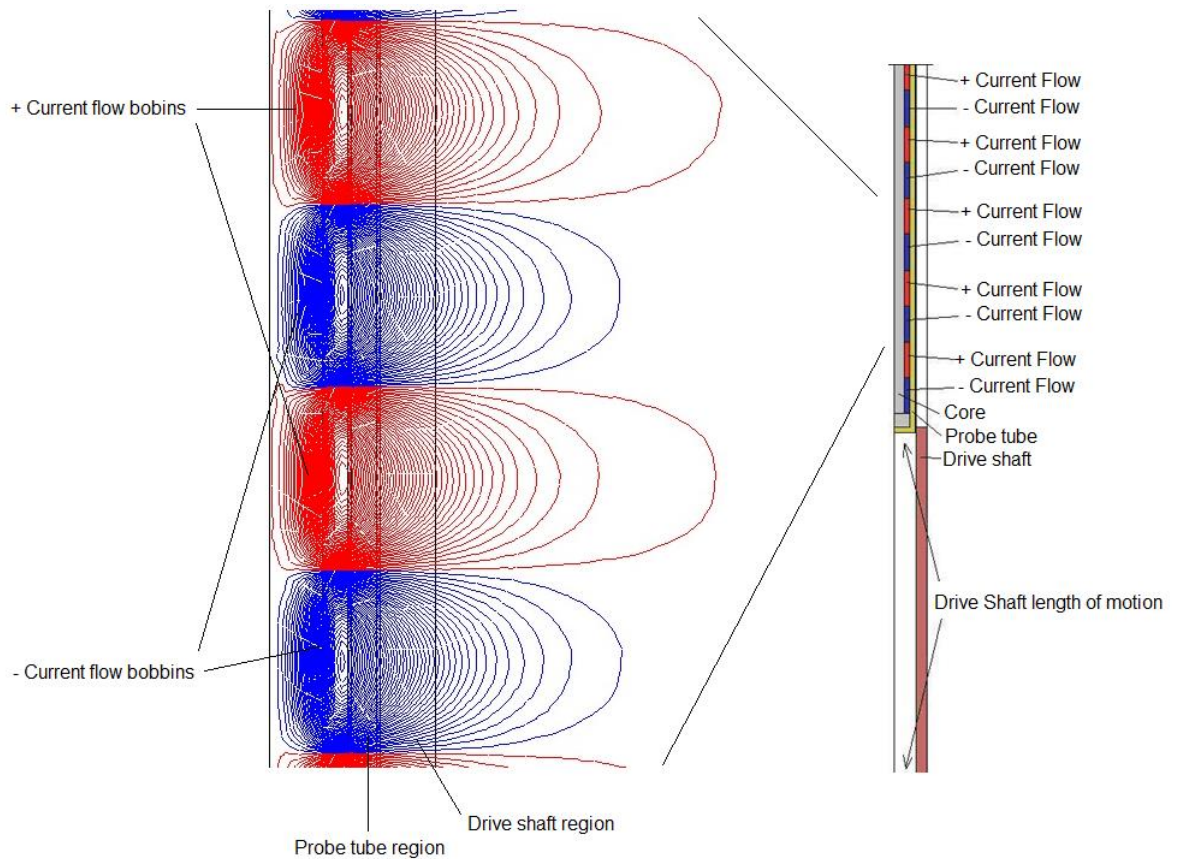


Figure 52 FLUX 2D magnetic model geometry of a multi-directional inductor

5.2 Option 2: Transformer rod position indicator principle

The principle used in the transformer rod position indicator has been used to detect control rod position for many years, and has been proven in service for its reliability and robustness. Section 2.2 Figure 17 illustrates the concept of the primary and secondary coil configuration of an existing solution and explains the reason why this cannot be adopted for use with the current design. The Transformer Individual Rod Position Indicator (TIRPI) is a variation of the illustrated design in Figure 17 to enable the principle to be used in this application. The primary and secondary coils are to be housed internally, rather than externally over the probe tube. The winding will be wound around a metallic core for mechanical strength. The primary coils are equally spaced and the secondary coils are placed between them, as shown in Figure 53.

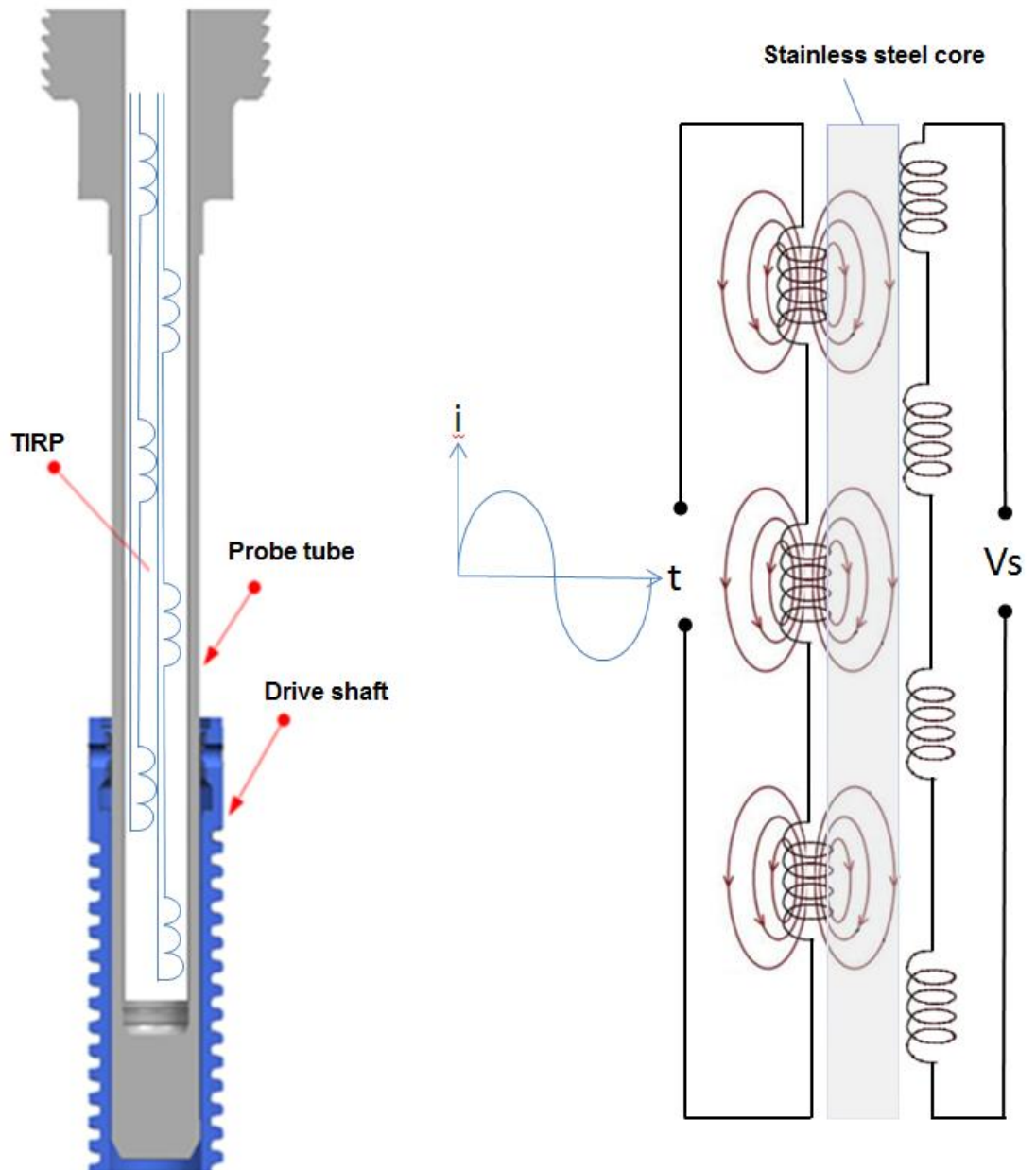


Figure 53 Transformer rod position indicator principle

When a sinusoidal constant current source is applied to the primary coils, a magnetic flux will be produced. The secondary coils are positioned such that the magnetic flux interacts with the coils and a voltage is induced at the secondary coil output. In situ, the magnetic flux produced from the primary coils will also interact with the probe tube. The probe tube is made of Inconel 625 and the driveshaft is made of 17.4PH condition H1100. Due to the magnetic relative permeability of the driveshaft material being greater than the probe tube material, the magnetic flux will propagate through the probe tube onto the secondary coils when the driveshaft is not present. However, when the driveshaft is in close proximity to the magnetic flux, the driveshaft absorbs the magnetic flux. This causes the induction of

the flux onto the secondary coils not to take place, thus causing the voltage on the output to reduce.

The TIRPI secondary output voltage span and sensitivity with respect to the driveshaft motion is determined by many attributes, including the magnetic permeability of the materials, their electrical conductivity, geometries and design of the TIRPI. The driveshaft and probe tube cannot be changed as these components interface with the control rod drive mechanism and are design constraints. These constraints limit the improvements which can be made to increase the overall system accuracy and only improvements to the TIRPI transducer can only be made.

5.2.1 Finite element model to optimise the transformer rod position indicator geometries to increase the output signal linearity

The secondary output signal linearity is important when trying to improve the accuracy of the TIRPI. As the driveshaft envelops the probe tube, the output signal changes, following an 'S' shape waveform. This effect causes the sensitivity of the TIRPI to change according to the position of the driveshaft, thereby limit the accuracy of the TIRPI. The sensitivity of the TIRPI can be improved by increasing the space between the primary and secondary coils to linearise the output waveform. Finite element method magnetics (FEMM) modelling was undertaken to optimise the coil spacing in the following chapter.

Chapter 6

6 Advanced Sensor Design and Analysis

6.1 Finite Element Model Approach

There are many approaches which can be taken when analysing a component using finite element modelling. A suggested sequence of modelling for the TIRPI is described below. Firstly the important parameters of the design need to be established and prioritised for modelling. For the TIRPI design the following correct sequence for modelling the design was established:

- the bobbin spacing length

The bobbin spacing length is the size of the space between each primary and secondary coil. The bobbin spacing length affects the induced EMF on the secondary coils and sensitivity of the signal output.

- the bobbin length best straight line

The bobbin length best straight line is the measure of linearity of the secondary output signal as the primary and secondary coil length is changed. This also affects the secondary output signal sensitivity however it is important to optimise the length of the primary and secondary bobbins to give the optimum linearity and thus secondary output signal resolution as this defines the TIRPI overall accuracy.

- the bobbin width best straight line model

This is similar to the bobbin length best straight line however this has a smaller effect on the secondary output signal sensitivity and resolution. This is usually defined by the number of coil windings needed and the capability of the TIRPI manufacturing possible in practice. Providing the mechanical requirements are met such as straightness and the wire size can fit within the space envelope of the bobbins then the width size can be optimised to aid the secondary output signal sensitivity and linearity.

- the span model

The span model is the optimisation of the secondary output signal sensitivity for the designated length of the TIRPI. There are only a finite number of primary and secondary

bobbins which can fit within a set length and a trade-off has to be made between number of primary and secondary bobbins, number of windings on each bobbin and linearity of the total secondary output curve from 0 to 100% driveshaft position. The secondary output is optimised to give the greatest sensitivity through the operational length.

- the optimised frequency

The optimised frequency is the frequency which the TIRPI gives the largest secondary output signal span. The frequency value must be determined when the TIRPI is within the operational location as the value changes with respect to the materials surrounding the TIRPI. An estimate of the optimum frequency can be determined using the TIRPI alone however this must be reanalysed once it has been installed in its final location.

The terms used above are illustration in Figure 54.

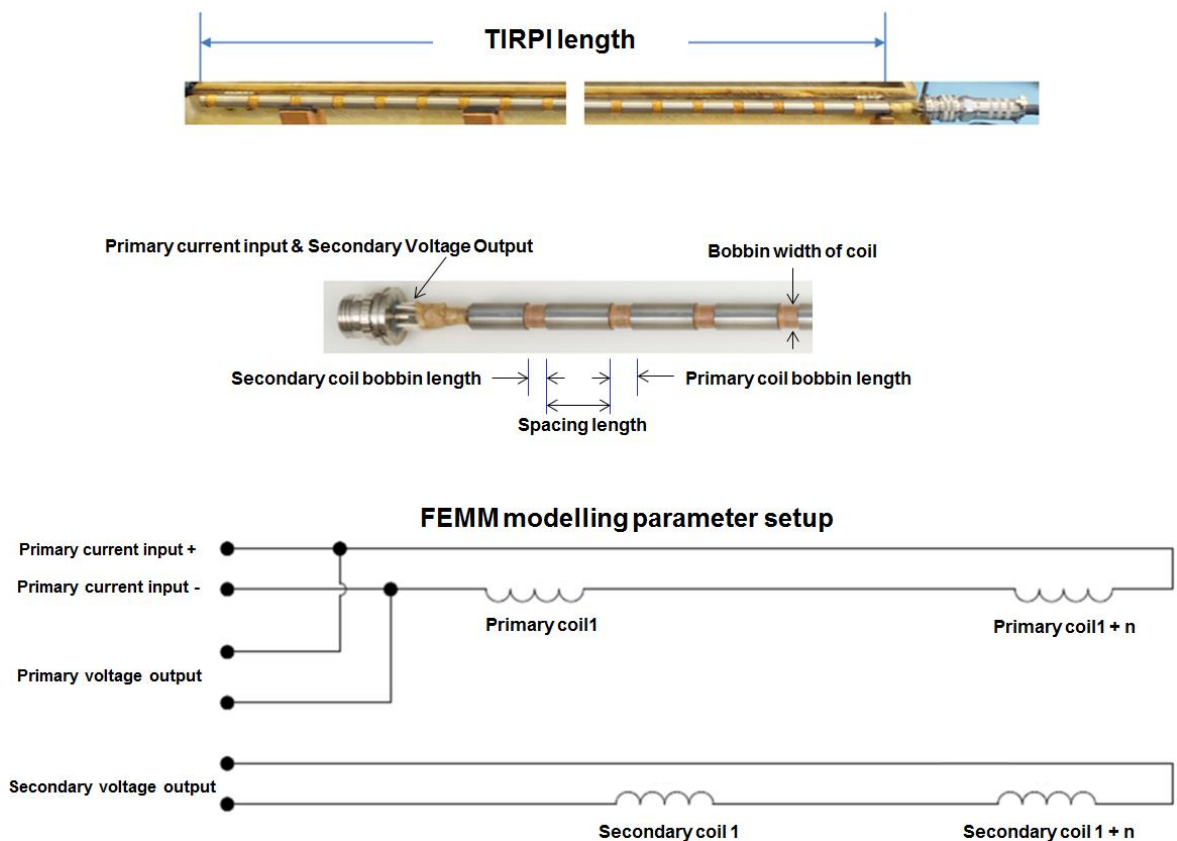


Figure 54 TIRPI terms

Although FE modelling is useful it is prudent to be aware of the software setup. The mesh sizing is to be small enough to achieve sufficient fidelity in the output results. However, if the mesh sizing is too small, the analyses will take too long to run and modelling may not be practical. A general rule of thumb is that the mesh size should be 2 to 3 times greater

than the smallest possible linear increment the TIRPI can move which is defined by the Control Rod Drive Mechanism (CRDM).

6.1.1 Bobbin spacing size and bobbin size model

The bobbin spacing and bobbin sizes of the TIRPI determine the linearity of the secondary output signal when the driveshaft envelops the probe tube. The length of the bobbin spacing is changed until a best straight line graph is achieved for the secondary output signal. The optimum length for the sensor parts is determined by the geometries and material characteristics of the sensor core, probe tube and driveshaft. These are fixed for the TIRPI design. The best straight line graph is calculated by measuring the “S” curve of the secondary output signal for the different bobbin spacing lengths and selecting the curve with the minimum deviation from a linear line or the best fit to a linear regression. The commonly known R^2 value can be used to determine which of the curves has the best straight line fit. A similar approach is employed to determine the optimum bobbin size after the bobbin spacing has been determined.

6.1.2 Hysteresis effects on TIRPI magnetic core material

When a magnetic material is magnetised it will not return back to its original state when the magnetic field has been removed. For the magnetic flux density to be zero within the material it will require the magnetic field strength to be reversed. This phenomenon can be thought of magnetic memory for the magnetic material.

The hysteresis within the TIRPI core material will cause the primary voltage back EMF not to be perfectly sinusoidal and this will affect the TIRPI secondary output voltage not to be perfectly sinusoidal. This harmonic distortion becomes greater as the hysteresis loop of the material becomes larger. A harmonic test was carried out using a constant voltage power source to the TIRPI to establish the harmonics of the TIRPI output voltage which resulted in a very small 2nd harmonic content shown on Figure 104, Figure 105 and Figure 106. Although This has been considered to be a negligible effect on the TIRPI secondary output RMS voltage and TIRPI sensitivity capability.

6.2 Design approach

The optimum TIRPI transducer design is determined by non-linearity characteristics of the output signal, the magnetic effects of the surrounding environment and the sensitivity of the transducer as defined by the span and the span divided by the offset of the secondary output voltage (SoR). The span of the output signal is the difference between the voltage output when the driveshaft is at its minimum position and the maximum position. The greater the voltage difference the greater the span. Another parameter which is important to the electrical instrumentation card is the TIRPI SoR as this defines how sensitive the TIRPI is with respect to the lowest voltage output the TIRPI can achieve known as the offset. This occurs when the driveshaft is in the maximum position. Generally this value is used when designing the input analogue to digital circuitry for the electrical instrumentation card and it is desirable to have a large as possible SoR to enable the electrical instrumentation card to detect the minimum required voltage change.

The SoR of the transducer is affected by the geometry of the driveshaft and core, the core material and the frequency of operation of the source signal. The TIRPI design target is to have the maximum allowable voltage on the secondary coil when the driveshaft is not covered by the probe tube, and the minimum possible voltage on the secondary coil when the driveshaft fully covers the Probe Tube. In practice it is extremely difficult to achieve this target as a trade-off occurs between non-linearity, SoR and signal magnitude.

However, it is possible to optimise the TIRPI transducer design by causing the induced magnetic field eddy currents to cancel at a particular desired frequency. This allows the minimum signal output to be determined when the driveshaft covers the probe tube. When the probe tube is in the uncovered position, the primary coil turns can be optimised for the maximum allowable primary voltage by the instrumentation card as both the primary and secondary voltages will be at their maximum signal output values.

6.2.1 Geometry Optimisation

When optimising an electromagnetic device (such as a sensor or transducer) for maximum sensitivity, the geometry of the sensor and associated components within the environment are significant factors to consider. The electromagnetic field produced by a

bar magnet or a solenoid produces a magnetic field distribution with a non-linearly varying magnetic field density in the surrounding environment, which is typically air. The non-linearity of the magnetic field produces higher and lower regions of magnetic flux density around its region. The magnetic field distribution also depends on the materials which are located within the source magnetic field.

In addition to a single source producing a magnetic field, a number of magnetic sources can be connected together to form an overall combined magnetic field. The resultant magnetic field is a combination of the individual source fields and is affected by the material types and material geometries.

The TIRPI consists of a number of magnetic field sources, known as the primary coils (solenoids), which are connected in series. Each solenoid produces a magnetic field distribution which interacts with its neighbour's magnetic field, producing a combined accumulative total magnetic distribution around the TIRPI. Between each solenoid there is an additional coil. These form a series of secondary coils (solenoids). The secondary coils do not produce a magnetic field, as they are not connected to a source current. However, they are located in the total field produced by the primary coils, hence an emf will be induced in the secondary coils if the total field has time variation, resulting in the production of a secondary electrical voltage.

As the geometry of the TIRPI changes, the primary magnetic field distribution and induced secondary voltage are changed. In addition, if the primary coils and secondary coils are situated too close to each other a high output secondary voltage is produced. However, the extent of the magnetic field area is also reduced, which results in a greater sensitivity output signal from the TIRPI as the driveshaft is situated within the magnetic field distribution area or location. Figure 55 shows the spread of the magnetic field produced by the primary coils and the magnetic field seen by the secondary coils along the profile lines. It also shows how the magnetic field decays radially outwards from the coil axis. The geometry of the TIRPI, probe tube and driveshaft has a significant effect on the capability of the TIRPI to detect driveshaft increments.

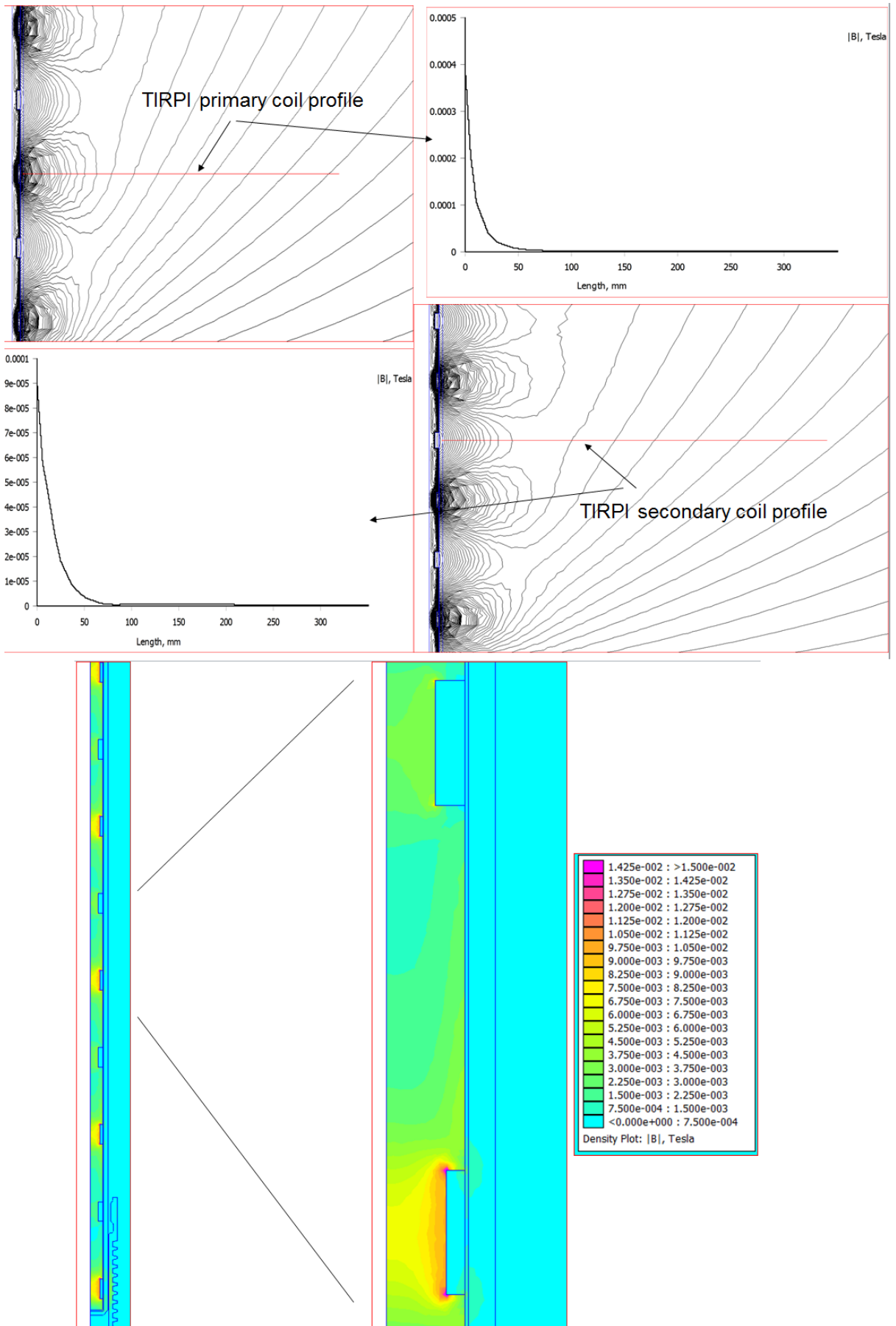
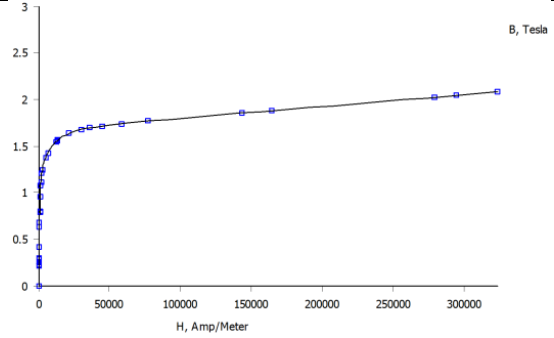
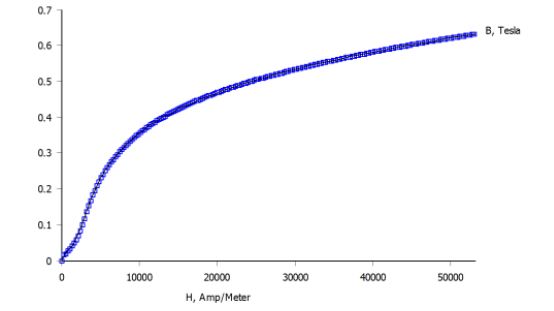
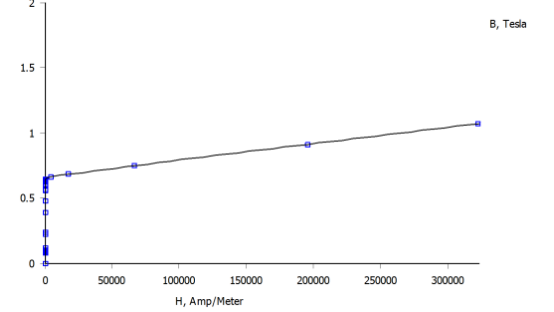
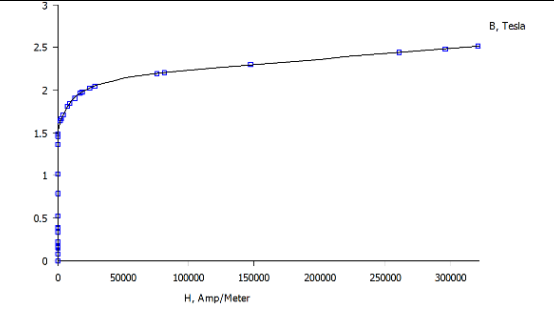


Figure 55 TIRPI magnetic fields

6.2.2 Core matching

The greatest influence on the design of the TIRPI has been the new concept of core matching. Using an FE analyse, it was found that the span and span to offset ratio (sensitivity of the TIRPI) are significantly increased when the core material of the sensor is closely matched to the driveshaft in terms of magnetic permeability and electrical conductivity. A number of different typical materials have been selected for analysis to demonstrate the core matching concept. A list of the materials tested is given in Table 2.

Table 2 List of TIRPI core materials

Material	BH Curve (Tesla) Used for FEMM Analysis	Material Conductivity (MS/m) Used for FEMM Analysis
416 Stainless Steel	 <p>The graph for 416 Stainless Steel plots magnetic flux density (B) in Tesla on the y-axis (0 to 3) against magnetic field strength (H) in Amp/Meter on the x-axis (0 to 300,000). The curve starts at the origin, rises steeply to about 1.5 Tesla at 10,000 Amp/Meter, and then continues to rise more gradually, reaching approximately 2.1 Tesla at 300,000 Amp/Meter.</p>	1.74
HAS4104 Condition A	 <p>The graph for HAS4104 Condition A plots magnetic flux density (B) in Tesla on the y-axis (0 to 0.7) against magnetic field strength (H) in Amp/Meter on the x-axis (0 to 50,000). The curve shows a smooth, non-linear increase from the origin, reaching approximately 0.65 Tesla at 50,000 Amp/Meter.</p>	1.28
Mu-Metal	 <p>The graph for Mu-Metal plots magnetic flux density (B) in Tesla on the y-axis (0 to 2) against magnetic field strength (H) in Amp/Meter on the x-axis (0 to 300,000). The curve shows a very low magnetic field strength for a given flux density, reaching approximately 1.1 Tesla at 300,000 Amp/Meter.</p>	1.74
Ingot Iron Annealed	 <p>The graph for Ingot Iron Annealed plots magnetic flux density (B) in Tesla on the y-axis (0 to 3) against magnetic field strength (H) in Amp/Meter on the x-axis (0 to 300,000). The curve shows a sharp initial rise followed by a gradual increase, reaching approximately 2.5 Tesla at 300,000 Amp/Meter.</p>	10.15

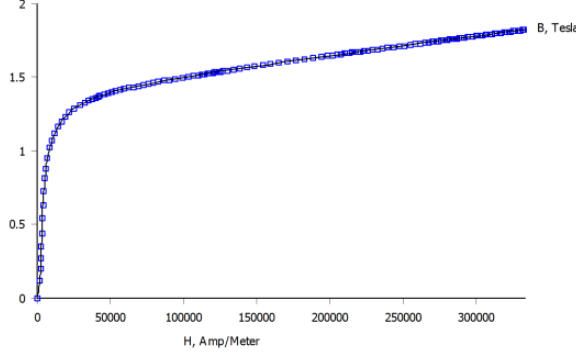
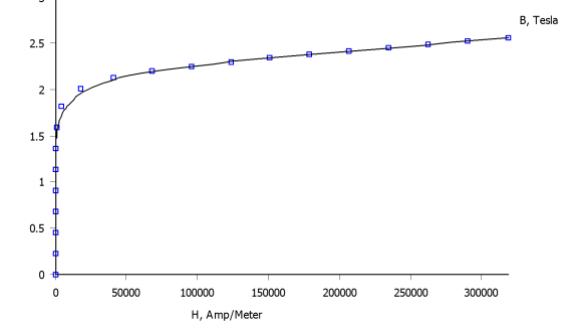
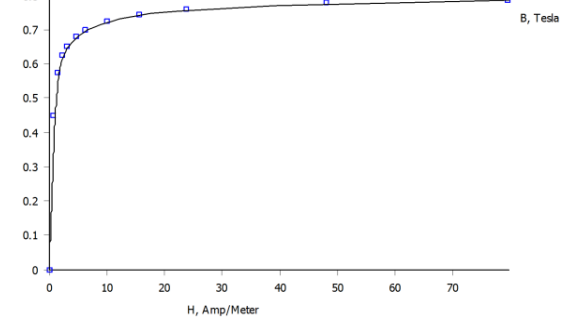
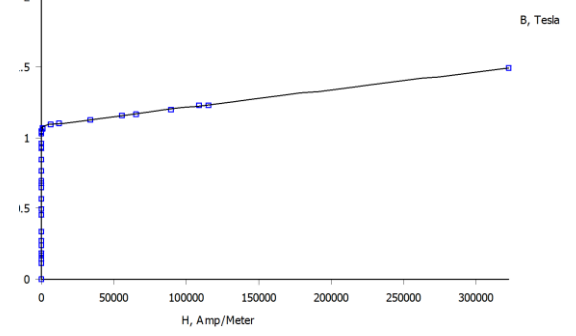
Material	BH Curve (Tesla) Used for FEMM Analysis	Material Conductivity (MS/m) Used for FEMM Analysis
17.4 PH		1.45
Pure Iron		10.44
Supermalloy		1.7
78 peramolly		2.32

Table 2 shows the characteristics of the magnetic materials which were selected and analysed to achieve the maximum secondary voltage span from the TIRPI. Typically these materials can be used within a nuclear environment, are suitable for machining and heat

treatments, and represent a range of B-H curve characteristics and electrical conductivities.

Testing of the effects of the bobbin geometries on the secondary voltage output span of the TIRPI was conducted using two TIRPI geometries, one being a “bobbin-optimised” test and the other a “bobbin-unoptimised test”. The bobbin-optimised test ensured the TIRPI bobbin size was such that it would provide the best straight line secondary output. The bobbin-unoptimised test analysed the core material output characteristics when the bobbin size was not optimised and at half the TIRPI original length to save cost of materials. This ensured that the FE results were not affected by the bobbin size and were a true representation of the core material permeability and conductivity effects.

6.2.3 Core matching analyses using optimised bobbin size

The FE model was used to investigate whether having an TIRPI core material that was the same as the driveshaft would give the maximum secondary span output. The permeability and conductivity of the core material differs in TIRPI secondary output response with changes in source current frequency applied on the TIRPI primary coil. It was originally intended to use a frequency range from 100Hz to 9.6 kHz for the TIRPI current source signal; however the cable being used to connect the TIRPI and the instrumentation card was very long and its capacitance limits the maximum current source frequency for use to lower than 2 kHz.

Although the materials listed in Table 2 exhibit a range of B-H curves and conductivity values, Figure 56 shows the maximum secondary span output of the TIRPI occurs at approximately 800 Hz with a voltage value of 3.4V. A reasonable explanation of the result is that the eddy currents within the materials are at a minimum at a particular frequency when the same materials are used for the core and driveshaft. The magnetic field vectors between the TIRPI, probe tube and driveshaft cancel out when the driveshaft is fully enveloping the probe tube.

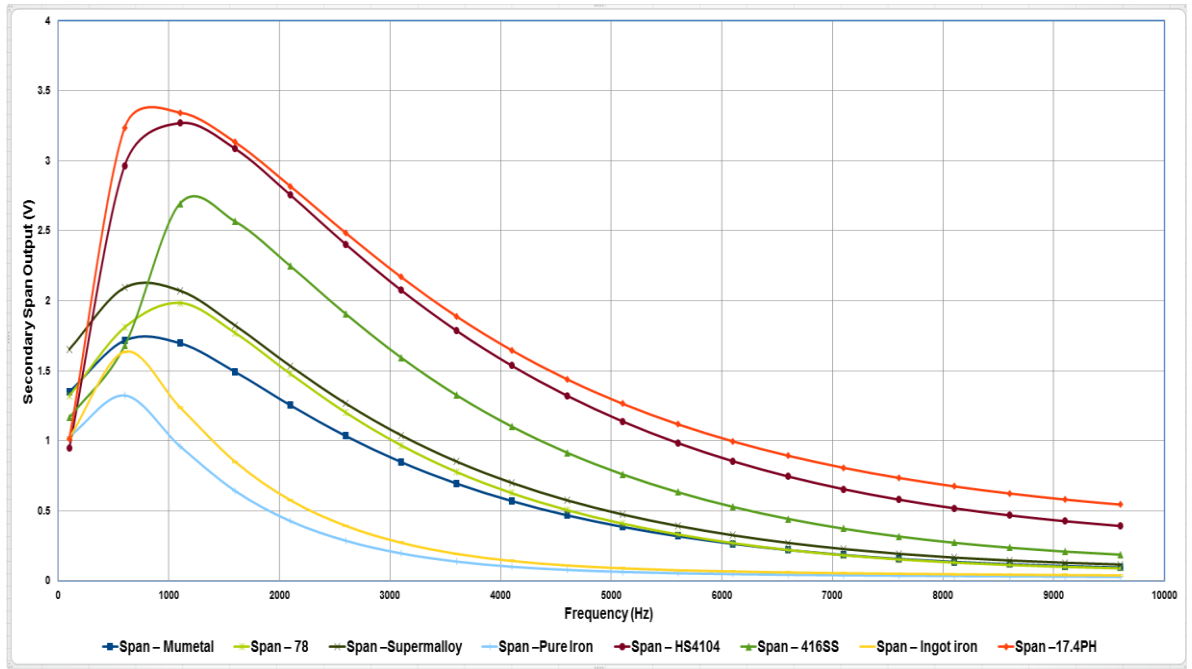


Figure 56 Span of the TIRPI with optimised bobbin size

The TIRPI span to offset ratio sensitivity (SoR) also changes depending on the primary source frequency used. The frequency value which produces the maximum SoR is not the same as the frequency value which produces the maximum span. Figure 57 shows the maximum SoR is achieved at a frequency of 5.5 kHz.

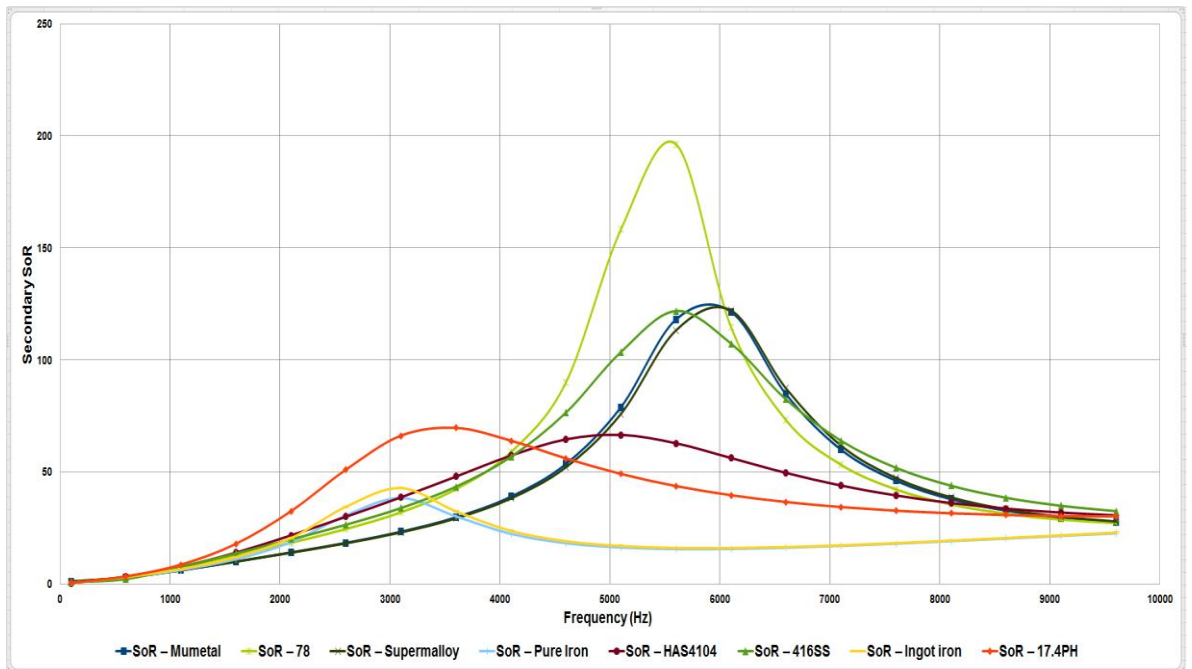


Figure 57 SoR of the TIRPI with optimised bobbin size

A discussion was made to choose the design which gives the maximum span output signal.

6.2.4 Core Matching Analyses using Un-optimised Bobbin Size

The FE model was also carried out using half-length primary and secondary bobbins to investigate whether this would affect the secondary output voltage span and SoR.

Figure 58 and Figure 59 show similar secondary span outputs, but significantly different SoR results due to the geometry being halved.

For the TIRPI, the significant parameter is the secondary output span as this directly affects the ability to detect a small change in driveshaft position; the greater the secondary span value, the greater the change in voltage output that will be achieved for a single CRDM pulse. This enables the instrumentation card to easily detect driveshaft position and maximises the resolution of the TIRPI channel.

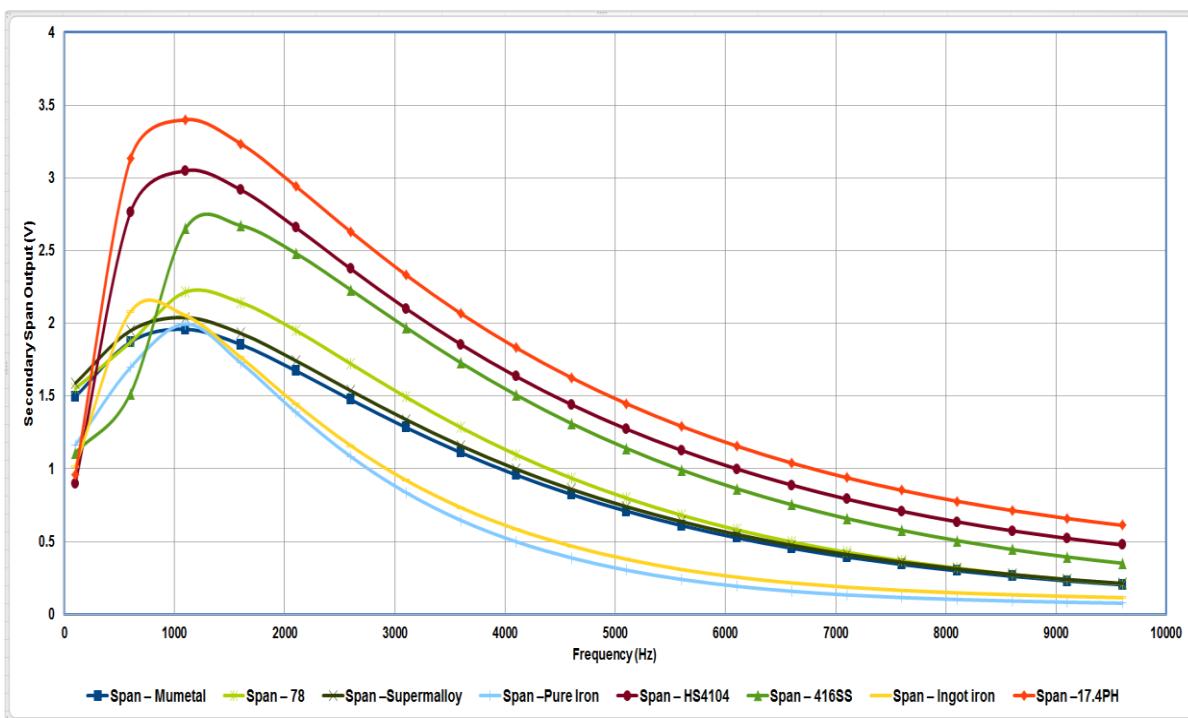


Figure 58 Span of the TIRPI with un-optimised bobbin size

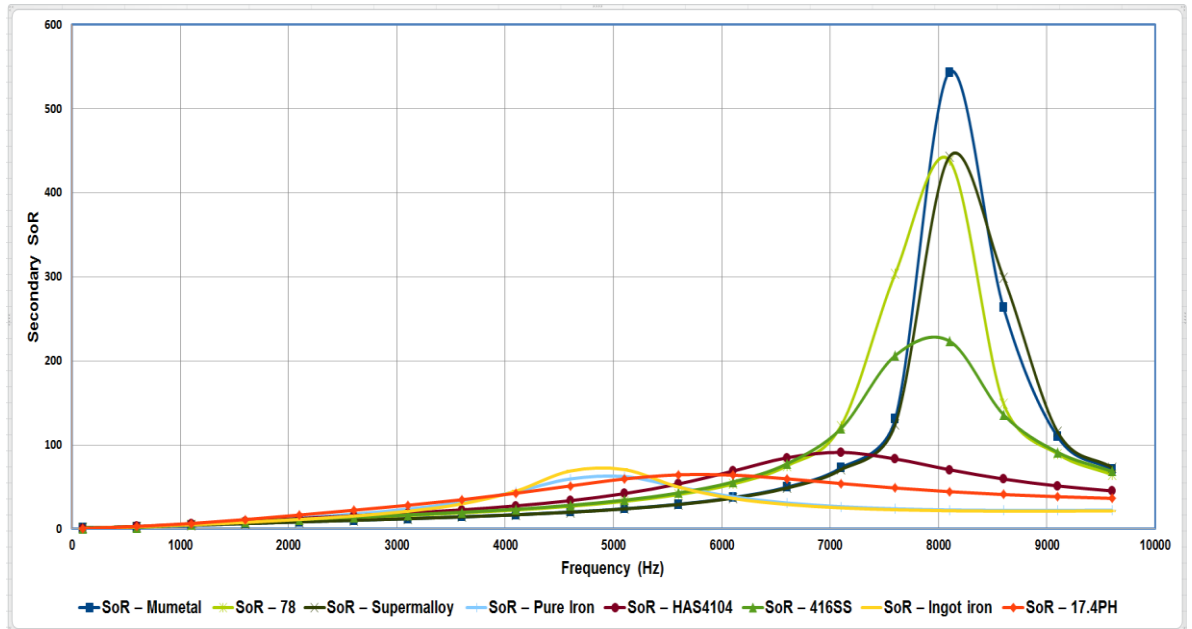


Figure 59 SoR of the TIRPI with un-optimised Bobbin Size

6.2.5 CRDM electro-magnetic analysis

Within an electro-magnetic circuit the frequency of the source signal has a significant effect on the operation of the component or device. Eddy currents are induced in most conductive materials, which can then interact with the magnetic characteristics of the component. The TIRPI is such a device as it is energised by a source alternating current at a particular frequency. In addition, the environment where the TIRPI is housed is also an electro-magnetic environment as it includes a large motor that operates large, moving rotor arms. To ensure an optimised source frequency value for the TIRPI design, an analysis of the CRDM motor effects and the TIRPI source current effects need to be undertaken.

An ideal method to analyse these effects would be to use a three-dimensional finite element modelling tool providing the material data valid. However, this would require considerable efforts and could not be completed within the time frame of this project. An alternative method would be to use a two-dimensional axisymmetric modelling tool, accepting the fidelity of the results would not be as good as those given by the three-dimensional modelling tool. Although the fidelity of the result would be reduced, the result should show an approximate frequency range that the design should be designed to. Using the two-dimensional axisymmetric modelling tool would require two separate

models to determine the electro-magnetic effects in the vicinity of around the CRDM. However using an birds-eye planar 2D model will determine whether any of the magnetic field produced by the CRDM will be present within the vicinity of the TIRPI and in addition provide a CRDM basic material arrangement model, which evaluates the TIRPI source magnetic field as part of the CRDM environment.

However, to increase confidence in the results from the analyses, the two-dimensional finite element tool is only used to model the TIRPI, probe tube and driveshaft. This is a relatively easy setup which can be manufactured on a bench to validate and compare the results against a two-dimensional axisymmetric finite element model of the same arrangement.

A frequency sweep of the TIRPI, probe tube and driveshaft carried out using the finite element modelling tool shows how the TIRPI behaves with different source current frequencies, and how the frequency of the current source signal affects the span output of the secondary output voltage. Ideally one wants to select a frequency which will give the maximum span on the secondary output voltage as this contributes to the sensitivity of the TIRPI output and the ability to detect the driveshaft. The increased secondary output signals from the TIRPI enables the instrumentation card to process the voltage signal more easily and reduce associated errors of the instrumentation card.

As described above, the initial model using only the TIRPI, probe tube and driveshaft was completed and results analysed. Figure 60 shows the 2D axisymmetric finite element model with the magnetic field distribution from the existing primary coils within the TIRPI, probe tube and driveshaft in the minimum position. The magnetic field is also distributed within the surrounding environment (air). The TIRPI secondary output characteristics were plotted against a source current frequency of 100 Hz to 5.9 KHz to determine the response with the driveshaft in the minimum and maximum position as shown in Figure 61. This enabled the span to be determined by subtracting the secondary output of the TIRPI when the driveshaft was within the minimum and maximum position.

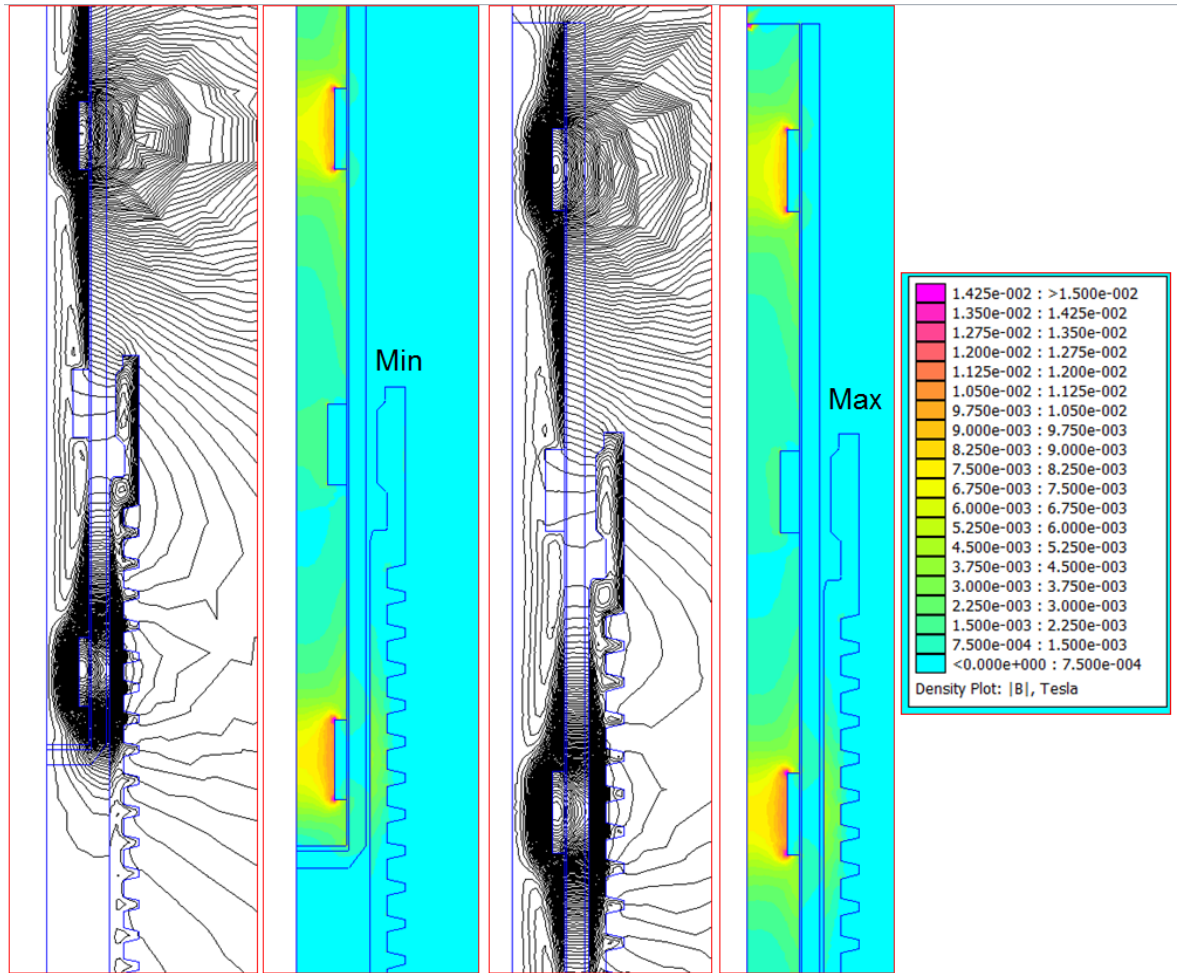


Figure 60 2D axisymmetric finite element model of TIRPI, probe tube and driveshaft in the minimum position and maximum position

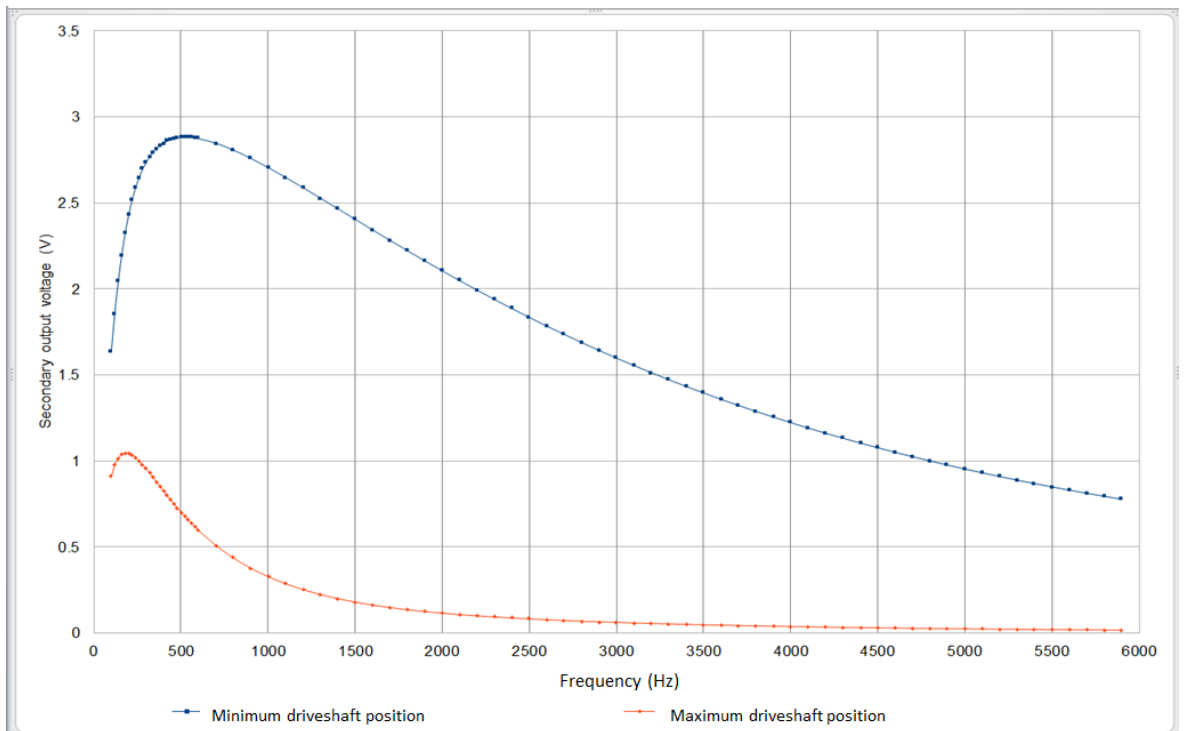


Figure 61 Bench analysis frequency sweep secondary output

Figure 62 shows the span of the bench analysis frequency sweep tests. As the frequency of the current source to the TIRPI increases the secondary output span initially increases and eventually starts to decrease, after peaking at a frequency of approximately 900 Hz. The response characteristic was as expected, as the increasing eddy currents within the materials would eventually cause the output of the TIRPI secondary voltage to reduce as the frequency increases. The analyses show that using a frequency value within the range of 600 Hz to 1100 Hz is the optimum range to achieve the maximum span value of the TIRPI using a bench setup. The bench analysis was subsequently verified by practical experimentation, and thus can validate the fidelity of the modelling tool. The analysis shows the peak value of the TIRPI secondary voltage to be approximately 900 Hz and the practical test results shown later in Figure 109 shows the peak span occurs at approximately 850 Hz. The FE models therefore have predicted the optimum frequency to be within 6% of the value. The finite element modelling tool was concluded to be of sufficient accuracy for use on the TIRPI design.

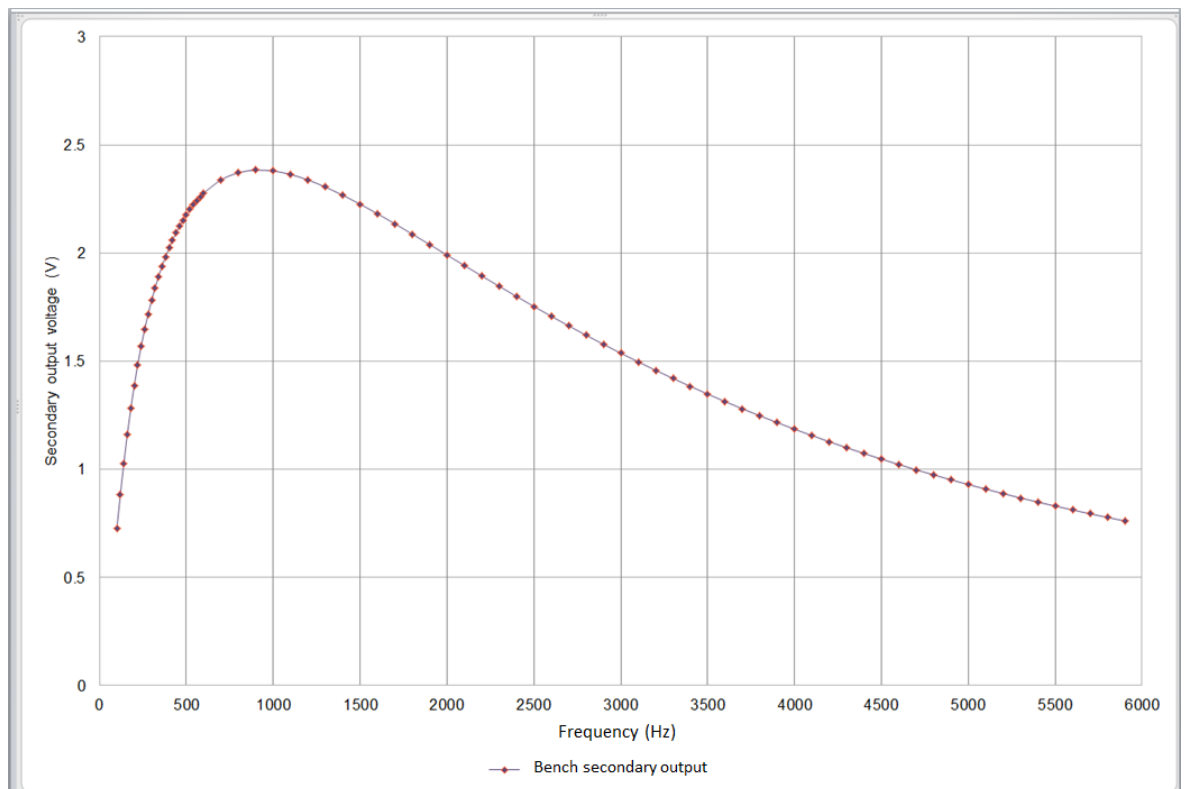


Figure 62 Bench analyses frequency sweep secondary span

The two mechanisms whereby the TIRPI can be affected by magnetic fields are by interference from an externally generated source magnetic field (such as the CRDM), or

any magnetic materials which are close to the TIRPI causing the magnetic field generated by the TIRPI to be concentrated within these regions. These can be evaluated using 2D finite element model that was verified previously by the bench analyses.

Initially, the external source magnetic fields from the CRDM stator were analysed to determine whether these physically come close to the TIRPI, probe tube or driveshaft. In addition, it was important to determine the magnitude of the magnetic field as this would also determine whether there would be any significant impact on the TIRPI compared to its own magnetic field from the source current.

Figure 63 shows the 2D planar finite element model of the CRDM where the TIRPI is housed. The CRDM stator generates a magnetic field which is used to energise and move the rotor arms into place. As the magnetic field rotates, the rotor arms follow the magnetic field as it rotates around the stator. Looking at Figure 63, the magnetic field of the stator does not interact within the TIRPI location and is contained predominately in the rotor arms. This was expected as the rotor arms are made of a highly permeable material to enable the CRDM to apply torque and radial force to lift the control rod with the driveshaft. From the analyses, it is concluded that the external CRDM stator magnetic field has a negligible effect on the TIRPI secondary output characteristics, and these are therefore not considered a significant factor in terms of magnetic interference illustrated within Figure 63.

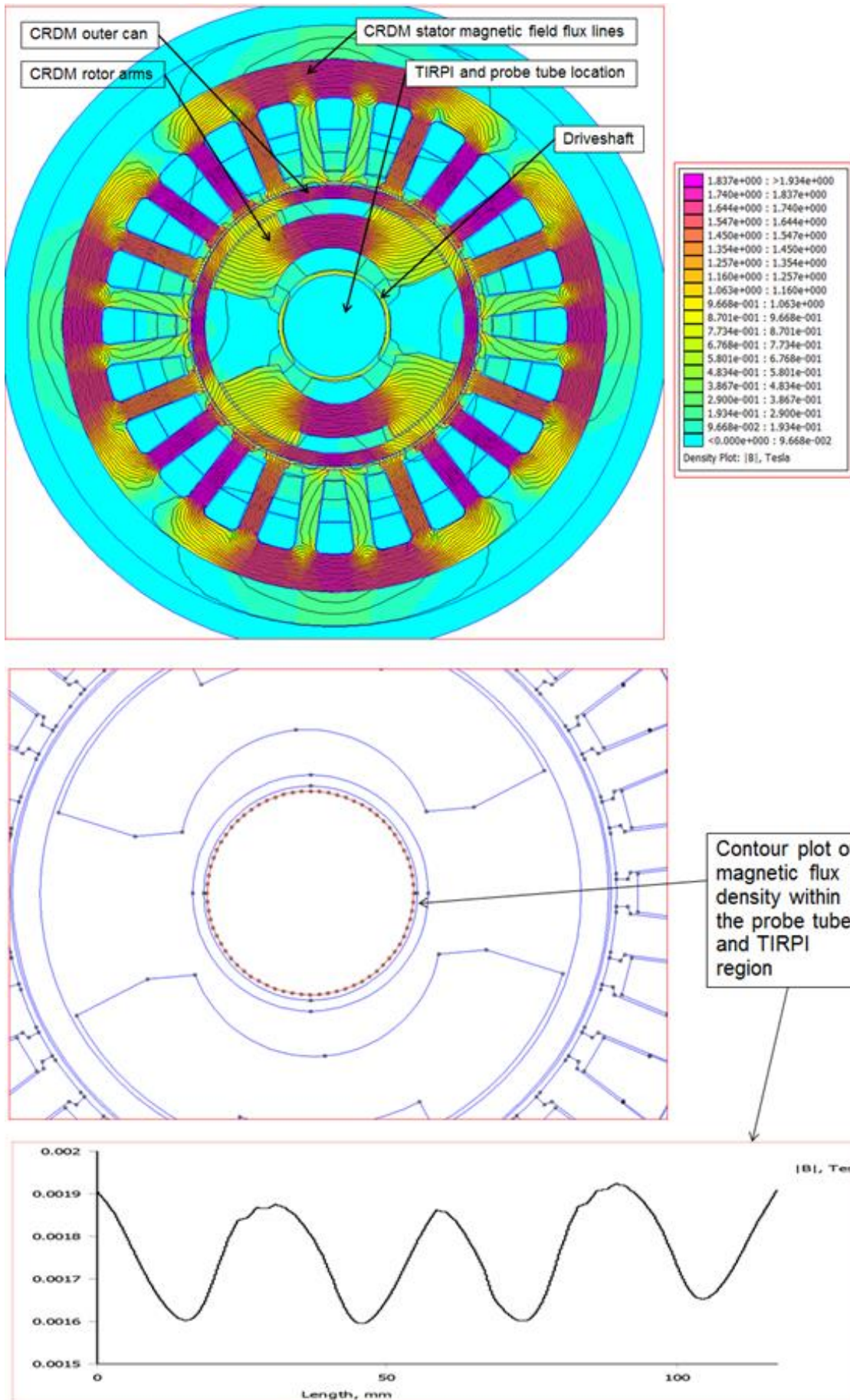


Figure 63 CRDM stator 2D planar finite element model

In addition to the external interference from the CRDM stator, the TIRPI source magnetic field effects need to be considered. From the previous analyses, the optimum frequency for the maximum secondary output span is 900 Hz. However, when the TIRPI is placed within the CRDM stator it is possible that the TIRPI source magnetic field may interact with the material in its environment.

The 2D axisymmetric finite element tool was used to determine how the surrounding environment would affect the TIRPI secondary output when changing the source current frequency. A simplistic geometry model was developed as the CRDM is a complicated piece-part machine and it would not have been practical to develop a like-for-like representation in the 2D finite element modelling tool. Although a simplistic model was used, the significant materials surrounding the TIRPI and the CRDM were included. These materials were presumed to be the significant components which could affect the TIRPI secondary output span characteristics. In addition, as a result of the previous 2D planar analyses of the CRDM stator model which showed negligible interaction from the stator, the CRDM axisymmetric model was developed using a bulk copper material without current flow that would create a secondary magnetic field source. This enabled the CRDM assembly to become part of the TIRPI sensing circuit and to interact only with the magnetic field from the TIRPI only.

For illustration, Figure 64 shows the CRDM assembly model using the 2D finite element asymmetric model. For the purpose of the model, it has been assumed that the CRDM is radially symmetrical. However, in practice this assumption is not accurate. This assumption will reduce the fidelity of the analysis. However, it is expected that the analysis will show the worse-case secondary output magnitude and span from the TIRPI to be within +/-10% of the actual values in practice.

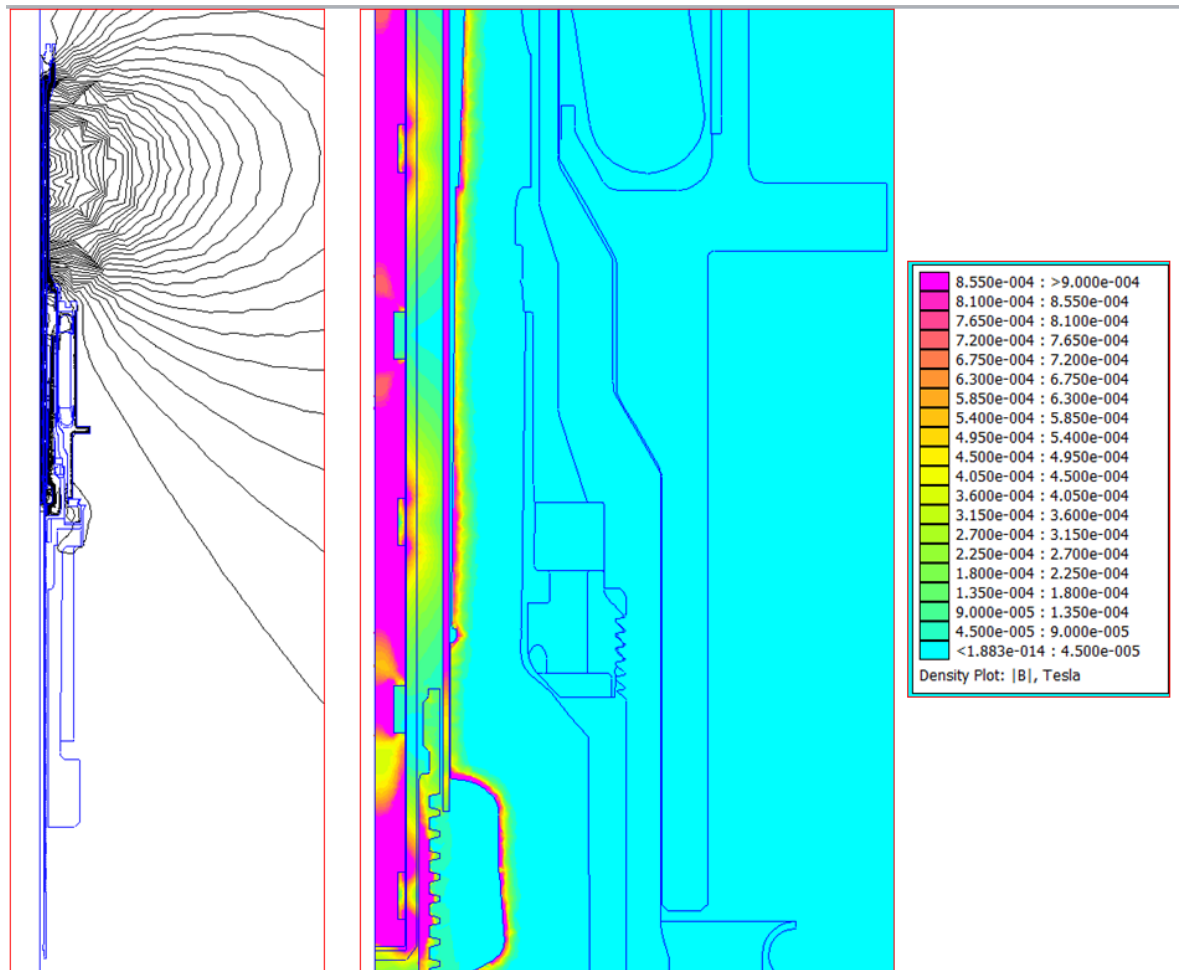


Figure 64 CRDM analyses frequency sweep 2D axisymmetric finite element model

Figure 65 shows a zoom sketch of the 2D axisymmetric finite element of the CRDM combined with the TIRPI, probe tube and driveshaft. It can be seen from the sketch that the TIRPI magnetic field distribution penetrates with the surrounding materials that make up the CRDM and particularly those that make up the rotor arms. This result is as expected, as the rotor arms are highly permeable to allow the CRDM to operate correctly. In addition, Figure 65 shows the magnetic field penetrating the driveshaft through to the rotor arms. This will also affect the secondary output signal and span performance of the TIRPI. In addition it is observed from Figure 65 the rotor arms show small magnetic loops, it is assumed that these are a results from the finite element discretisation and are actual indicating the build-up of eddy current on the rotor arm edge.

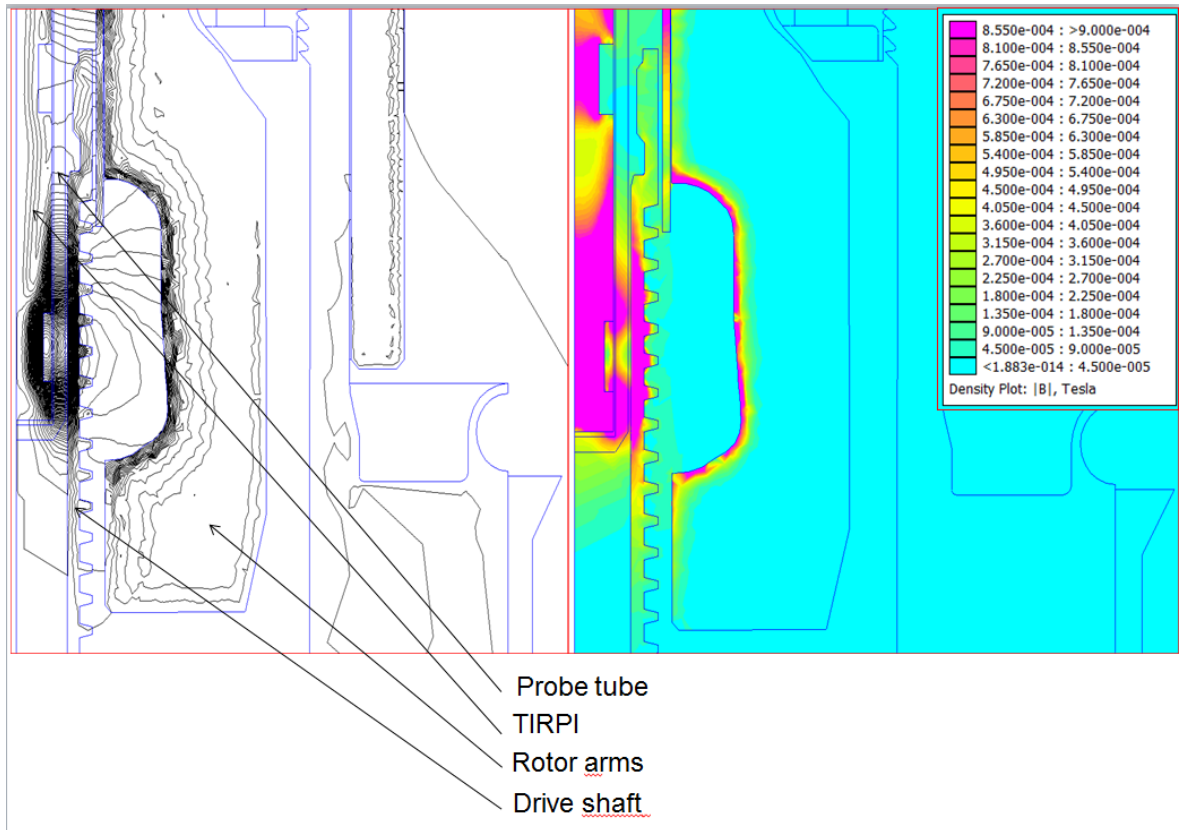


Figure 65 CRDM analyses frequency sweep 2D axisymmetric finite element model

A frequency sweep similar to the previous analysis was carried out using the 2D axisymmetric finite element model. This will determine the changes introducing the CRDM materials around the TIRPI environment and their effect on the secondary output signal and span. Figure 66 shows the results obtained for the minimum and maximum positions of the driveshaft. The general trend of the output has a similar shape to the bench analyses produced previously; however, the amplitude of the secondary output signal has been reduced by approximately 30%. In addition, the peak frequency for both the minimum and maximum driveshaft positions has reduced. This is a cumulative effect of all the components that were affected by the TIRPI source magnetic field.

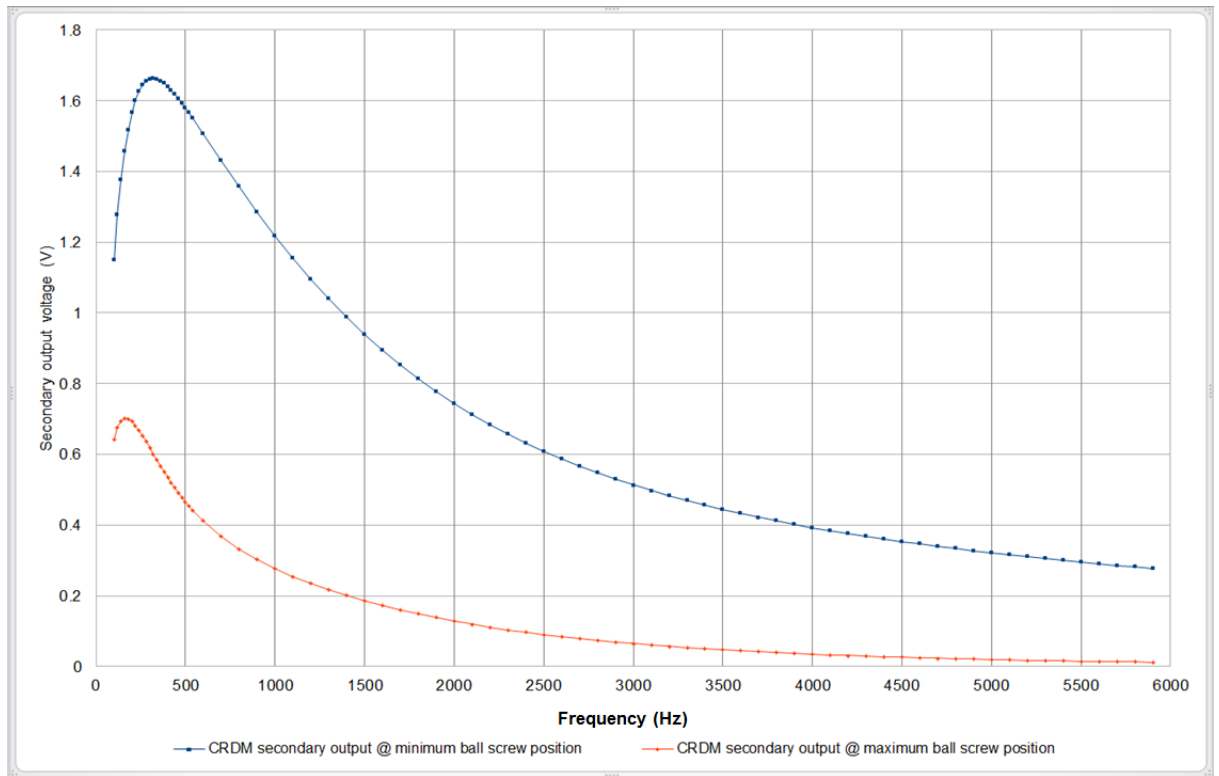


Figure 66 CRDM analyses frequency sweep secondary output

The most significant parameter of interest in the analysis is the secondary output signal span. The greater the span, the greater the signal the instrumentation card will have to process. As a result, the accuracy of the system will also increase. Figure 67 shows the secondary output signal span of the TIRPI within the CRDM. The analysis shows the peak amplitude occurs at a frequency of 480 Hz. This is only an approximate value as the geometry of the CRDM in the model was a simplistic representation of the actual CRDM component. The results from the analysis shows lower frequencies will give greater secondary output signal span values at higher frequencies. A rough order of magnitude value for an optimum frequency of the TIRPI would be 500 Hz. This would be verified when the prototype TIRPI was built and tested.

It is important to note that the 2D axisymmetric finite element analysis can only be carried out when the TIRPI is at room ambient temperature and not at its actual in-service operating temperature unless the materials characteristics can be tested to give the correct B-H curve and conductivity parameters for the model at the operating temperature. In practice, the TIRPI will be subject to a thermal gradient across its length. An assumption was made that the optimum frequency of the TIRPI would not deviate significantly with the introduction of a thermal gradient across its length.

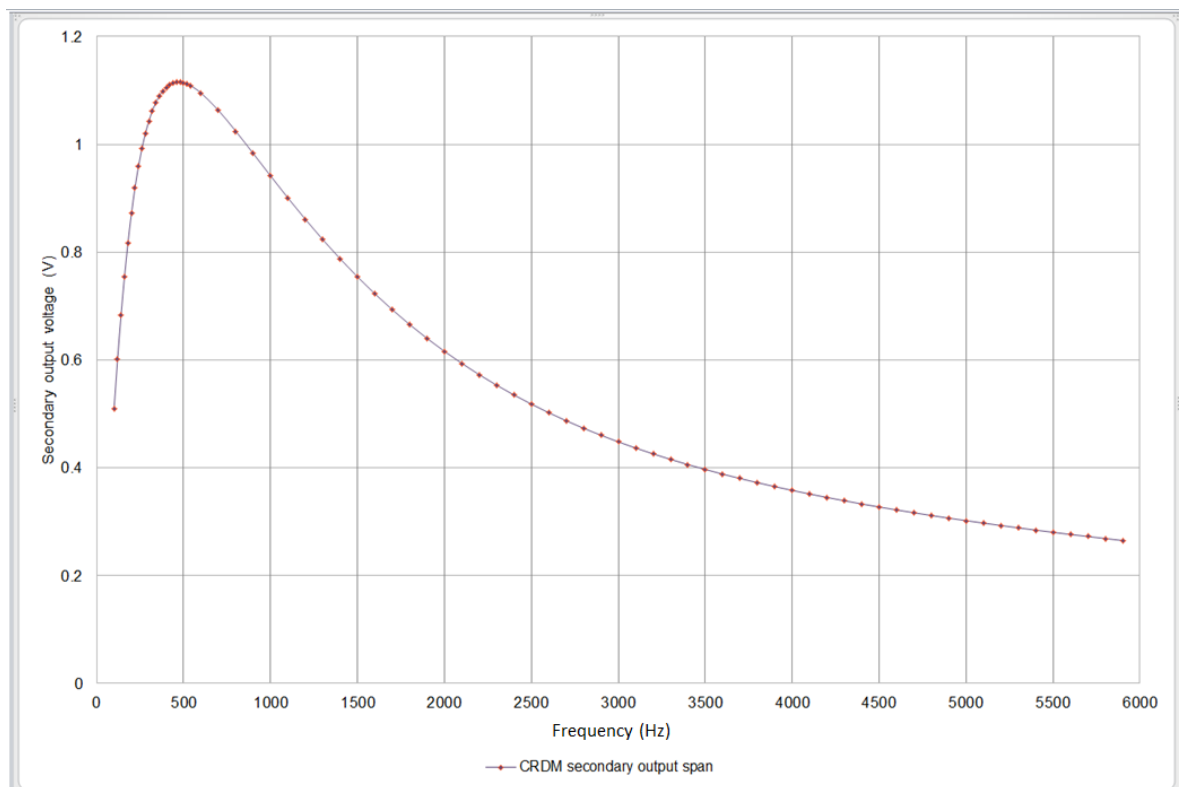


Figure 67 CRDM analyses frequency sweep secondary span

The results from the finite element model can only be verified by manufacturing a prototype TIRPI and testing its characteristics within an actual CRDM component. The data from the testing phase will confirm whether the finite element tool has predicted the characteristics of the TIRPI with sufficient accuracy. The results of the experimental tests carried out are shown in the following chapters.

The characteristics observed in Figure 66 and Figure 67 is a function of the CRDM and TIRPI system, where the response is a combination of the magnetic interactions of all the components in the system. However, it would be useful to understand whether or not the TIRPI makes a significant contribution to this overall response. Although the amplitude of the TIRPI secondary output signal is lower than that obtained during the bench and CRDM tests, the general characteristic shape is similar. This suggests that the shape of the characteristic shown in Figure 67 is dominated by the TIRPI magnetic core. The 2D axisymmetric finite element analysis tool could be used to do a sensitivity study to observe the effects of changing individual components, giving even greater confidence in the hypothesis.

6.2.6 TIRPI cable capacitance model

Parasitic capacitance is unavoidable capacitance which occurs in an electrical circuit due to the close proximity of the conductors. Inductors have parasitic capacitances between each winding turn. The value of the reactance depends on the value of its source frequency supplying the inductor. At low frequencies, the parasitic capacitance is negligible and is generally considered to be zero.

The TIRPI would normally be connected to a long cable before it is connected to the instrumentation electronics. The cable would be approximately 100m long then cut to size and located in the harsh environment. The cable would be constructed from multiple of layers of materials to help it survive in the service environment. These materials act as dielectrics between the conductors.

A finite element electrostatic cable analysis was used to predict the cable capacitance of the TIRPI and whether the value would have a significant effect on the TIRPI resonant frequency value. This should be avoided as electrical ringing could occur and cause errors in the TIRPI secondary output signal. The maximum voltage applied to the cable by the TIPRI was assumed to be 5.5V rms, and the maximum cable length was assumed to be approximately 25 meters. For the purpose of the analysis a 30 metres cable length value was used to allow for any analysis errors. The FE 2D planar electrostatic model shown in Figure 68 gives the cable charge and voltage applied per core pair. The capacitance of the core pair is defined as the charge divided by the voltage on the cable producing a cable capacitance value of 10nF per core pair.

The FE modelling showed the capacitance values do not cause a resonant condition when an AC current source is connected to the TIRPI at the frequency chosen.

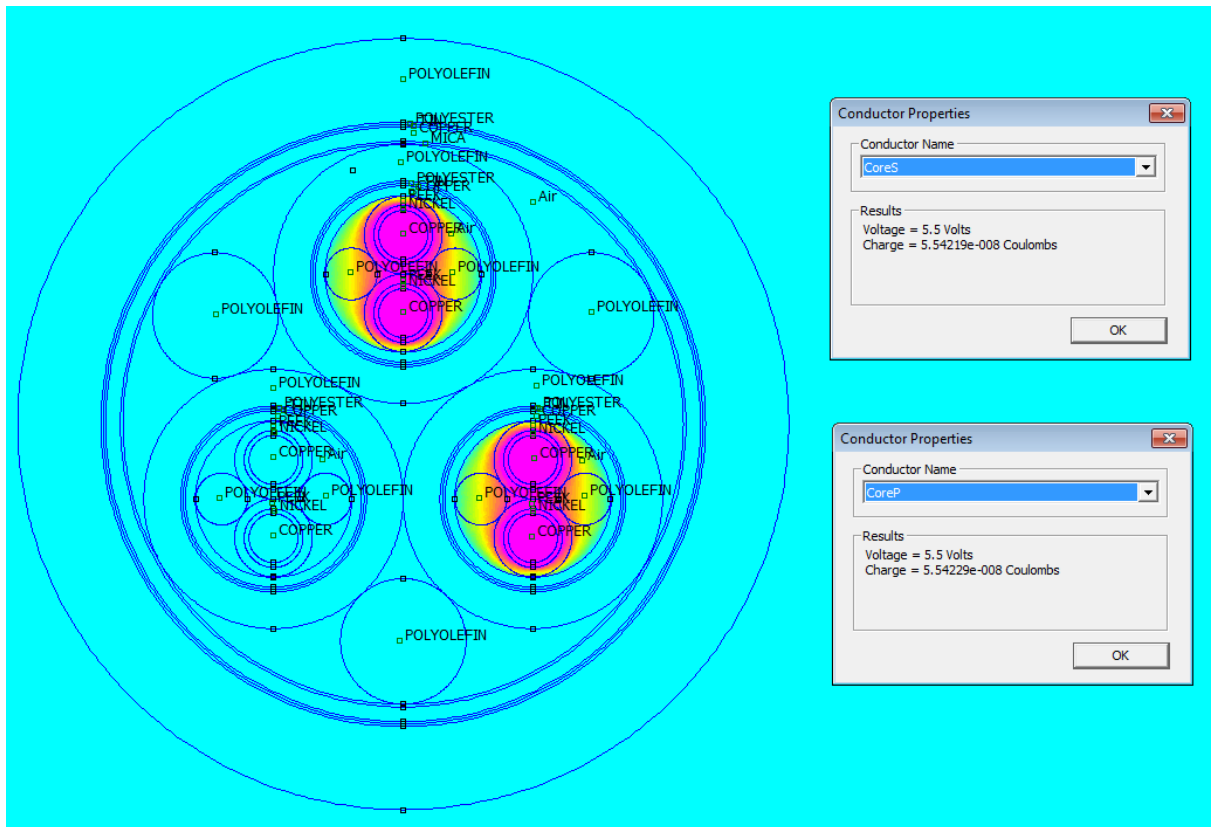


Figure 68 TIRPI cable

6.2.7 Power factor of TIRPI

AC circuits have resistive and reactive components which produce current and voltage phase shifts. The real and reactive power representation of the TIRPI can be shown using a phase diagram shown in Figure 69. The power factor of the system is represented by the phase angle, theta. It is normal to try and keep the power factor as close to unity as possible.

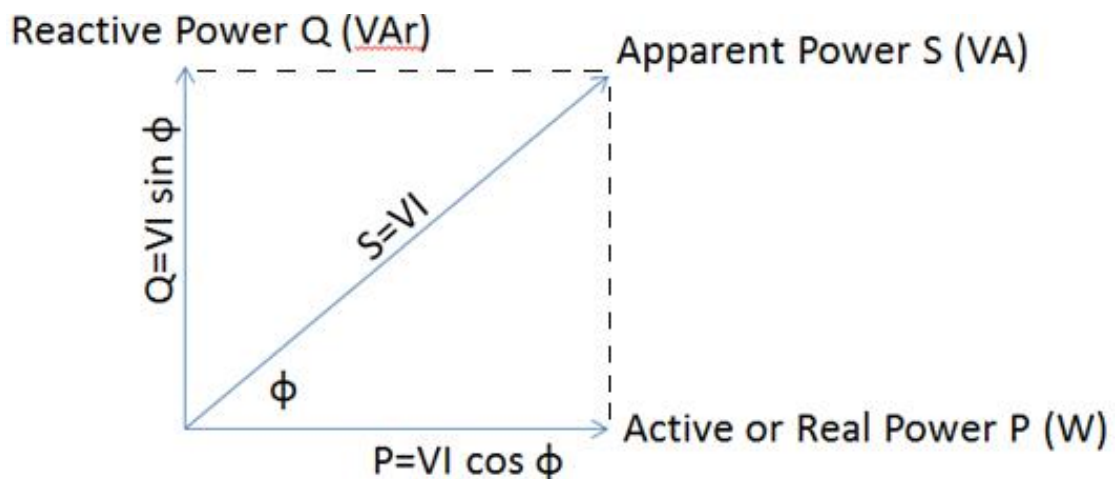


Figure 69 TIRPI power phase diagram

To determine the power factor of the TIRPI system and its individual components, the finite element modelling tool was used. The model provides the Real, Reactive and Apparent power values for the individual components which can be used to calculate the overall efficiency of the TIRPI. Table 3 shows the simulated result for the TIRPI core, primary coils and secondary coils. The results show the TIRPI with the probe tube and at the driveshaft at minimum and maximum positions. The active or real power value is known as the efficiency of the system as this gives an indication of the useful energy in the system. The results show the TIRPI power factor is between 0.719 and 0.748.

Table 3 Power efficiency of TIRPI

Power	Driveshaft at 0%	Driveshaft at 100%
Real (W)	0.245959	0.25993
Reactive (VAr)	0.217798	0.250707
Apparent (VA)	0.32853	0.361134
Efficiency (Real (W) / Apparent (VA))	0.748	0.719

The analysis was repeated for the CRDM. The modified efficiency was re-calculated, and it was found to have increased to a value between 0.815 and 0.821 as shown in Table 4. The change in magnetic loading with the CRDM materials has in this case increased the power efficiency of the TIRPI within the CRDM.

Table 4 Power efficiency of TIRPI within an CRDM

Power	Driveshaft at 0%	Driveshaft at 100%
Real (W)	0.32129	0.332135
Reactive (VAr)	0.222627	0.236009
Apparent (VA)	0.390883	0.407447
Efficiency (Real (W) / Apparent (VA))	0.82195	0.81516

Chapter 7

7 Design Optimisation Process

The following chapter describes the sequential steps used to design a TIRPI with an optimised span and linear secondary output voltage.

It is important to understand the initial requirements and constraints for the design before starting the design process as these will determine the final engineered solution. The sequence of events to ensure a suitable set of initial requirements is derived for the TIRPI is shown in Figure 70.

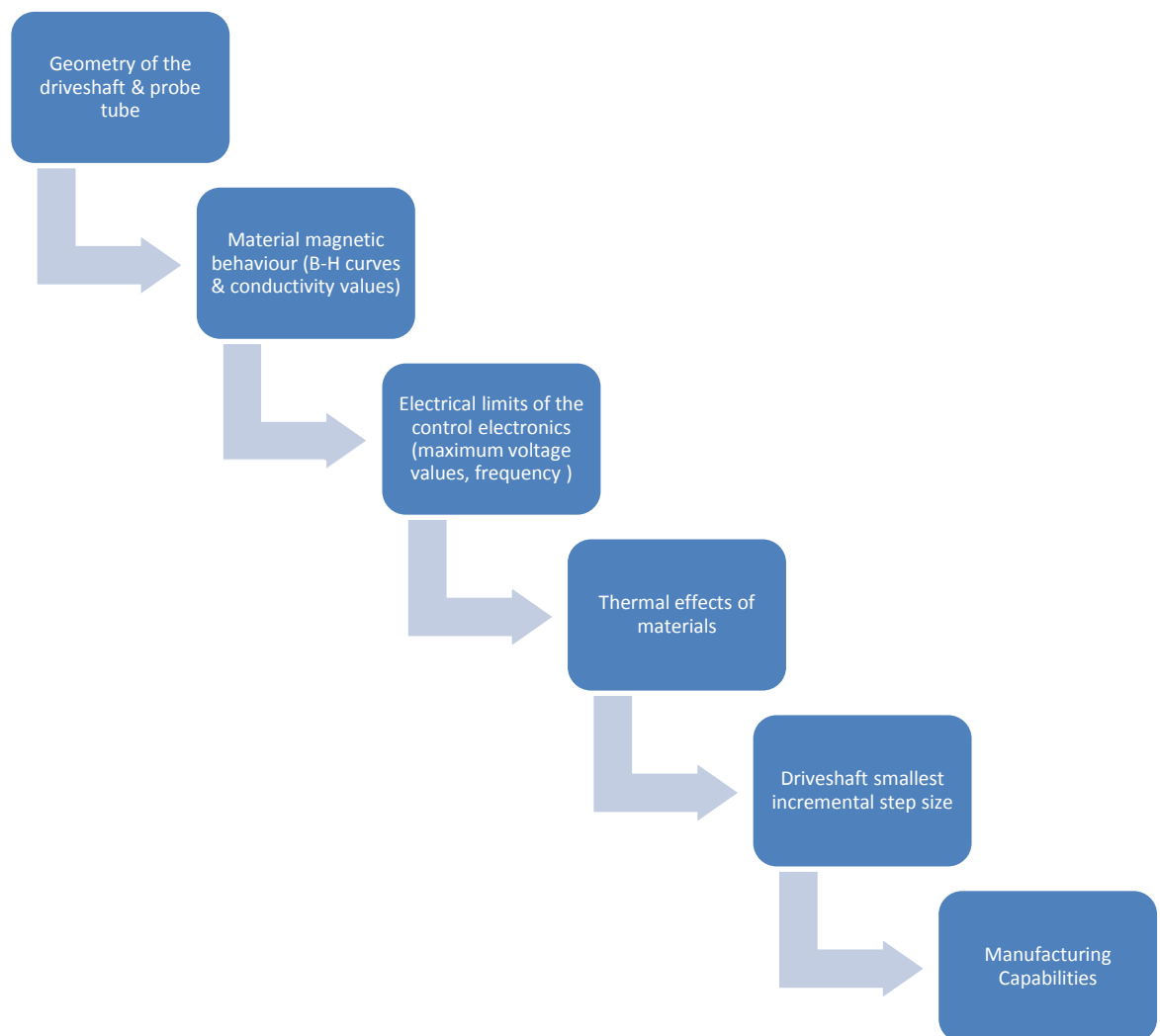


Figure 70 Design optimisation sequence diagram

Following definition of the requirements, the geometry of the probe tube and driveshaft are input to a finite element modelling tool package. It is important to ensure B-H characteristics and conductivity values for all the materials used are defined correctly as these affect the design. Materials should be tested prior to analysis to determine their effects on the electromagnetic fields. This will provide the relevant B-H curve and conductivity values. Following the geometry and material definition, the correct mesh type and sizing is important. In addition, skin effects and source voltage frequency will also need to be considered. A general rule is to have a mesh size three times smaller than the smallest skin depth required for any of the materials used.

After defining the initial modelling conditions, the model software tool can be run manually. Alternatively it is possible to develop a macro within a FEMM-supported environment such as LUA to run the FEMM commands in a sequential manner. This reduces analysis time significantly when doing repeat analyses at different driveshaft positions.

Once a characteristic curve has been developed from the FE software, an Excel software package can be used to determine the span and linearity of the data. Initially, the data will consist of two points for the smallest driveshaft increment ensuring all driveshaft positions are analysed. This ensures that the peaks of the data characteristics are all included and the result does not give a false linearity due to large step increments from the driveshaft. It was found that using the cubic spline fitting function in the excel software package enables larger driveshaft increments to be used instead of the smaller 0.13mm increments. This enables the processing time of the analyses to be significantly reduced as the driveshaft increments could be increased to 10mm instead of 0.13mm.

It is important to be aware that when the geometry of the item being analysed is changed (such as changes to the spacing size or bobbin size), the maximum output voltage of the primary and secondary outputs also changes. These changes will also affect the span and linearity of the analysis. To address this issue the primary and secondary wire turns on the TIPRI need to be changed until it equals a selected secondary output voltage value every time the geometry is changed or redrawn. This will enable a correct comparison of the results to be determined. The initial analysis will need to be configured with the correct

number of primary and secondary wire turns on the TIRPI prior to running the analysis as the instrumentation control electronics has a maximum voltage limit. These voltage values will be the maximum values present on the primary coil and secondary coil when interfaced to the control circuit as they decrease when the driveshaft envelopes the probe tube.

The size of the spacing and bobbin can be incremented as necessary; it is prudent to make the changes to these as small as possible as this will give more accurate results for span and linearity. However, this is at a cost of increasing the number of iterations and the solution time so the increment size should be adjusted accordingly.

The TIRPI exhibits coil end effects as the driveshaft moves towards the end windings. This is due to the changing magnetic field within these areas. These areas should be avoided when the TIRPI is in use as the span of the TIRPI is reduced in these regions significantly. As the space between the bobbins and bobbin sizes change, the location of the end effects will also change and these should also be considered. To determine the actual span and linearity of the TIRPI without the end effects being considered, suitable locations are determined on each TIRPI secondary voltage characteristics curve as shown in Figure 72. The span can then be calculated as a ratio of the span divided by the a predefined distance. Using this method helps to achieve the correct optimised solution. A practical start size for the TIRPI spacing and bobbins must be determined initially and this must be treated as the datum. By understanding the manufacturing process for the TIRPI allows an initial design to be determined which can be manufactured in a repeatable production sequence. If only a single unit is being developed, this is not as important. However, it is good practice to keep any design concept as simple as possible. If time permits, a number of prototypes could be manufactured and compared to the models to improve the FE modelling fidelity and further improve the optimisation process. However, this will result in carrying out many solutions where the benefits of optimisation gained are less than the amount of time and cost invested.

Following the sequence of process events described above the TIRPI design parameters for the TIRPI bobbin spacing and bobbin sizes were established.

7.1.1 Driveshaft increment size analyses

To reduce the time taken to define the TIRPI design, the excel software cubic spline fitting function was used to infer the TIRPI output characteristic curve. To show this method was feasible, a FE analysis using 0.13mm ball screw increments was compared to solution for 1mm and 10mm ball screw increments. The output curves were inferred using the cubic spline fitting function. The results showed that the three curves using the different methods gave comparable secondary output voltage characteristics and such a coarse 10mm driveshaft incremental step would still give valid results as long as the excel cubic spline fitting function is used to fit the TIRPI secondary output voltage curve. This causes the time taken per analysis to reduce significantly. Figure 71 shows the results for 10mm, 1mm and 0.13mm driveshaft incremental steps.

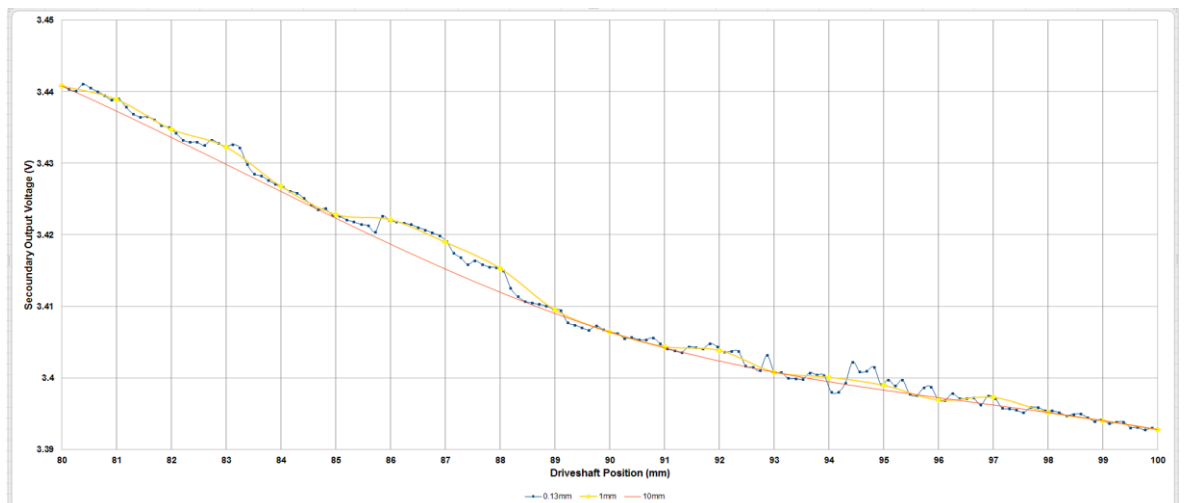


Figure 71 Comparison of driveshaft increment size

7.1.2 Spacing optimisation

The optimisation of the space between the bobbins was achieved by calculating the span and linearity of the secondary output voltage, providing the maximum value for each simulation starts from the same voltage value. This was achieved by adjusting the number of primary and secondary turns on the TIRPI until both output voltages were the same for all the spacing sizes as they are changed. A start spacing size of 41mm was used as this gave a reasonable initial output curve. The number of primary and secondary turns was calculated for the control instrumentation capability. Figure 72 shows a secondary output

voltage of approximately 5V peak to 0.8V peak when a 41mm length was used as the spacing between the bobbins. The figure also shows the winding end effects where the driveshaft has fully enveloped the probe tube. These end effects should not be considered in the analyses as they will falsify the results of the optimisation. Two peak points were selected eliminating the end effects. The process was repeated for spacing values of 41mm, 43mm, 45mm, 47mm, 49mm, 51mm and 55mm.

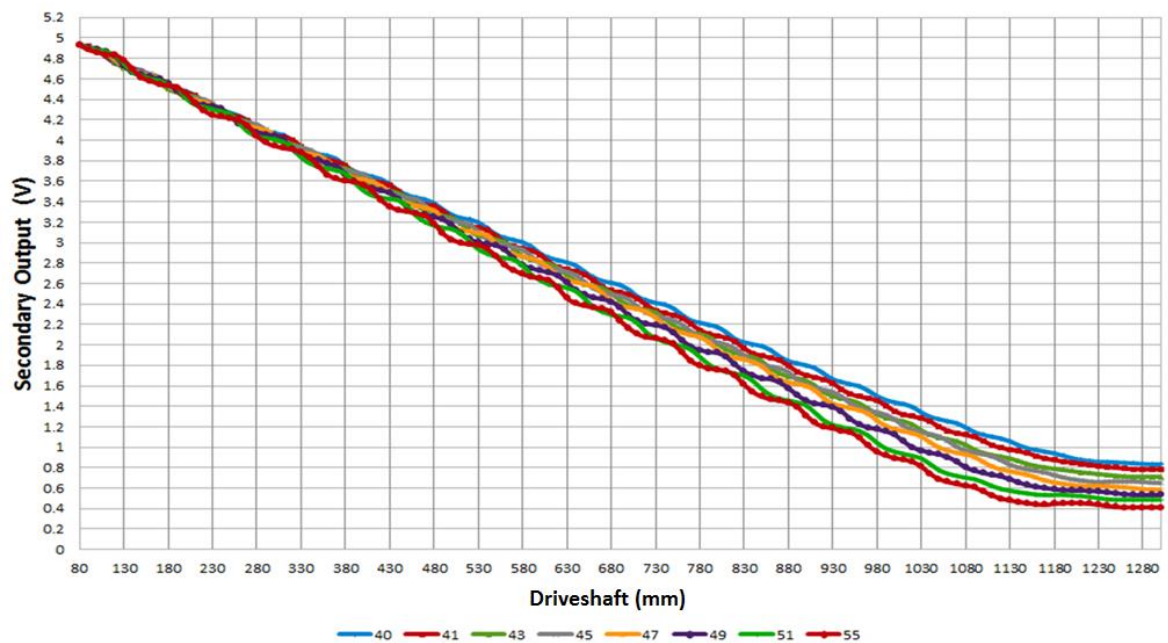


Figure 72 Spacing optimisation

Figure 73 shows the selected regions where the first peak value occurs and the last peak value occurs. It is important to compare like-for-like regions of each curve for the different ranges of spacing lengths to calculate the span values for each secondary output at different spacing values. Due to changes in the spacing length however, changing these peaks will occur at different driveshaft distances. This can be addressed by dividing the span values by the distance between the peaks to give a span per millimetre value. The linearity can also be calculated by using the excel regression function to obtain a value for the best straight line. The linearity was calculated for all the spacing values simulated. The spread of the results can be seen within Figure 73; these however results need to be plotted on a separate graph to determine the maximum peak values of span and linearity. The numbers on the figure indicates the size of the space between the bobbins in millimetres.

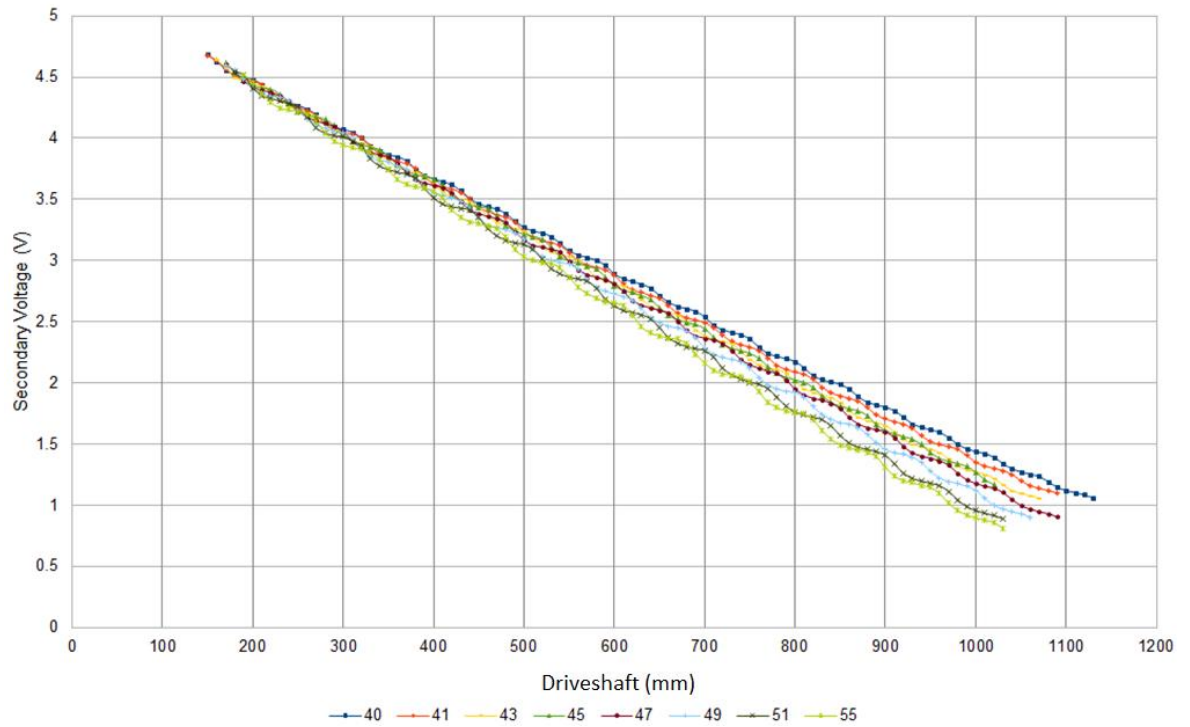


Figure 73 Spacing optimisation

The span and linearity characteristics were plotted as each spacing length was analysed. This determined the proceeding increments of spacing length defined by the trend of the results. The ideal scenario would be to use very small increments of spacing length, but the number of analyses needed would take an excessive time to complete. This option therefore is not practical. The results from Figure 74 show the peak span performance was obtained for a space length of 55mm. However, the results in Figure 75 show the linearity peak performance occurs at a 45mm spacing length. Taking into consideration the importance of span and linearity, the peak performance occurs at a 45mm spacing length. The span is important to maximise the sensitivity of the TIRPI; it is also important however to have a linear response to minimise any flat regions in the curve. The span response shown in Figure 73 shows a relatively large span response, and thus it would be prudent to maximise the linearity of the results. The selected optimised space length was 45mm.

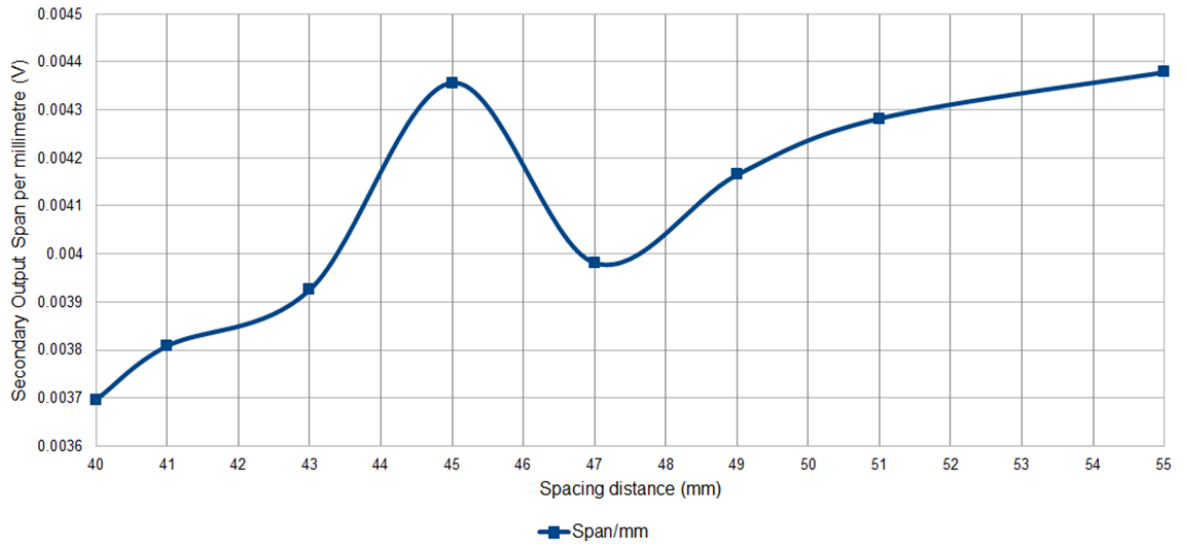


Figure 74 Span spacing optimisation characteristics

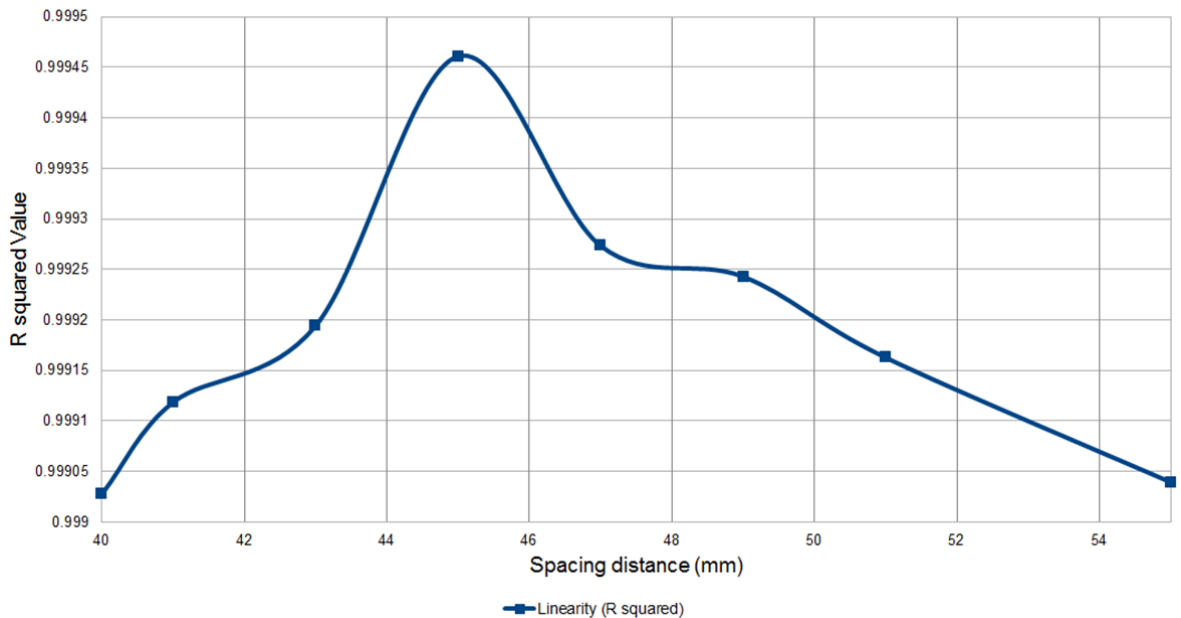


Figure 75 Linearity spacing optimisation characteristics

7.1.3 Bobbin optimisation

Bobbin optimisation followed a similar process as the spacing optimisation to achieve the optimum span and linearity. However, the initial start geometry of the TIRPI bobbin length was changed to accommodate the optimised spacing of 45mm. The parameters of the primary and secondary windings were re-calculated to give the same initial primary and secondary voltages as the spacing optimisation. The bobbin optimisation, bobbin optimisation of selected regions, span optimisation characteristics and linearity optimisation characteristics graphs were produced in a manner similar to that used for the

spacing optimisation above. The results for these characteristics are shown in Figure 76, Figure 77, Figure 78 and Figure 79. The numbers on the figure indicates the size of the space between the bobbins in millimetres.

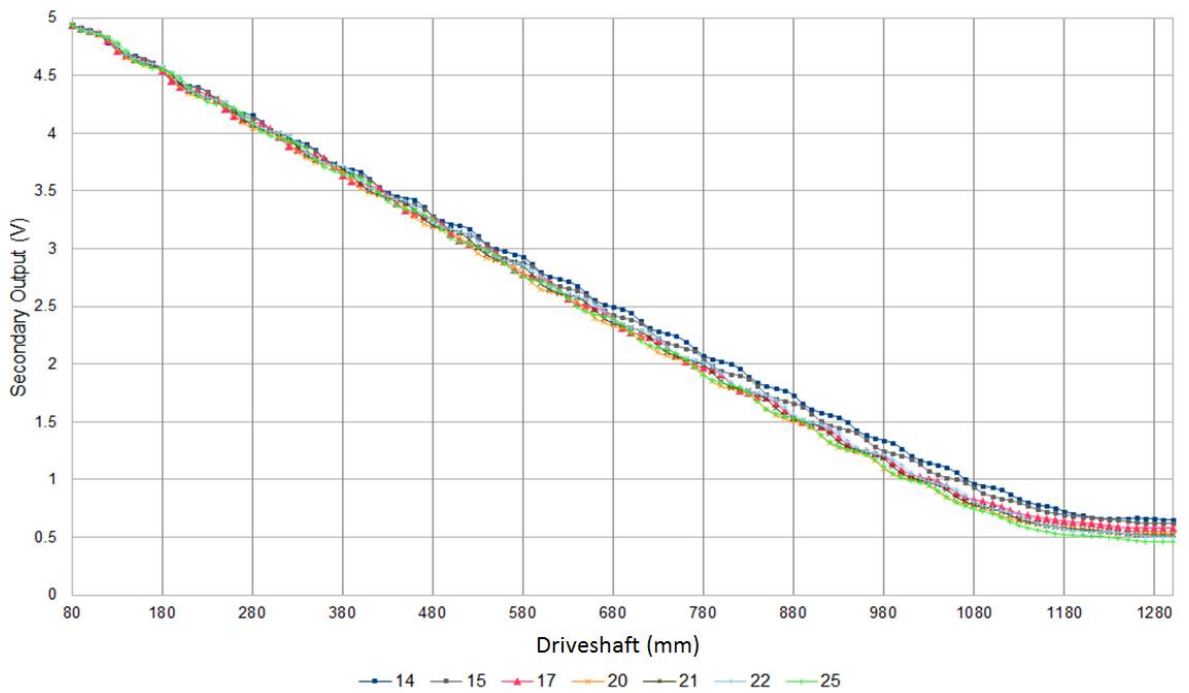


Figure 76 Linearity optimisation

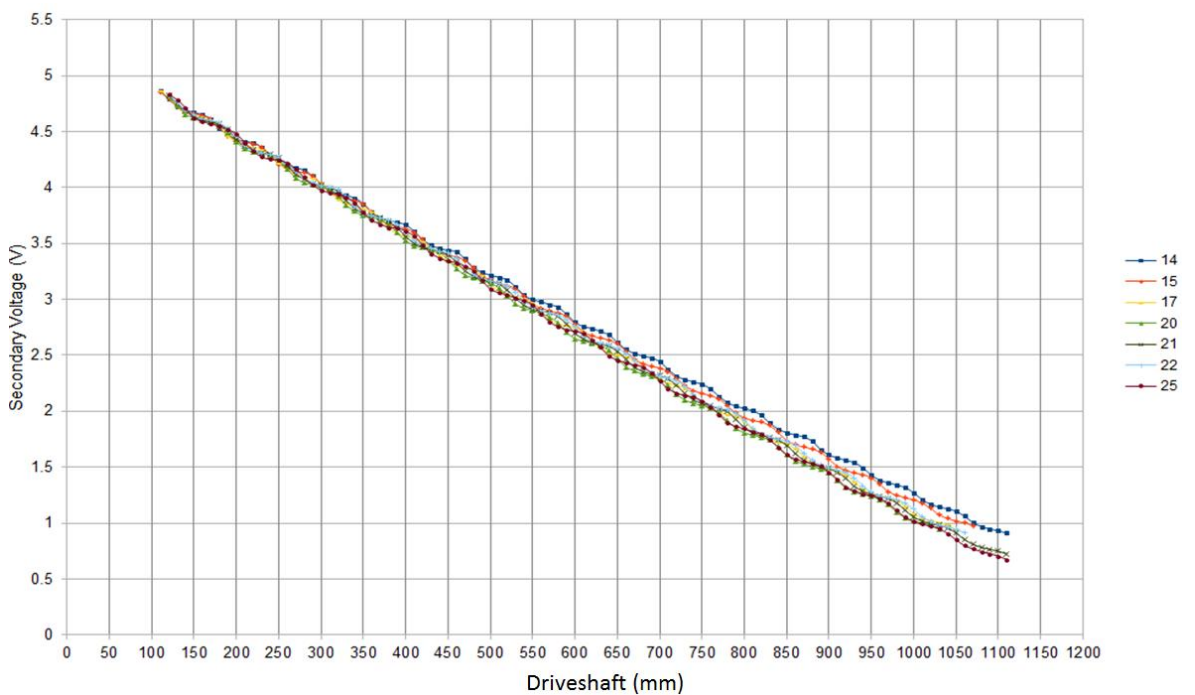


Figure 77 Bobbin optimisation of TIRPI Selected Regions

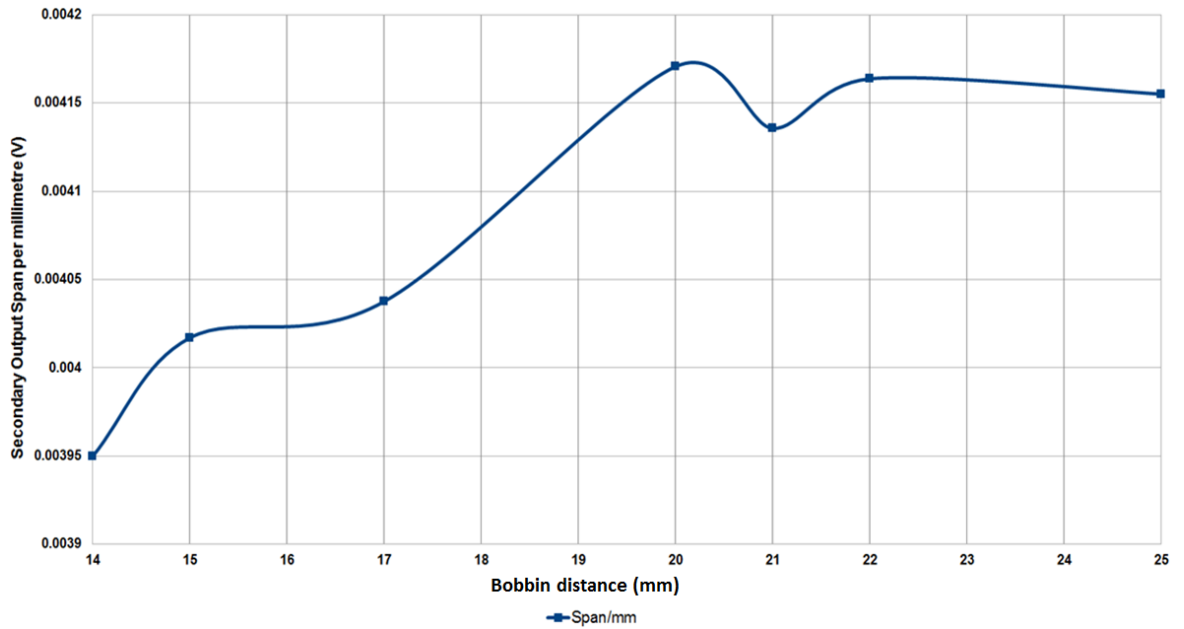


Figure 78 Span bobbin optimisation characteristics

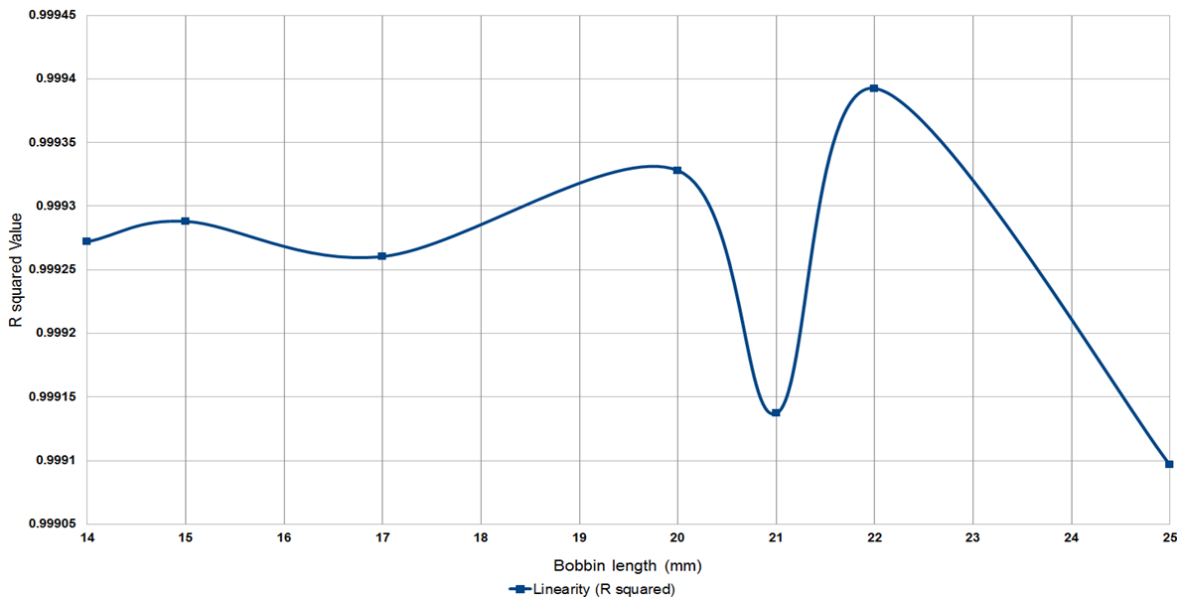


Figure 79 Linearity bobbin optimisation characteristics

In much the same way, the space optimisation trade-off between span and linearity, it can be seen from Figure 78 and Figure 79 that the optimum bobbin spacing is 22mm.

Additional FE modelling could be carried out to give a more accurate value for the bobbin length but this will likely result in the benefit gained from the optimisation being less than the amount of time and cost invested.

7.1.4 **Summary**

This chapter shows how you would optimise the TIRPI design and which parameters to take into consideration. It is important to consider that each of the parameters affects the other so it is important to select which is the important parameter for the design such as the span of the TIRPI secondary output voltage.

Chapter 8

8 Magnetic Sensitivity Analyses

8.1 Core Matching Sensitivity

The fundamental principle of matching the core material of the TIRPI to the driveshaft material is intended to increase the TIRPI sensitivity. The validity of this relies on the magnetic permeability and conductivity of the core and driveshaft remaining constant throughout the period of use. In practice, magnetic variations will occur due to the thermal environment, magnetic materials variations within the CRDM environment and the initial manufacturing of the materials. The thermal variations are compensated for within the instrumentation electronics, and any small variations due to material structure can also be compensated for in the thermal calibration process. However, should the material characteristics change significantly through-life or be significantly different from when the TIRPI was manufactured, the TIRPI will suffer from accuracy errors. This study investigates how much the primary and secondary voltages of the TIRPI would change if the permeability and conductivity of the TIRPI core change through life.

The permeability of the 17.4PH H1100 material used for the core was defined as a B-H curve from an electromagnetic perspective. This is simplified to a single curve for analytical purposes of the modelling software. The B-H curve was constructed by testing a piece of the 17.4PH H1100 material and determining its magnetic characteristics from the results. Although this is assumed to give a typical response, the material tested could show slight manufacturing variations to the magnetic response. To understand how the output of the TIRPI is affected by variation in the core material, an analysis of the percentage of material magnetic deviation was plotted against the actual primary and secondary output voltages. For the purpose of the study, the B-H curve of the 17.4PH H1100 material was changed to plus and minus ten percent of the peak saturation value. This is an excessive variation for the material, but it will give a worse case TIRPI secondary output voltage variation. Similarly, for conductivity variations of 17.4PH H1100,

the conductivity value of the material has been changed by plus and minus ten percent of its nominal value as illustrated in Figure 80.

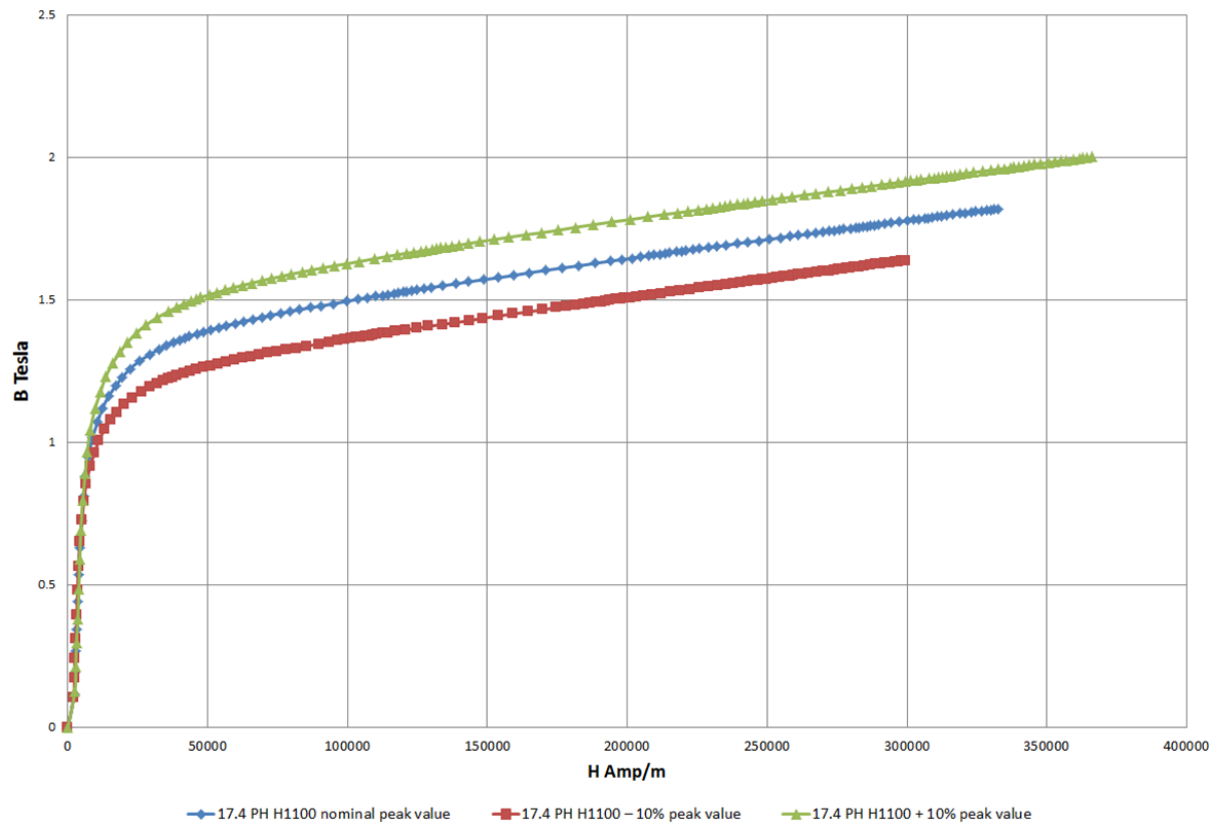


Figure 80 17.4PH H1100 TIRPI core material permeability variation

8.2 Core permeability sensitivity

The assumption of a ten percent variation in the core material permeability was used in the model. This variation includes all initial variations due to manufacturing influences and process variations during machining. The variation has been calculated from the nominal value B-H curve, and a theoretical B-H curve with errors has been developed. The secondary output voltage was compared with the nominal B-H curve and the modified B-H curves illustrated in Figure 81. Figure 82 shows the effects of the core material variation to be a very small secondary output voltage offset error of less than 0.01%. This was considered to be negligible variation, and was not unsurprising as the core material does not operate near its saturation point.

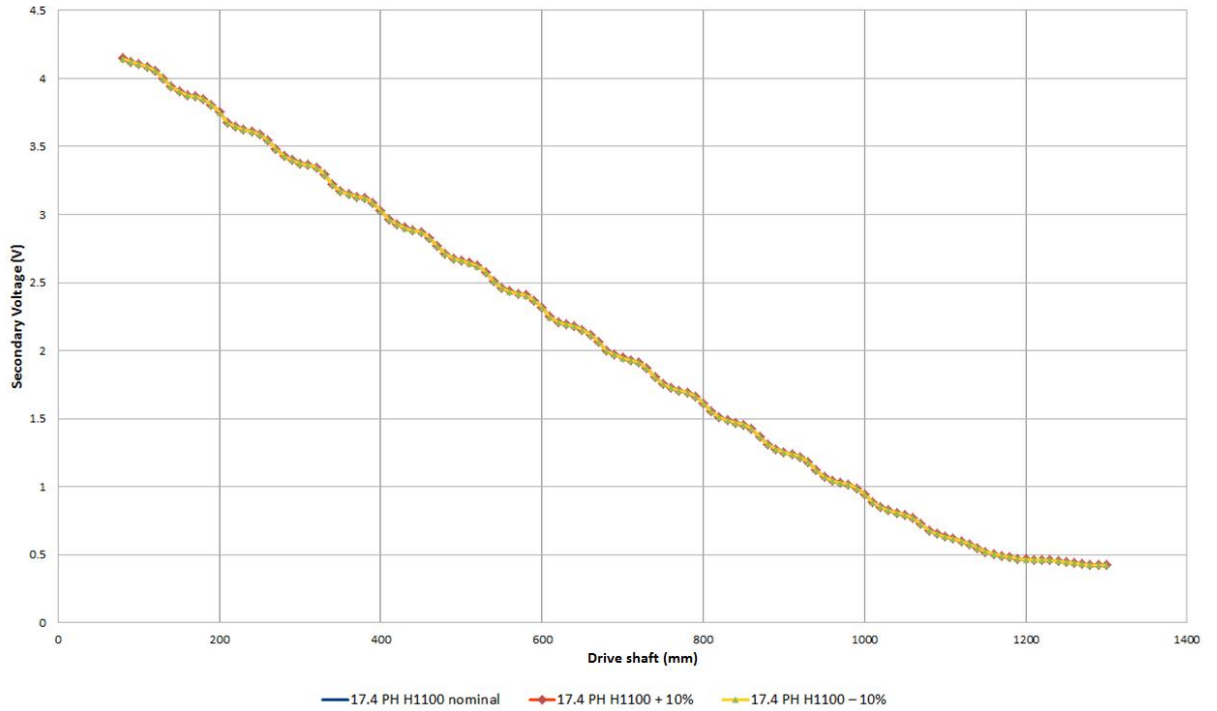


Figure 81 Secondary voltage Vs core material permeability variation

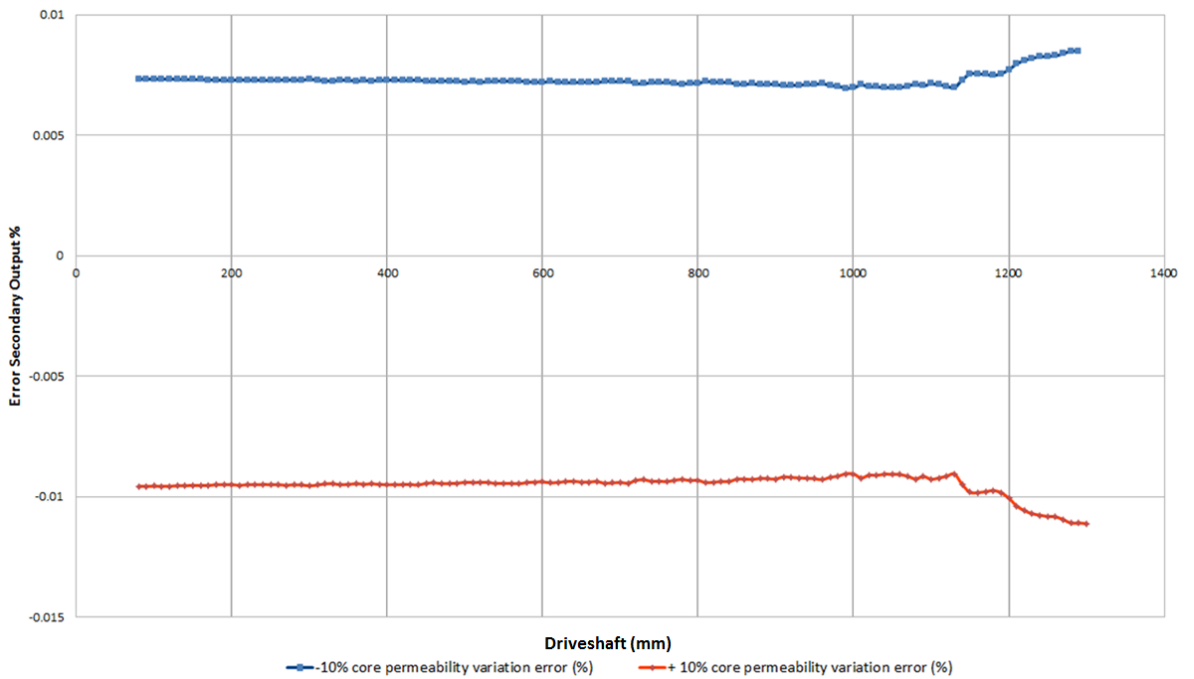


Figure 82 Secondary voltage Vs core material permeability variation error

8.3 Core conductivity sensitivity

In addition to the effects of core permeability variation, the core material conductivity also needed to be modelled to determine the secondary output voltage when the core conductivity varies using a tolerance of plus and minus ten percent. In a manner similar to the core permeability variation above, the nominal conductivity value of 1.45MS/m was changed in the FE model to 1.305MS/m and 1.595MS/m corresponding to the ten percent

variation. The results showed that the secondary output voltage of the TIRPI relied significantly on the conductivity of the 17.4PH H100 core material. However, a major deviation detected during the TIRPI testing cycle after machining could be compensated for within the control electronics providing the deviation remained constant after calibration. Should the conductivity of the TIRPI core change after calibration, but not as a result of thermal effects, the secondary voltage output will give a significant output error as this type of variation cannot be compensated for in the electronics. Figure 83 shows the secondary outputs for the nominal conductivity values, and plus and minus ten percent. It shows a significant span difference, which will result in a significant error in accuracy.

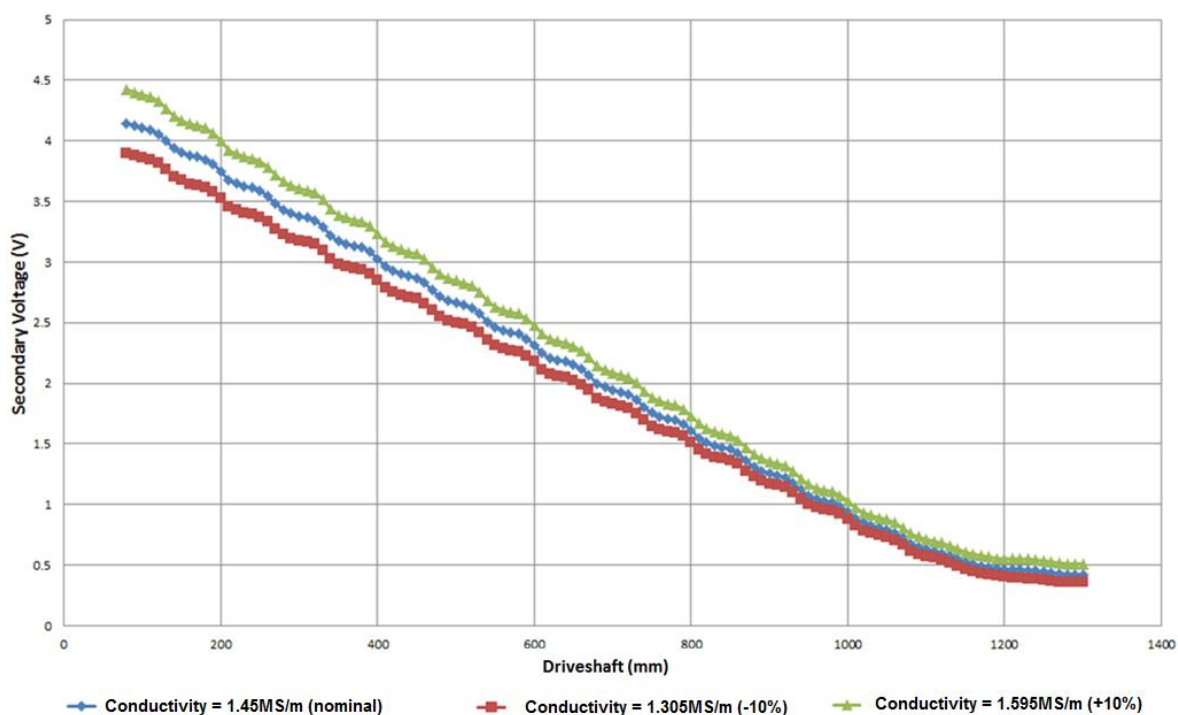


Figure 83 Secondary Voltage Vs Core Material Conductivity Variation

Figure 84 shows the secondary output voltage error as a percentage of the secondary output voltage. The graph shows the errors becoming greater after the driveshaft has enveloped the probe tube at a position of 1000mm. This is due to the end effects of the coils amplifying the errors; however in practice the driveshaft would not travel to the end of the coils.

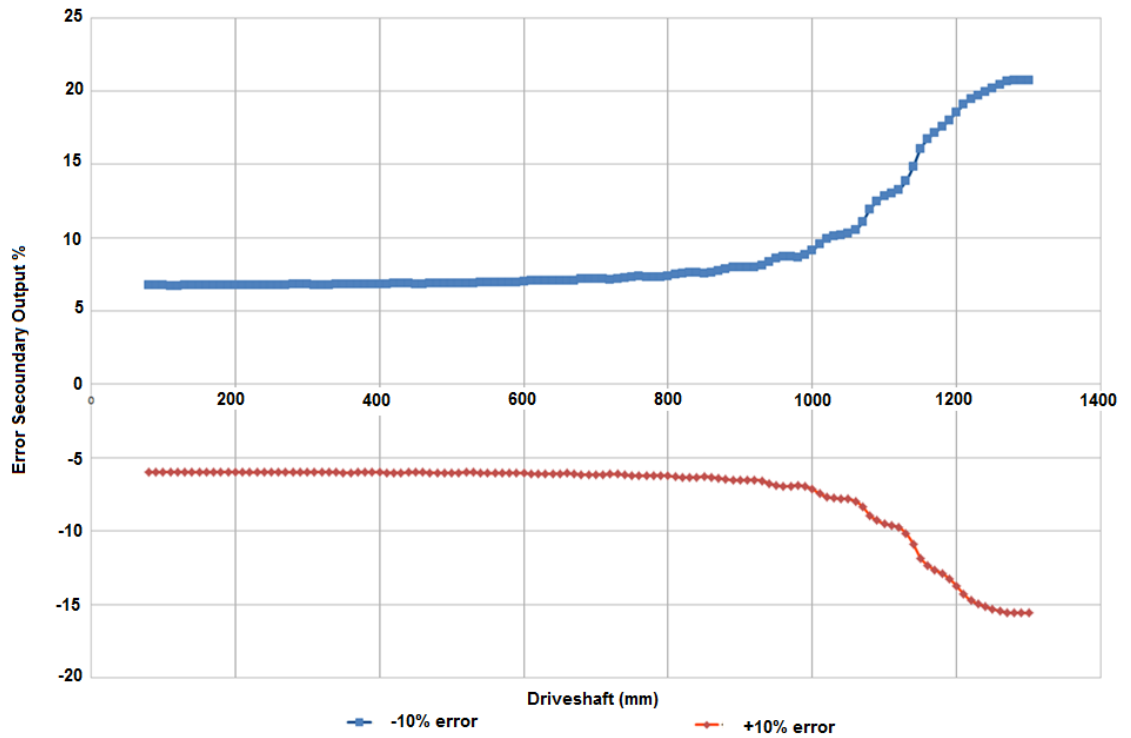


Figure 84 Secondary voltage Vs core material conductivity variation error

The FE models show the conductivity of the 17.4PH H1100 core material needs to be controlled with a greater degree than the permeability. In addition any conductivity errors occurring after calibration but which are not present when the thermal compensation factors are calculated will cause a significant error of approximately 7% on the secondary voltage output. This error would manifest itself as driveshaft positional error.

Chapter 9

9 Octave/FEMM Expert-Based TIRPI Optimisation

9.1 Octave

Octave is a high-level programming language initially intended for numerical computations. It is similar to Matlab as it can be used to solve numerical linear and nonlinear equations. It has a visual interface and can directly interface with the FEMM software. Octave has been used to develop FEMM commands and output the characteristics of the TIRPI using the constraints and variables defined within the requirements in section 1.3. Table 5 shows what the constraints are and which variables can be changed to give a preferred, optimised TIRPI design. The optimised TIRPI design is the design which is deemed to be the most desirable solution that meets the requirements taking into consideration the applied constraints, as determined by an expert-based optimisation approach.

Table 5 Variables and constraints

Parameter	Variable or Constraint	Description
Primary current	Constraint	Fixed value of 100mA r.m.s
Primary and secondary wire size	Constraint	Fixed value of 0.3mm and 0.2mm wire
Spacing between the primary and secondary bobbins	Variable	Defined by the span and linearity using a range of 1mm to 60mm space lengths
Primary bobbins length size	Variable	Defined by the span and linearity using a range of 5mm to 50mm bobbin length.
Primary bobbins wire turns	Constraint	Defined by the maximum voltages the instrumentation card can tolerate and the maximum mechanical length of the TIRPI

Parameter	Variable or Constraint	Description
Secondary bobbins length size	Variable	Defined by the span and linearity using a range of 5mm to 50mm bobbin length
Secondary bobbins wire turns	Constraint	Defined by the maximum voltages the instrumentation card can tolerate and the maximum mechanical length of the TIRPI
Secondary bobbins depth size	Constraint	Defined by the primary wire turns and manufacturing capabilities of the manufacturer.
Number of primary bobbins	Constraint	Defined by the maximum voltages the instrumentation card can tolerate and the maximum mechanical length of the TIRPI
Number of secondary bobbins	Constraint	

9.2 Approach to expert-based optimisation

Initially, it is important to determine which parameters of a design are most important to meeting the requirements. Often optimisation can only be achieved for a single parameter, so an order of priority of requirements is important. For the TIRPI, the three most important parameters are the signal voltage output span, linearity and the upper end effect when the driveshaft has fully enveloped the probe tube. However, engineering design is usually a trade-off of the requirements, and a compromise between a number of the priority variables is often necessary.

The optimisation approach adopted was to observe the characteristics of the span, linearity and end effects while changing only a single variable. The sensitivity of the secondary voltage output is considered for its optimum output span and linearity at a particular variable value. A similar process is repeated for all the variables while observing the effect on the secondary voltage output. This is a deterministic approach which relies on the expertise of the designer or engineer. After determining the sensitivity variables which have the greatest influence on the secondary output voltage, the analyses to find the optimum secondary output voltage for a particular single requirement were carried out.

9.3 Spacing optimisation

The spacing optimisation was carried out with an initial condition for all the variables and constraints. This was a baseline to start the process. The initial conditions and final conditions are shown in Table 6.

Table 6 Variables and constraints initial and end conditions

Variables and Constraints	Start Values	End Values
Spacing length	1mm	60mm
Primary bobbin turns	69	176
Secondary bobbin turns	177	2156
Primary bobbin length	22mm	22mm
Primary bobbin depth	4mm	4mm
Secondary bobbin length	22mm	22mm
Secondary bobbin depth	4mm	4mm
Total size of a space, primary bobbin and secondary bobbin	46	164
Total number of a space, primary bobbin and secondary bobbin	20	7

As the spacing length changes, other variables also are changed. An example of this is the total number of primary and secondary bobbins. These values will change for a given fixed overall TIRPI length if the spacing length between them changes. If we specify a single space, primary bobbin and secondary bobbin as a section, then Table 6 shows the number of sections must decrease as the spacing length increases providing the primary and secondary bobbin length remains constant. In addition, the number of sections also affects the secondary output voltage. This must also be considered when analysing the secondary output results of the TIRPI.

It is also prudent to ensure any design suggested by a theoretical analysis can be manufactured in practice. For example the secondary bobbin turns increases as the spacing is increased but the secondary bobbin length is constant. This may result in an

impractical manufacturing solution as the length and depth of the secondary bobbin cannot physically house the wire turns within the slots.

Figure 85 shows the results from the optimisation where the spacing between the primary and secondary bobbins was changed. The geometry of the TIRPI was re-drawn every time the spacing values were changed to ensure that the overall design complied with the constraints placed upon it, such as mechanical length. The results show how the secondary output changes when the space length is changed. The secondary output characteristics span, linearity and 'S' shaping are all affected by the spacing length. This is an excellent example of an engineering trade-off and where the optimised solution is dependent on the priority of the requirements and not an overall best solution in general. Using the expert-based optimisation approach, the selected best spacing value was found to be 45mm as this give good span and linearity values. In addition, the 'S' shaping was such that it could be detected by the instrumentation card. It is also important to note that the secondary output voltage tends to flatten towards the higher driveshaft values as the spacing length increases. This is due to the end effects of the TIRPI and cannot be removed without adding an additional primary bobbin. However, doing this will then reduce the span of the secondary output. Although the slope significantly changes due to the end effects, this was still considered to be a sufficient rate of change for the instrumentation card to detect positional change of the driveshaft.

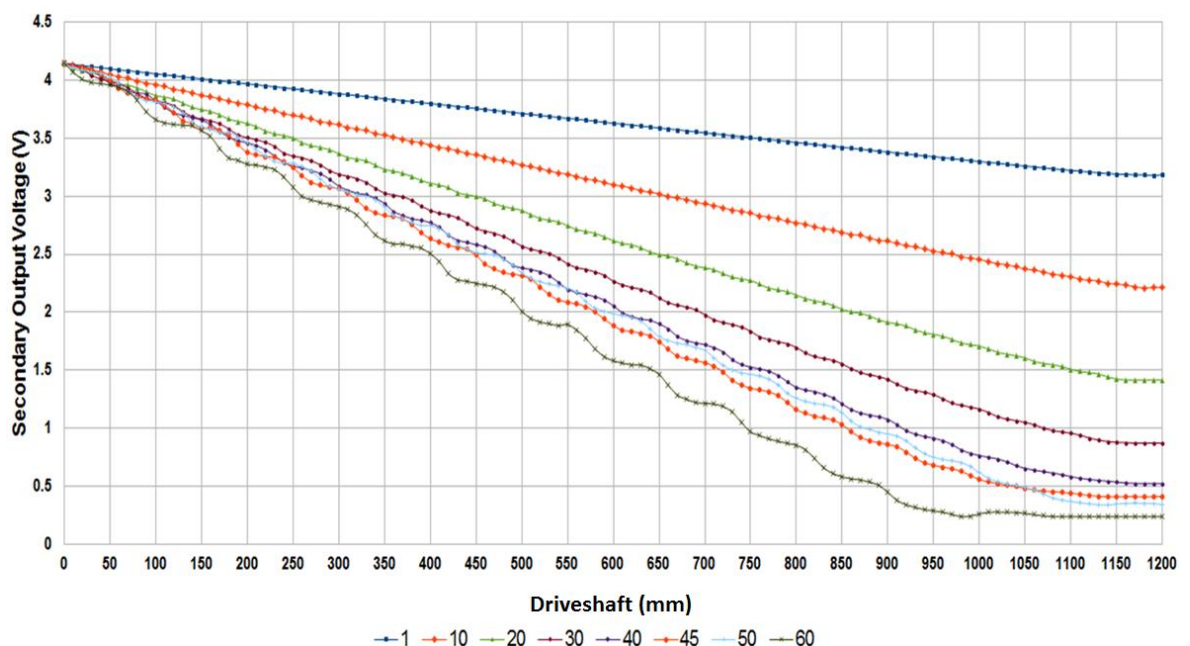


Figure 85 Spacing optimisation using Octave and FEMM

9.4 Primary bobbin optimisation

The optimisation analysis was modified to use a fixed spacing value of 45mm as this was deemed the best solution to satisfy the requirements. In addition, the primary bobbin length was changed from 5mm to 11 mm and the results observed. Figure 86 shows minimal significant changes to secondary output voltage span, linearity and 'S' shaping results when the primary bobbin length is increased. However, at a specific value of primary bobbin length, there is a significant step change in the span. This is a direct result of the number of sections consisting of a primary bobbin, a space and a secondary bobbin which fit within the fixed TIRPI length. The step change in the span observed in Figure 86 is due to the length of the primary bobbin being large enough to reduce the number of sections which can physically fit in the TIRPI length. This change resulted in a section being omitted from the design. Although the span of the TIRPI secondary output voltage has increased, the linearity and 'S' shaping values have become worse. It was concluded from the results that the primary bobbin length does not have a significant effect on the optimisation of the design; however, it does have an impact on the number of bobbins which can be added due to the limits on the TIRPI length.

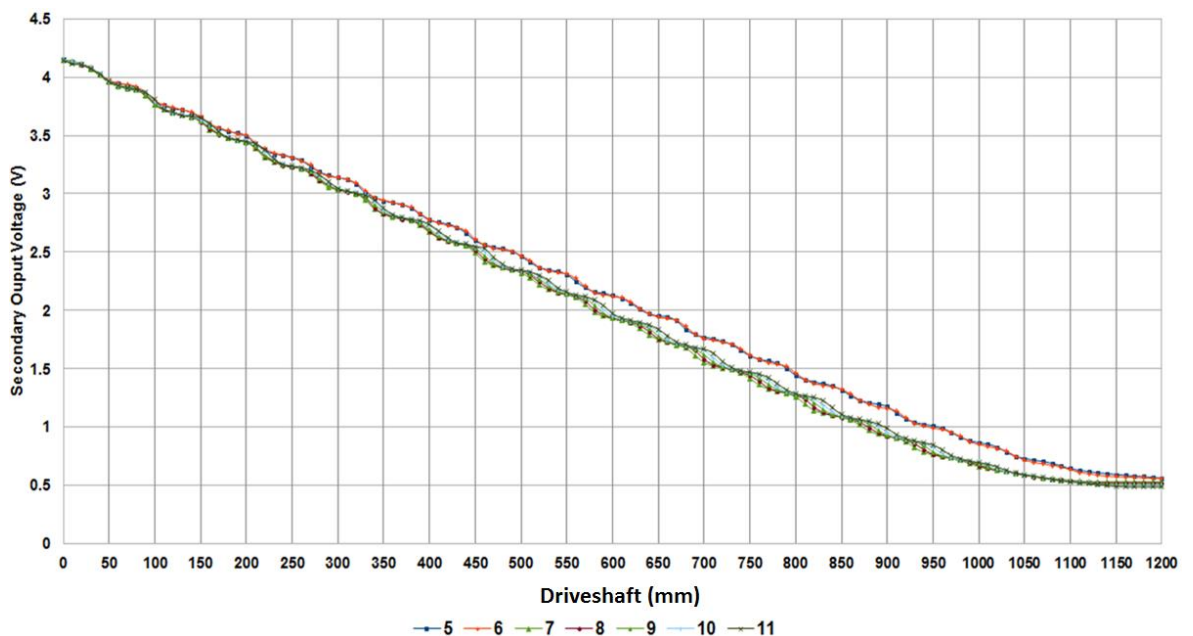


Figure 86 Primary Bobbin optimisation using Octave and FEMM

9.5 Secondary bobbin optimisation

Due to the design of the serial transformer the number of secondary bobbin wire turns is significantly greater than the number of primary wire turns. This is an important factor to be considered initially before carrying out optimisation of the secondary bobbin length. Due to the increased number of secondary turns however a practical length of secondary bobbin length had to be calculated as the ideal secondary bobbin length would not physically house the number of turns required. The results showed that the number of secondary wire turns required could never fit within the allocated secondary bobbin length unless the primary bobbin length increased. This would then reduce the turns required on the secondary bobbins. It was concluded that keeping the primary and secondary bobbins the same length would be the optimum solution and would ensure the secondary bobbin was able to house the required number of wire turns. The minimum primary and secondary bobbin lengths were calculated to be 16mm. This was again a trade-off of span, linearity and 'S' shaping, similar to that done for the spacing optimisation.

9.6 Expert-based optimised TIRPI design

The expert-based optimisation technique relies on the best judgement of the person doing the analysis. The judgement is aided by analytical data providing a generalist approach solution by analysing which parameters need to be controlled to ensure a fit-for-purpose design. The optimum expert-based design for the TIRPI is shown in Table 7.

Table 7 Expert-based optimisation parameters

Variables	Values
Spacing length	45mm
Primary turns	122
Primary length	16mm
Primary depth	5mm
Secondary turns	866

Variables	Values
Secondary length	16mm
Secondary depth	5mm

Figure 87 shows the secondary output curve of the optimised TIRPI using Octave and FEMM.

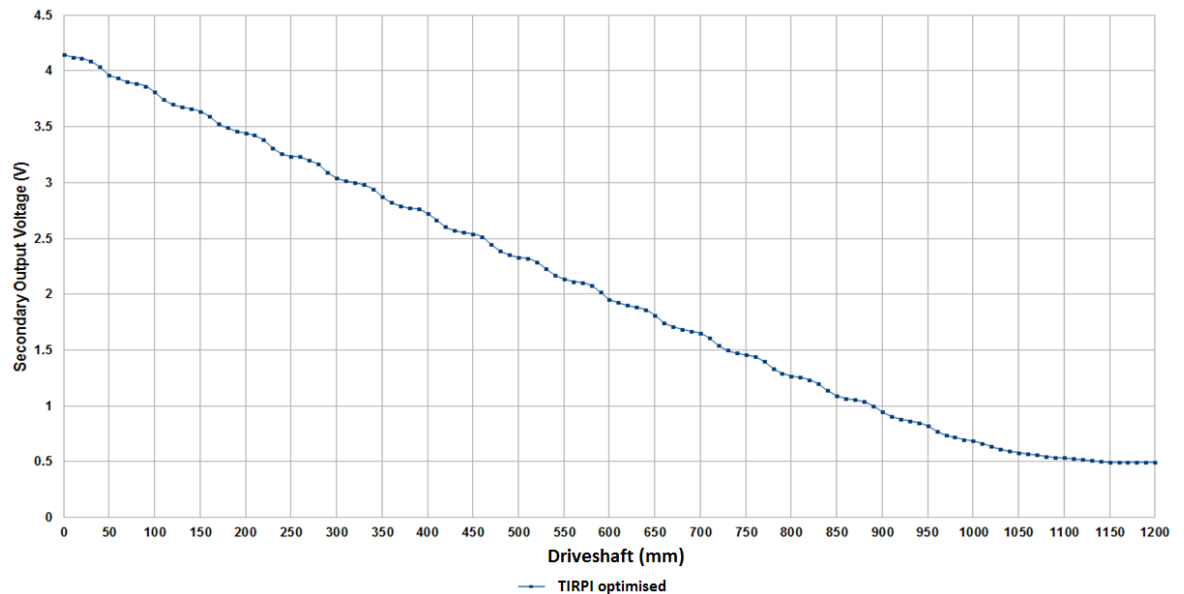


Figure 87 Primary Bobbin optimisation using Octave and FEMM

Although the characterised secondary output waveform within Figure 87 is considered to be the optimum design for the requirements, it is very important to consider the capability of the instrumentation card. For safety-critical applications such as this, the nuclear regulator requires that data is presented in as simple a manner as possible. Analysing the 'S' Shape of the curve, it can be seen that the rate of change of the output differs depending on the position of the driveshaft. A generalised approach can be applied where the accuracy of the system is considered to be directly proportional to the smallest rate of change section of the total curve. If this approach is taken, the span no longer becomes the priority parameter and the greatest rate of change of the secondary output signal dominates.

Two solutions have been considered: a minimum span output of the TIRPI secondary output signal with the optimum linearity of the output curve; and the solution which is considered the compromise optimised solution shown in Figure 87. The bobbin primary

and secondary lengths have been kept the same as these are not considered a significant contributor. Table 8 shows the actual variable for each analysis.

Table 8 Comparison of optimisation parameters

Variables	Expert-based Values	Best linearity Values
Spacing length	45mm	0.1mm
Primary turns	122	43
Primary length	16mm	16mm
Primary depth	5mm	5mm
Secondary turns	866	90
Secondary length	16mm	16mm
Secondary depth	5mm	5mm

The method to determine which of the two solutions will give the best accuracy involves determining the minimum rate of change of the secondary output signal between each of the smallest driveshaft position increments. Increment values of 10mm and 1mm have been chosen for the analysis and the rate of change of the secondary output signal was measured.

The solution that gives the minimum rate of the change value of the secondary output signal would be the least accurate solution for the TIRPI, as this will be the one that the instrumentation card will find hardest to detect.

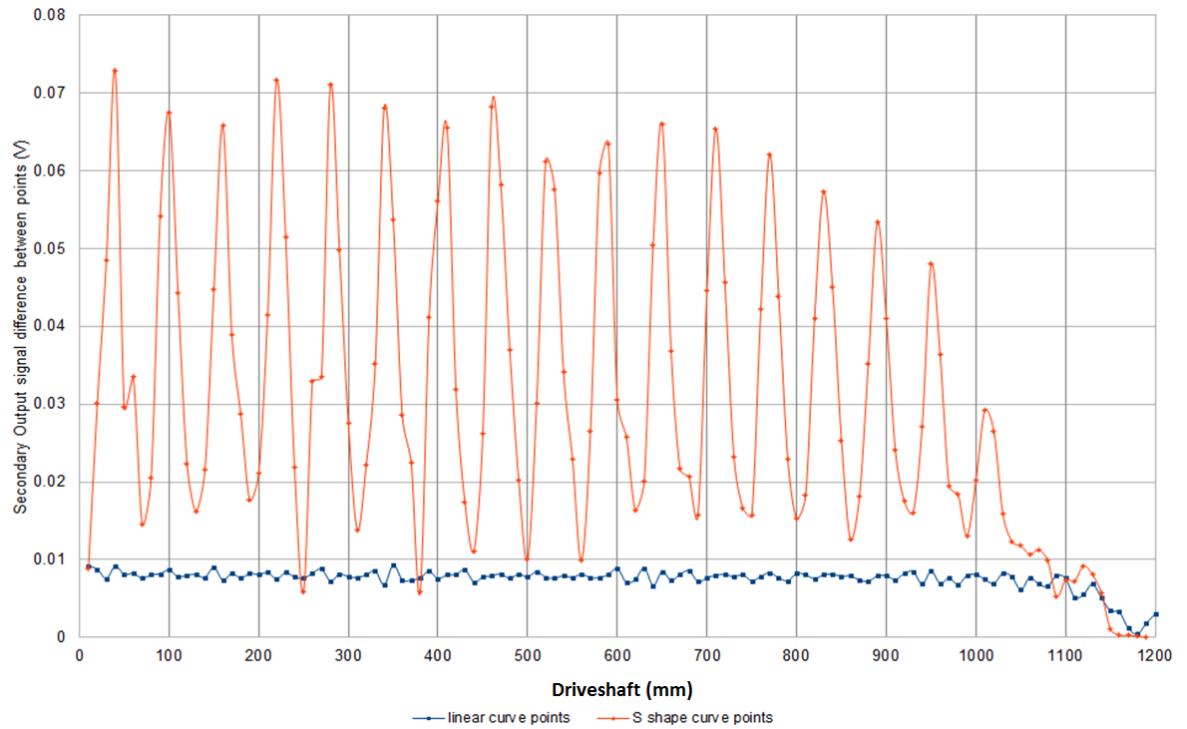


Figure 88 Comparison of expert-based optimisation and linear optimisation for 10mm increments

Figure 88 shows the expert-based solution and an optimised linear solution using the same primary and secondary bobbin dimensions. It is clear from the data that the expert-based optimisation provides a better secondary output signal rate of change than the linear solution. However, at particular points it can be seen that the linear solution exhibits a greater rate of change for the secondary output signal. Intuitively, the expert-based solution is considered a better design, although the data suggests that the linear solution is the optimum design for a more consistent secondary voltage difference. Care must be taken however as the analysis has considered large, 10mm incremental steps of the driveshaft. In practice, the incremental step resulting from a single CRDM pulse is much smaller. A repeat analysis using a driveshaft 1mm incremental step was carried out to determine how sensitive the incremental step is to the results of the secondary output signal.

The analysis for the 1mm incremental step shows similar results to the 10mm incremental step analysis. There is a greater difference between the secondary signal outputs at each point for the expert-based optimisation, as shown in Figure 89. Thus the solution

proposed by this technique would enable the instrumentation card to provide an overall better accuracy.

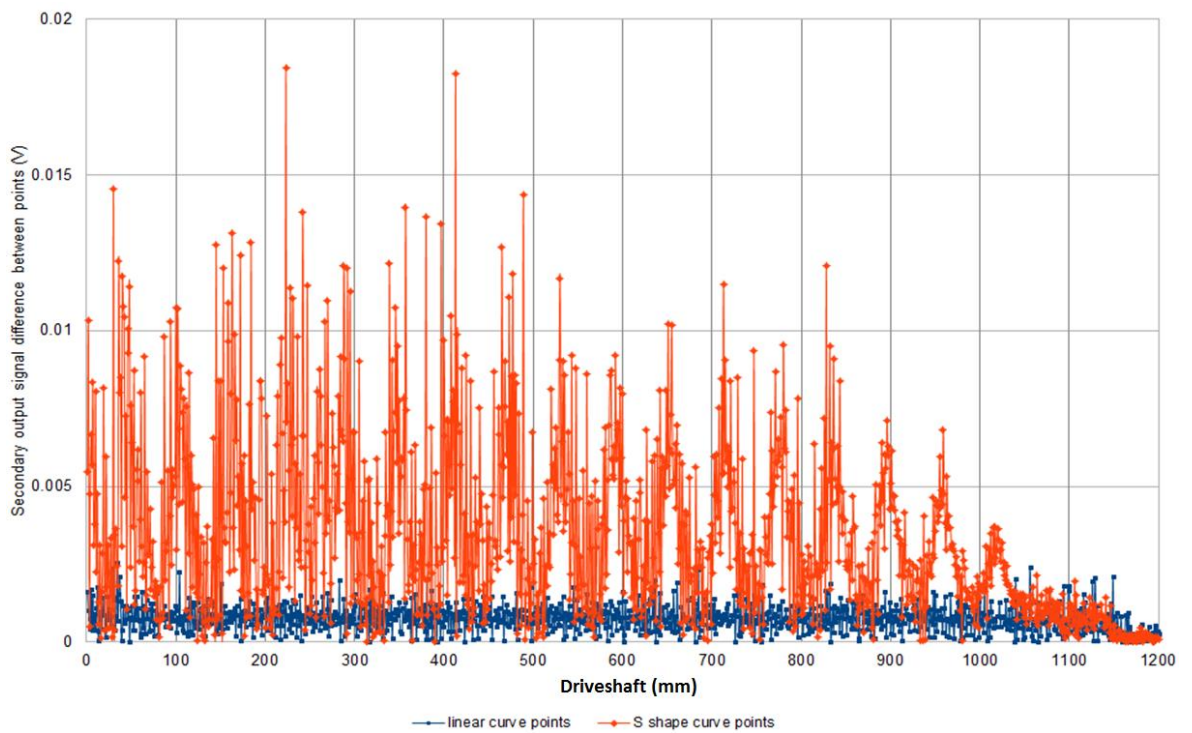


Figure 89 Comparison of expert-based optimisation and linear optimisation for 1mm increments

Chapter 10

10 TIRPI Prototype 1 Build

10.1 Introduction

The physical size of the TIRPI design was limited by the probe tube dimensional and environmental envelope. The probe tube is a long thin tube where the TIRPI is housed. In addition the probe tube design has an upper connector-flange arrangement which enables the TIRPI to be rotated in 5 degree steps to aid connector and cable alignment. The TIRPI is also held in place by a flange plate which secures the TIRPI and probe tube together. The TIRPI connector, flange plate and cable arrangement are qualified to withstand a Loss of Coolant Accident (LOCA).

10.2 Design Concept

The TIRPI consists of two subassemblies these being the connector-flange and the coil former. The coil former is made from a series of bobbins which house the primary and secondary coils. The coil former has electrical insulation tape to insulate the coil former from the enamelled copper wire wound onto the bobbin.

When the TIRPI is housed within a probe tube, the complete housed assembly is inserted into the driveshaft. The upper section of the probe tube also interfaces with the motor tube of the control rod drive mechanism as illustrated in Figure 90 and Figure 91. The TIRPI is attached to the probe tube via a plate with a bolting arrangement to hold the TIRPI in place.

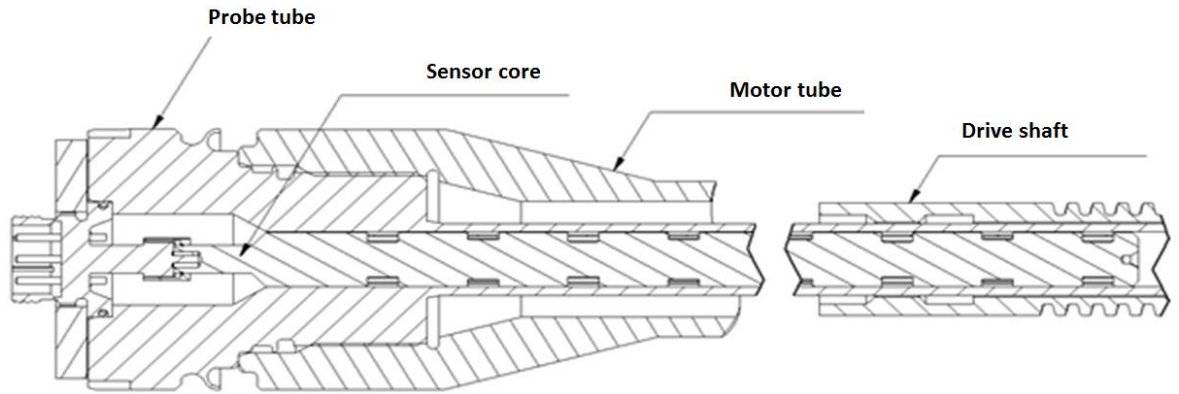


Figure 90 Upper arrangement assembly

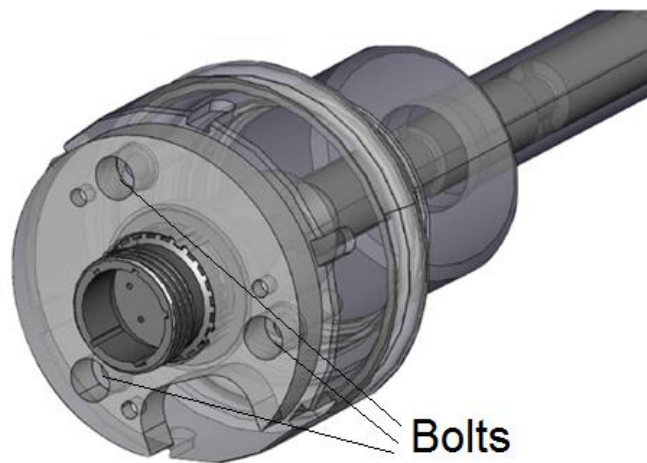


Figure 91 Upper arrangement assembly bolting location

10.3 Electrical Connector

Due to the harsh environment the TIRPI operates in and the safety critical application, a MIL-C-38999 connector using a series 3 shell size 17 receptacle shell as its basis was selected as the connector for the TIPRI. A novel connector sealing arrangement was developed for the connector, where the pins were sealed in place using a PEEK seal, as illustrated in Figure 92. This enabled the connector to meet requirements to withstand excessive thermal radiation, radiation and pressure demands. The connector flange was also been designed with a stepped thread around its upper side. The stepped thread ensured the TIRPI could not be twisted once it had been fixed in position, and only allowed the connector flange to rotate through a maximum of 15° when lifted from the probe tube. Figure 93 shows the connector flange and connector flange housed within the probe tube with the upper plate fixing the assembly into position.

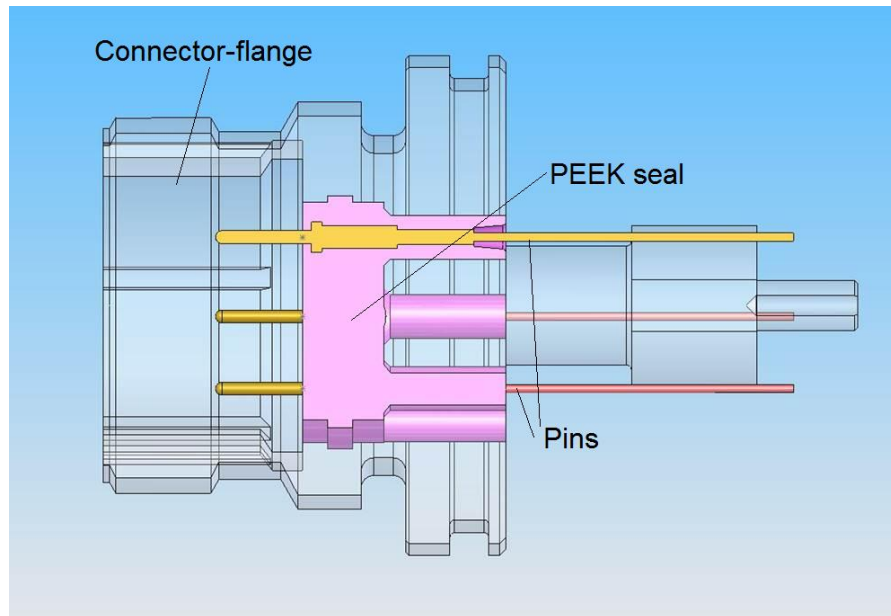


Figure 92 Connector-flange PEEK sealing

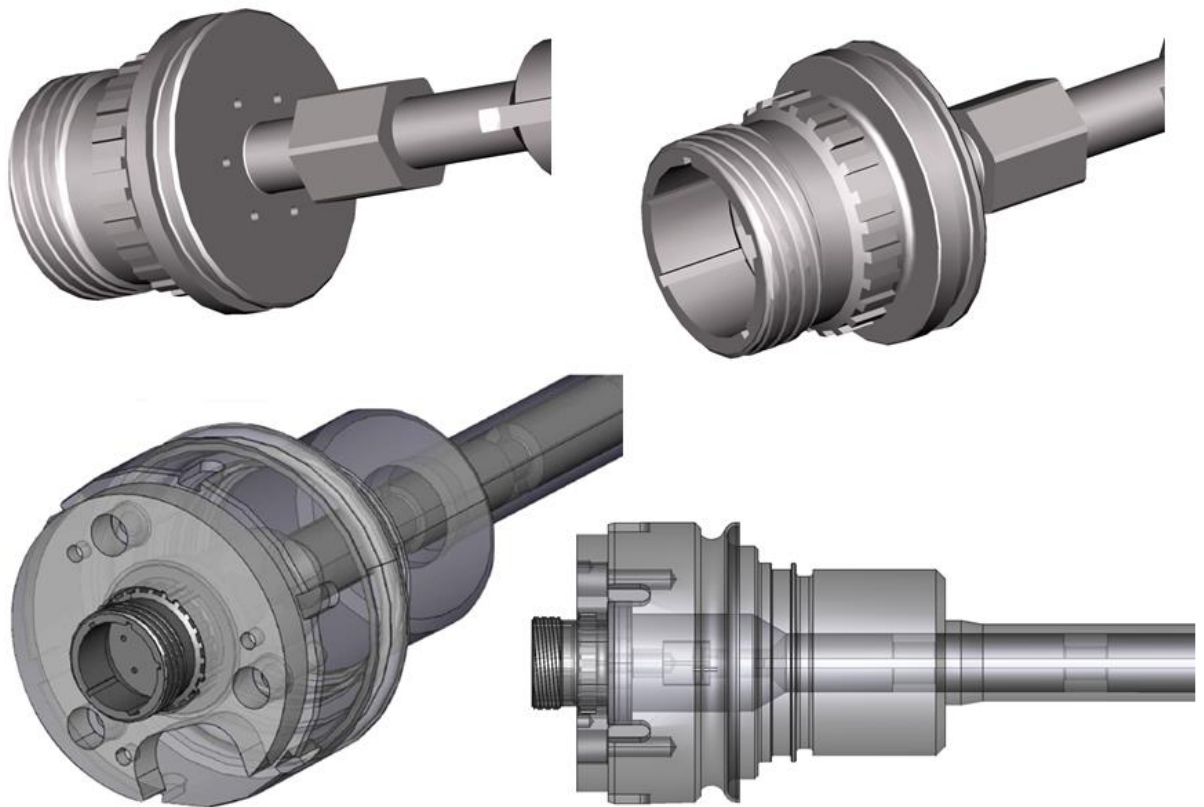


Figure 93 Connector-flange arrangement

10.4 Coil former

The coil former is machined from a single piece of 17.4PH stainless steel bar. This was chosen as it was the same as the driveshaft material and this would give the optimum

core performance due to the matched electromagnetic characteristics. Bobbin slots were machined into the 17.4PH stainless steel bar, along with two continuous slots on opposite sides. The slots would house the enamelled copper wire and enable the wire to be threaded from one bobbin to another. The 17.4PH material was a precipitation-hardened stainless steel which provided high strength, good corrosion resistance and good mechanical properties up to temperatures of 316°C.

The coils were wound in two distinctive sections: the primary and secondary sections. The enamelled copper wire for the primary section was fed through the coil former slots and then wound around the primary bobbins. The winding must be continuous without any physical breaks, as any breaks would invalidate the safety case for the design. The enamelled copper wire for the secondary section was then fed through the opposite coil former cavity and wound into the secondary bobbin slots. The secondary winding must also be a single continuous wind without any physical breaks. This was ensured by crossing the secondary wire over the already completed primary bobbins to ensure a serial wind. The top of the TIRPI would have lead out wires so the enamelled copper wire connections were mechanically supported by the enamelled wire thin diameter. An illustration of the bobbins with the finished primary and secondary windings is provided by Figure 94.

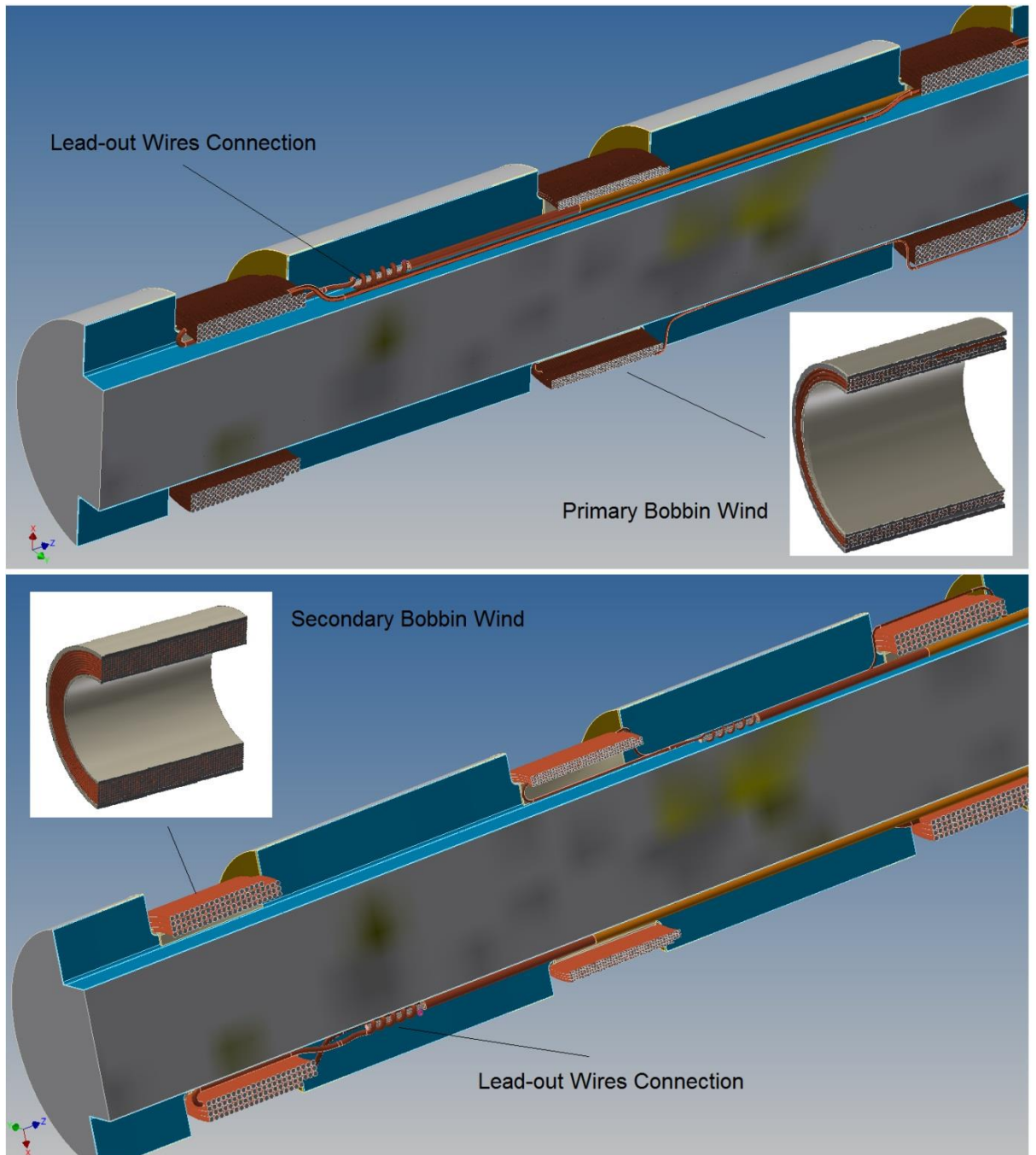


Figure 94 TIRPI windings (courtesy from Centronics Ltd)

10.5 Coil varnish impregnation

The enamelled copper windings must maintain their mechanical strength throughout the TIRPI life. This was achieved by using a varnish to give the bobbins mechanical resilience. An additional electrical insulation layer made of kapton tape was placed between the core former and the windings. The proposed varnish was Elmotherm 073-1010, which has a thermal rating of 200°C. The varnish impregnation was carried out using a capillary action process. This gave good penetration characteristics, but ensured

high flexibility with high bond strength. The varnish also exhibited good chemical and water resistance and did not emit solvent gases after it had undergone curing. The varnish had pedigree of use in other radioactive environments and was deemed suitable for use in this application.

10.6 Winding coil wire

The coil wire was insulated with polyimide insulation grade 2 and had a continuous thermal rating of 240°C. The operational life of this wire reduces by 50% for each 10°C over the operational service temperature however; the TIRPI environment was below the maximum value of 240°C. This would ensure the wire enamel did not degrade due to overheating.

10.7 Lead-out wire connection

The lead out wire was mechanically wound and soldered using BSENISO 9453 alloy 191 liquidus 301°C. This met the operational thermal requirements. Post soldering, the joints were potted using Dow Corning 3145 RTV and sleeved using Vidaflex series 300 or 111 'E' glass sleeving. This ensured mechanical strength and a good electrical insulation illustrated in Figure 95.

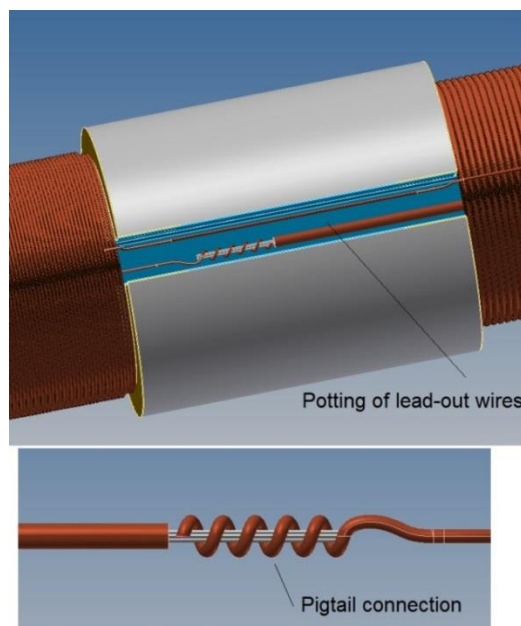


Figure 95 TIRPI lead-out wire (courtesy from Centronics Ltd)

The lead out wires were polyimide insulated wire and run from the coils to the connector-flange pins.

10.8 Rod core insulation

The rod core insulation consisted of polyimide tape (Kapton) that was cut into suitable shapes to fit the bobbin space envelope. The insulation of the core former was carried out prior to the bobbin being wound. In addition to the polyimide tape a layer of 3M Glass Tape type 69 (MIL-I-19166C) was put in place to aid the electrical insulation of the core as illustrated in Figure 96. After the insulation was put in place, the varnish impregnation process encapsulates the coils, giving them a surface temperature withstand capability of 220°C.

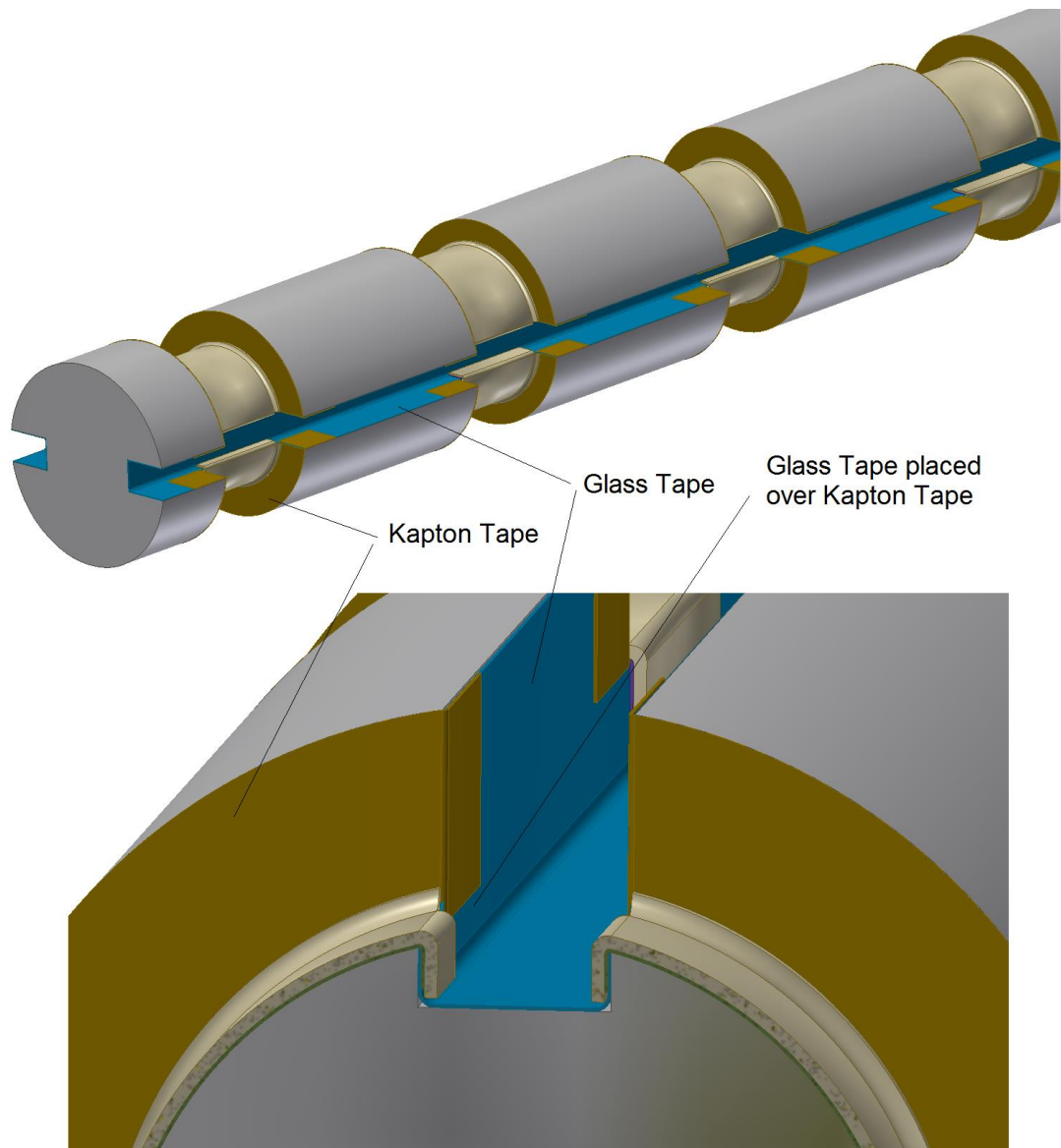


Figure 96 Polyimide and glass tape insulation (courtesy from Centronics Ltd)

10.9 Seal of TIRPI to probe tube

The TIRPI was protected from ambient pressure and environmental ingress by a Viton 'O' ring. The operating temperature of the Viton 'O' ring was 205°C although its location would only experience a temperature of approximately 94°C in this application. This ensured the maximum life of the Viton 'O' ring was preserved.

10.10 Failure Modes and Effects Analysis (FMEA)

A Failure Modes and Effects Analysis (FMEA) is a stepped approach that is used to assess all possible failures in a design, manufacturing assembly, product or service. The FMEA looks at how a design might fail to meet the requirements placed on it. This is investigated further within chapter 10.15.

10.11 Mean Time before Failure (MTBF)

The Mean Time Before Failure (MTBF) is a measure of the time that is supposed to elapse before a device fails. This is usually calculated as the average time between failures or the arithmetic mean between failures. The analysis of the MTBF showed the TIRPI to operate for a period of 84.5 years before failure. The analysis is shown in section 21.

10.12 Demonstration mini unit development for manufacture

A demonstration unit was built to ensure that manufacture of the production units was feasible. The manufacturing of the core former used an automatic machine which cut the former material into the correct shape. After the former materials were cut, the core former was assembled by hand in a production workshop to produce the TIRPI. The TIRPI was finally placed into a thermal oven to be cured. The curing process cures the varnish used and produced a final assembled component. Figure 97 shows a completed mini-TIRPI demonstration unit. It is important to recognise that the connector-flange assembly has not

yet been developed, and will be part of a separate, but related, project as only the electrical characteristics were being tested at present.

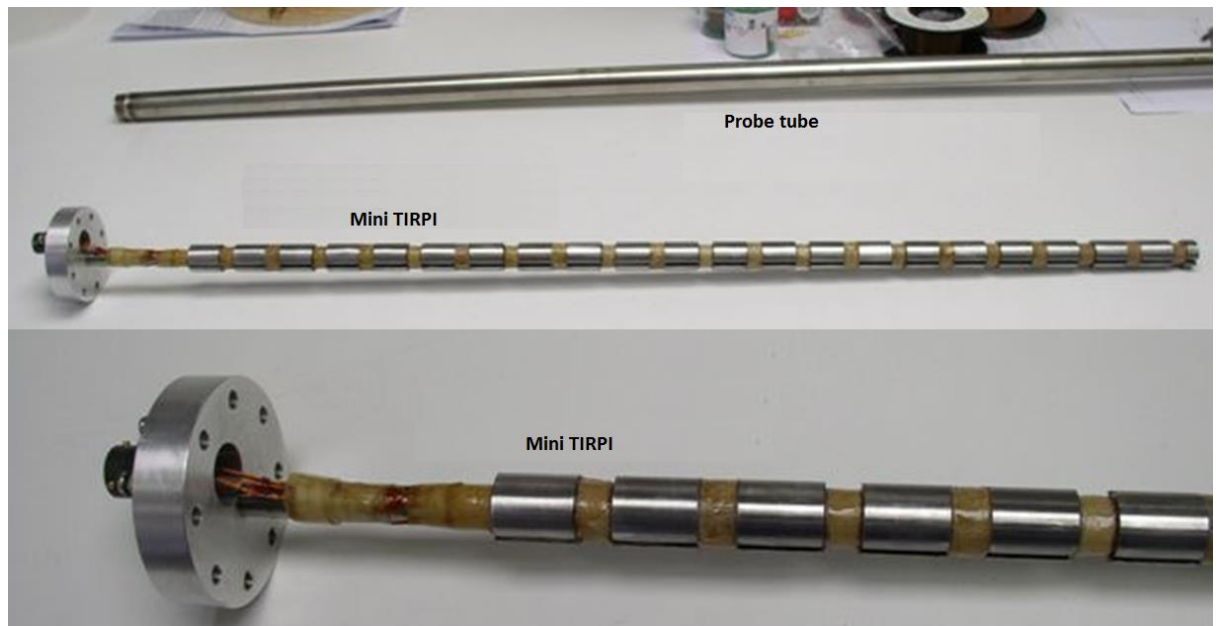


Figure 97 Demonstration for manufacture TIRPI (courtesy from Centronics Ltd)

10.13 Assembly of connector-flange to the core former

The assembly of the core former to the connector-flange was achieved by means of using a spiral retaining ring, location dowels and a locking nut as shown in Figure 98. The locking nut was coated in a varnish, which was cured to ensure the nut would not loosen during operation. This method of connection is the preferred option as the concentricity of the TIRPI is highly accurate. In addition, the mechanical methodology of the connection enables correct mating of the TIRPI core bar with the probe tube which has an internal precision bored cavity to house the TIRPI core bar. Alternative methods, such as welding of the connector-flange, would distort the concentricity of the assembly, and were thus undesirable.

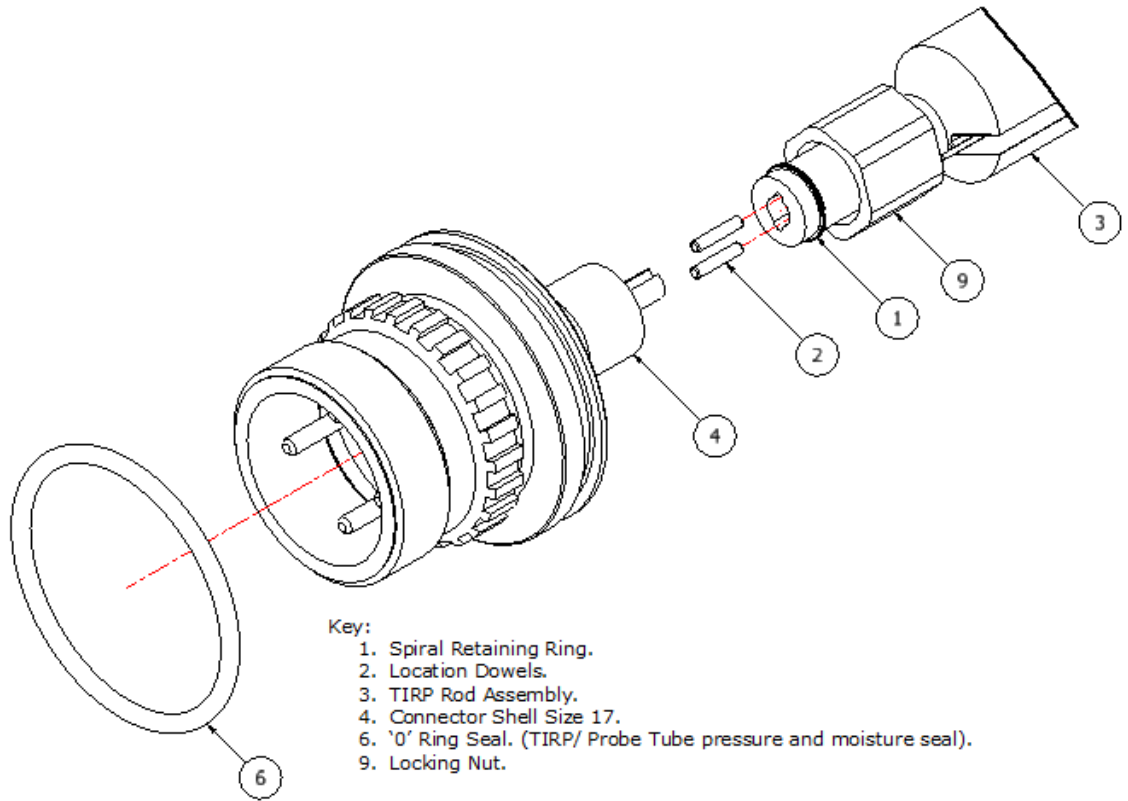


Figure 98 Connector to core former connection (courtesy from Centronics Ltd)

10.14 TIRPI Prototype 2 Build

An alternative version of the TIRPI was designed. This design uses a different geometry for the driveshaft and probe tube. This alternative prototype demonstrates how the procedure developed for the TIRPI prototype 1 was robust and could be repeated when the driveshaft and probe tube design is changed. It also demonstrated that the manufacturing processes used for the TIRPI were repeatable and could accommodate slight differences within the design. In addition extra time was allowed to increase the fidelity of the FE modelling tools used in the design of the second prototype. This information was used to enhance the span of the secondary output voltage compared to the first TIRPI prototype. The models used for the TIRPI prototype 2 gave an optimal spacing length of 45mm and a bobbin length of 22mm. These values were used to determine the number of primary and secondary bobbins and the primary and secondary turns. For a given TIRPI length of 1335mm, it was calculated that there should be 140 primary turns using 0.2032mm enamelled copper wire, and 1033 secondary turns using 0.315mm enamelled copper wire. A schematic of the TIRPI prototype 2 is shown in Figure 99.

An enhanced feature was incorporated in the design of the lower end of the TIRPI prototype 2 to aid its insertion within the probe tube. The end of the TIRPI has a chamfer allowing it to rub against the probe tube without causing scoring or scratching to the probe tube. This is an important feature as the probe tube is the thinnest part of the nuclear plant that contains the radioactive water and should not be allowed to breach the probe tube and into the TIRPI.

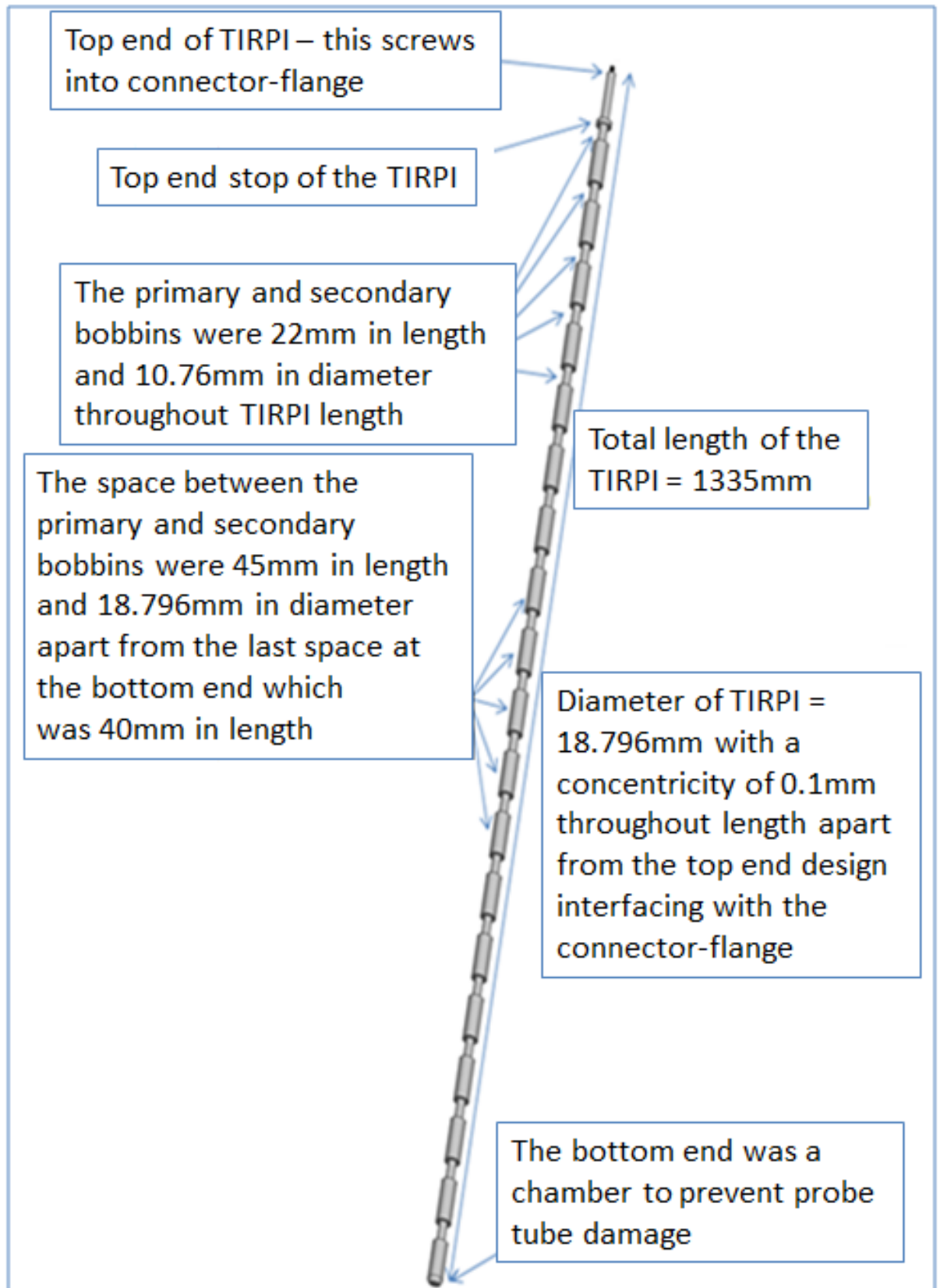


Figure 99 TIRPI prototype 2 schematic

10.15 DFMEA and PFMEA

DFMEA (Design Failure Mode and Effects Analysis) and PFMEA (Process Failure Mode and Effects Analysis) are structured and systematic techniques for failure analysis using inductive reasoning to determine single point failures. These are usually considered as the first step in reliability studies that review all the components and sub-components within a design or process, and identify failure modes and their causes and effects. The analysis is usually carried out within a worksheet, where qualitative analysis is used to assign numerical ratings and rankings to the TIRPI component parts.

The steps carried out in a DFMEA analysis are shown below.

- **Design review** – Use of the design drawings and documents to identify the individual components and their relationship to the other sub-components.
 - Ensures team members are familiar with the design and product.
 - Identifies the main components and determines their individual functions and associated functions with their interfaces.
 - Ensures all the components are considered within the design.
- **Expert-based brainstorming potential failure modes** – Consider potential failure modes for every component and interface.
 - Ensures all potential modes are analysed which will affect the intended use of the components and its interfaces.
 - All single and multiple failure modes must be considered, whether or not these are likely to occur.
 - Use previous experience and knowledge of similar products which have a pedigree of use to determine potential, similar failures.

- **List of potential failure modes** – This relates to the ability of the specific component to perform its intended function.
 - The effect of the failure, should it occur.
 - Should be meaningful to product performance so potential risks can be identified.
- **Assign severity ranking** – These are very important for the process as these determine the basis for identifying the relative risk of a failure occurring.
 - The ranking is usually based on a relative number of 1 to 10 where 10 is a high severity leading to a hazardous situation without any warning and a 1 is a low severity.
- **Assign occurrence ranking** – Based on the frequency of the failure occurring, this is a function of the failure. A better understanding of the failure can determine the likely frequency of its occurrence.
 - Different approaches can be determined using time based, event-based or piece-based methods.
- **Assign detection ranking** – To determine the assigned controls in place for each failure mode, and then to assign a detection ranking to each control method.
 - Prevention determines the frequency of failure or the likelihood of the failure occurring.
 - Detection controls of the failures post the event occurring stopping a design being released for manufacture.
- **Calculate the RPN value** – This is a risk priority number which shows the relative risk of the design.

- The RPN is calculated by multiplying the severity ranking, occurrence ranking and the detection ranking for every failure mode and effect considered.
- **Develop action plan** – The various means of reducing the RPN can be determined by minimising the rankings for the severity, occurrence and detection.
 - Severity ranking can be reduced by a design change.
 - Occurrence ranking can be reduced by controlling or removing the potential failure causes.
 - Detection ranking is reduced by adding or improving prevention or detection controls.
- **Complete the action plan and re-calculate the RPN value** – Ensure all actions developed in the action plan have been completed. Then review all RPN values determined from the beginning of the DFMEA analysis.
 - Ensures the overall RPN value has been lowered to an acceptable value.

The DFMEA for the TIRPI is shown in Section 17 of this thesis.

Although a product can be designed to have an acceptable failure rate the process of manufacturing the product can also contribute to a potential failure. It is important to analyse the processes used in manufacturing to ensure the potential failure mechanisms are minimised.

The steps carried out with and PFMEA analyses are shown below.

- **Process Review** - Identifies the process components and reviews the intended functions of each component.
 - Use of a flow chart is required to ensure a process route is understood.
 - Identify components which have more than one function.

- **Expert-based brainstorming potential failure modes** – Consider potential failure modes for every component and interface.
 - Ensure all potential modes that may affect the intended use of the components and their interfaces are considered.
 - All single and multiple failure modes must be considered, whether or not these are likely to occur.
 - Use previous experience and knowledge of similar products which have a pedigree of use to determine potential, similar failures.

- **List potential effects causing failure** – Analyse the effects associated with each failure mode. This is related to the ability of the component to perform its intended task.
 - The effect is the impact should a failure occur.

- **Assign severity ranking** – The severity is a measure of how serious an effect is, should it occur.
 - The ranking is usually based on a relative number of 1 to 10, where 10 is a high severity leading to a hazardous situation without any warning and a 1 is a low severity.
 - Consider the impact on severity through life of the component.

- **Assign occurrence ranking** – Consider the potential cause and failure mechanisms within the process for each failure mode, and assign a potential occurrence ranking.
 - This is based on the likelihood or frequency of the failure occurring.

- **Assign detection ranking** – To determine the process-assigned controls in place to detect each failure mode, and then to assign a detection ranking to each control method.

- Prevention affects the frequency of failure or the failure occurring.
- Detection controls of the failures post the event occurring stopping a design being released for manufacture.
- **Calculate the RPN value** – This is a risk priority number which shows the relative risk of the design.
 - The RPN is calculated by multiplying the severity ranking, occurrence ranking and the detection ranking for every failure mode and effect considered.
- **Develop action plan** – The various means of reducing the RPN can be determined by minimising the rankings for the severity, occurrence and detection ranking.
 - Severity ranking can be reduced by modifying the process usually equipment modification or manufacturing layout.
 - Occurrence ranking can be reduced by controlling or removing the potential failure causes.
 - Detection ranking is reduced by adding or improving prevention or detection controls by adding process shut down devices and alarms etc.
 - Mistake-proofing, statistical process control and design of experiments techniques can be adopted.
- **Complete the action plan and re-calculate the RPN value** – Ensure all actions developed in the action plan have been completed. Then review all the RPN values determined from the beginning of the PFMEA analysis.
 - Ensure overall RPN value has been lowered to an acceptable value.

The PFMEA the TIRPI is shown within the appendix of the report.

Chapter 11

11 Experimental Testing and Model Validation

Testing of the TIRPI prototype was carried out at two locations: the manufacturing Vendor and Rolls-Royce Raynesway Engineering Laboratory (REL). The REL was used for bench testing, CRDM In-Air testing and CRDM Hot and Pressurised Water testing. The Vendor was used for the environmental chamber testing prior to the CRDM Hot and Pressurised Water testing.

11.1 Bench test at room ambient temperature

The TIRPI bench testing setup consisted of the TIRPI, a probe tube and a driveshaft with a high-precision control facility on a bench. The bench test control system moved the driveshaft over the probe tube in small increments. The TIRPI primary voltage, primary current and secondary voltages were measured during the test at a constant room temperature of approximately 22°C. This test showed how the characteristics of the TIRPI output voltages changed as the driveshaft enveloped the probe tube without the CRDM.

Figure 100 shows the bench test facility used.



Figure 100 Bench test facility

The bench test result in Figure 101 shows the primary and secondary voltage outputs of the TIRPI as the driveshaft envelops the probe tube. It also shows the primary voltage to be a relatively constant value, implying the temperature of the bench test facility was relatively constant throughout the test.

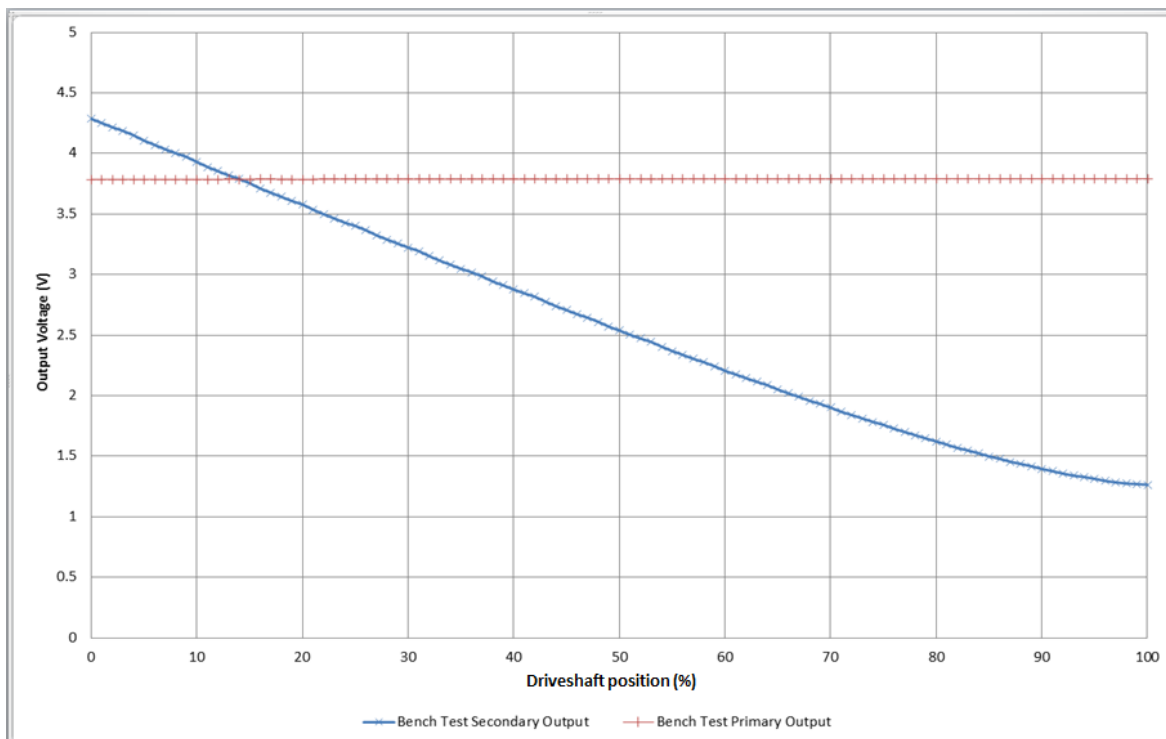


Figure 101 TIRPI Bench test – secondary voltage output

However, if the primary voltage is analysed with greater resolution, as shown in Figure 102, it can be seen that the driveshaft affects the primary voltage output value as the driveshaft envelops the probe tube. The effect of the driveshaft on the primary voltage output is similar to the effects due to thermal change on the TIRPI from the view of the instrumentation card. This is considered a thermal change which will cause an error in the secondary voltage which translates to driveshaft position. The change in primary voltage in Figure 102 is approximately 5.7mV between the 0% and 100% driveshaft positions. However, this error is incorporated within the thermal cold and hot compensation test errors as a lumped value and, as such can be compensated for within the thermal compensation algorithm.

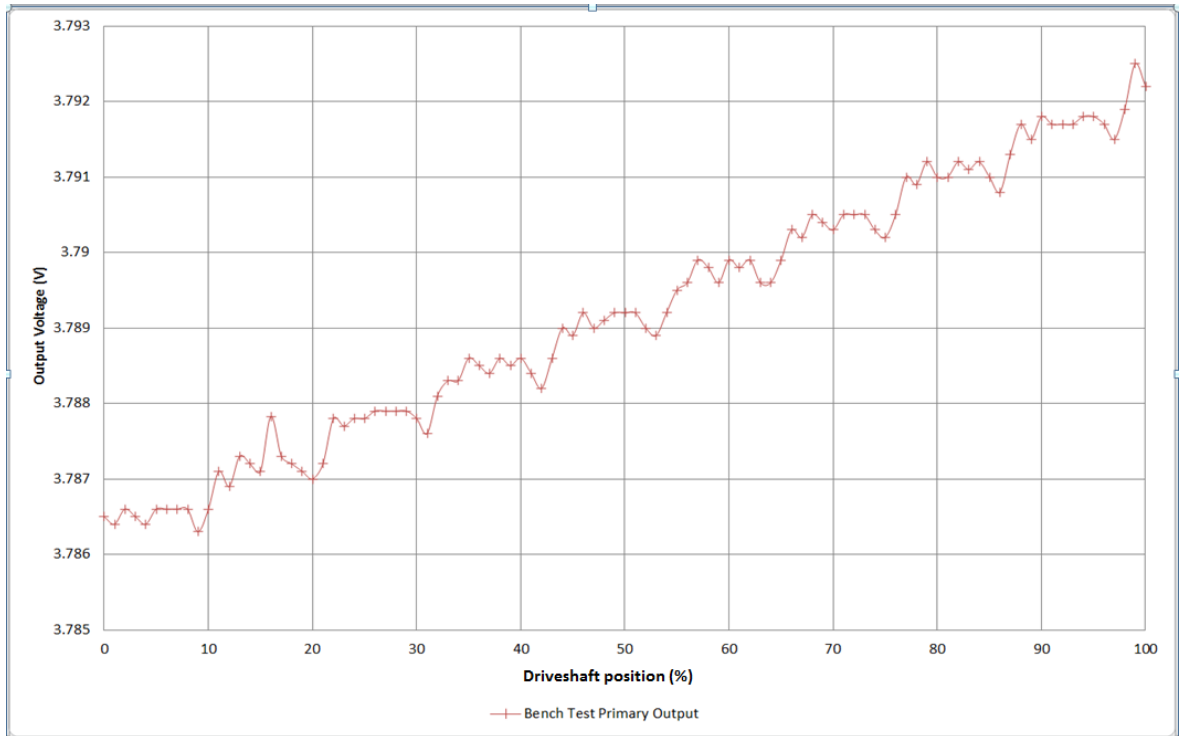


Figure 102 TIRPI Bench test – primary voltage output

11.2 Thermal environmental test

The TIRPI is subject to thermal gradients throughout life which require an instrumentation card compensation algorithm. To determine the thermal response of the TIRPI, a thermal environmental chamber was used to test how the TIRPI performs. The results are shown in Figure 103. The span and offset of the secondary output voltage will increase due to the rise of TIRPI temperature. The maximum voltage achieved by the TIRPI is when the driveshaft is in the minimum position and the temperature of the TIRPI is at its maximum value. This values needs to be considered when designing the instrumentation card otherwise a signal output error could be introduced when the TIRPI is being used in situ.

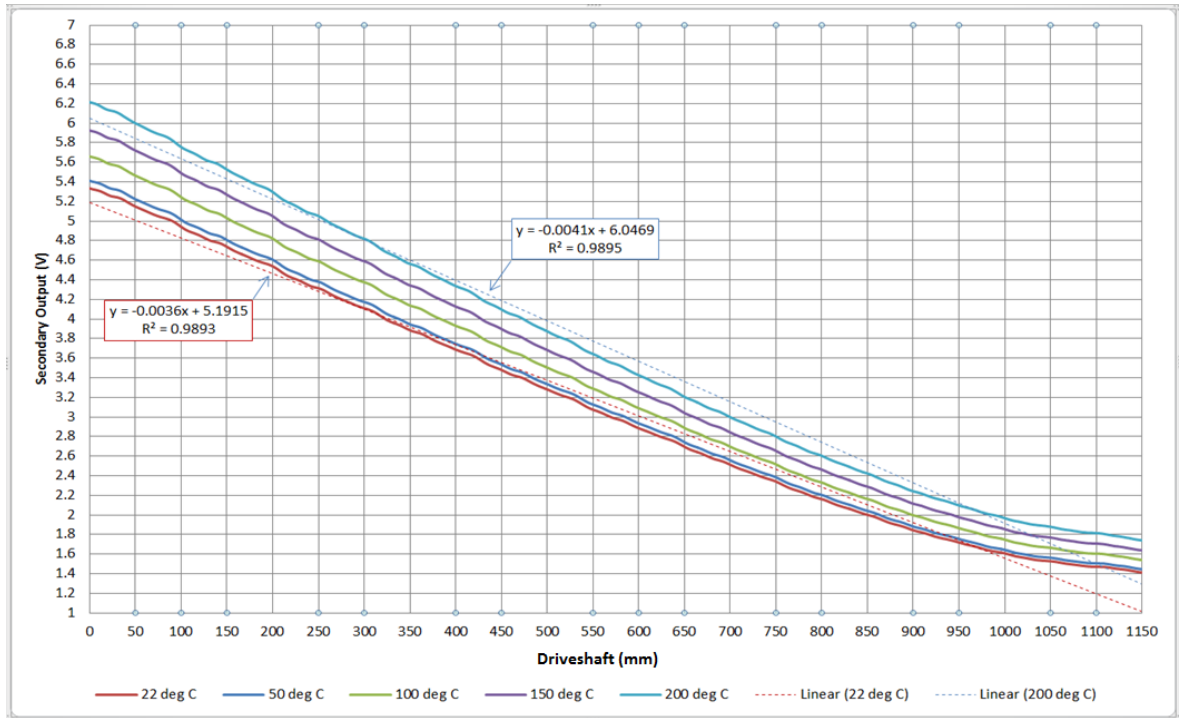


Figure 103 TIRPI environmental thermal Test

11.3 Harmonics Test

For transformers such as that used in the TIRPI design, the secondary output signal is a function of the primary current producing the magnetic field which couples the primary and secondary windings. However, voltage sources are easier to implement and therefore if a voltage source is used to generate a primary current the current, can become distorted due to the magnetic non-linearity of the transformer magnetic circuit. Distortion of the secondary load however also causes non-linearity of the secondary output voltage.

Harmonics are defined as multiples of the fundamental frequency and produce voltages at other frequencies. They consist of a number of sinusoidal waveforms at multiples of the fundamental frequency. These can contribute to the error of a sensor or sensing device.

The fundamental frequency used for the TIRPI was 400Hz; harmonics were considered at frequencies of 99 Hz, 502 Hz, and 2 kHz to evaluate possible effects caused by the variation of probe response with frequency. These values were selected as these are close to the operating frequency of 400 Hz as our available test equipment had limited capability.

Testing was conducted using a range of supply current values to investigate the effect of the harmonic response at different power levels. Figure 104, Figure 105 and Figure 106 shows the harmonic effects under various conditions.

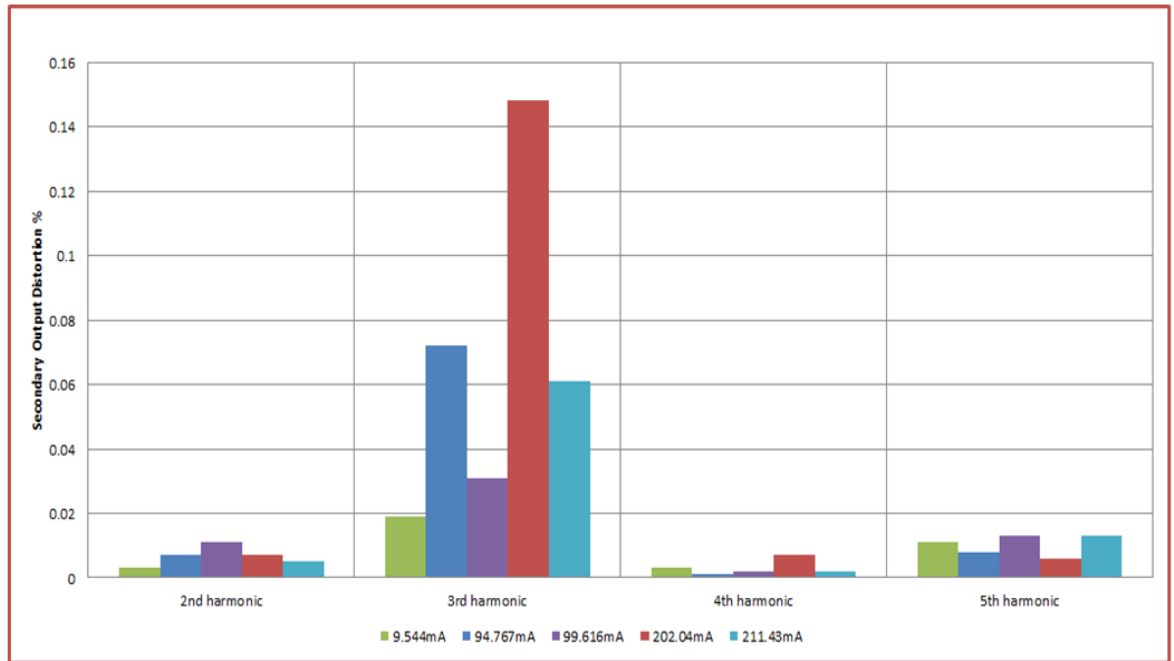


Figure 104 Cold harmonic testing at 400Hz

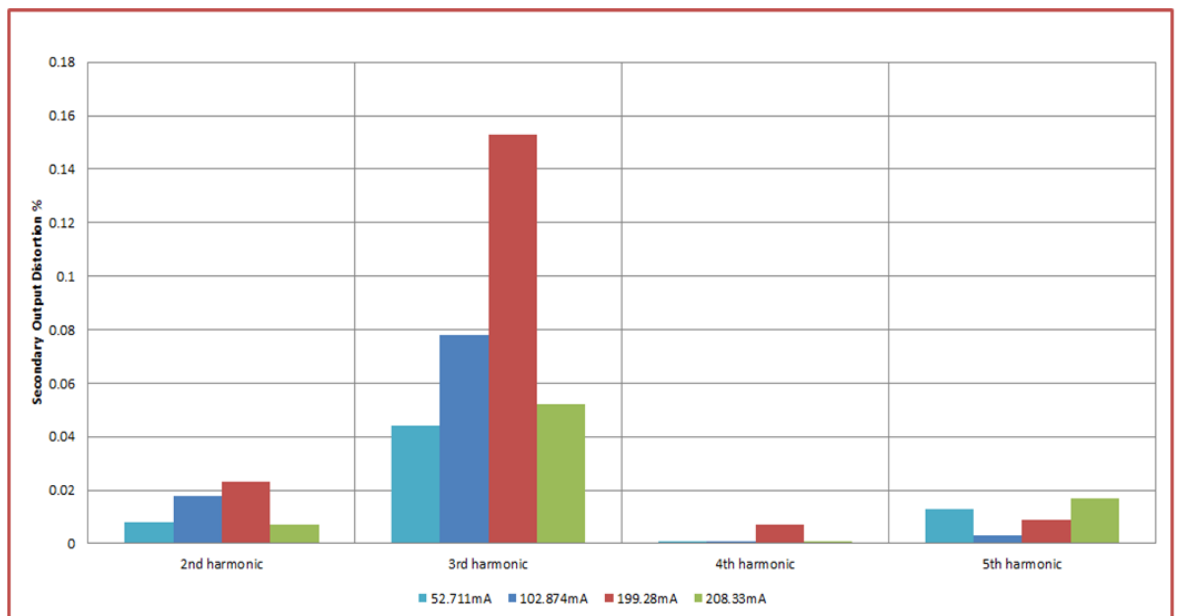


Figure 105 Hot harmonic testing at 400Hz

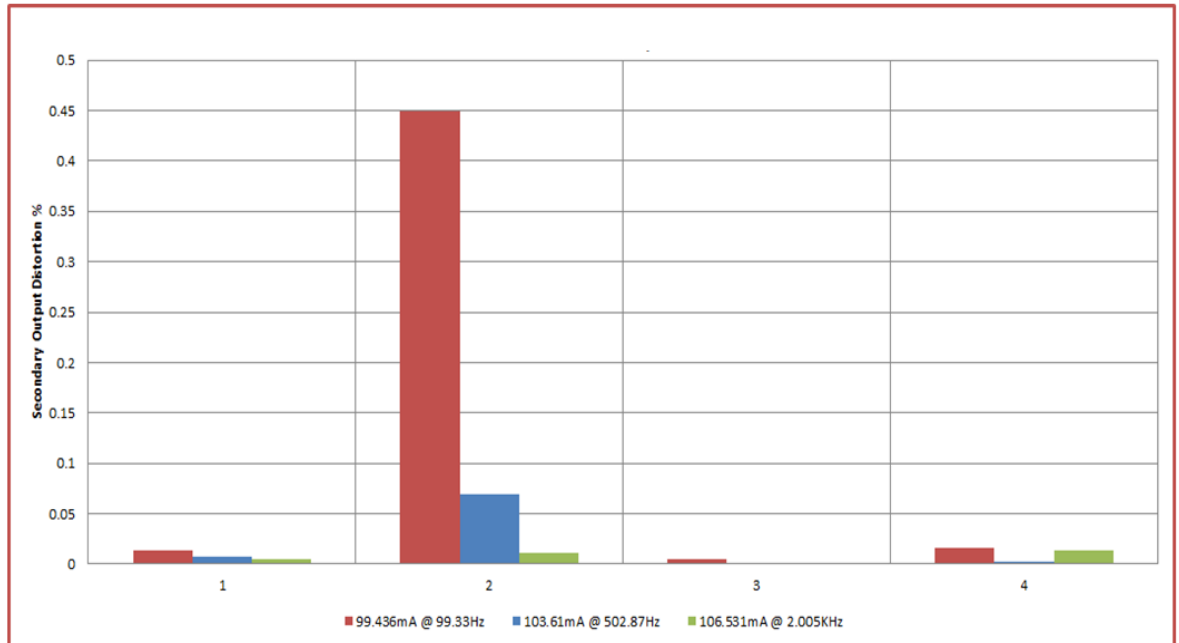


Figure 106 Hot harmonic testing at 99Hz, 502Hz and 2kHz

The harmonics test results show relatively low 2nd, 3rd, 4th and 5th harmonic effects at different supply current values and frequency values. The low values of the harmonics were not as a result considered a major source of error. Thus the harmonics are a low contributor to TIRPI sensor overall errors.

11.4 Secondary output voltage and primary voltage during warm-up

The TIRPI primary voltage was used to compensate for any secondary voltage output variations due to changes in the ambient temperature. This test showed the behaviour of the secondary voltage as the temperature of the TIRPI rose from 20°C to 200°C. The behaviour of the secondary voltage in response to temperature will be characterised as a mathematical function within the instrumentation electronics to allow for temperature compensation.

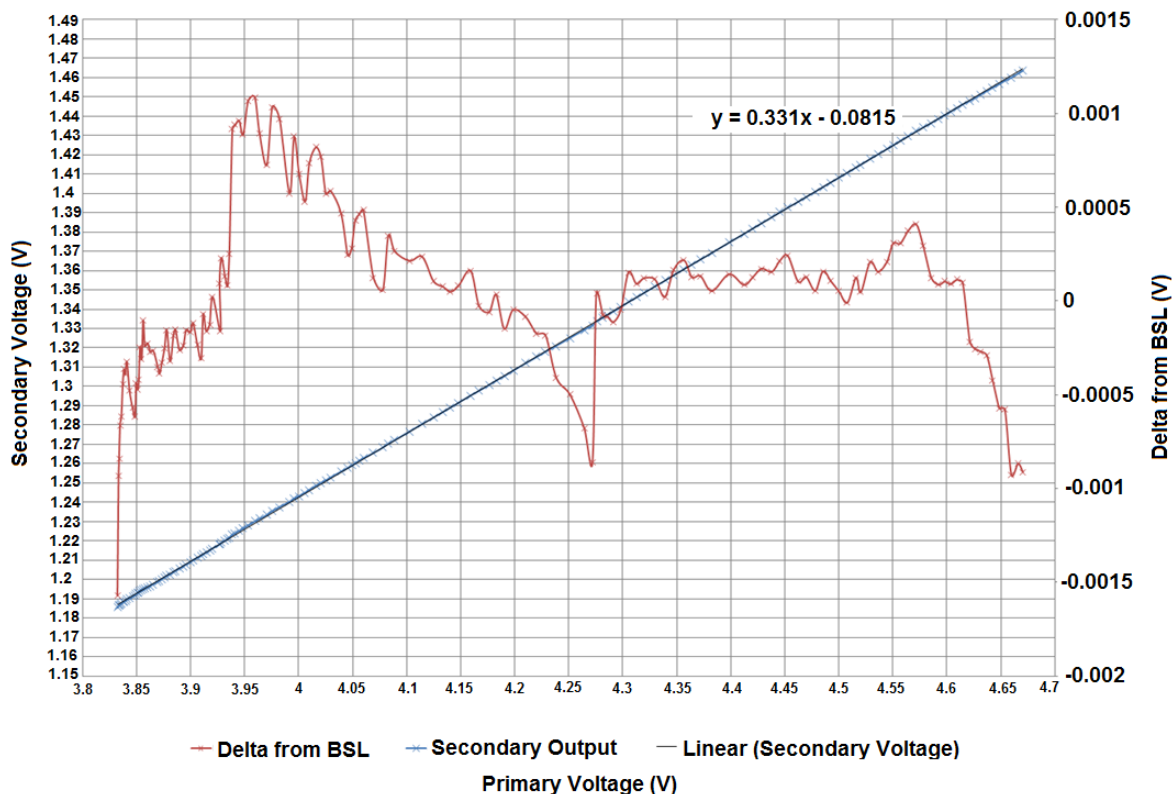


Figure 107 Secondary voltage as a function of primary voltage output

Figure 107 shows the secondary and the primary voltages increase due to the temperature of the TIRPI increasing. The relationship between the secondary curve and a best straight line fit of the secondary curve shows a linear relationship. Figure 107 shows the delta from the best straight line fit as approximately 0.001V. These results have a significant effect on the complexity of the instrumentation card because a linear thermal response is the most favourable to simplify the software algorithm required within the processor.

11.5 Frequency response test

One of the fundamental parameters which govern the sensitivity of the TIRPI is the operating frequency of the source signal. As this frequency changes, the induced eddy currents within the TIRPI, probe tube and driveshaft will change in amplitude and phase. The vector addition of the eddy currents at a particular frequency affects the resultant induced secondary voltage output of the TIRPI.

Figure 108 and Figure 109 show the secondary output voltage response curves when the primary current source frequency is increased from 100Hz to 2000Hz at constant primary current and temperatures of 200°C and 20°C respectively. In addition, the response of

secondary output voltage is shown when the driveshaft is at 0% and 100% percentage withdrawal. The voltage difference between 0% and 100% withdrawal is indicated as the span of the TIRPI, and the sensitivity is calculated by dividing the span of the TIRPI by the 100% driveshaft position value. The maximum span value is at 800Hz.

The hot frequency sweep test results are only valid when the sensor is used in the current bench setup condition, and a different result would be expected when the sensor is housed in a CRDM.

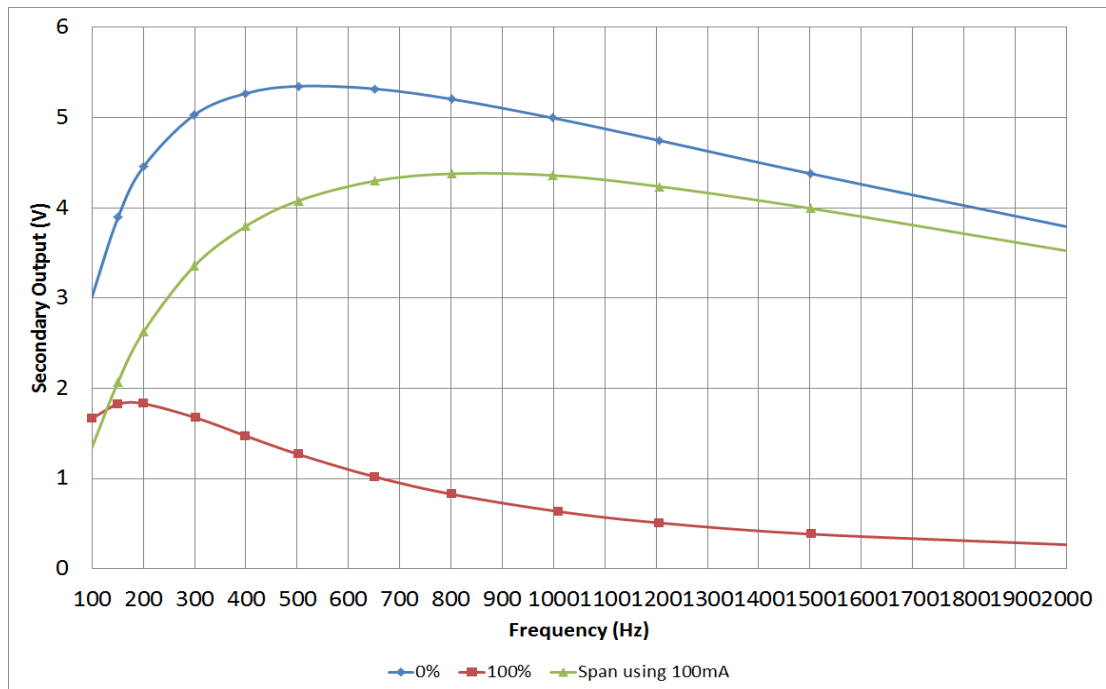


Figure 108 Bench hot frequency sweep test

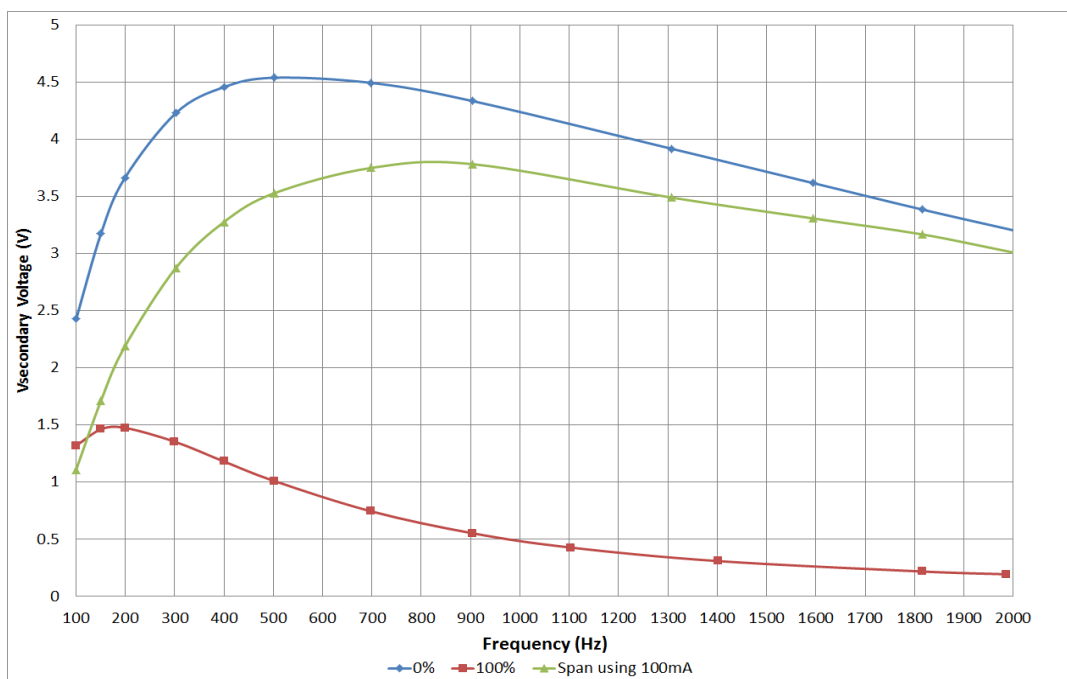


Figure 109 Bench cold frequency sweep test

11.6 Secondary voltage and primary current test

The TIRPI secondary output induced voltage is a function of the primary current amplitude. The secondary voltage was measured at three driveshaft positions: 0%, 50% and 100% of full scale driveshaft position. The primary current was increased from 0 to 210mA at the three stationary driveshaft positions at temperatures of 20°C and at 200°C. Figure 110 and Figure 111 shows how the TIRPI secondary voltage changes when the primary current is increased. The secondary output voltage TIRPI data changes linearly with respect to the primary current at all three driveshaft positions. These results were as expected. The smallest current possible should be used the limit self-heating effects of the TIRPI. Usually this is determined by the instrumentation card capability.

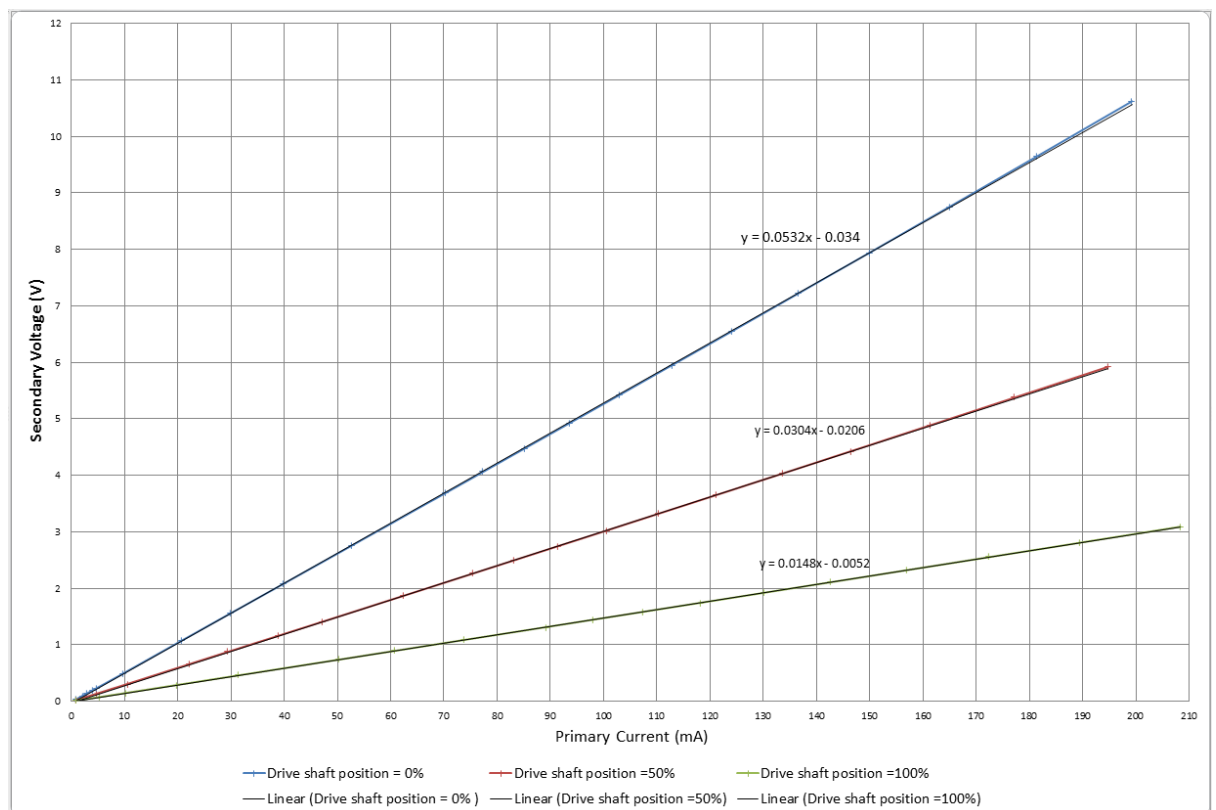


Figure 110 Hot primary current sweep

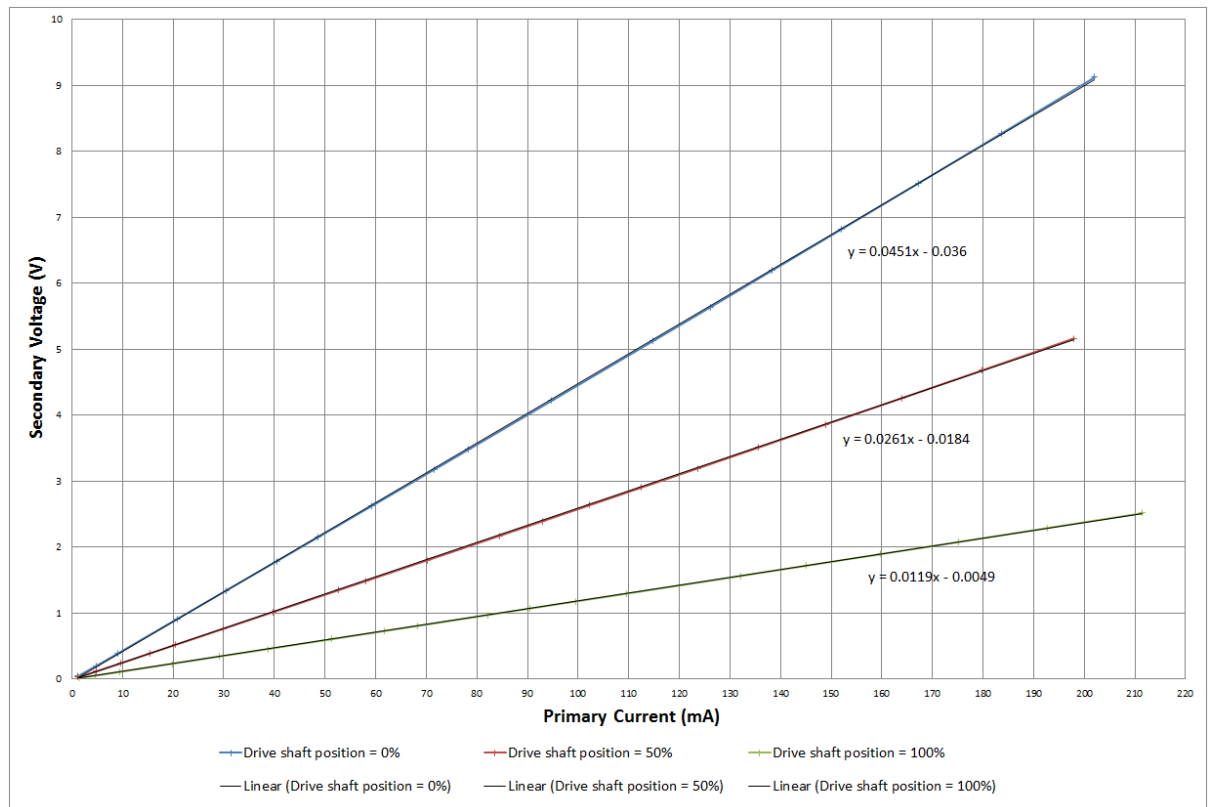


Figure 111 Cold primary current sweep

11.7 Secondary sensitivity sweep test at 400Hz

The CRDM uses a four-pole stator motor powered by a three-phase 12-step power supply to move the driveshaft. The CRDM (when powered) produces a radial force which engages the rotor arms onto the driveshaft. When the three-phase power supply is cycled, a torque is produced on the rotor arms causing them to rotate. Because the rotor arms are engaged to the driveshaft, the rotation causes the driveshaft to move upwards or downwards depending on the direction of the power supply cycle. The smallest rotational step of the rotor arms produces a linear driveshaft movement of 0.25mm.

To date, the current rod position transducer can only detect CRDM steps of 22mm. This results in an inaccurate position reading for the driveshaft. The prototype TIRPI transducer has an overall magnitude resolution better than the smallest increment of driveshaft movement produced by the CRDM (0.25mm), and hence an error of zero percent. However, any horizontal movement due to the mechanical tolerances of the driveshaft and probe tube can produce a position error of +/-0.25%.

Figure 112 shows a 40mm portion of the TIRPI secondary output voltage when the driveshaft overlaps the probe tube from 30mm to 40mm. The driveshaft position is shown

in steps of 0.25mm and readings for the primary current, primary voltage and secondary voltage were taken between each 0.25mm driveshaft increment. The results show that the secondary output voltage is monotonic and the TIRPI transducer can detect driveshaft steps of less than 0.25mm. As the minimum step generated by the CRDM can be detected by the TIRPI, the TIRPI sensitivity error is zero percent, not accounting for horizontal driveshaft motion producing +/-0.25% error.

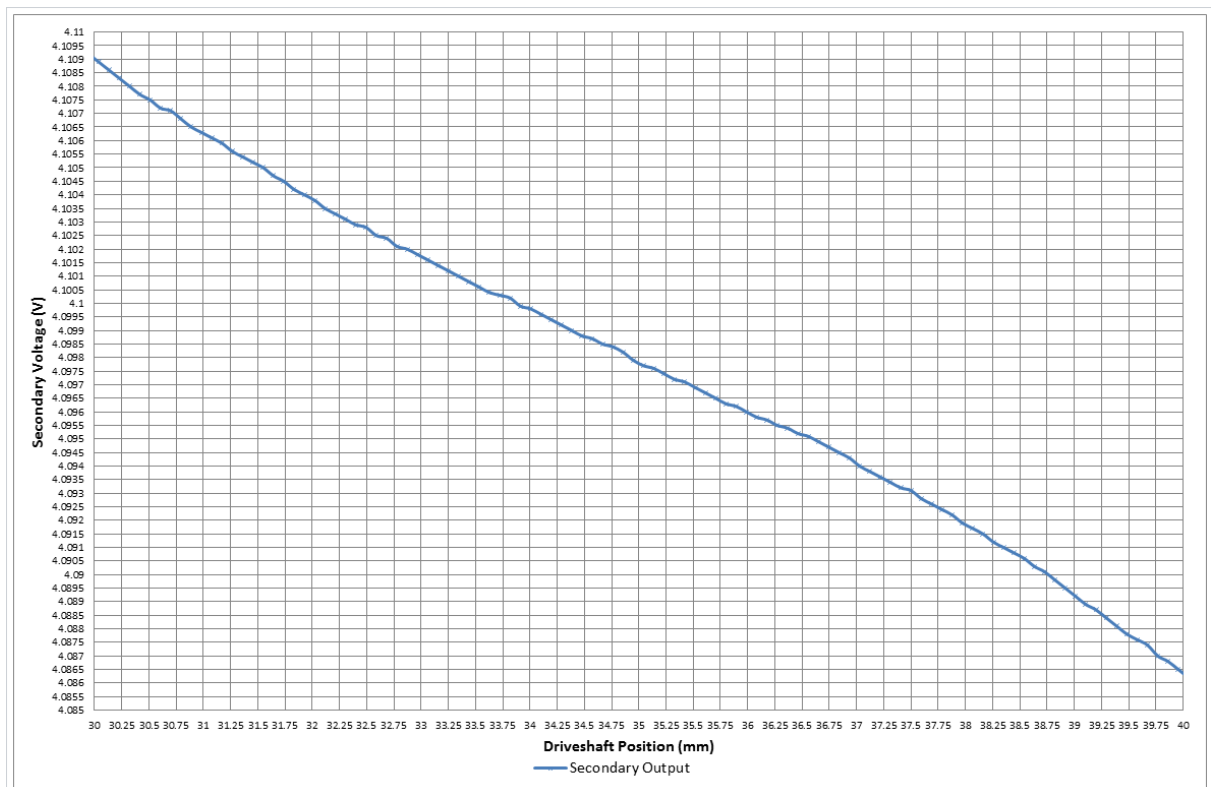


Figure 112 Sensitivity sweep test at 400Hz, 100mA

The most important characteristic of the secondary output voltage is the linearity of the curve. Linearity determines the slope of the curve, and therefore the sensitivity of the TIRPI transducer. Figure 113 shows a linear curve superimposed onto the secondary voltage output of the TIRPI transducer. For a sensor with the ideal linearity, sections A and B within Figure 113 would have as small as possible but equal areas. Figure 113 shows the practical test results of section A and B are similar. This would suggest the design of the TIRPI transducer has been relatively well optimised. The linearity of the TIRPI is affected by the geometries and materials used for the probe tube, driveshaft and TRIPI transducer.

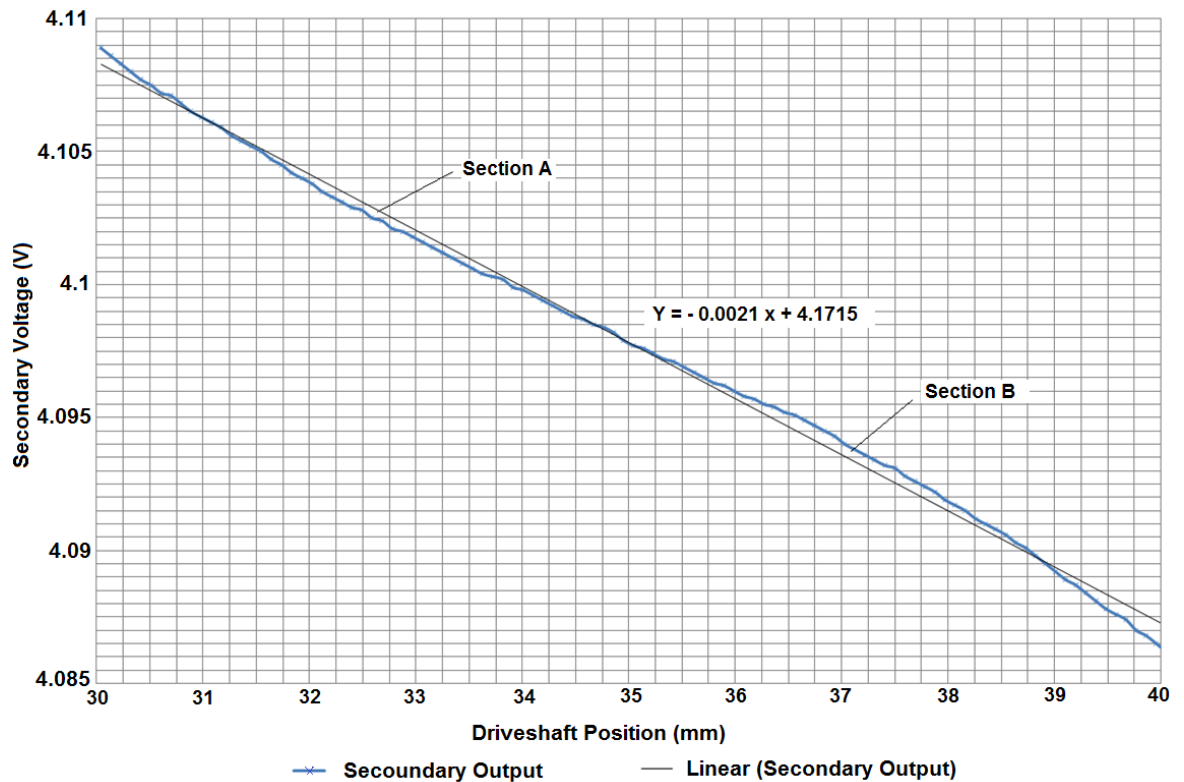


Figure 113 Linearity test

11.8 TIRPI cable capacitance test

The TIRPI is an inductive transducer. Electrical resonance can occur when the electrical circuits include inductive and capacitive elements. Inductance exists within the primary and secondary coil windings of the TIRPI. In addition, the cable connected to the TIRPI and the instrumentation electronics has capacitance. A practical test was carried out using the TIRPI at a nominal primary voltage of 4.28Vrms and a variable capacitance box to simulate changing cable capacitance of the cable changing when used in situ on a submarine individual rod position channel. Figure 114 shows the capacitance characteristics versus the secondary TIRPI voltage output. It shows that the maximum secondary voltage is within the range 6.5Vrms to 7Vrms. Within this range, a cable with a capacitance of approximately 360nF will produce a resonance condition between the cable and TIRPI.

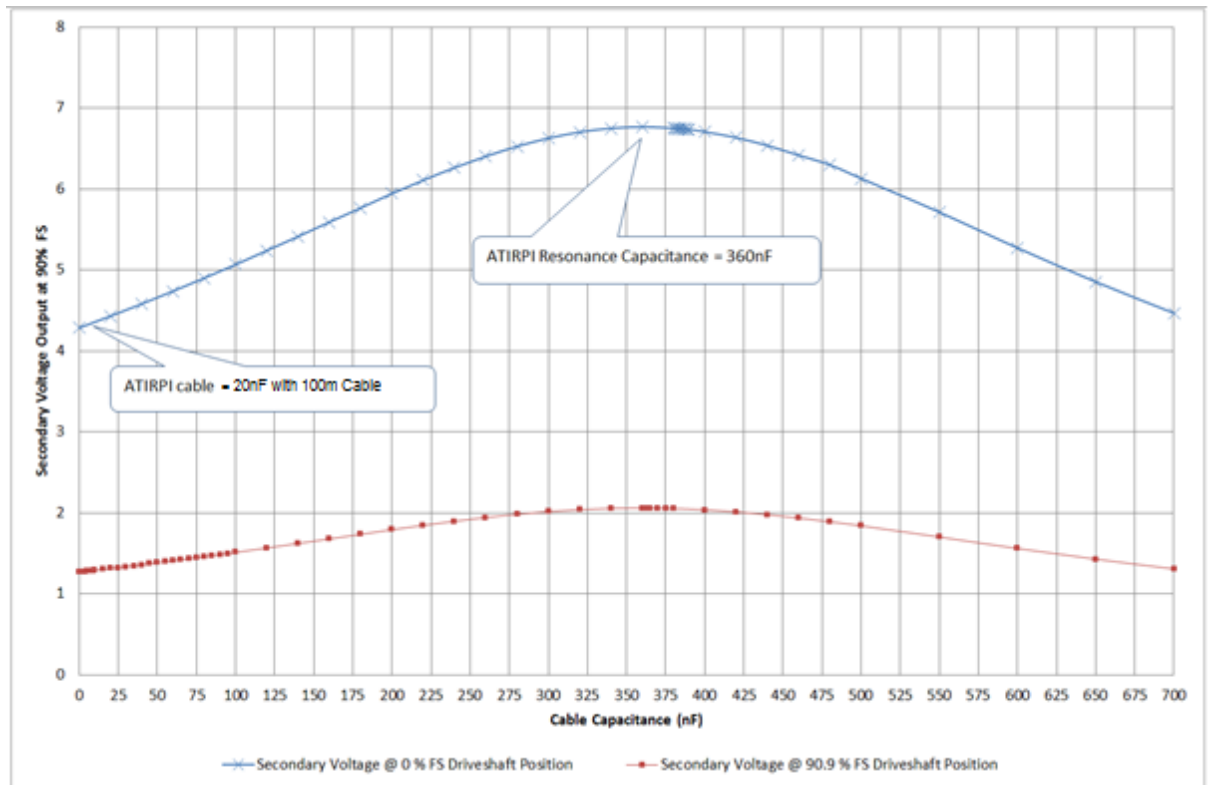


Figure 114 TIRPI and cable capacitance test

11.9 Mini TIRPI with manganin wire

An additional shorter length TIRPI was prototyped for the core material testing. The core characteristics are fundamental to the performance of the TIRPI. These enable the secondary output signal to be higher amplitude for the instrumentation card input circuitry. This enables the instrumentation card to provide a higher accuracy measurement capability. An ideal design of the TIRPI would be one which would give the same secondary output voltage throughout the thermal operating range experienced by the sensor and system. The Mini TIRPI components which could change behaviours and characteristics with temperature are assumed to be the core material and electrical copper wire. However, without testing, this cannot be confirmed. When electrical copper wire is used instead of manganin wire, the resistance of the wire increases with temperature significantly enough to require thermal compensation within the instrumentation card. However, it is not known whether this is also true for the core material. Ideally assuming the ideal core material is S14 3SS(17.4PH) and its characteristics do not change with temperature, then a material with a different thermal coefficient can be used for the wire

instead of the copper or manganin for example. As a result, the TIRPI secondary output signal would not be temperature dependent and would not require thermal compensation. To fully understand whether this hypothesis is correct an investigation into the thermal effects of the core material and surrounding materials was undertaken.

To investigate behaviour of the core material, the wire material was initially changed to manganin. Manganin is known for its good thermal characteristics, and its electrical resistance changes with temperature are negligible. As the secondary output signal is governed by the wire resistance and the core material effects varying with temperature, we can use the secondary output signal as a method of sensing the thermal effects on the core material.

A smaller TIRPI was manufactured to test the thermal core material behaviour (known as the Mini TIRPI). The Mini TIRPI has a design that is similar to the TIRPI, with a primary coil and a secondary coil throughout its length. However, in addition, a copper wire coil was wound on the primary coil. The function of the copper primary coil was to allow a temperature measurement to be obtained when the temperature was changed. This was needed because the manganin wire would not indicate any significant resistance variation due to temperature increase. The additional copper wire was supplied by a direct current supply, and a resistance meter to measure the resistance. As a result, the addition of the copper wire would have no effect on the primary and secondary manganin coils as no induced voltage would be generated.

Figure 97 shows the manufactured Mini TIRPI. The Mini TIRPI has been manufactured to the same standard as the full length TIRPI previously described. This manufacturing standard ensured the test piece was fit for its intended use within the environmental chamber, where it would be thermally cycled and provide results which can be compared to a set of expected or simulated results.

The experimental core thermal response of the mini TIPRI produced absolute values of primary and secondary voltages which are not important; it is the difference between them that is important. The ideal results would be no change in the secondary output voltage when the Mini TIRPI environment temperature was changing. However, due to the core material being both an electrical and magnetic conductor we can only analyse the

measurement of the change in the secondary output signal and evaluate how this would result in measurement errors.

Figure 115 shows the test results of the Mini TIRPI temperature at a number of specific driveshaft positions: nominally at 0mm, 100mm, 200mm, 300mm, 400mm, 500mm, 600mm, 700mm and 770mm. The results show that when the temperature of the Mini TIRPI is increased and the driveshaft envelops the probe tube, the secondary voltage decreases. It also shows that all the curves trend in a linear fashion in the same direction as the temperature increases. It can be concluded therefore that the core material or a material surrounding the core is affected by temperature and this is a significant parameter for TIRPI accuracy. However, it also shows that the temperature compensation algorithm used in the instrumentation card can be a linear compensation. This is a major advantage as the instrumentation requires software computation to be simple as possible for the nuclear safety case approval.

To verify that the environment of the Mini TIRPI was at the intended temperature value, the resistance of the copper wire adjacent to the manganin wire on the Mini TIRPI was measured. The temperature coefficient of copper is $0.4\%/^{\circ}\text{C}$, and a correlation of the resistance and temperature value was recorded and shown in Figure 116. The results were as expected, showing a linear trend of resistance versus temperature. It was therefore concluded that the Mini TIRPI was operating at the intended temperature.

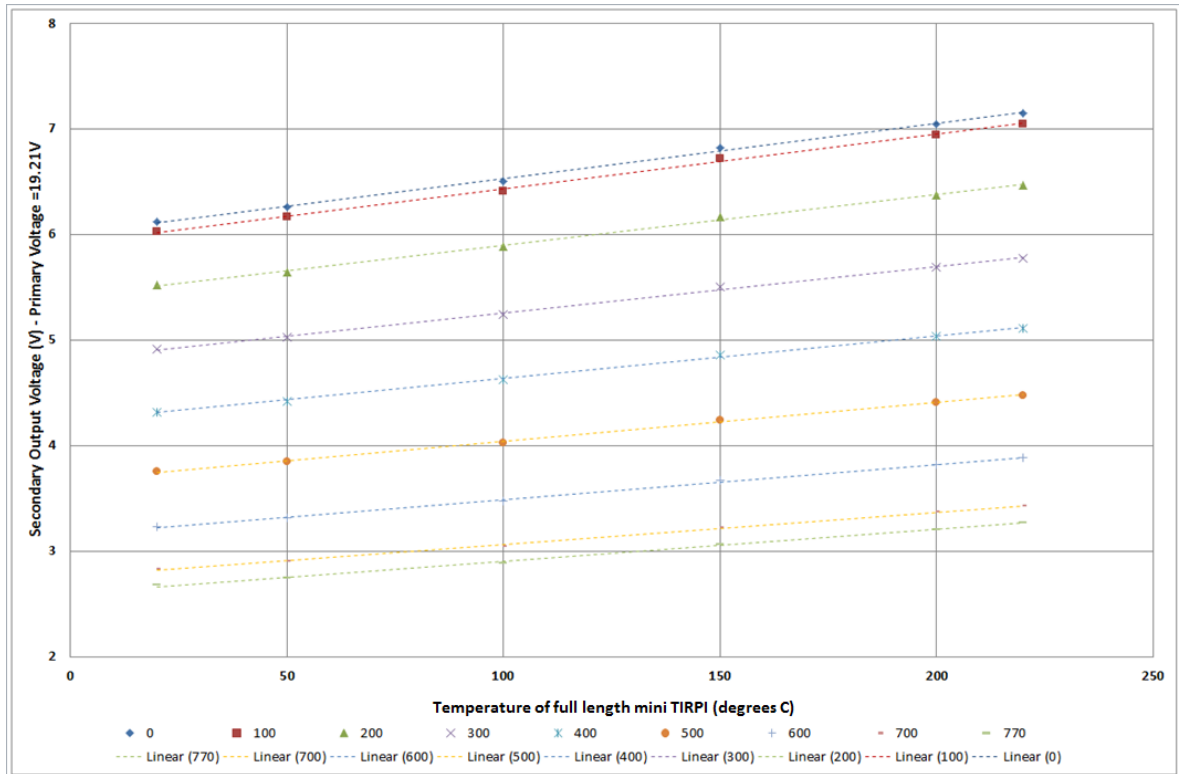


Figure 115 Mini TIRPI thermal effects

The two parameters which could cause a material to change its electro-magnetic behaviour when its temperature is increased are the material electrical conductivity and the magnetic material B-H curve characteristics. The physics which explains why this occurs are not within the scope of this thesis, however, a hypothesis could be formed to explain whether the conductivity of the material is the dominant parameter affecting the change in the material characteristics with temperature, or whether it is the permeability of the B-H curve characteristics which is more dominant.

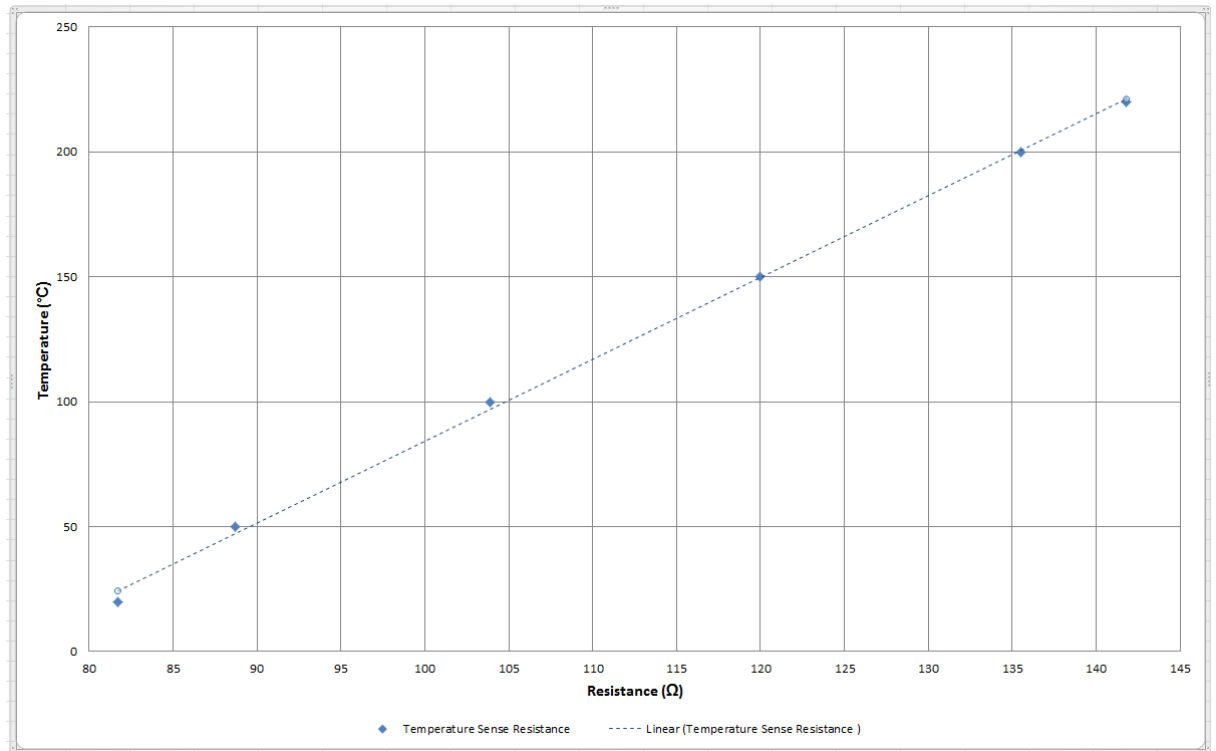


Figure 116 Mini TIRPI temperature sense wire results

To provide the basis for this hypothesis, the effects of increasing the temperature on the material characteristics of the Mini TIRPI core former and probe tube need to be investigated independently. The B-H curve characteristics can be tested using unique thermal B-H testers; however, this is not a practical option for this project due to cost. The conductivity of the material however can be initially measured using an accurate ohm meter, and then re-measured as the core material is heated up within an oven.

It is important to measure the small resistances without external influences such as changes in the resistance of the external ohm meter wire when the oven temperature increases. A test procedure consisting of spring-forced probes (shown in Figure 123) was used to enable a good electrical contact on the probe tube and TIRPI core being tested. These required the user to press down when taking the measurement and a reading was taken only when a good contact was established.

In addition to the material characteristics of the Mini TIRPI, the geometry of the surrounding materials (such as the probe tube and driveshaft) is very important. Not only do the material properties define the TIRPI secondary output voltage, but the position of materials relative to the generated primary magnetic field is also a factor. To understand which materials are dominant, a systematic approach is required to analyse how the Mini

TIRPI secondary output voltage changes with temperature. The components which require further investigation are the Mini TIRPI core and the probe tube. It is important to recognise that the driveshaft effects can be inferred from the results shown in Figure 115. Comparing the slope of the curves for each temperature value in Figure 115 shows the driveshaft has a negligible effect on the TIRPI secondary output voltage as it envelopes the probe tube. The testing was carried out on the Mini TIRPI using a heat plate and high accuracy megger ohm meter to identify the thermal conductivity of the probe tube and the TIRPI core former. The probe tube was subjected to an additional magnetic permeability test, as this is was not magnetic and could be tested using a magnetoscope. The data from the results could then be used to confirm what affects the TIRPI secondary output voltage by isolating each component and parameter in turn, and then using an alternative analytical method (such as a finite element modelling tool) to confirm its individual effect on the overall system.

Testing was initially carried out on the probe tube which is made of Inconel 625. The probe tube was laid onto a hot plate, where the upper of the probe tube would be in contact with the hot plate. The surface of the hot plate was then warmed up to 250 °C. The arrangement for the heating of the upper side specific area of the probe tube as illustrated is Figure 117 and Figure 118. These arrangements established a thermal distribution of heat throughout the probe tube length.

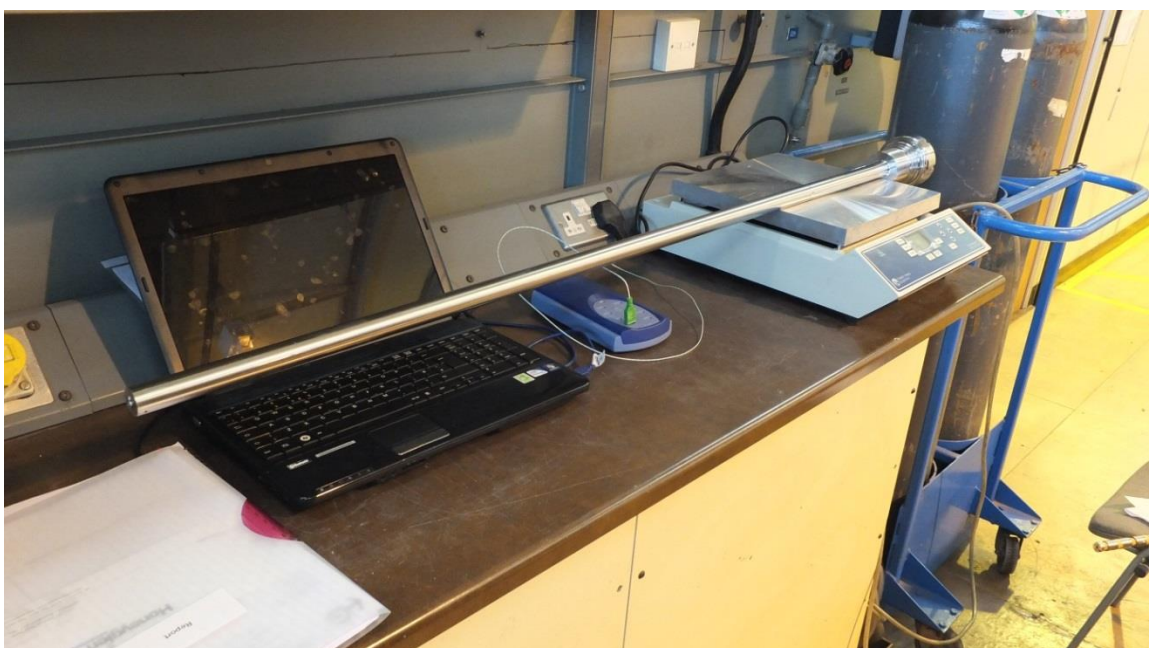


Figure 117 Probe tube hot plate testing PC and data logger



Figure 118 Probe tube hot plate testing setup

The probe tube was divided into a numbered scale 1 to 14 shown in Figure 119 to allow a specific point to be repeatedly tested as the hot plate heated up.

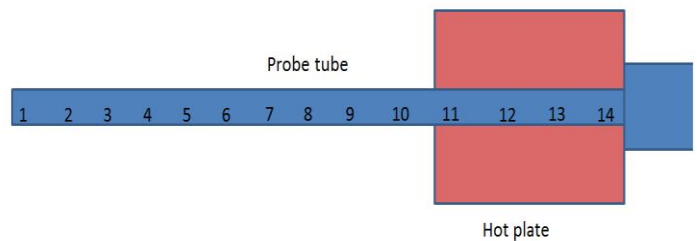


Figure 119 Probe tube hot plate testing positions

This test would determine the temperature of the selected specific point using a PC-driven thermometer and a sigmatest conductivity meter (shown in Figure 120) to measure the electrical conductivity at the measured temperature.



Figure 120 Electrical conductivity meter

The probe tube was laid onto the hot plate where it was supported by its own weight and geometry. Further inspection noted that the surfaces of the probe tube and hot plate were in better physical contact at a specific region around reading position point 12 (as shown in Figure 121) due to the flatness of the surface straightness of the hot plate. This resulted in point 12 being the optimum test position to determine the thermal effects on the probe tube conductivity due to the heat transfer between the hot plate surface and the probe tube surface.

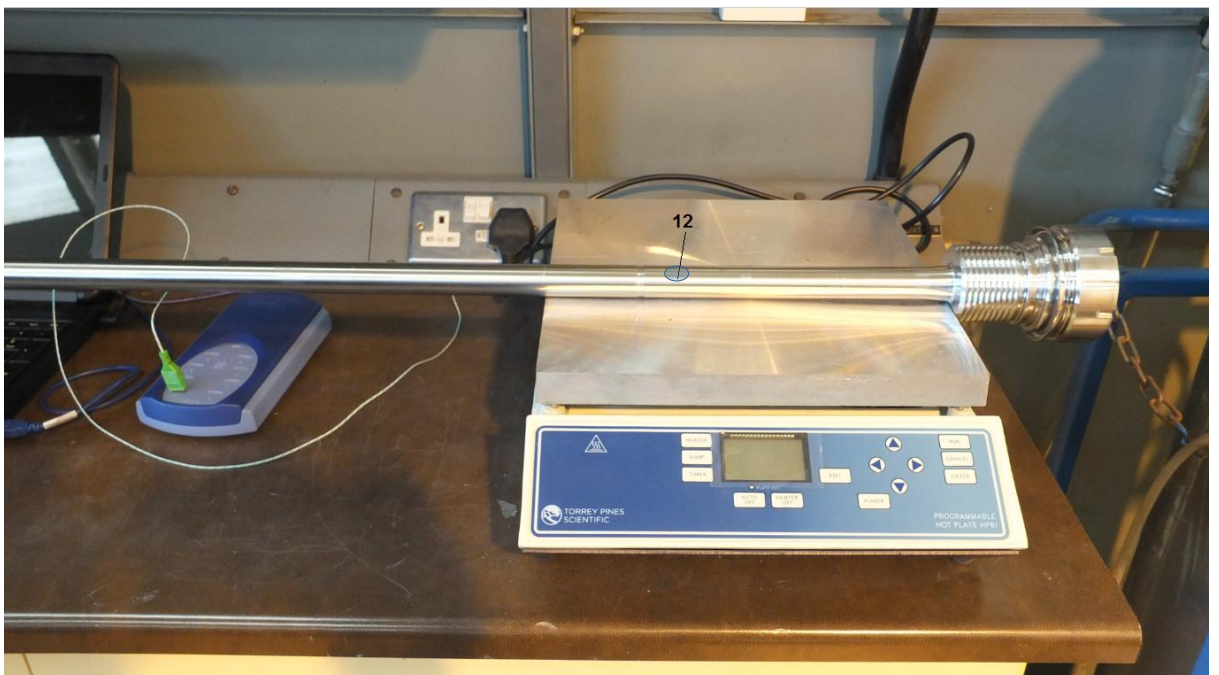


Figure 121 Probe tube hot plate testing reading position

Following the thermal electrical conductivity tests for the probe tube, a similar approach was adopted to measure the magnetic permeability of the probe tube when subjected to a thermal gradient along its length. For this test, the same PC thermometer system was used. A magnetoscope shown in Figure 122 was used to determine the magnetic permeability of the material subjected to the thermal gradient. Similar to the electrical conductivity test, the temperature and magnetic permeability readings were taken along the length of the probe tube while the hot plate was heating up to 250 °C. For both the electrical conductivity and magnetic permeability results a linear average line was determined and therefore an equation which described the thermal behaviour of the probe tube in terms of electrical conductivity and magnetic permeability. These calculations were used to predict what the electrical conductivity and magnetic permeability would be at a specific temperature such as 220 °C. This in turn enabled a direct comparison to be made between the test results previously observed (see Figure 115) and the finite element analytical model using the practical electrical conductivity and magnetic permeability values from the thermal tests.



Figure 122 Magnetic permeability meter

Part 2 of the testing was to test the core former material as this affects the secondary output of the Mini TIRPI. This was made of 17.4PH and exhibits magnetic properties including magnetic permeability. The results obtained previously using the sigmatest

electrical conductivity meter could not be repeated for magnetic materials as the AC test current used would generate eddy currents and these eddy currents would interfere with the electrical conductivity measurements. To overcome this challenge, a digital low-resistance ohm meter was used which would measure the resistance of the 17.4PH material at different temperature values. This meter is shown in Figure 123. The digital-low resistance meter produces a 10A DC current measures low resistance values down to milliohms. The meter was used to measure the value of material resistivity value and calculate the electrical conductivity for the 17.4PH material. The meter uses a set of 4-point measurement probes to carry out the test.



Figure 123 Digital low resistance ohm meter

In addition to determining the electrical conductivity of the 17.4PH material, it would be useful to determine its magnetic behaviour and establish B-H curves for different values of material temperature. However, this would require a significant investment and was not practical for a single test. An alternative approach would be to calculate the conductivity of the 17.4PH and use finite element modelling tools to show whether the electrical conductivity variation due to temperature was similar to the results observed in Figure 115. Should the electrical conductivity show negligible influence on the results, it could be concluded that the TIRPI core material magnetic permeability was the significant

factor causing the TIRPI secondary output voltage to change when subjected to a temperature increase.

The Mini TIRPI was laid onto the hot plate in a manner similar to the probe. Two locations, the 4th and 15th bobbins were selected for the conductivity testing as shown in Figure 124. The contact to the core was made using a 4 point measurement probes. It was observed that the 15th bobbin on the TIRPI made better contact with the hot plate. It was decided therefore that this position should be used as the reference temperature to increase the accuracy of the results obtained.

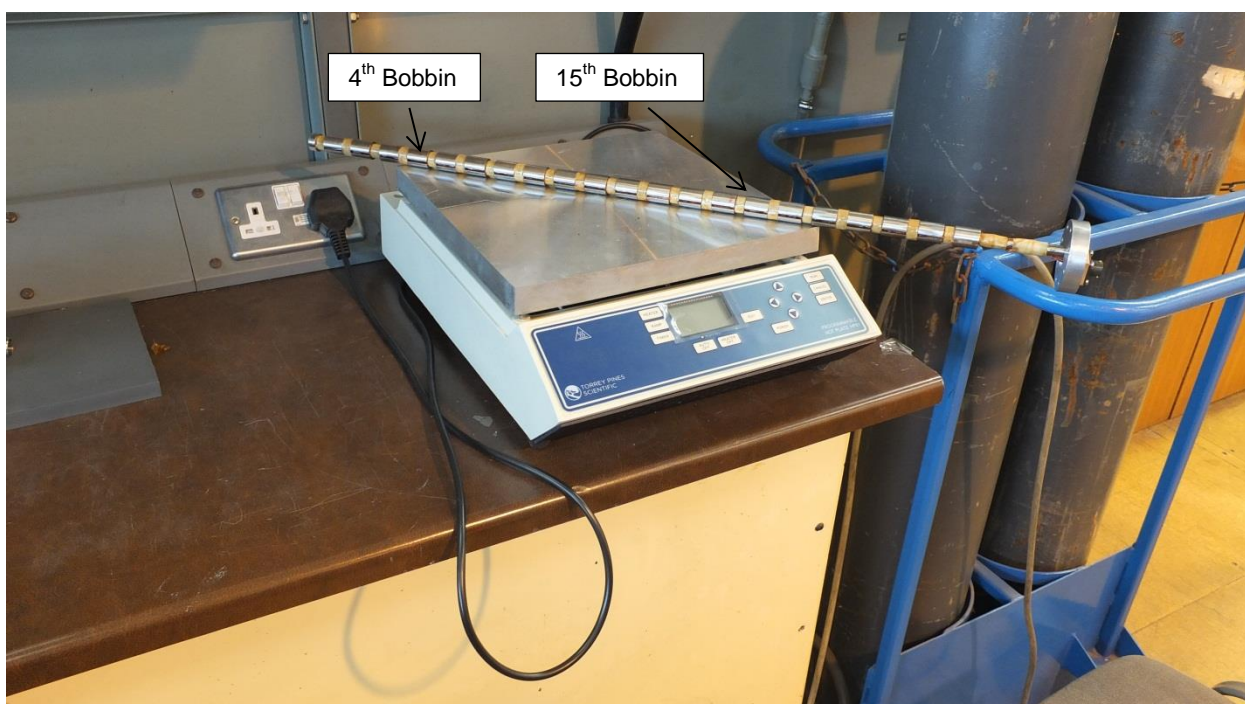


Figure 124 Mini TIRPI hot plate testing positions

The resistivity of the Mini TIRPI was measured continuously across points 4 and 15 to ensure the same of length of the Mini TIRPI core was being measured. Initially, the temperature at points 4 and 15 were measured and as quickly as possible followed by the resistance. The digital low-resistance ohm meter enabled a good contact to be established and therefore an accurate reading. The testing was repeated over a range of temperatures as the hot plate increased to a temperature of 250 °C.

The results from the probe tube and Mini TIRPI testing shall be discussed within this section and conclusions made to determine whether the conductivity of the system way the dominant effect on the Mini TIRPI secondary output voltage.

The electrical conductivity of the probe tube was tested at specific location points 1 to 14 (as shown in Figure 119) at an ambient temperature of 23.31 °C.

When the hot plate was cold, an average normalised electrical conductivity value across the probe tube length was recorded shown in Figure 125. The average value of the electrical conductivity was 0.6191 MS/m. This correlated with the expected value of approximately 0.6 to 0.7 MS/m.

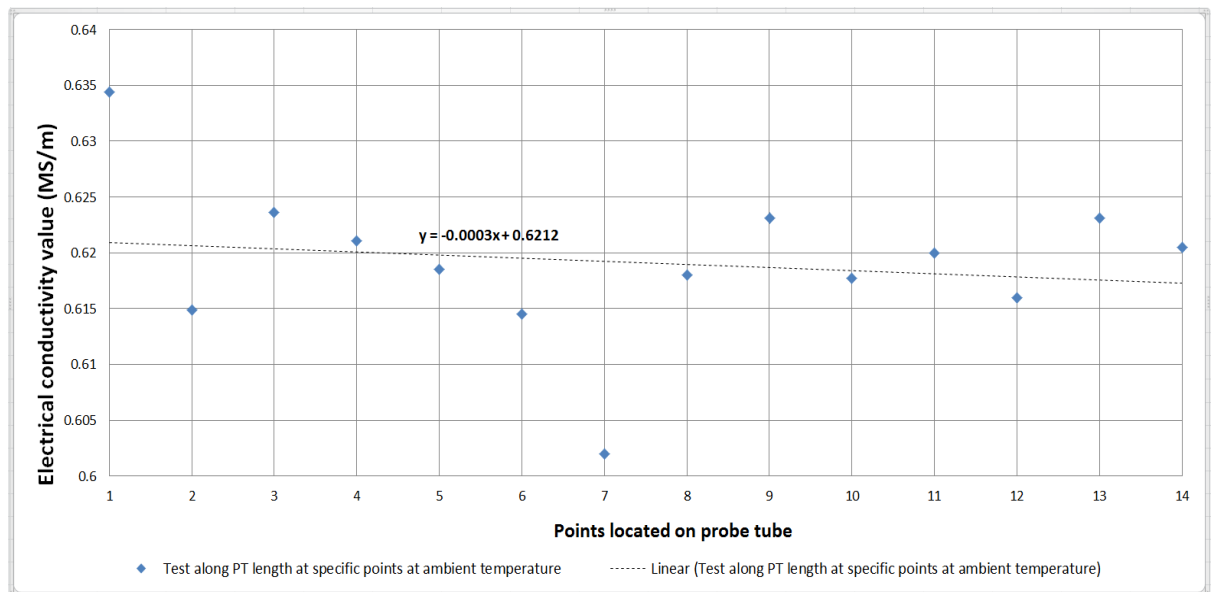


Figure 125 Probe tube electrical conductivity at ambient temperature

After the ambient measurements, the hot plate was set to 250 °C and the upper surface was heated of the probe tube. The probe tube was only in contact with the hot plate between the points 11 to 14 (as illustrated in Figure 119). The specific temperature at each numbered point was measured prior to taking the electrical conductivity values. Although the hot plate only had a surface temperature of 250 °C, the amount of heat being dissipated was relatively large as the metal volume of the probe tube was larger than the hot plate surface. Each temperature and electrical conductivity value was taken individually to limit inaccuracies in temperature gradients developed across the probe tube. The thermal gradient produced by the hot plate and probe tube setup was considered to be more representative than heating the probe tube to a single temperature as the thermal gradient developed would be similar to a CRDM environment in practice.

Physical contact between the probe tube and the hot plate is important for the heat transfer. As a result point 12 was used as this was observed to have the most surface area in contact with the hot plate. As the temperature of the hot plate and the temperature of the probe tube increased, the temperature and the electrical conductivity of the Mini TIRPI core material was recorded at point 12. Figure 126 shows the results obtained. This concludes that there is negligible change in the measured electrical conductivity as the temperature increases.

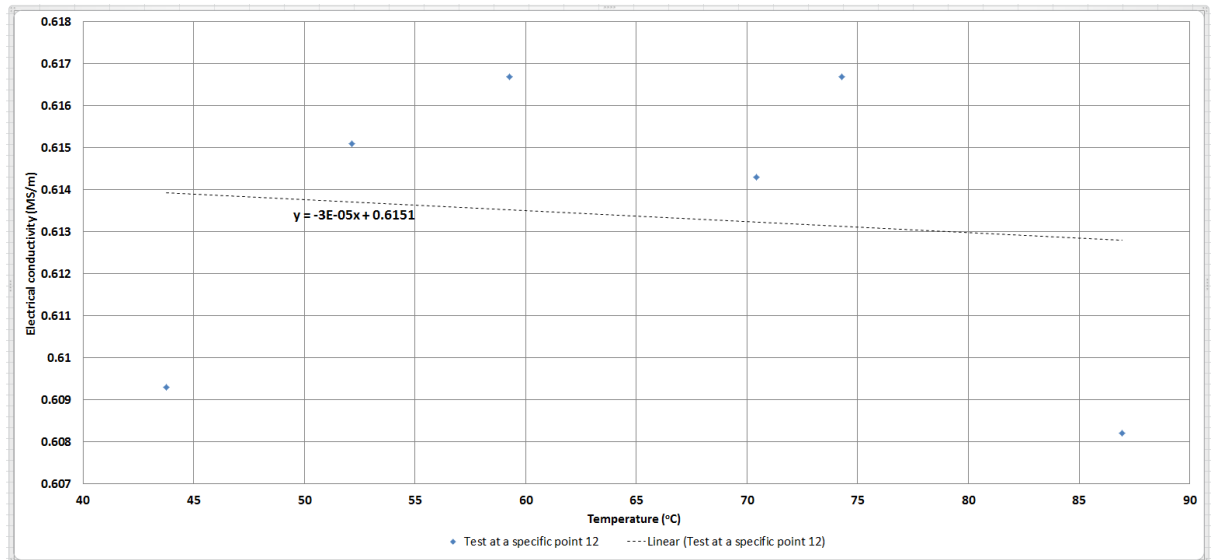


Figure 126 Probe tube point 12 electrical conductivity at temperature

The temperature and electrical conductivity readings were taken at all the points 1 to 14, diametrically opposite the hot plate surface. This was done to ensure that the probe tube was at the soaked temperature illustrated in Figure 121. The data collected (shown in Figure 127) can be normalised with a linear curve fit as the effects of temperature versus electrical conductivity throughout the probe tube length are assumed to be linear. As such, a prediction can be made of the electrical conductivity value at a temperature value of 220 °C which is close to the temperature used in operation. This predicted value could then be compared to the Mini TIRPI secondary output change illustrated in Figure 115 to identify whether the temperature changes was totally due to the probe tube electrical conductivity.

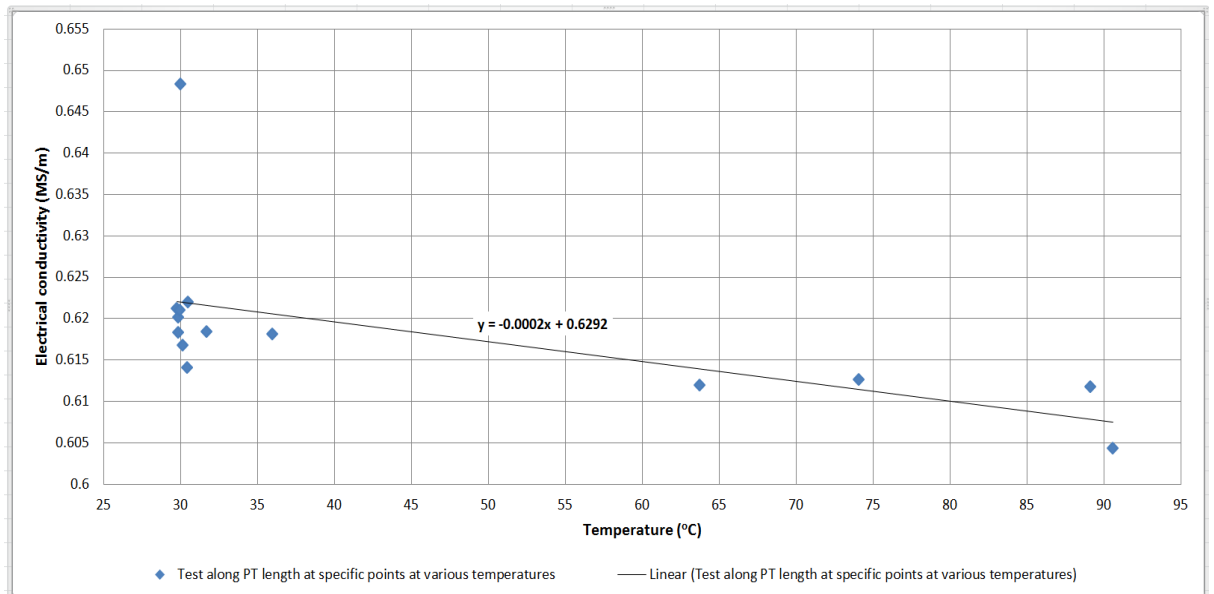


Figure 127 Probe tube electrical conductivity at temperature

Using the derived linear fit equation shown in Figure 127, the electrical conductivity could be derived at the probe tube temperatures of 20 °C and 220 °C. These values could then be used in the FE model to analyse the effect on the secondary output voltage. The percentage change obtained from the FE model for the Mini TIRPI secondary output could then be compared to the practical test results shown in Figure 115. This would determine whether the probe tube electrical conductivity was a significant factor and needed to be considered when operating the Mini TIRPI at elevated temperatures.

The difference in temperature of the secondary output voltage was 1.029V over a temperature range of 200 °C. This equates to a 16.81% change in secondary output voltage, as observed in Figure 115. The probe tube conductivity could be calculated using the linear equation in Figure 127. This resulted in conductivity values of 0.6252MS/m at 20 °C and 0.5852MS/m at 220 °C. The electrical conductivity values were analysed using the FE model tool. The results showed that the secondary output voltage changed by only - 0.07843V. This equates to a 1.2 % change of the secondary output voltage. It could be concluded therefore that the electrical conductivity was not the dominating parameter that influenced the output when the Mini TIRPI core bar material was subjected to thermal change.

In addition to the electrical conductivity of the probe tube, the magnetic permeability of the Mini TIRPI core bar material could also change with temperature. A similar approach to the electrical conductivity testing was adopted with magnetic permeability values recorded

at different temperatures. Initially, the ambient temperature magnetic permeability was recorded across all the probe tube points. The results showed a value across the total probe tube length of approximately 1.000 as expected. This is illustrated in Figure 128. The results showed that the effects of the manufacturing and heating processes were consistent along the probe tube.

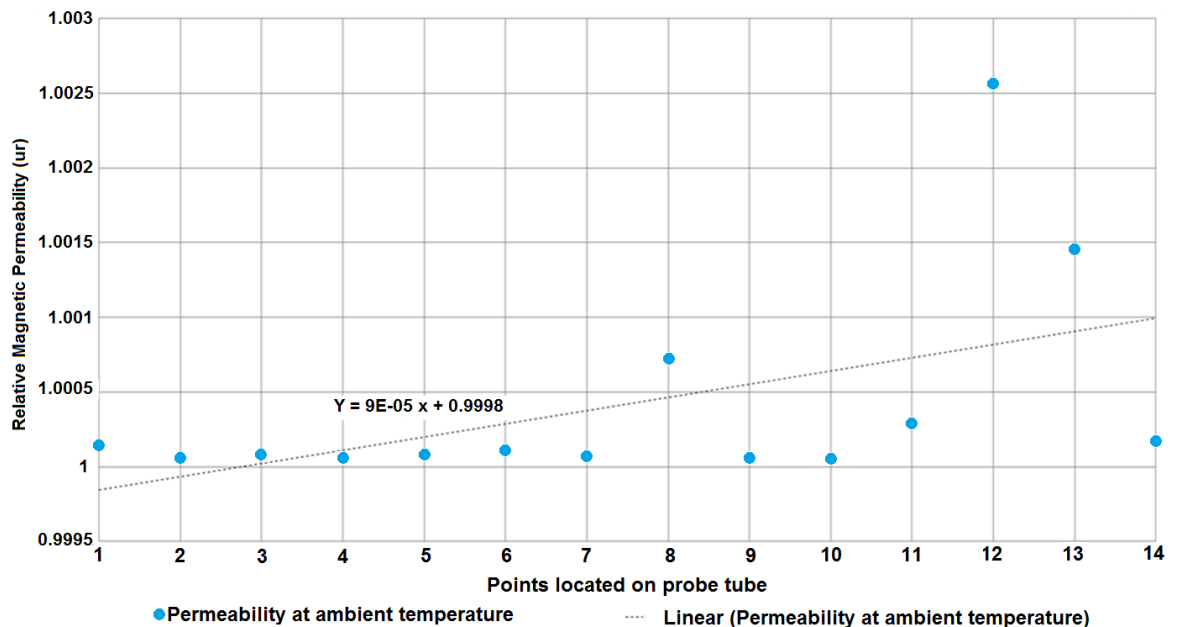


Figure 128 Probe tube magnetic permeability at ambient temperature

As the hot plate was heating up the probe tube would also heated up and produced a thermal gradient throughout its length. The temperature and magnetic permeability were taken periodically to establish a trend of the temperature versus the magnetic permeability. The results in Figure 129 show the relative magnetic permeability reducing as the temperature increases; however the change is very small. Using a linear fit curve, the change in magnetic permeability is 1.0024 to 0.9624 when temperature change of 20 °C to 220 °C is applied. To establish the effect on the secondary output voltage, the FE model was used to analyse the effect of the changing magnetic permeability. The secondary output voltage changed by 0.0216V, which equates to an equivalent change of 0.35 %. Such a small change was considered negligible.

The total effect of the probe tube on the Mini TIRPI secondary output voltage due to the increasing in temperature was calculated by adding the effects of both the electrical conductivity and magnetic permeability. This resulted in a total 1.55 % change of the

secondary output voltage for the mini TIRPI. The result falls significantly short of the 16.81% change that was observed for the secondary voltage when the temperature was increased. It was concluded therefore that the probe tube was not a component which had a significant effect on the secondary output voltage.

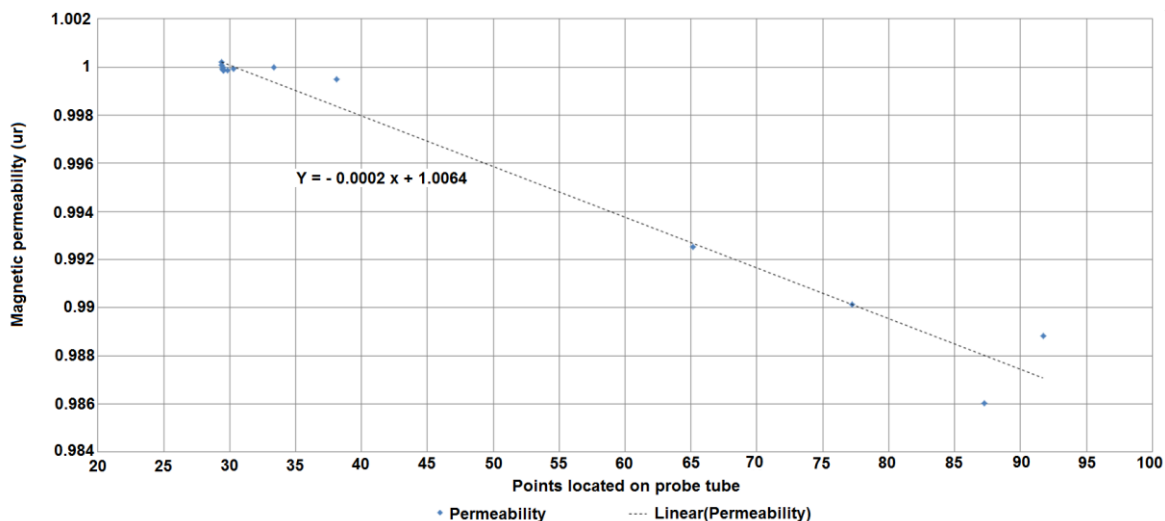


Figure 129 Probe tube relative magnetic permeability at temperature

The other component which required testing was the core bar former. The core former was placed onto the hot plate in such a way that at least a single bobbin section was in good contact with the hot plate surface. Bobbin number 15 (as shown in Figure 124) had the best physical contact with the hot plate.

The hot plate was set to 250 °C, and the temperatures of bobbin numbers 4 and 15 were taken and the resistance between bobbin 4 and bobbin 15. Once the hot plate reached the equilibrium temperature of 250 °C the core former was at a temperature of 91 °C. The results are shown in Figure 130. The results show that electrical conductivity increases with an increasing core former temperature. Using these results, the resistivity values could be calculated at different temperature values. This would allow the electrical conductivity values of the core bar former to be determined using a linear fit equation.

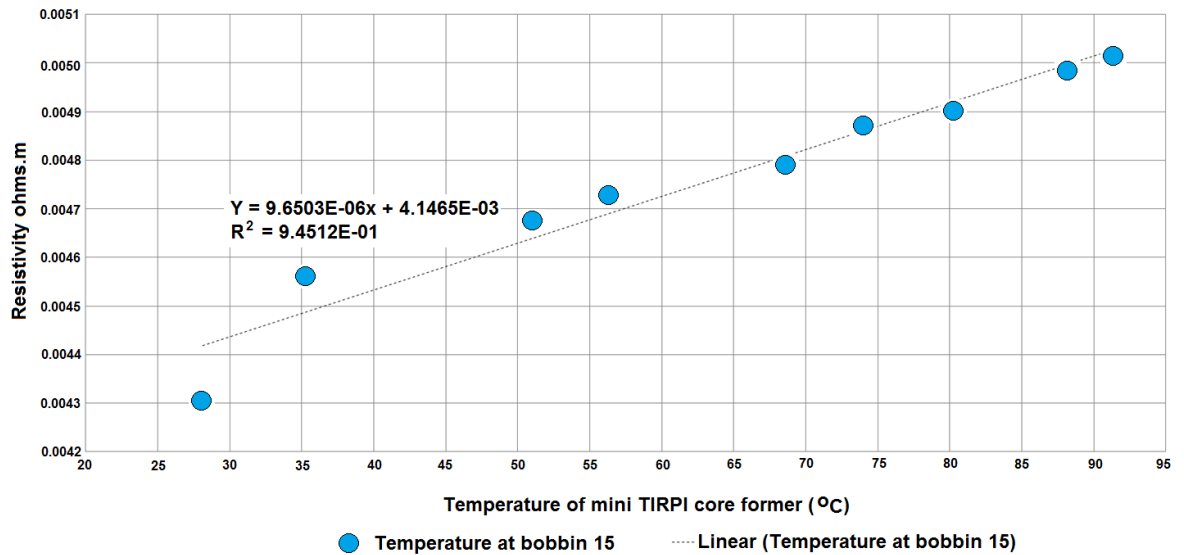


Figure 130 Core former electrical resistivity temperature

The data showed that the electrical conductivity varied with temperature. A linear curve fit of the data points was established as shown in Figure 131. This was used to predict the variation in electrical conductivity for the core former when the temperature was increased from 20 °C to 220 °C.

Using the equation for the linear curve fit, the electrical conductivity changed from 1.164E6 MS/m to 0.806E6 MS/m. These electrical conductivity values were then used in the FE model to determine the secondary output voltage. The predicted change in the secondary output voltage was 1.08V which equated to a 16.85 % variation. The practical testing of the Mini TIRPI secondary output showed a change of 16.81 %. This result suggested shows that the core former electrical conductance was the significant component that influenced the secondary output voltage when the temperature was increased.

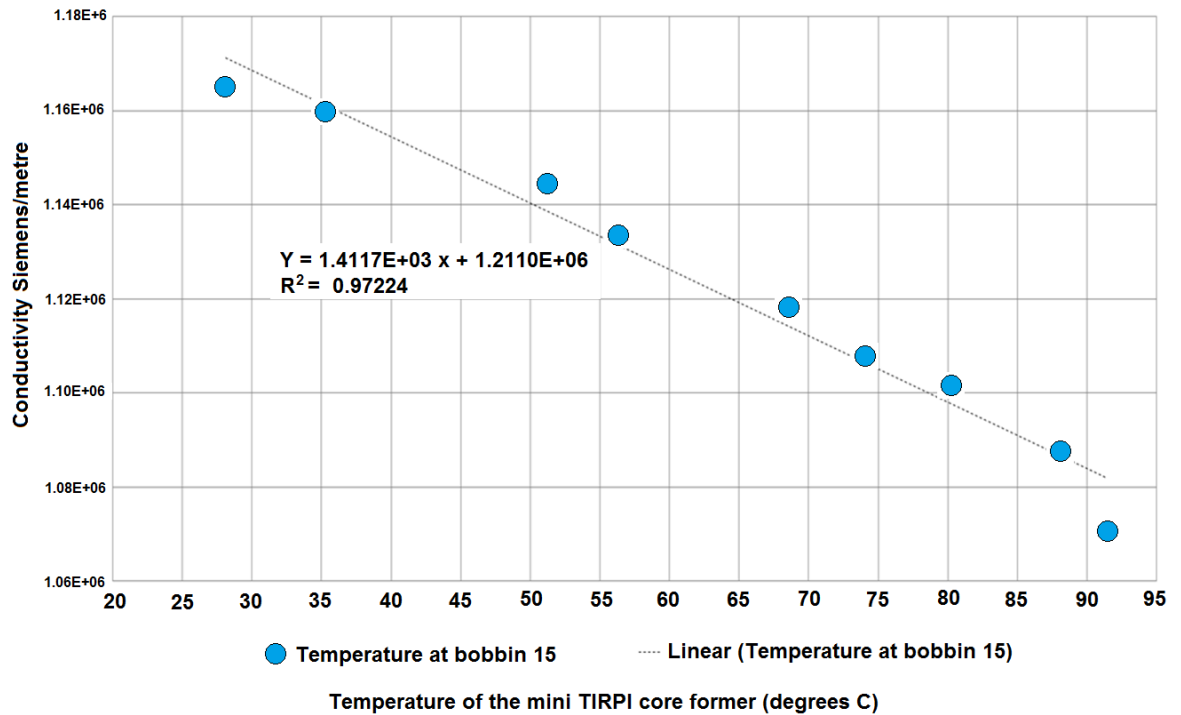


Figure 131 Core former electrical conductivity at temperature

11.10 Probe tube electrical conductivity effect

The presence of the probe tube has a significant effect on the TIRPI secondary output voltage. This is a consideration which needs to be taken into account when designing the TIRPI output interface to the instrumentation card. Although the probe tube has negligible magnetic permeability, it does have electrical conductance which enables eddy currents to be generated within the material. This suggested that the source current supplying the Mini TIRPI primary voltage needed to be designed prior to the Mini TIRPI itself because the eddy currents were determined by the source frequency and could affect the Mini TIRPI secondary output voltage. An experiment to determine the change was developed so that the performance of the Mini TIRPI with and without a probe tube could be compared and highlight any changes in the secondary voltage.

Initially a system shown in Figure 132 was used to enable a constant current of 100mA to be generated for the TIRPI and the secondary output voltage to be recorded. In addition, the primary voltage was also monitored to show the effect of the probe tube when the temperature remained constant. Any primary voltage change would then be a direct consequence of the probe tube being installed.



Figure 132 TIRPI system without probe tube

As shown in Figure 133 the primary current of 100mA produced a primary voltage of 4.812V and a secondary output voltage of 8.444V for the TIRPI was without the probe tube. In this system configuration, the TIRPI was not affected by the probe tube, driveshaft or CRDM. As a result, the output voltage was expected to be the maximum value that could be produced. The CRDM material was expected to produce a 30% reduction in the TIRPI secondary output voltage; the effect of the probe tube however could be determined both practically and analytically.

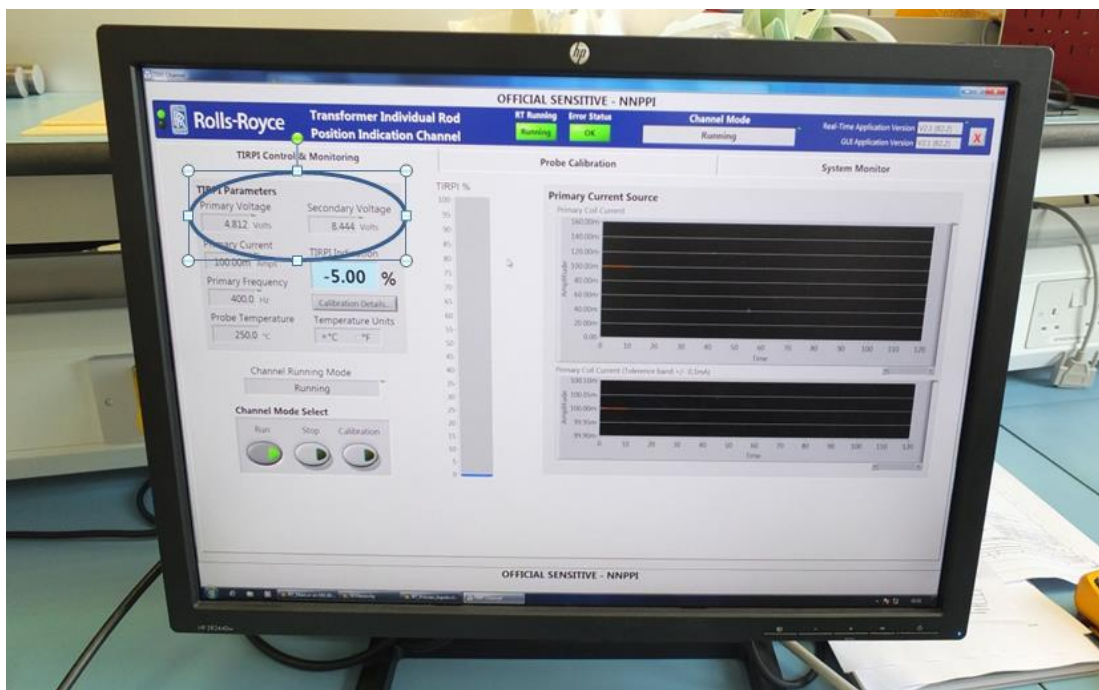


Figure 133 TIRPI without probe tube

The TIRPI was installed in a probe tube and the test was repeated using the setup shown in Figure 134. Without changing the system input of 100mA the TIRPI secondary voltage dropped significantly.

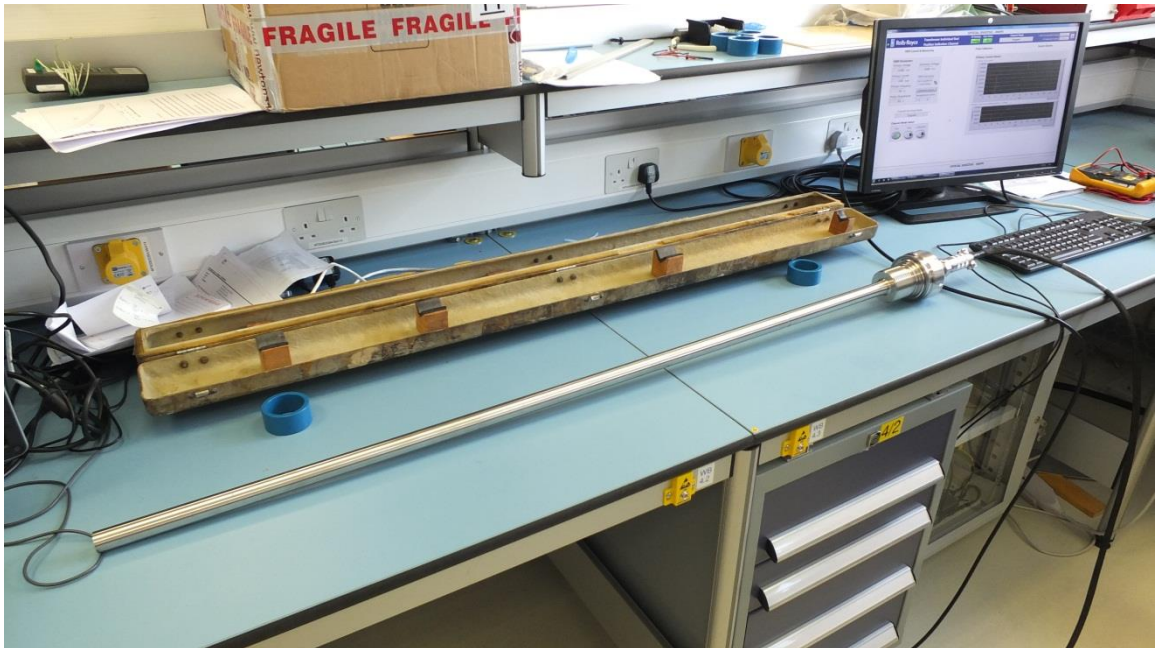


Figure 134 TIRPI system with probe tube

The TIRPI secondary voltage changed from 8.444V to 5.909V as shown in Figure 133 and Figure 135. This represented a -30% change, similar to that seen with variations in the CRDM materials. It is important to note that the TIRPI primary voltage also changed due to the probe tube. The TIRPI primary voltage dropped from 4.812V to 3.941V which is a change of 18.1%. The primary voltage has changed less than the secondary voltage as this is controlled by a constant current generator of 100mA. Although the primary voltage has changed, it would not affect the accuracy of the system as the instrumentation card compensation is carried out is the CRDM when it is in its operating environment. The primary voltage is an indication of the temperature and material and as such is a measure of changes in the thermal conditions and the driveshaft position. It is not directly related to an actual value of temperature.

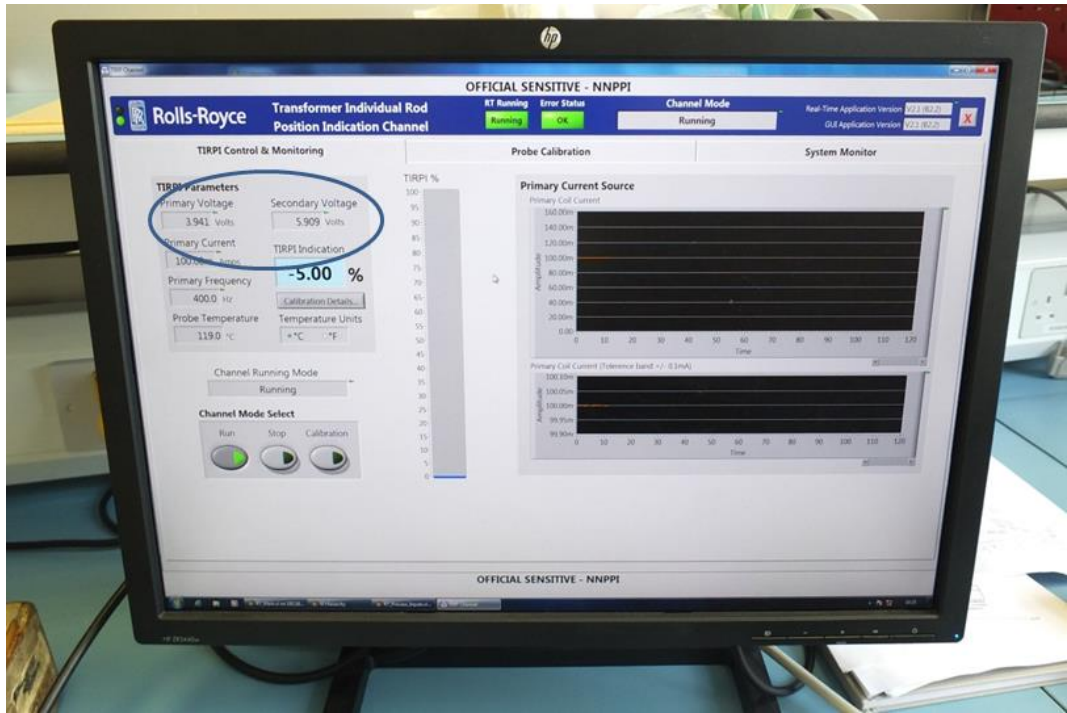


Figure 135 TIRPI with probe tube

To confirm the probe tube electrical conductivity effects, the FE model was used to analyse the results. The TIRPI was tested using a DC low-resistance meter to determine the correct value of electrical conductivity. The resistance of a metre length of the TIRPI core former gave a resistance of 4.067×10^{-3} ohms. The location of the test probes is shown in Figure 136 between bobbin 1 and bobbin 19. To calculate the electrical conductivity value for the FE model, the initial electrical resistivity value needs to be determined. This was determined by multiplying the resistance per metre length and divided by the length in metres of the TIRPI core bar former.



Figure 136 TIRPI core former DC resistance test

To establish the effects of the probe tube in the FE model, the electrical conductivity of the core bar former was measured and the magnetic permeability of the material was derived by using the B-H curve in the FE model. The secondary output voltage from the testing and the model output was normalised with the probe tube being omitted. The secondary output voltage predicted by the FE model was 4.79V without the probe tube, reducing to

3.23V when the probe tube was inserted. This equates to a 29.18% change of output voltage. When this was compared to the results from the practical testing above, the change in the secondary output voltage was very similar to that predicted by the model. The experimentation and analysis both concluded that the effect of the probe tube on the system when it envelopes the TIRPI was a reduction of approximately 30% in the secondary output voltage.

It is important to note that the actual values obtained from the model are not the same as those obtained from the experiment. It was assumed that this was due to the source signal used in the experiment having an additional higher frequency harmonic superimposed on the 400Hz source current signal, producing higher output voltage values.

11.11 CRDM Hot and Pressurised Water Testing Results

The CRDM Hot and Pressurised test facility is a representative setup of a nuclear power plant. The heat however is produced by heaters rather than nuclear fission. In addition, the pressure to the plant is provided by water pumps and not a pressuriser system.

Despite these differences, the CRDM experiences the same environmental conditions as it would see in a nuclear fission power plant except for nuclear radiation.

This facility was used to prove the operation of the TIRPI and provide data to support the design and capability of the TIRPI within a operational CRDM. A schematic of the facility is shown in Figure 137.

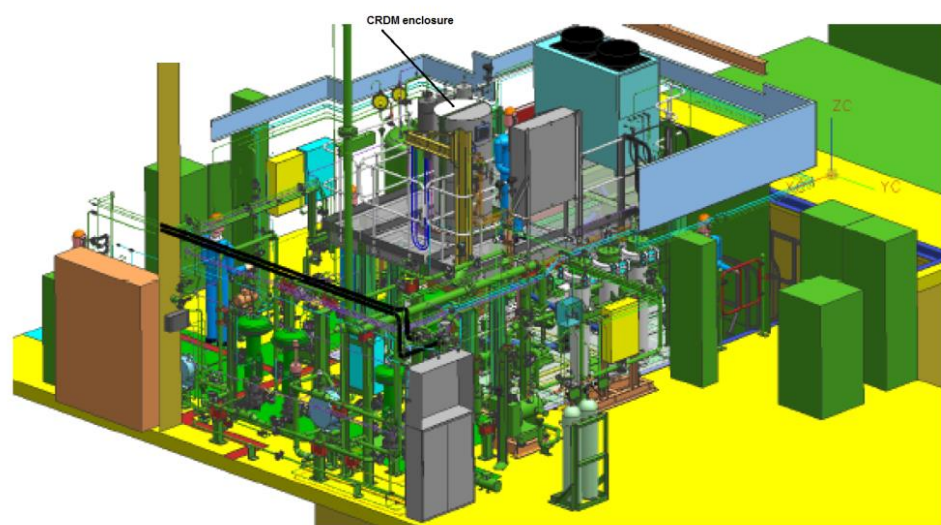


Figure 137 Hot and pressurised CRDM test facility

The TIRPI warm-up test showed how the primary and secondary output voltages respond to the CRDM temperature varying from approximately 23°C to 180°C. When the TIRPI and probe tube are housed in a nuclear reactor, the CRDM has a hot region and a cold region. The hot region of the TIRPI would be located in the lower coil assembly whilst the cold region is located in the upper coil assembly. The locations of these regions are shown in Figure 138. The difference in temperature causes a thermal gradient along the probe tube length and changes the resistance of the copper windings and the magnetic properties of the core former.

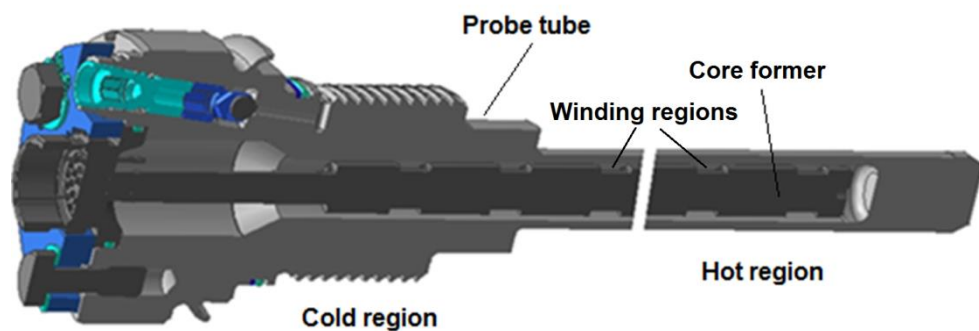


Figure 138 TIRPI thermal regions

The instrumentation card compensation algorithm needs to include an equation which relates the primary and secondary voltages to thermal effects in order to mitigate the impact. The compensation equation is determined by plotting the primary voltage and secondary voltage when the driveshaft is at various positions and the CRDM is heated from the minimum to maximum operating temperatures.

Figure 139 shows the test results from the warm-up test. The secondary voltage changed in a linear manner with respect to the primary voltage producing a linear characteristic curve. The linear equation for the curve was then used to compensate for the thermal effects on the TIRPI.

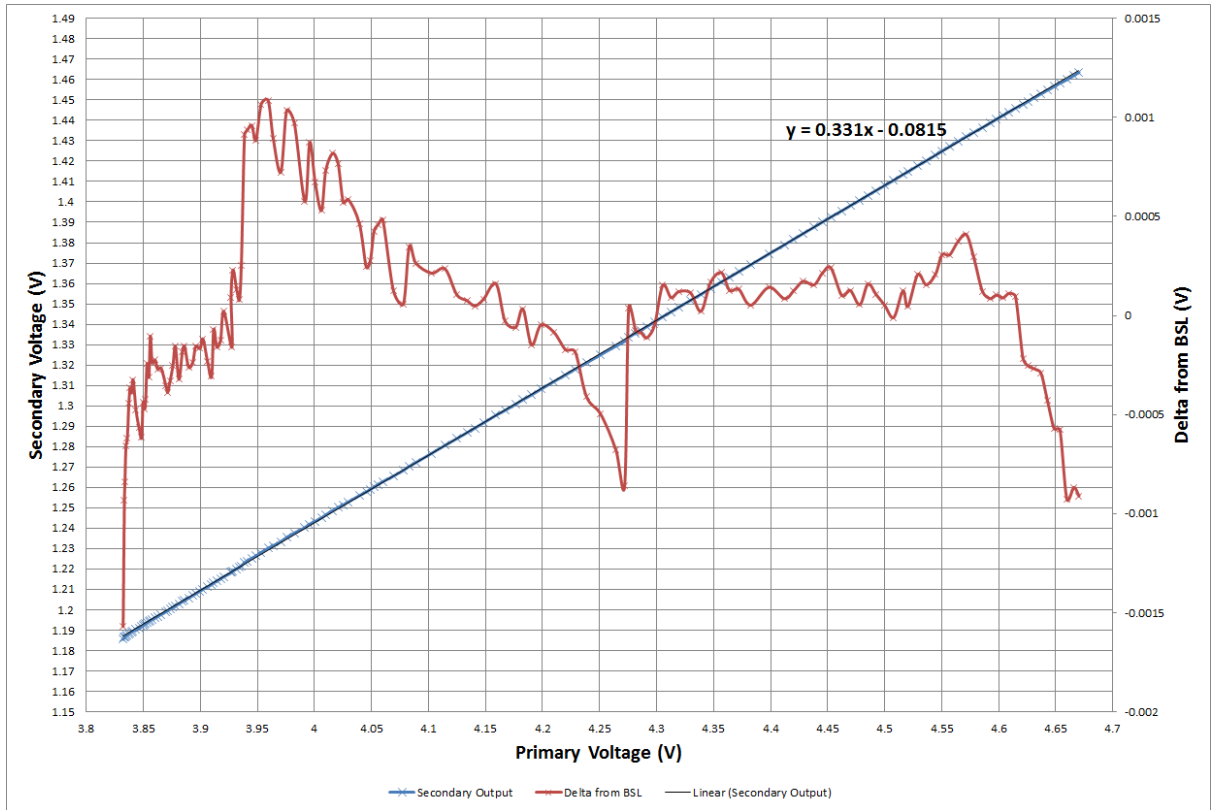


Figure 139 TIRPI warm-up test

The warm-up test was carried out by heating the CRDM and noting how the primary and secondary voltage reading changed until the CRDM temperature stabilised. Following the cold and hot calibrations curves shown in Figure 140, the thermal compensation algorithm could be calculated to infer the rod position at different temperatures using linear interpolation.

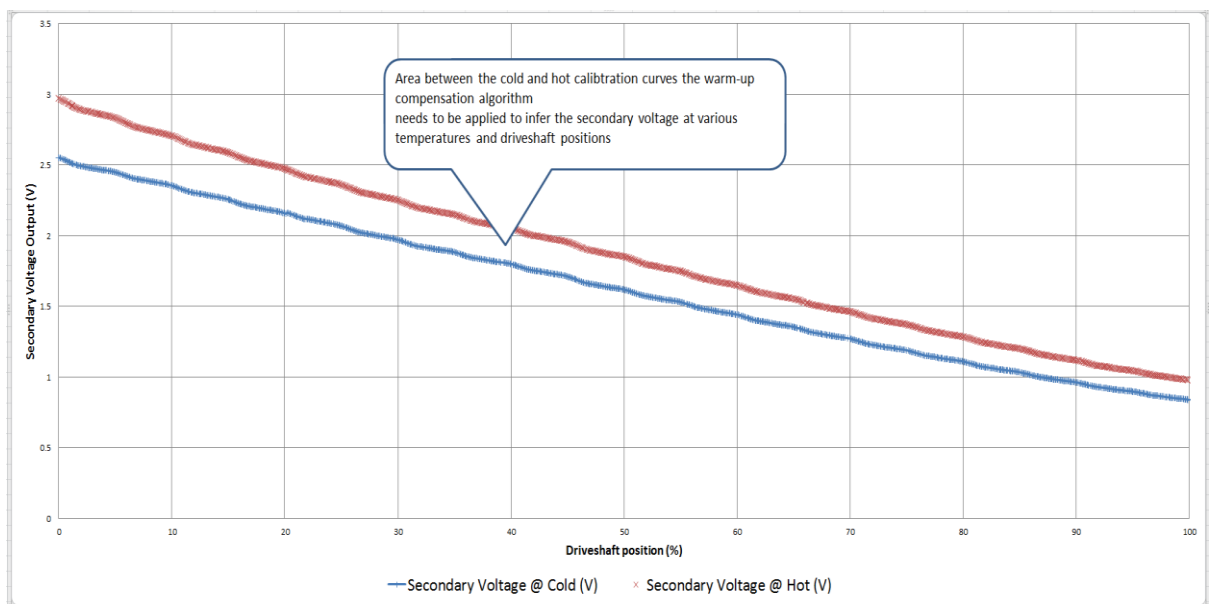


Figure 140 TIRPI thermal compensation

The linear equation which defines the driveshaft position between the hot and cold calibration curves will be calculated between every pair of adjacent cold and hot calibration points, as illustrated in Figure 141. The instrumentation card would use the primary voltage to defines the temperature change and then apply a modified secondary voltage output value.

The sum of the driveshaft position and thermal effects results in a single TIRPI secondary output value. The cold and hot calibration points are required at the same positions throughout the driveshaft length for the linear equation to be applied and avoid accumulation of errors.

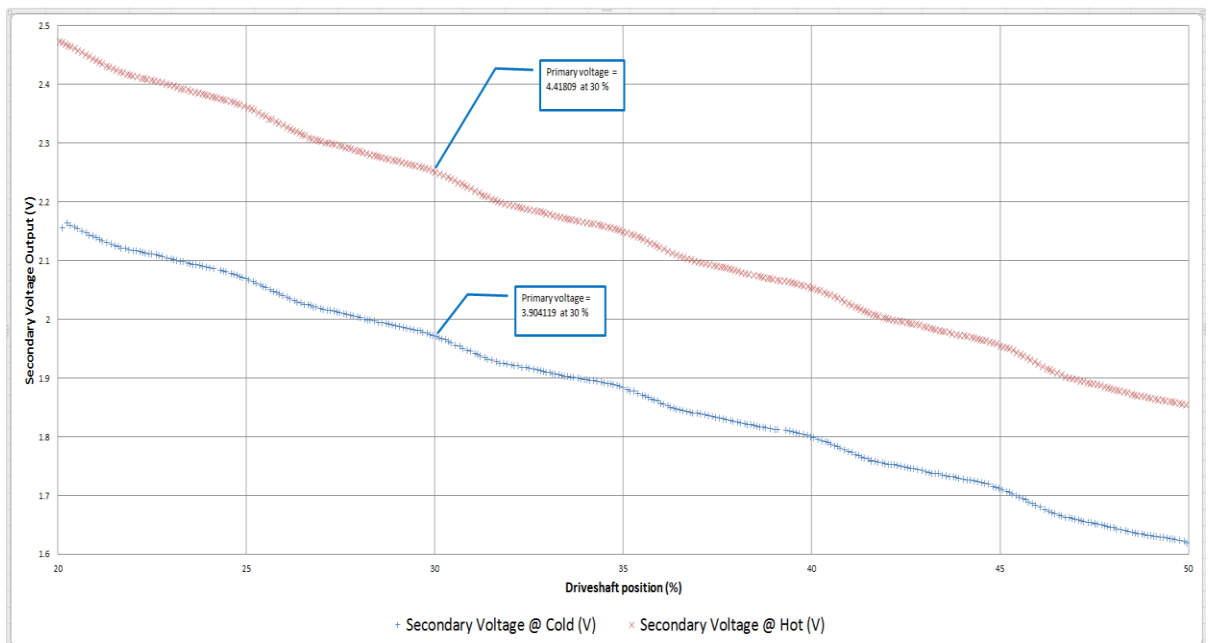


Figure 141 TIRPI thermal compensation technique

An example of a secondary voltage inferred from the linear equation is given in Table 9.

The results are for a TIRPI output at 30% driveshaft withdrawal.

Table 9 Thermal linear expression compensation equation

Primary voltage at driveshaft 30% withdrawn	Secondary voltage at driveshaft 30% withdrawn	Linear Expression ($y=mx+c$)
4.41809V (Hot)	2.25048V (Hot)	$2.25048V=m4.41809V+c$
3.90411V (Cold)	1.97105V (Cold)	$1.97105V=m3.90411V+c$

The thermal compensation linear equation for the 30 % driveshaft position is:

$$(1) \quad \text{Secondary voltage (V)} = 0.543 \times \text{Primary voltage (V)} - 0.15146$$

A graph made up of seventeen inferred secondary voltage values is shown in Figure 142. For each pair of cold and hot calibration points, a linear expression will be defined within the instrumentation card. This would allow real-time thermal compensation of the TIRPI transducer.

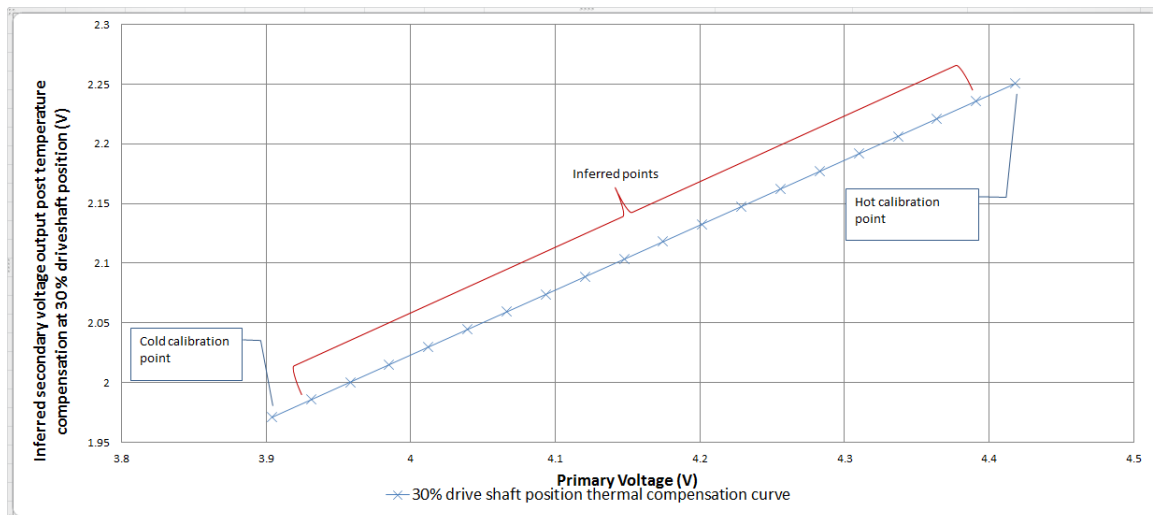


Figure 142 Thermal compensation characteristics @ 30 % driveshaft withdrawal

11.12 CRDM current test

The CRDM generates a large electromagnetic field to generate the radial forces on the rotor arms. This enables the rotor arms to latch onto the driveshaft thread. The CRDM electromagnetic field is also used to generate rotary motion of the rotor arms by cycling the three-phase, four-pole motor. The electromagnetic field produces stray fields in the TIRPI resulting in electrical noise errors on the secondary output.

The TIRPI is at the centre of the CRDM and has a number of metallic components between itself and the source of the electromagnetic field (the stator). Fortunately, the driveshaft is surrounded by the motor tube which is made of a ferrous material. The motor tube acts as a shield to most of the stator electromagnetic field, reducing the stray fields in the TIRPI. In addition, the TIRPI has been designed with a permeable core (made from 17.4PH H1100), which also has a high magnetic permeability. The highly permeable core further limits the electromagnetic stray field effects from the stator.

Figure 143 illustrates the CRDM stator location with respect to the TIRPI. A planar view of the stator with the surrounding components is also shown.

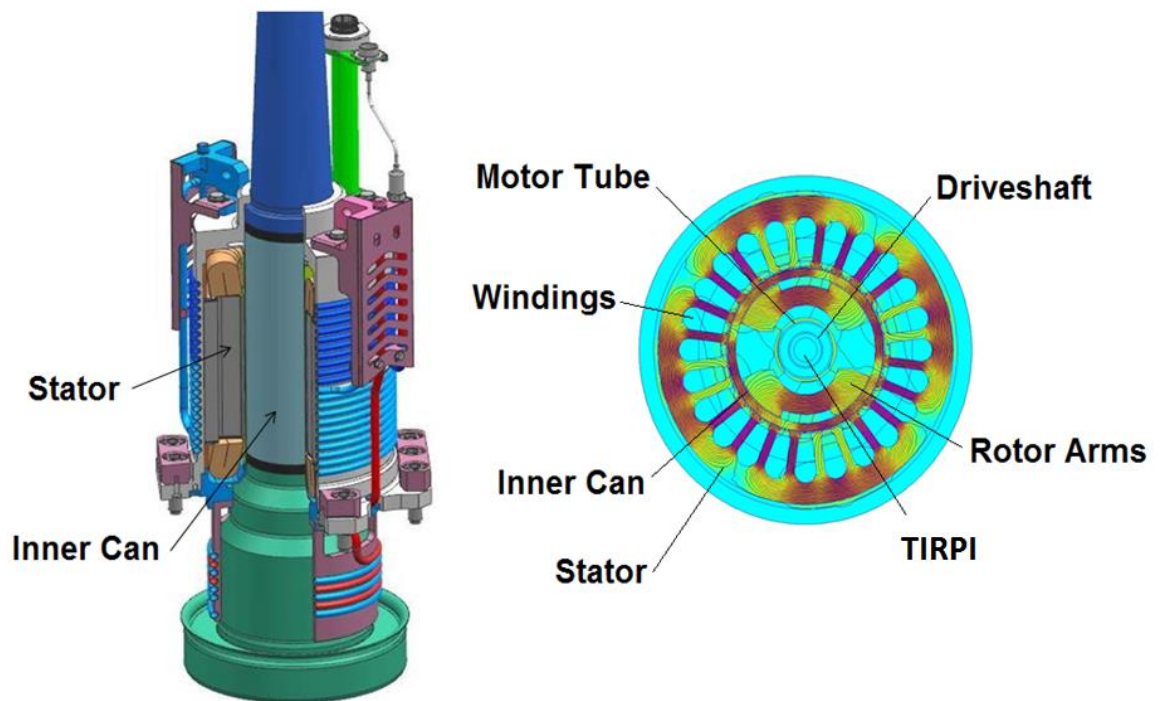


Figure 143 CRDM stator

The CRDM was subjected to a variation in source current which changed the electromagnetic field produced by the stator. To verify how the stator magnetic field affected the secondary output voltage of the TIRPI, the source current to the stator was changed from 4A to 11A in discrete static steps. The CRDM current variation test was conducted when the driveshaft was at a position of 1.2% withdrawal.

This was considered as a typical worst case condition for CRDM electromagnetic interference due to the driveshaft not enveloping the probe tube and absorbing any electromagnetic field produced by the CRDM stator. Figure 144 shows the results of the CRDM electromagnetic testing.

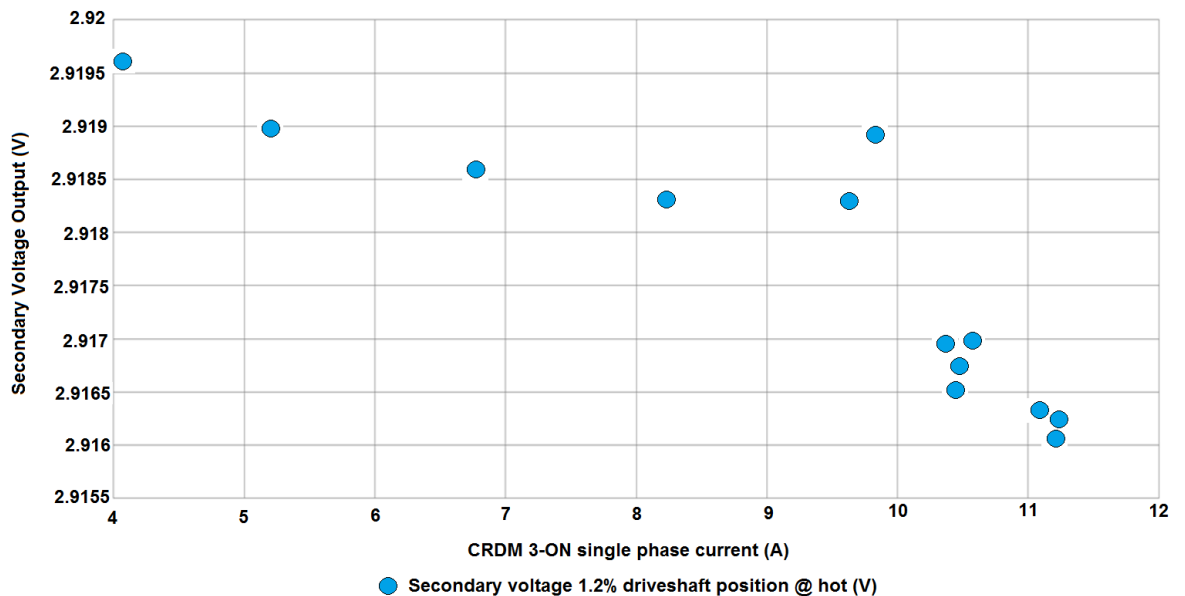


Figure 144 CRDM current test

The test results show that the CRDM electromagnetic interference changes the secondary output voltage by 3.5mV, with a CRDM current variation of 1.38A. The change in secondary voltage equates to an error of approximately 0.07% variation in driveshaft position. In practice, the CRDM stator current will be controlled and will not vary significantly. The CRDM electromagnetic interference errors are considered therefore negligible.

11.13 Channel alignment test

The alignment test compares the measured rod position output from the TIRPI with the output from the CRDM Synchronous Individual Rod Position Counter (SIPRIC) to assess the channel accuracy. The accuracy of the channel is expected to be within +/-1% FS to enable the reactor to operate within the specified requirements.

The test was carried out in the Hot and Pressurised rig facility using cold and hot water. The results in Figure 145 shows the TIRPI errors at 5 % steps as the driveshaft is raised and lowered. The results show a dc offset of 0.3% FS error and an additional +/-0.2%FS error. The reason a dc offset error is exhibited within the data results from the cold and hot calibration is because the TIRPI was calibrated with the driveshaft fully engaged which corresponded with the ball nuts of the driveshaft moving the driveshaft slightly in an upwards direction to fully engage. This position was recorded as 0% on the TIRPI calibration position.

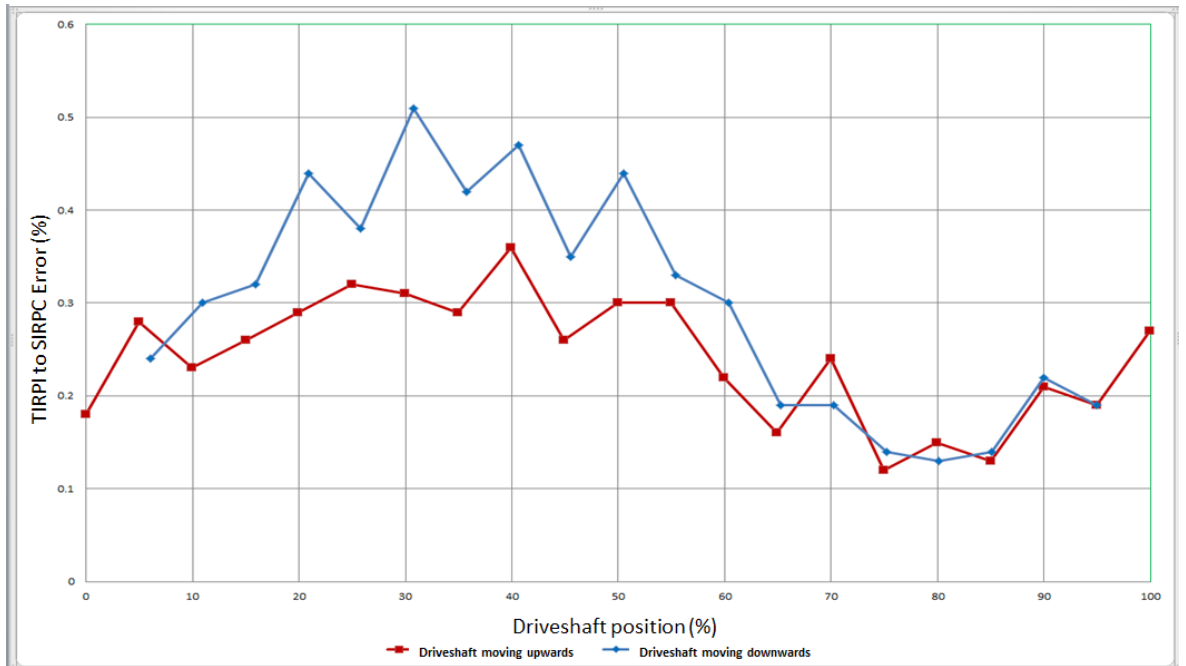


Figure 145 TIRPI cold alignment test

Within an actual operating nuclear power plant, the offset would not be normalised and an offset channel error would exist. This is shown in Figure 146. The normalisation is achieved by driving the driveshaft downwards until the CRDM exhibits a pole slip. This process enables the dc offset error to be eliminated in the TIRPI calibration procedure as the driveshaft is physically driven to the bottom of the control rod mechanism before the calibration procedure begins which enables a forced datum driveshaft position of zero.

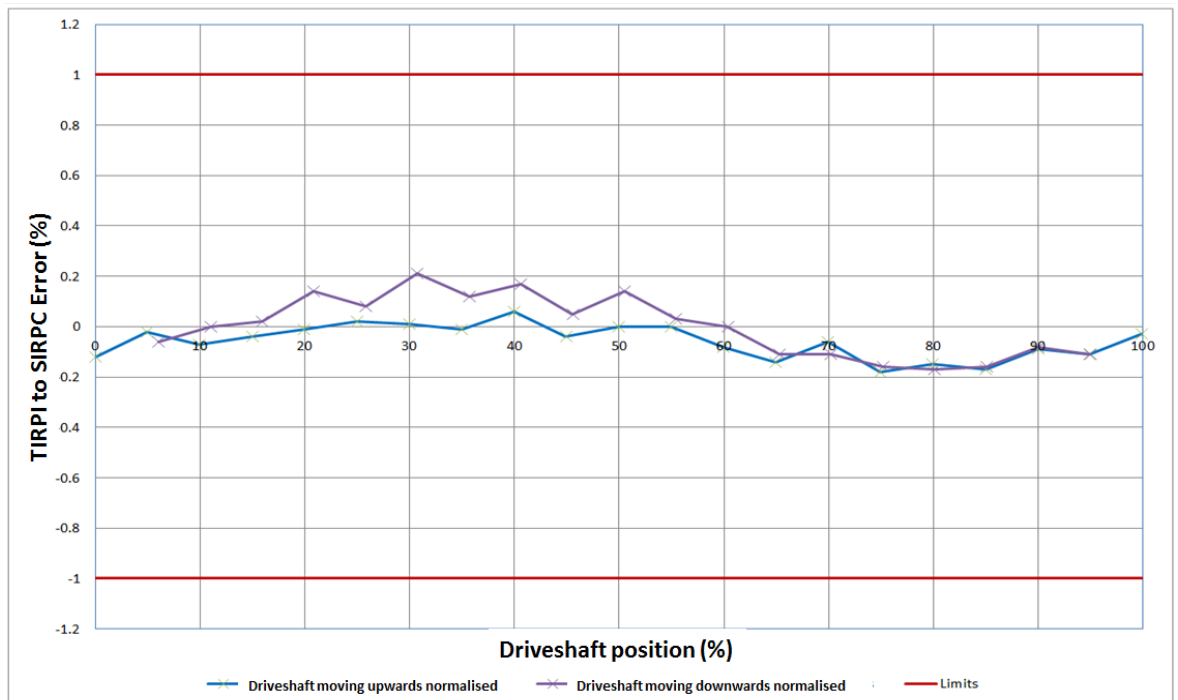


Figure 146 TIRPI cold alignment test normalised

11.14 CRDM frequency sweep test

The frequency of the TIRPI current source signal is a very important factor as it determines the capability of the transducer and thus the overall channel accuracy. The frequency values of the current source determine the magnitude of the eddy currents induced within the surrounding materials of the TIRPI and within the TIRPI itself.

It is very important to determine the frequency that produces the maximum sensitivity of the TIRPI when the transducer is within the CRDM as the CRDM becomes part of the sensor when used in situ. The optimum frequency values were determined by setting the CRDM to the minimum temperature and minimum driveshaft position. Data was taken from the secondary output voltage in the frequency range 50 Hz to 5KHz while keeping the temperature and source current constant. This experiment was repeated at the maximum driveshaft position.

On completion, the frequency sweep experiment was repeated using the maximum CRDM temperature. This was done to determine the effects of temperature on the optimum frequency value. The results are illustrated in Figure 147. Any current deviations throughout the tests have been normalised, as previous tests have shown a linear change in secondary output voltage were caused by current or temperature changes.

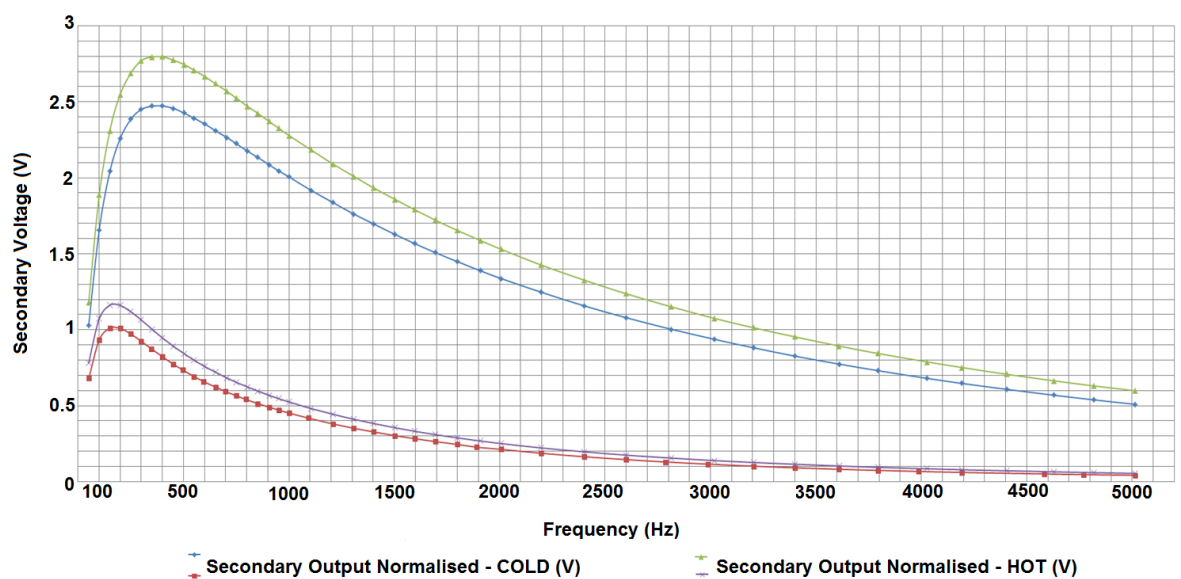


Figure 147 TIRPI frequency sweep normalised

To determine the optimum frequency for maximum TIRPI sensitivity, the span of the minimum and maximum driveshaft position was calculated and plotted against the source frequency. It is clear from Figure 148 that the optimum TIRPI frequency is the same for the minimum CRDM temperature and the hot CRDM temperature profiles. The optimum TIRPI frequency was approximately 550Hz.

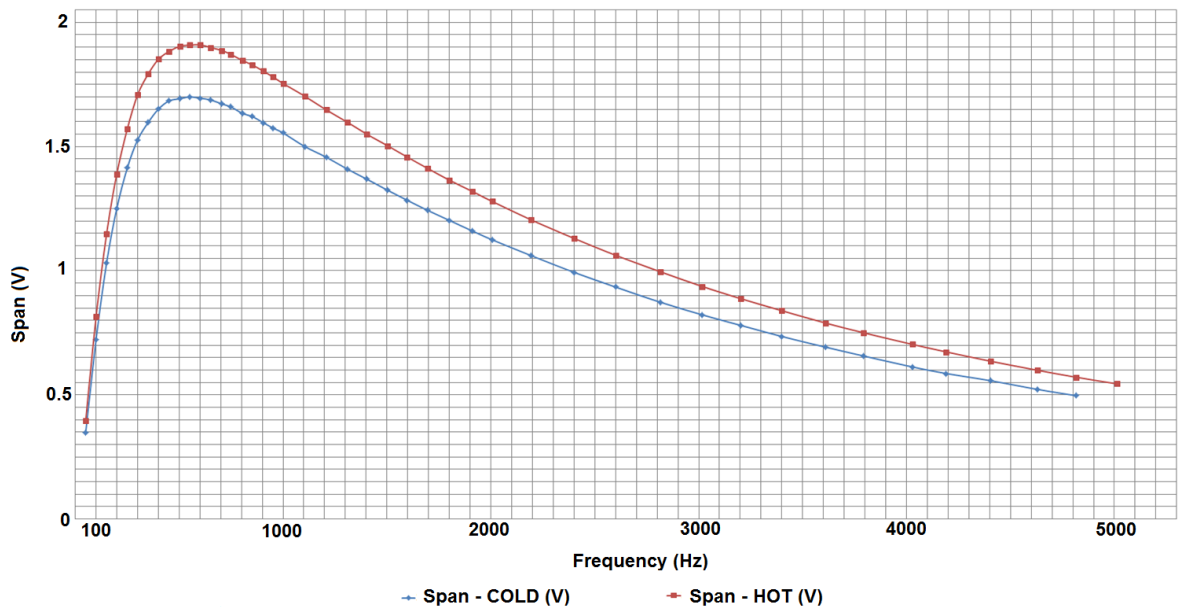


Figure 148 TIRPI frequency sweep span normalised

Within an actual nuclear rod position system, the limiting parameter for cables is the TIRPI primary coils source frequency. As the frequency rises the capacitance increases and with an inductive circuit the TIRPI secondary output signal amplifies significantly. This is due to the resonance in the system and care must be taken to avoid reducing the rod position measurement accuracy. Instrumentation card designers impose frequency limitations on sensors and transducers to avoid this issue. A maximum frequency of 400Hz was chosen to be a practical value for use on this project. Following the hot and pressurised rod position alignment testing, it was found that the transducer was capable of detecting the smallest movement increment of the CRDM. It was therefore concluded that the frequency selected met the requirements.

11.15 SCRAM engagement repeatability test

Following a SCRAM condition, the ball screws are not engaged with the driveshaft. When the control rod needs to be raised, the ball screws engage the driveshaft; however, their

position is not known and upon engagement they can engage onto the thread of the driveshaft or on the outer surface of the thread. Should the ball screws engage onto the outer surface of the driveshaft then the control rod will not be raised until the ball screws are in a position where they are engaged with the thread. This will cause a mis-alignment between the outputs of the TIRPI and the synchronous indicator rod position counter thus a generating error.

The CRDM was scrambled five times to determine the error associated with SCRAM engagement. Figure 149 shows the errors to be approximately 0.8% of full scale. This would not be an acceptable error and therefore a revised calibration procedure was developed. The calibration would require the driveshaft to be driven to the bottom of the control rod limit while engaged and a pole slip forced to occur within the CRDM. This would enable a fixed datum point to be established for the TIRPI and SIRPI. Having a known datum point would allow the SIRPI to be reset to zero at that bottom of the control rod platform and normalise any TIRPI to SIRPI mis-alignment errors.

The results from the test are shown in Figure 149. This shows an offset error of 0.75% FS error and an approximate 0.1% to 0.3% FS error after normalising the offset errors. This is an good result as it shows the TIRPI is operating as expected.

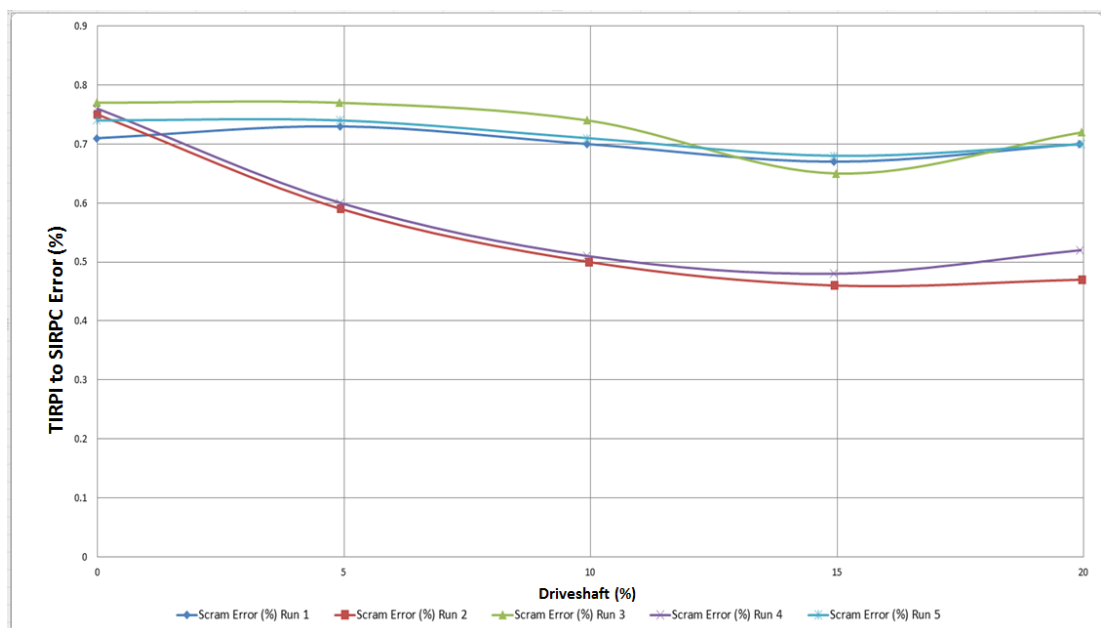


Figure 149 SCRAM to engagement repeatability

11.16 Rod drop test

In a SCRAM event it is very important to insert the rod properly within the required time in order to stop the nuclear reaction. Rod insertion is achieved simply by the weight of the control rod and a spring mechanism that drives the control rod down to the 0% control rod withdrawal to prevent thermal core damage as the nuclear reaction is limited or stopped. Core damage occurs when the heat generated by the nuclear reactor exceeds the heat being removed by the cooling system and at least one of the reactors fuel elements exceeds its melting point. To ensure the nuclear reactor will not sustain any damage, the core performance needs to be assessed and rod drop profile limits defined. This determines a maximum rod drop time to prevent core damage. The TIRPI allows measurements of the rod position as a SCRAM is initiated, and can be used to prove rod drop times. Accelerometers have been used to infer the time taken for a rod drop; however no actual measured output was available.

In addition to the rod drop times, the TIRPI allows additional parameters to be determined to ensure the health of the SCRAM system throughout its life. These parameters include driveshaft descent times, the velocity of driveshaft, driveshaft buffer impact time, driveshaft hit bottom time and driveshaft bottom bounce. Examples of these are shown in Figure 150. These parameters enable the nuclear reactor to shut down within a specific time which satisfies the nuclear regulator safety limits. The development of the TIRPI has enabled these tests to be performed as the existing sensor is not capable of carrying out rod drop tests. Currently accelerometers are used to do rod drop testing.

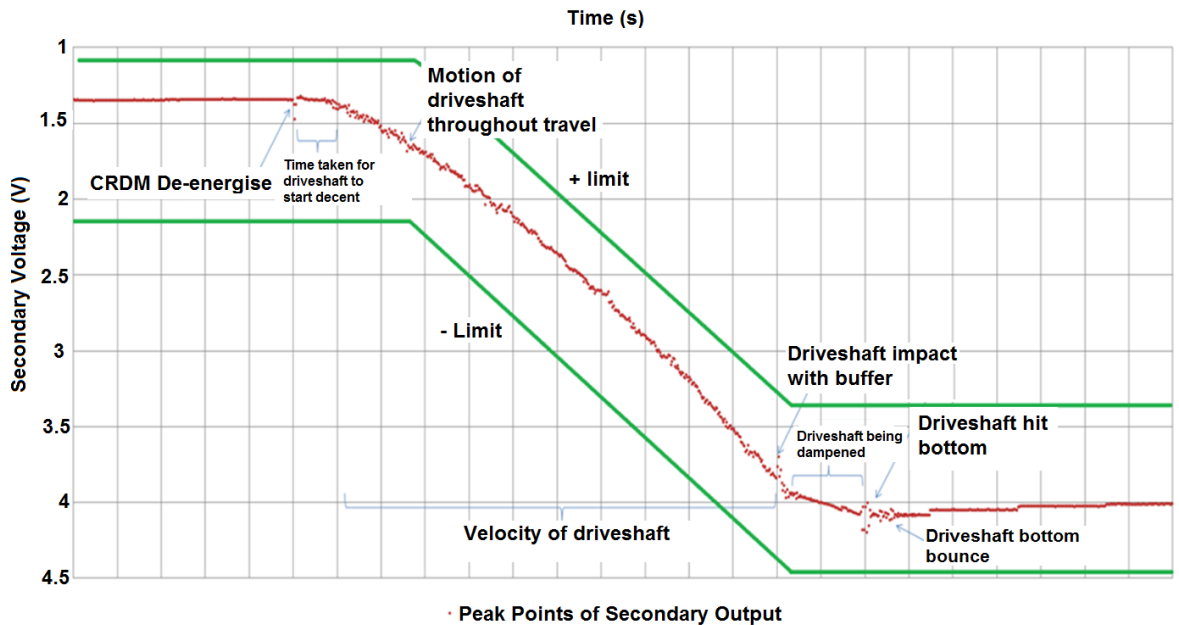


Figure 150 Rod drop test

11.17 Rod motion measurement accuracy

On the current system, determining the position of a control rod has been achieved by stopping the control rod at an estimated position and reading the value indicated by the rod position indicator. The incremental steps of the driveshaft are controlled such that overshooting the desired value is minimised. However, when the control rods are in motion, the CRDM is moving the driveshaft and is therefore producing an alternating magnetic field within the TIRPI region. The magnetic field generated by the CRDM causes the rod position indication to be noisy and non-readable. To overcome the noise problem the control rod is stopped and a static rod position is read.

Following a number of tests and trials, the TIRPI has been shown to be extremely accurate when measuring static control rod values, and also when the control rod is in motion. This is a significant benefit as the operator can seamlessly move to the required position without excessive overshooting from the required position.

The accuracy of the TIRPI within the hot and pressurised test facility is determined by comparing the synchronous indicator rod position counter to the actual rod position while the control rod is in motion. It has been concluded that there is no error reduction while the control rod is in motion.

11.18 CRDM to CRDM interference

Within a nuclear reactor plant there are many CRDM's fitted together to minimise space occupied by the nuclear reactor core. Each CRDM core houses a TIRPI within it. As the CRDM's are located as close as physically possible, the TIRPI are within close proximity to each other. Each TIRPI emits an electromagnetic field which is used to detect the position of the control rod, however as the surrounding materials around the TIRPI upper region are Inconel 625 and non-magnetic stainless steel, the TIRPI primary coil generated electromagnetic field can be detected by the adjacent TIRPI's. A finite element model was generated to investigate how this effect would cause an error on the secondary TIRPI outputs. Any changes in the TIRPI secondary voltage due to the adjacent TIRPI's would result in an additional error on the accuracy of each TIRPI within the nuclear reactor core as shown Figure 151.

Within the nuclear reactor core the individual TIRPI will undergo a calibration to characterise the TIRPI secondary output voltage with respect to the driveshaft position and temperature of the surrounding region. This is achieved by only moving a single rod at a particular time, however in practice the use of the control rods will be moved as a bank (a number of control rods together) which will be different to the original calibration procedure with only a single control rod being moved.

A 2D planar model was constructed of two CRDM's to investigate the differences in the TIRPI secondary output voltages when a single driveshaft moves compared to both driveshaft moving as shown in Figure 151.

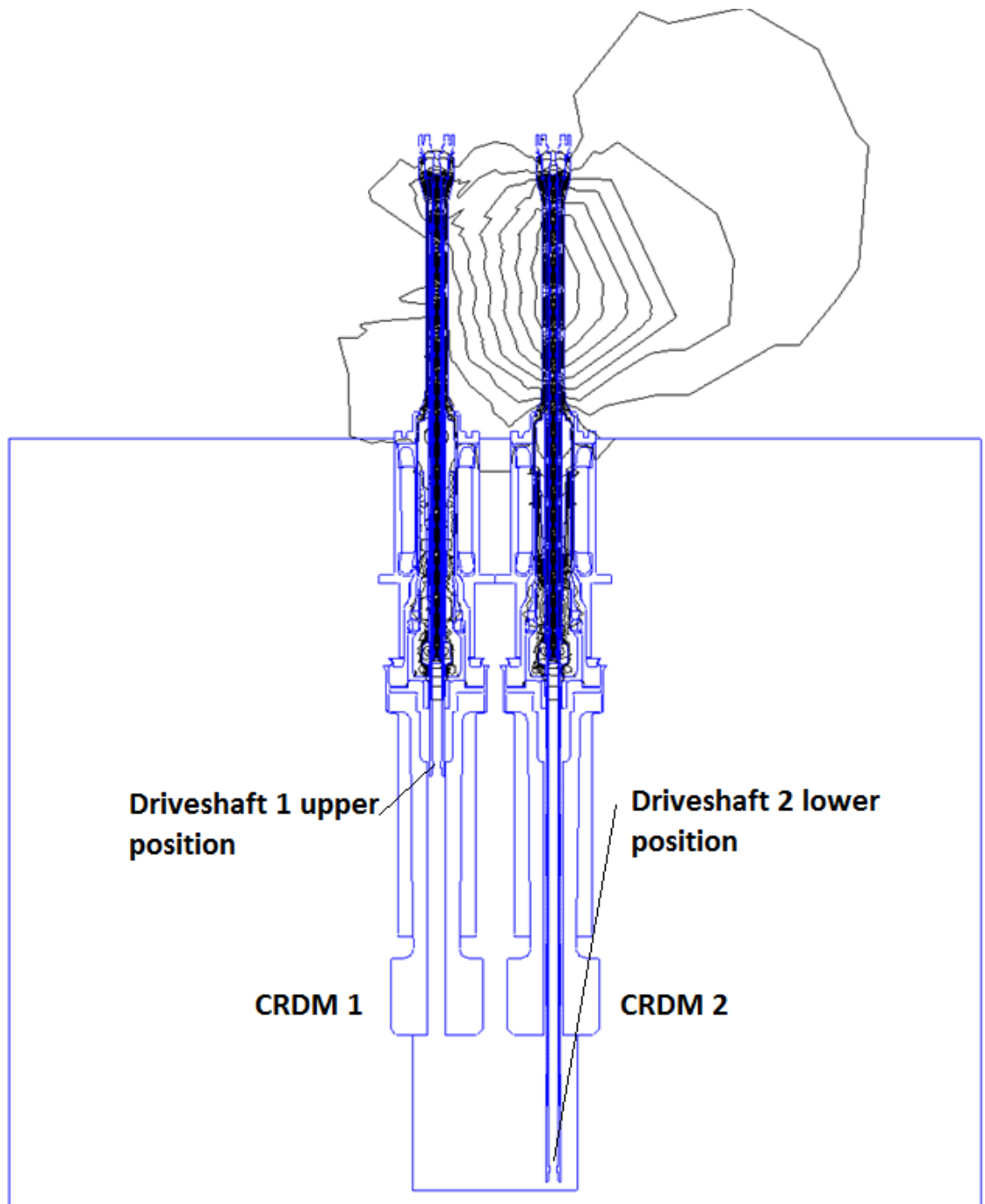


Figure 151 CRDM adjacent interference

The FE model moved the driveshaft of CRDM 1 in steps of 5% while CRDM 2 driveshaft was stationary. The model repeated the simulation with both the driveshaft moving together in increments of 5%. The results were compared to check for differences in the secondary output voltage shown in Figure 152 and the error calculated in Figure 153.

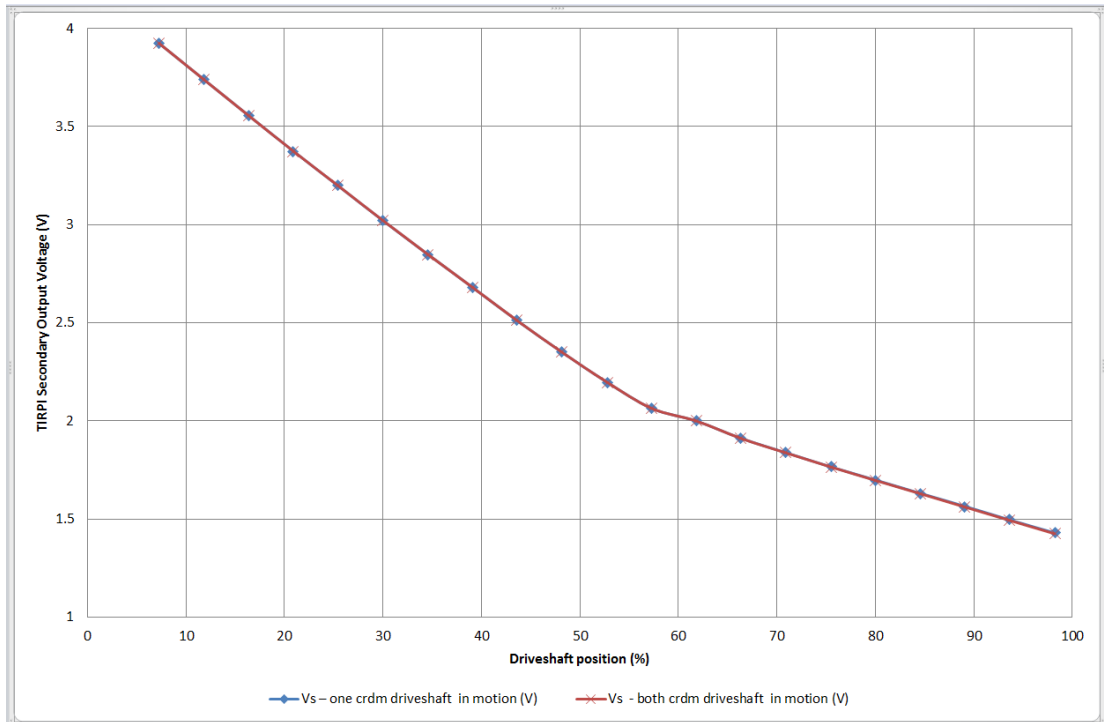


Figure 152 TIRPI secondary output of two adjacent CRDMs

The results show that the interference that is caused between the adjacent CRDMs is very small and causes a worst case error of 0.025% above the 90% driveshaft position operating region. Typically this magnitude of error is considered practical and acceptable for the TIRPI design.

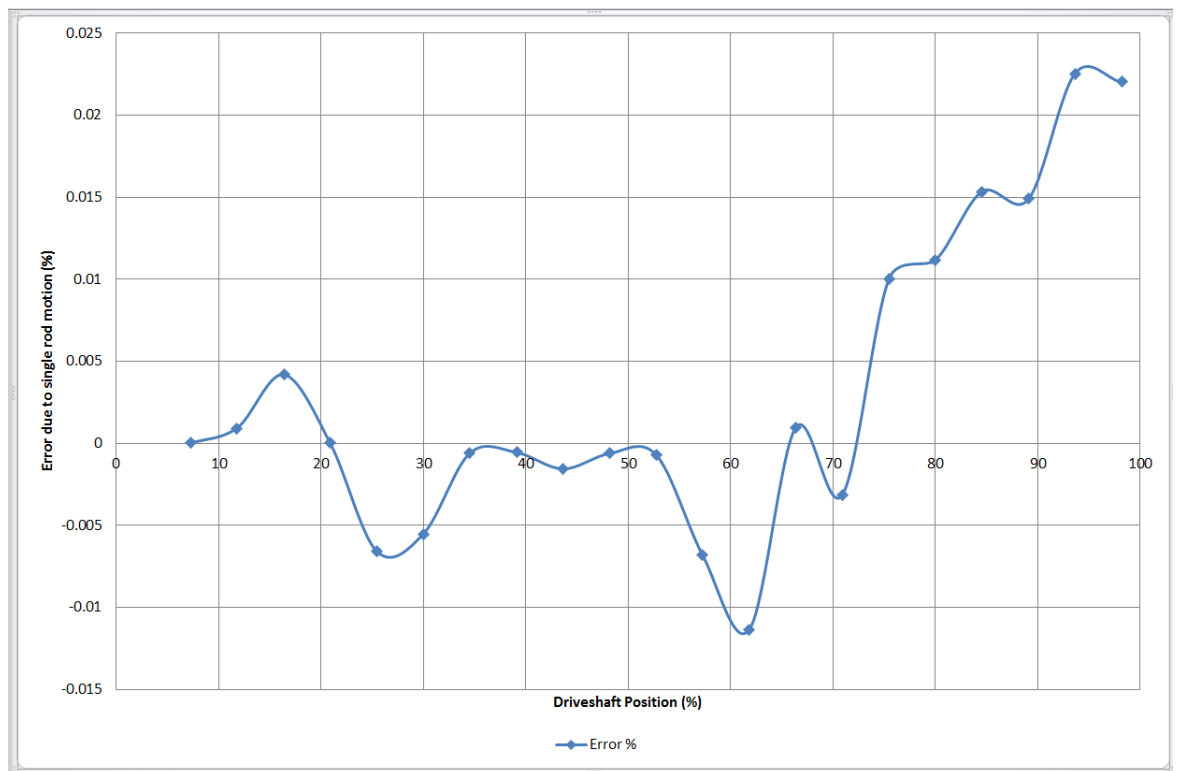


Figure 153 Error of TIRPI output with two adjacent CRDM

11.19 Conclusion

The overall accuracy target for the TIRPI channel is +/- 1% of Full Scale (FS). The test results showed that the TIRPI can detect a single CRDM pulse rotation, and thus the accuracy error is 0% FS. However, with the addition of the driveshaft horizontal variation, the error becomes +/-0.25%. The channel alignment test within the Hot and Pressurised rig has shown an error of +/- 0.2% error with a 0.3% error offset. To date the TIRPI has performed beyond expectations and has achieved a higher accuracy than expected.

11.20 Post CRDM testing inspection

Following the CRDM hot and pressurised testing the TIRPI, CRDM and the sub-components associated with the CRDM were taken apart and inspected. The TIRPI operated throughout the CRDM testing phase as expected.

On closer inspection it was found that the tip of the TIRPI had become dis-coloured and the potting compound had split within the hot region shown in Figure 154 and only slightly discoloured in the colder region as shown in Figure 155.



Figure 154 TIRPI post testing thermal inspection discolouration of hot region

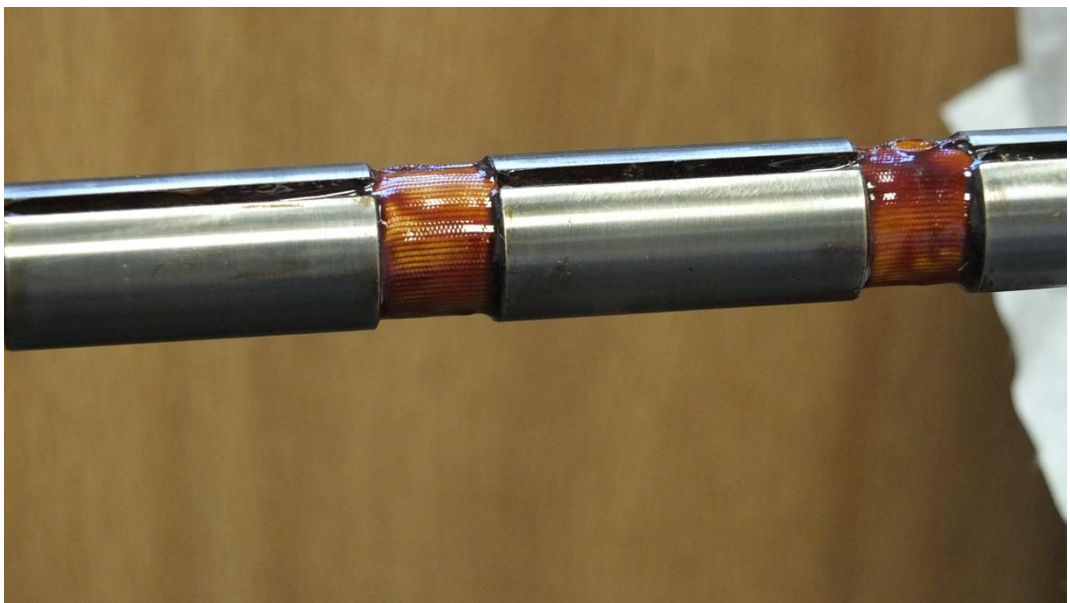


Figure 155 TIRPI post testing thermal inspection discolouration of cold region

Although the initial inspection shows discoloration caused by the heat generated within the CRDM, the actual recorded temperature of the TIRPI hot region was 140°C. This is well below the suggested temperature limit of approximately 220°C for the materials used on the TIRPI. An engineering assessment by the manufacturer has concluded that the manufacturing of the prototype unit was the root cause of the potting fracture and will be addressed in future products. In addition, the manufacturer has stated that discoloration of the TIRPI will not impede the operation through life.

Chapter 15

12 Thermal Induced Stress

12.1 Introduction

Thermal stress or thermal deflection is produced by strains within a structure of object due to the temperature applied to it. This occurs when the structure or object is prevented from freely expanding or contracting due to thermal strain or at a point where different materials with different thermal coefficients are physically in contact. It is important within this application because the TIRPI is inserted into the probe tube when they are both at ambient temperature. When heated due to the reactor temperature, the TIRPI cannot expand more than the probe tube which would lead to thermal stress within the internal bore of the probe tube. This ensures good engineering practice because the TIRPI will be required to be operational for very lengthy periods of time and removal maybe required from the probe tube and thermal expansion should not prevent extraction. To develop confidence in the mechanical thermal design, a thermal stress model was developed to determine the expansion of the TIRPI and probe tube when operated over the normal operating temperature. Two separate models have been developed and the thermal displacements compared to ensure thermal expansion will not causes stresses within the internal bore of the probe tube.

12.2 Mechanical and thermal properties

Table 10 shows the properties used for the thermal simulations. These are typical values for the Inconel 625 probe tube material and tested values for the TIRPI 17.4PH H1100 material. In addition, three temperature values of 200 °C, 100°C and 70°C were defined at different regions of the probe tube and TIRPI. The location of these temperature values is shown in Figure 156. The separation gap between the probe tube and the TIRPI has been considered to be very small and once the temperature has reached the equilibrium state the difference between them is negligible. An assumption has been made that both the

TIRPI and probe tube will be modelled starting from their respective length of zero at the hottest end.

Table 10 Thermal stress material properties

Material properties	TIRP variant values	Probe tube values
Thermal distribution	Isotropic	Isotropic
Thermal Conductivity ($\text{W}\cdot\text{m}^{-1}\text{K}^{-1}$)	18.1	10.8
Spacer 1 Fixed Temperature ($^{\circ}\text{K}$)	473.15 (200°C)	473.15 (200°C)
Spacer 2 Fixed Temperature ($^{\circ}\text{K}$)	375.15 (100°C)	375.15 (100°C)
Spacer 3 Fixed Temperature ($^{\circ}\text{K}$)	343.15 (70°C)	343.15 (70°C)
Young's Modulus (Gpa)	186	76.5
Poisson's Ratio	0.31	0.286
Density (Kg/m^3)	7700	8440
Thermal Expansion Coefficient [x 10-6] $\text{m}/(\text{m } ^{\circ}\text{K})$	11.7	13.1
Initial Temperature ($^{\circ}\text{K}$) - The reference temperature is the initial temperature of the nodes that are now at the temperatures which were transferred from the thermal analysis solution.	295.15	295.15

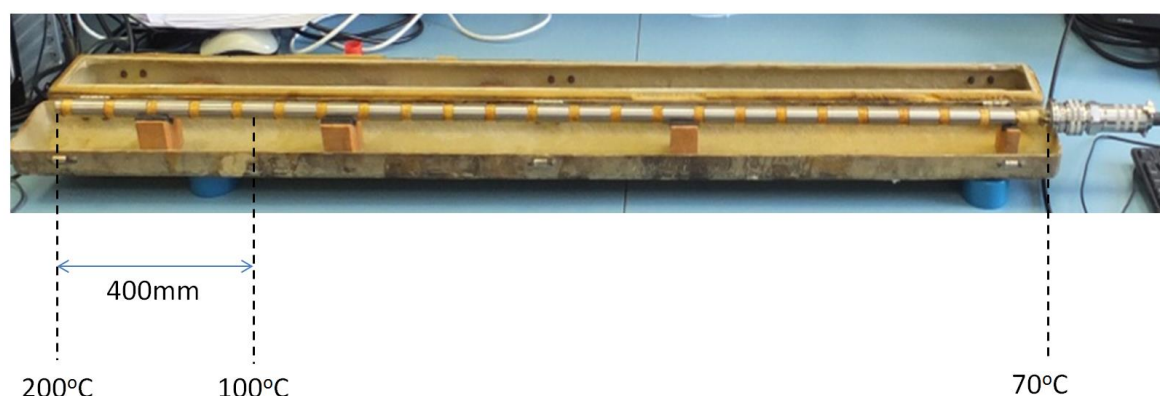


Figure 156 TIRPI temperature distribution

12.3 TIRPI variant thermal stress model

The minimum and maximum clearances between the TIRPI and probe tube was 0.055mm and 0.165mm depending on machining tolerances of the TIRPI and taking into account the minimum tolerance in the bore diameter of the probe tube. Ideally the design of the TIRPI should not exceed the 0.055mm gap restriction when it is operating at temperature which ensures no stresses will be induced by thermal expansion.

The 3D finite element models of the TIRPI thermal expansion are shown Figure 157, Figure 158 and Figure 159 along the x, y and z. In the x direction the expansion of the TIRPI had a maximum value of 25.02um in the positive direction and 13.92um in the negative direction. The addition of these two values gives the total maximum expansion of the TIRPI within the hot region of 38.94um. Similarly for the thermal expansion in the y direction, the positive and negative expansion values 19.82um +19.11um are added to give the total expansion. The x and y direction values were extremely close as expected because the TIRPI core former is axi-symmetric. Finally the thermal expansion was measured in the z direction where the TIRPI was expected to have the greatest expansion. The models show the maximum expansion along the z axis to be 1.269mm. This represents is a value greater than the perimeter of the TIRPI former. The probe tube had a bored cavity 10mm longer than the TIRPI and as such could accommodate the maximum thermal expansion of 1.269mm. Thermal expansion of the diameter could also be accommodated as the clearance around the TIRPI circumference allowed an expansion of 55um and the models predicted an expansion of approximately 39um. In addition it was assumed that the probe tube could not expand and create a longer cavity for the TIRPI. The models however would show the effect of the thermal gradient on the probe tube and whether it would actually results in a longer cavity for the TIRPI.

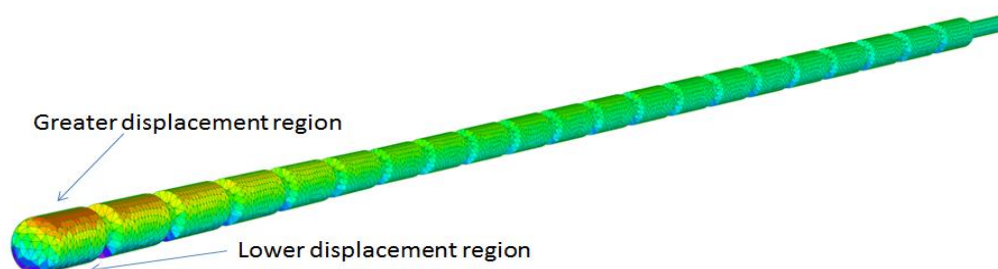


Figure 157 TIRPI thermal induced stress distribution within the x-direction

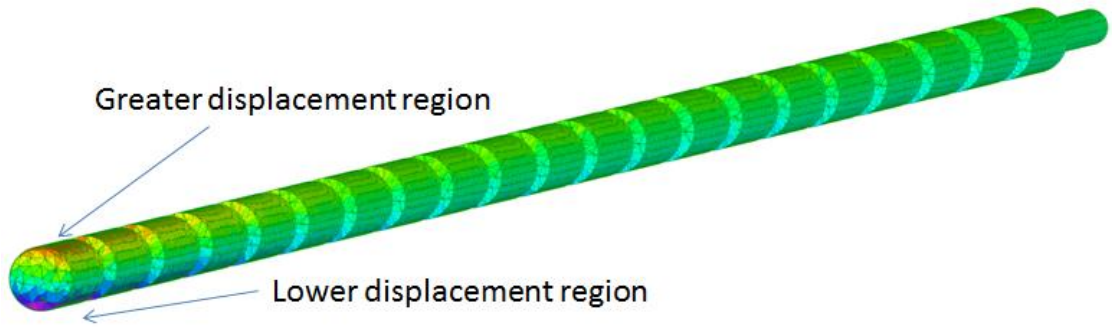


Figure 158 TIRPI thermal induced stress distribution within the y-direction

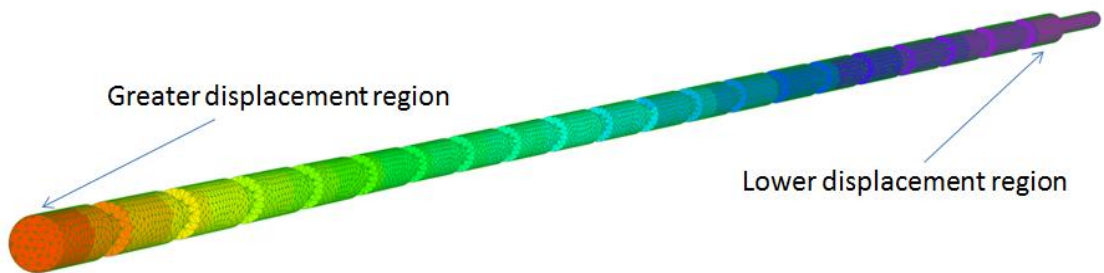


Figure 159 TIRPI thermal induced stress distribution within the y-direction

Figure 160, Figure 161 and Figure 162 show the thermal expansion models of the probe tube and how it expands internally and externally. The external thermal expansion is of no interest to the TIRPI and so is not part of the TIRPI design. However the internal expansion of the probe tube is of interest as the models show that the internal cavity circumference increases which creates for an addition gap between the TIRPI and probe tube. This enables the TIRPI to expand freely without risk of it coming into contact with the probe tube and leading to induced stresses.

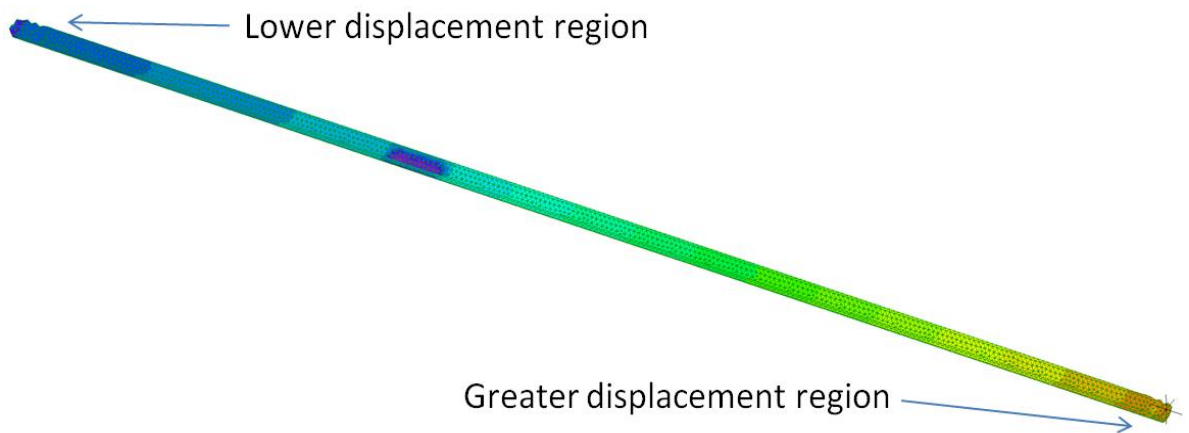


Figure 160 PT thermal induced stress distribution within the x-direction

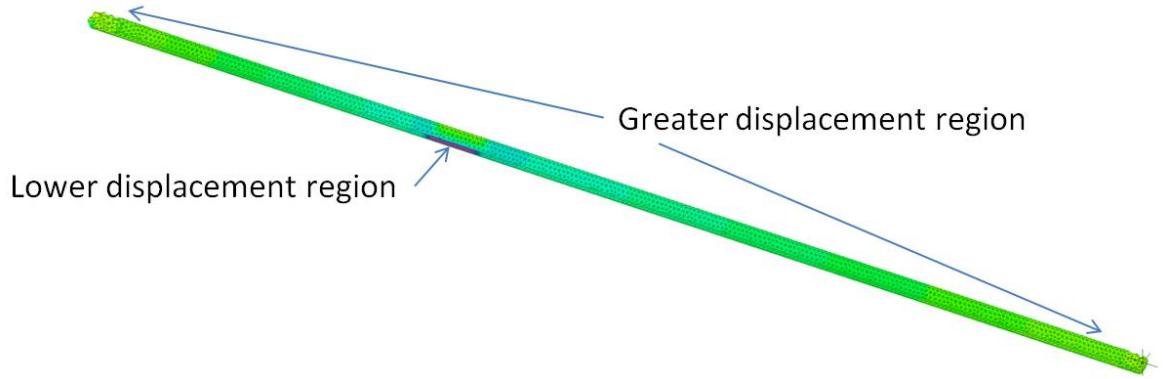


Figure 161 PT thermal induced stress distribution within the y-direction

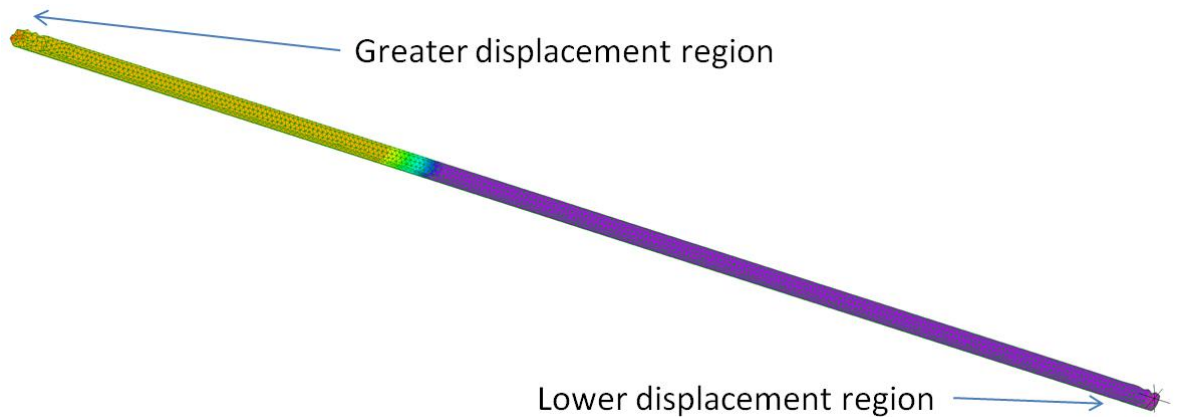


Figure 162 PT thermal induced stress distribution within the z-direction

To create a visual representation of the finite element model demonstrating how the internal cavity within the probe tube increases as the temperature increases, a section was taken where the temperature of the probe tube transitions from 200 °C to 100°C and onto 70°C. This illustrates how the variation in temperature affects the expansion. In addition the model has been amplified artificially by a factor of 100 to aid visualisation of the changes in the probe tube. The model in Figure 163 shows the probe tube sectioned along its centre line to enable the internal bore cavity to be visible. As the temperature along the length of the probe tube changes the expansion of the probe tube cavity follows the trend and becomes larger thus increasing the available space to the TIRPI.

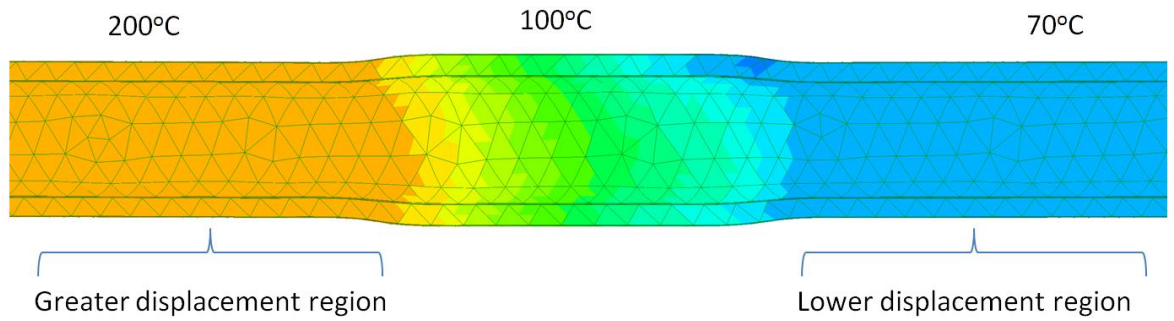


Figure 163 PT thermal induced stress amplification distribution within mid-section

The conclusion from the analyses shows that thermal stresses will not be induced within the TIRPI and probe tube as they both heat up to the operating temperature because they will not be in contact due to the thermal changes of the materials. Thermal induced stress is therefore considered to be not an issue or risk.

Chapter 16

13 Conclusion and Future Work

13.1 Conclusion

This thesis investigates potential technologies which can be used to detect the position of a nuclear reactor control rod position using a magnetic detector. It investigates current detector designs and develops a novel TIRPI method to improve the accuracy of the control rod position. The novel TIRPI has been optimised using finite element modelling, manufactured, and tested within a representative CRDM environment. The results show the new TIRPI operated as expected and achieved the requirements initially set out by the project. In addition, this report shows additional benefits made possible by the new TIRPI when a “SCRAM” is initiated and control rod accurate position is required as the rod is in motion. It was concluded that a TIRPI design needs to consider the core materials and the geometries of the design as well as the wire size and turns to increase the sensitivity of the TIRPI to detect the smallest increment of the CRDM stator rotor arms moving the driveshaft in a linear motion. The optimum TIRPI design is dependent upon the materials surrounding the location where it will reside and the air gaps around its location. It was discovered that the material of the TIRPI core should be of the same materials as the drive shaft to achieve high secondary output voltage resolution and the wire is to be made of copper to enable a larger primary voltage change when the driveshaft envelopes the probe tube. This would allow a compensation to be achieved for variations in temperature and drive shaft effects on the primary coils reflected on the TIRPI secondary output signal. In addition it was concluded that the frequency of the source current is very important to the accuracy of the TIRPI due to the eddy currents within the conductive components of the system. The optimum frequency was determined by using an FE model to simulate the TIRPI and the surrounding components while ensuring an electrical resonant condition

is not caused due to the capacitance of the individual parts of the system such as wiring and connectors.

13.2 Future Work – Design optimisation

13.2.1 Design optimisation

When a requirement needs to be met by creating or designing a product, the natural human reaction is to find the most efficient way to satisfy the need or requirement. This is a loose form of optimisation. When a product is engineered, the tendency is to repeat previous designs and processes. The new design therefore does not lend itself to having any novel features as a consequence. The process is usually driven manually, involving a lot of time using a calculated step by step approach to produce what is deemed the best solution. This method of optimisation is commonly termed an expert-based optimisation approach. Although this is a viable and acceptable approach, it does not allow thorough exploration of the solution space and therefore inherently cannot finding the optimum design.

For low-volume bespoke products where cost is not the priority but the product performance is the key factor such as the TIRPI, the manual stepped approach is suitable. In high-volume products where cost is the highest priority, it is necessary to design products which will satisfy not only the generic requirement but which are also optimised for specific attributes such as efficiency, cost, reliability and so on.

In theory, the optimisation approach for attributes is a logical step forward; however, in reality, identification of optimised designs is not often possible due to the size of the problem and the initial lack of knowledge. In industry, design optimisation is labelled as design improvement, and the term optimisation is used as a loose statement without explaining what techniques are considered to carry the optimisation out.

Design variables used for optimisation are usually characterised into quantitative or qualitative terms. Problem variables (such as length, temperature, span and weight) are referred to as quantitative design variables. When defining a real life design problem there are often variables associated with the product that are difficult to measure. These are known as qualitative variables. Examples of these are aesthetics and manufacturability. In

order to bound a design space, minimum and maximum values limits of the variables are defined which forms the boundary of the variables. In addition, constraints on a design need to be defined as limitations to the functional requirements.

The expert-based optimisation approach uses knowledge gained either from the experience of qualified personnel or by using simulation techniques (such as finite element analysis techniques) where the designer requires no additional skills to carry out the optimisation task. This approach usually provides incremental improvements to a design relying on the experts based knowledge shown in Figure 164. It also shows an overview of the engineering design optimisation methods used over the last ten years, where the designs are initially assessed against the priority constraints such as cost before deciding the optimisation approach to be used.

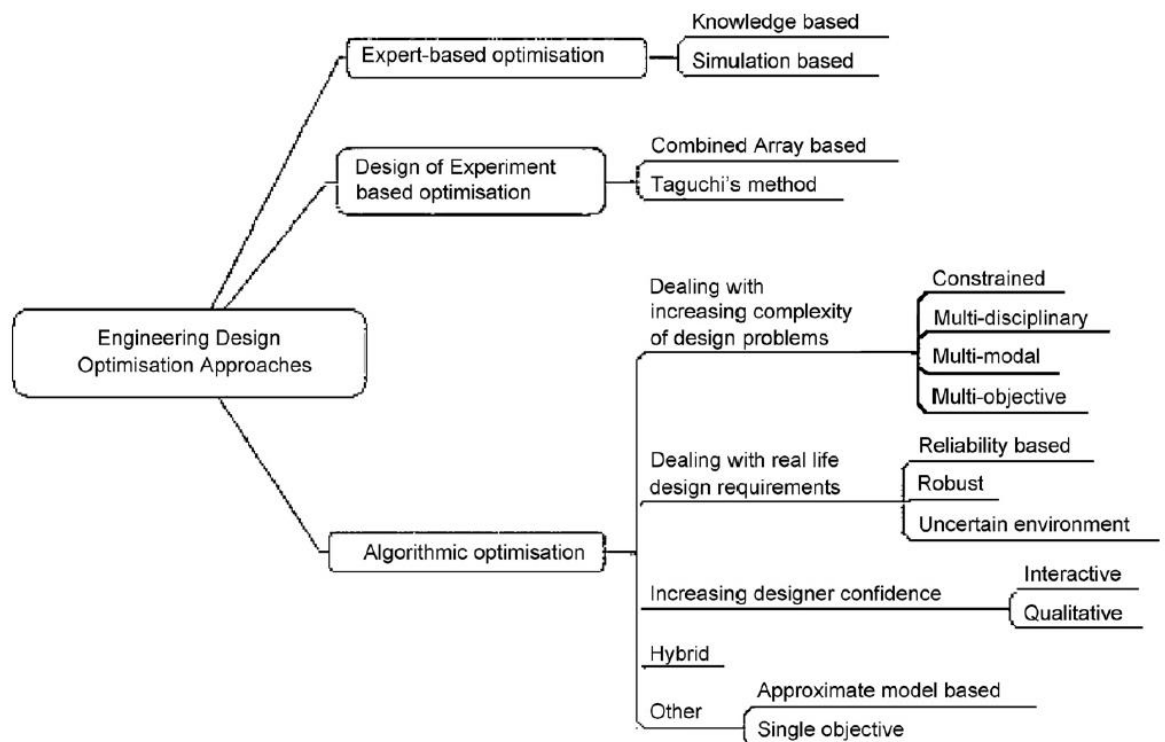


Figure 164 An overview of engineering design optimisation methods [23]

It is evident that algorithm based optimisation requires significant research to develop the optimisation approach. The design of experiments (DoE) methodology is a structured and organised methodology to determine the inputs (denoted the X factors) affecting the design and the outputs (denoted Y factors) of the design. Once the design variables have been identified, an ideal set of parameters is assumed to give the optimised set of results.

This DoE approach can reduce design time and can produce better performing designs that are usually a surprise to designers.

At the start of a project, it is difficult to gauge whether it is more beneficial to use an engineering design optimisation approach or rely on the expert-based approach.

Figure 165 shows an indication of which optimisation technique to use, depending on the size of the engineering design or problem.

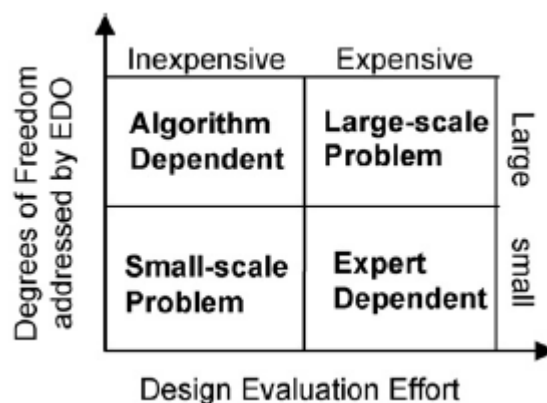


Figure 165 Engineering design approach Vs class of optimisation [23]

It has been observed widely that scalability is the largest challenge when selecting an optimisation methodology; algorithmic optimisation however is becoming popular.

Although this is generally correct, industry is still not widely accepting formal optimisation use. Generic algorithm-based optimisation is still the most popular algorithmic approach.

Further work should include formal optimisation is considered for future iterations of the TIRPI design to identify any shortfalls that may occur as a result of the expert-based approach adopted here. This effort would need to be planned in at the start of the requirement capture stage of the programme and planned as an integrated activity which supports and defines the final design solution.

13.3 Future work – TIRPI CRDM stator immunity

The CRDM currently changes the characteristics of the TIRPI secondary output signal span by 30% compared to the results from a bench test. This is due to the operational frequency of the primary current used to energise the TIRPI. Currently at a frequency of 400Hz, the frequency of the TIRPI primary source is low and the magnetic field generated by the primary bobbins penetrates the probe tube, driveshaft, the surrounding CRDM motor tube and any other surrounding components. As the frequency of the primary

current is increased, the generated eddy currents increase and limit the penetration of the magnetic field into the CRDM components. Ideally the magnetic field should only penetrate up to the driveshaft circumference isolating any other CRDM components. This should reduce the effect of the surrounding CRDM materials on the TIRPI. However this is not practical. Currently, the optimal solution would be to select the frequency which gives the maximum span of the secondary output signal.

13.4 Random optimisation

When using FE design tools, optimisation is used to determine the intended design objective while complying with the constraints of the analyses using a combination of input variables. The optimisation approach used is known as the Direct Optimisation (DO).

A DO optimisation routine was carried out to verify the TIRPI design using expert-based optimisation was sufficiently close to a mathematical analytical model. The expert-based design for the TIRPI was sufficiently accurate allowing the smallest single CRDM motion to be detected thus improving the TIRPI sensitivity further will not give the overall measurement system further benefits. However, the mathematical analysis model would be able to give an optimised design much faster for future developments.

It is very important that the correct mathematical optimisation method is applied for the tools you are using for example the use of FE lends itself to use an optimisation method known as “Random Optimisation”. This is a beneficial method as errors caused due to variations in meshing when different geometries are used cancel out.

A program was developed using Octave to run the FE tool implementing the “Random Optimisation (RO)” technique. A flow chart of the program is shown in Figure 166 of how the program sequentially creates random geometries within the FE tool and checks the span of the TIRPI secondary output signal. If the output is better than the previous result it keeps the latest solution else the solution becomes discarded. This process is continued until either the maximum iterations of the generator are reached or the solution converges.

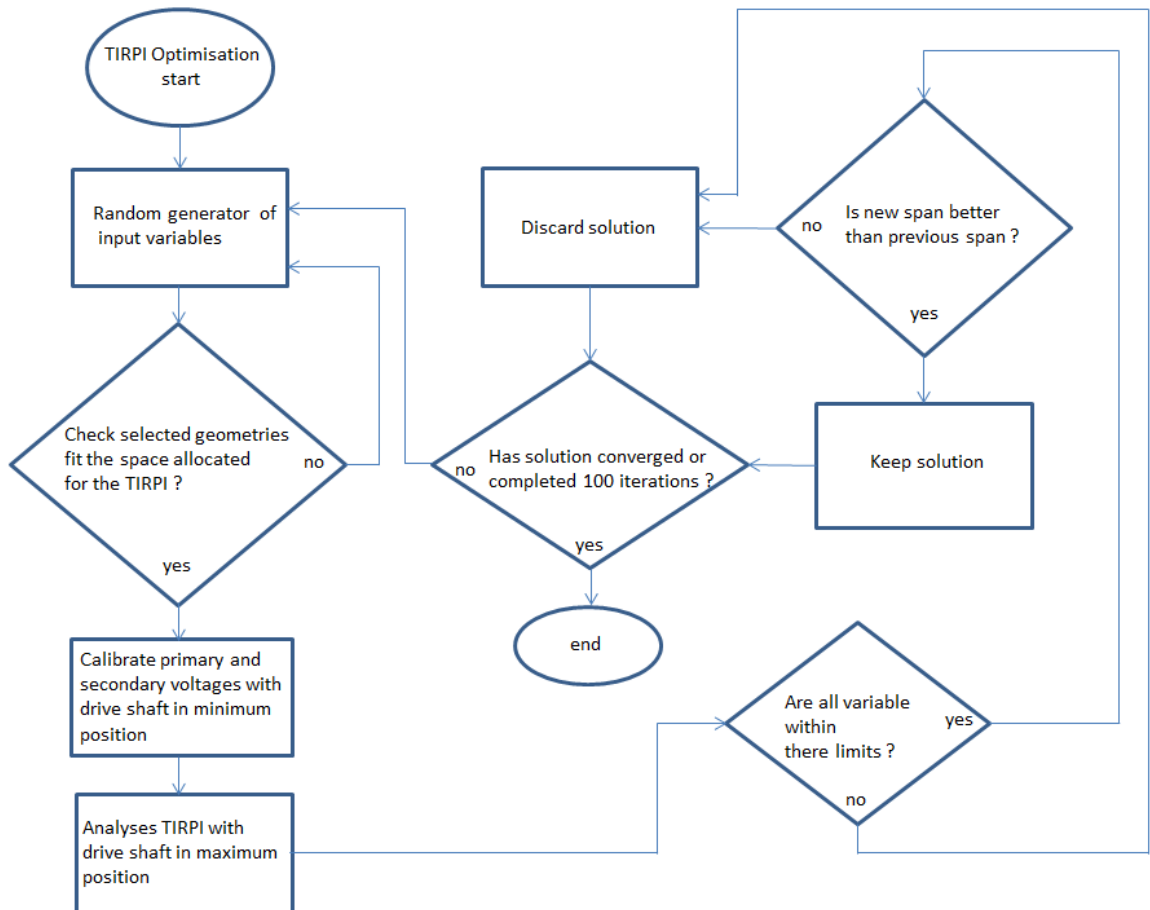


Figure 166 TIRPI Random optimisation flow sequence chart

The results in Figure 167 shows the RO techniques gives greater secondary voltage span output and Figure 168 shows the secondary voltage output difference between each 10mm driveshaft increment to be greater. In addition the RO technique resulted in a lower operational frequency. Although the RO technique is better than the expert-based optimisation the differences between the solutions are relative little demonstrating the expert-based design being suitable as a valid solution.

Given additional effort programming the optimisation software, the RO technique could be improved to find an optimised solution with the addition of the surrounding components. The advantage of using the RO technique is the little amount of time taken for a design to be completed is significantly less compared to the expert-based technique. This would allow more time for the meshing of larger geometries to be considered such as the environment of the TIRPI (CRDM) as part of the optimum solution rather than utilising time visually checking every iteration from the FE model to carryout expert-based optimisation.

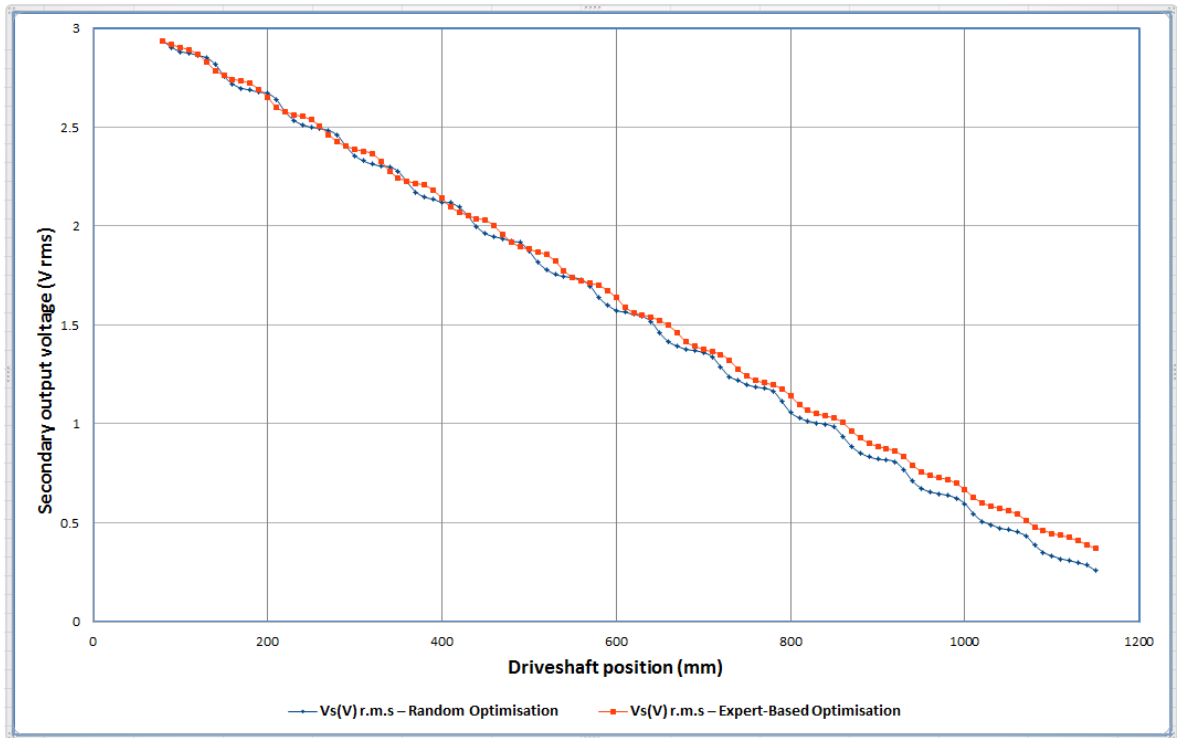


Figure 167 TIRPI secondary Output using Random Optimisation

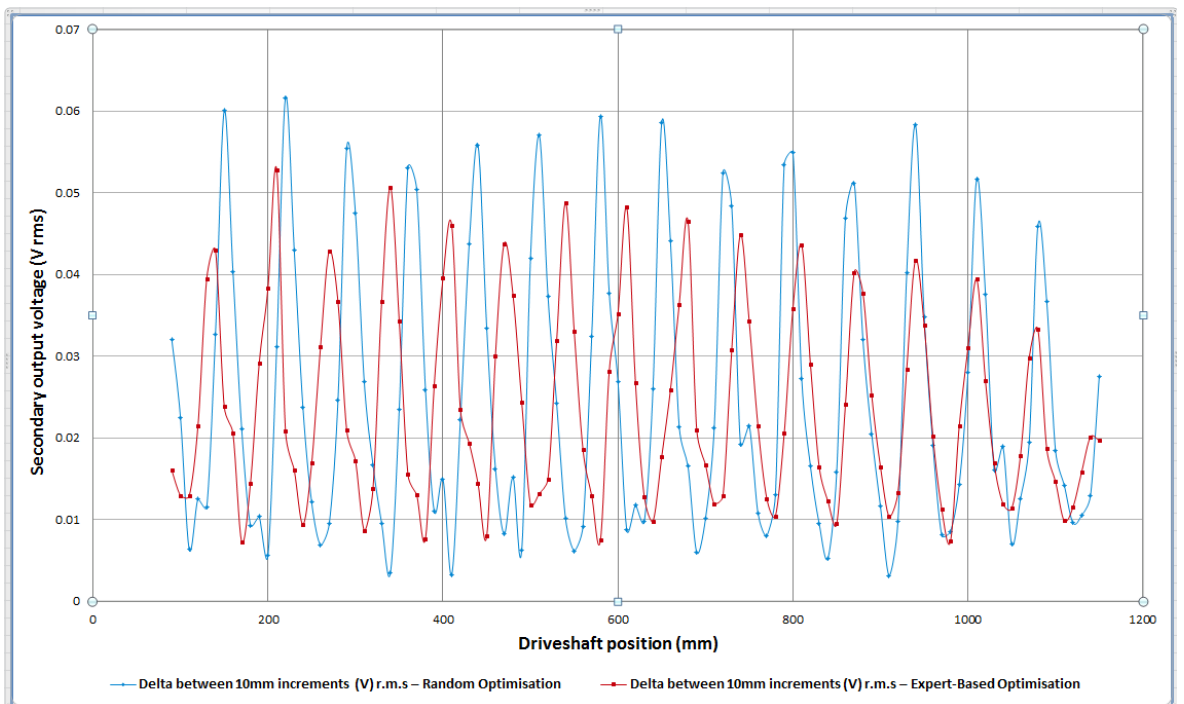


Figure 168 TIRPI secondary voltage output at 10mm incremental driveshaft positions

Table 11 shows the input parameters and the secondary output voltage span for the expert-based and random optimisation. The results show the random optimisation span is 4.12% greater than the expert-based solution than the random optimisation technique however the input power for the random optimisation technique consumes greater power.

Table 11 TIRPI comparison of optimisation techniques

Parameter	Expert-based optimisation	Random optimisation
Frequency (Hz)	400	398.69
Primary Current (A)	0.1	0.14
Primary Voltage (V)	3.29	3.35
Span (V)	2.56	2.67

Although the random optimisation gives an optimum solution, the model only includes the TIRPI, probe tube and driveshaft. This provided a result which could be compared to a known practical solution. However, a better random optimisation model would be to include the CRDM materials around the TIRPI as this is a more realistic environment when in use. Figure 169 shows the results with the random optimisation including the CRDM materials. Within the practical hot and pressurised testing it was discovered that the CRDM material reduces the secondary output span by approximately 30%. Using the random optimisation model the reduced span will be automatically compensated the difference within the solution thus providing a larger secondary voltage output span than using the expert-based TIRPI solution. The model was repeated using the expert-based TIRPI solution to gauge the benefits of using the random optimisation method. The random optimisation solution gives a larger secondary output signal span shown in Figure 169 and Table 12 compared to the expert-based solution resulting in a better result. In addition the sensitivity of the random optimised solution is better as shown in Figure 170 which also reduces the burden on the instrumentation card detecting the voltage changes from the TIRPI secondary output.

It was concluded that using a random generator to achieve an optimised design was successful and significantly reduces the design time of the TIRPI project.

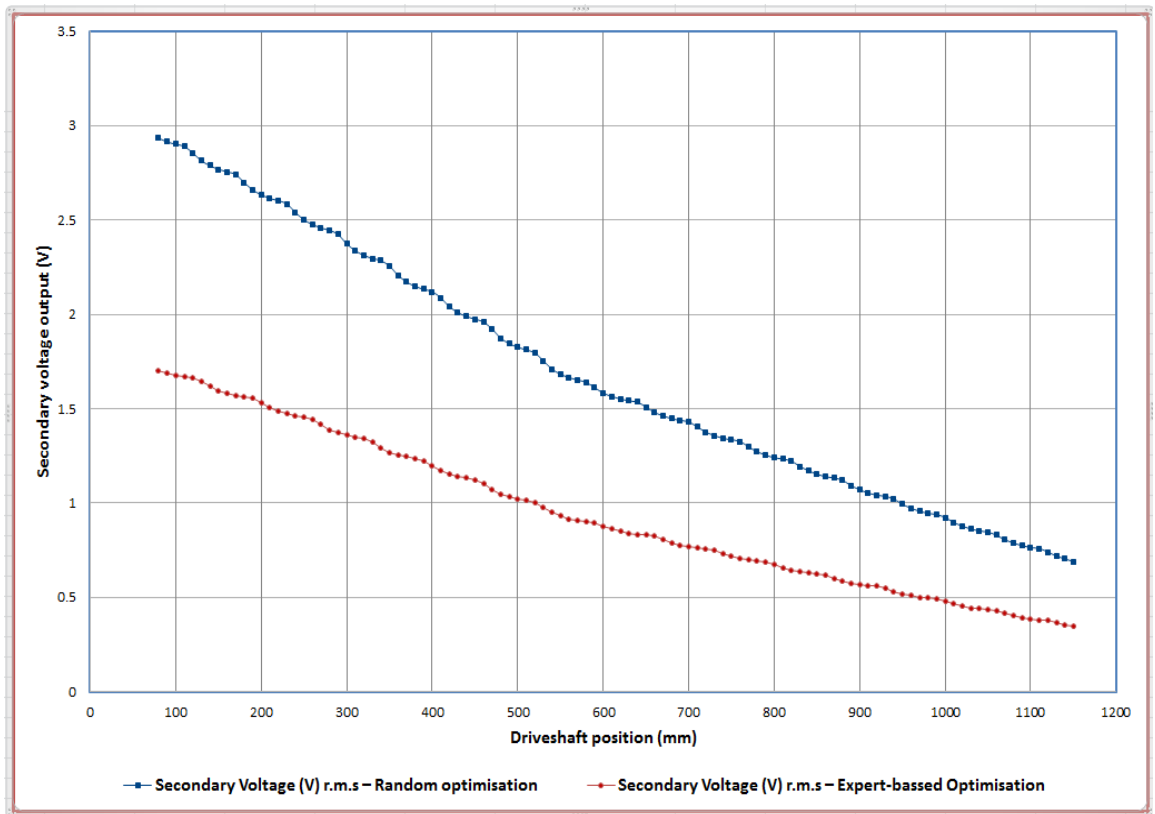


Figure 169 TIRPI within CRDM using Expert-based and Random Optimisation

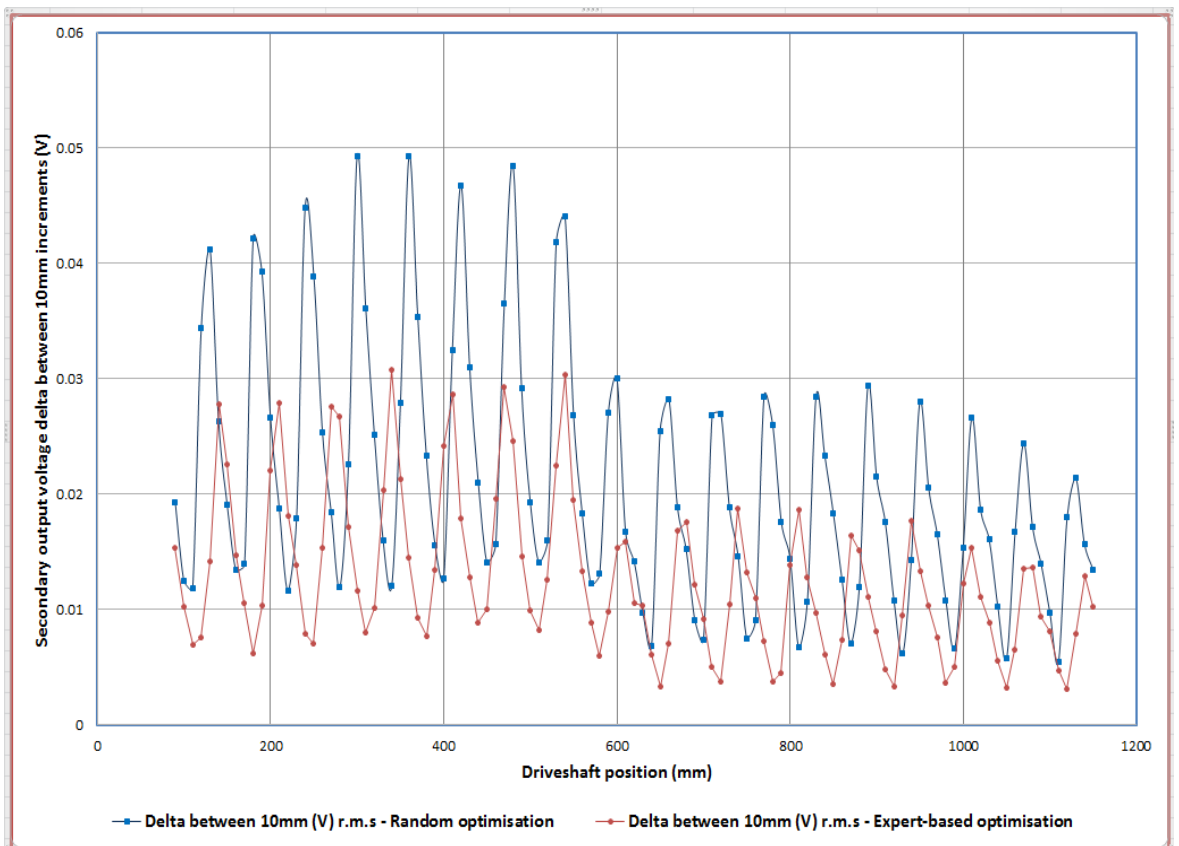


Figure 170 TIRPI sensitivity within CRDM using Expert-based and Random Optimisation

Table 12 CRDM/TIRPI comparison of optimisation techniques

Parameter	Expert-based optimisation	Random optimisation
Frequency (Hz)	400	389.90
Primary Current (A)	0.1	0.179
Primary Voltage (V)	3.03	3.27
Span (V)	1.35	2.24

13.5 Future Work - Electromagnetic Compatibility

(EMC) Environmental Withstand

The TIRPI has to be able to withstand an electromagnetic DC field within free space when used within a submarine environment. The TIRPI is expected to operate to the accuracy requirements for the rod position measurement once the magnetic field is removed. A finite element model could be used to simulate the effect of interference from the external electromagnetic fields on the TIRPI measurements and compared to testing. An initial model was developed to predict the magnetic effects on the TIRPI within the CRDM however further work would be required to validate the results. This would require large infrastructure investment as the CRDM is a large component and specialist Helmholtz coils will need to be manufactured.

Chapter 17

14 Additional Work

A second TIRPI was manufactured called the TIRPI Variant using the same materials as the first TIRPI. It was optimised however for a slightly different geometry probe tube and driveshaft. The solution for the TIRPI Variant would normally be very similar to the TIRPI as the materials are the same however the customer required a greater span output of the secondary voltage. The increased span output from the secondary output results in an increased 'S' shaping of the output signal. This was predicted using the TIRPI FE model. The TIRPI Variant worked as predicted first time giving the increased sensitivity results. The TIRPI Variant was tested within a thermal environmental chamber to ensure the secondary output signal changes linearly as the environmental temperature increases similar to the TIRPI. Figure 171 and Figure 172 shows the TIRPI Variant secondary output characteristics as the temperature of the environment increases. The results show the span of the secondary output voltage and offset increases. As each temperature is calibrated using the primary voltage the thermal effects are cancelled within the instrumentation card. It was important to show the thermal changes cause the TIRPI Variant secondary output voltage to change linearly as this is assumed within the instrumentation card.

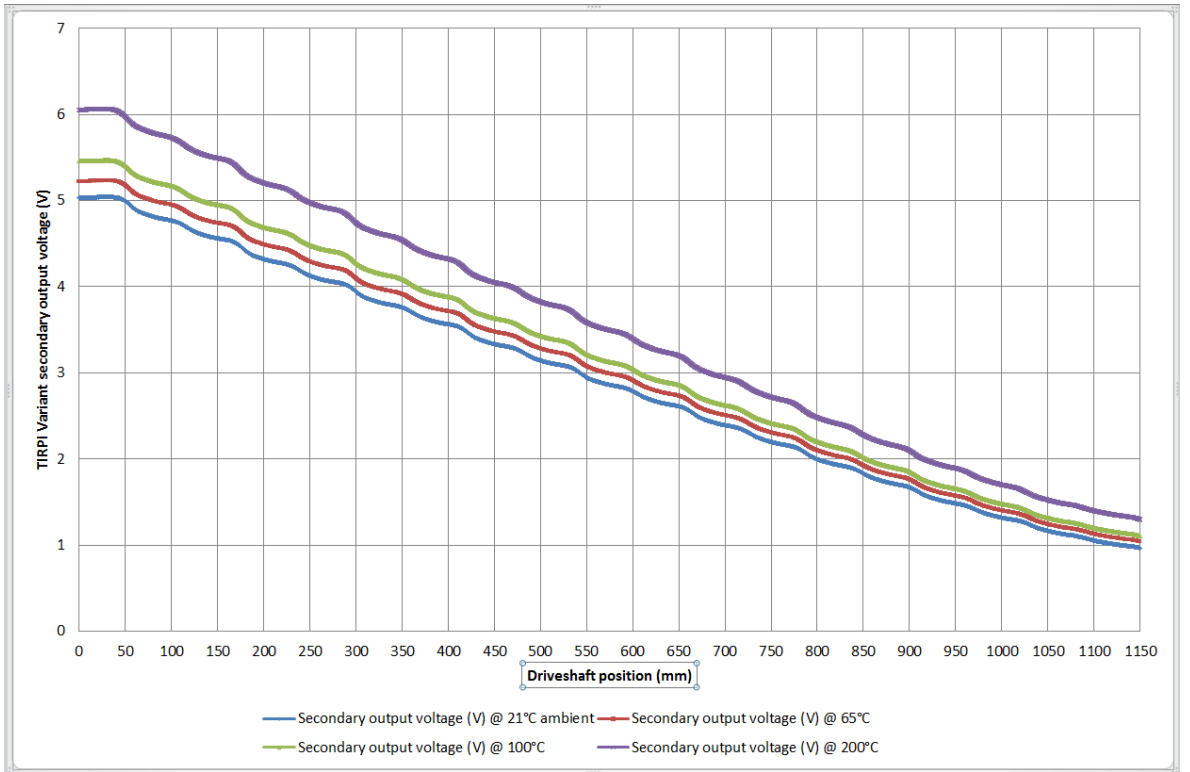


Figure 171 TIRPI Variant secondary output characteristics at 21°C, 65°C, 100°C and 200°C full sweep

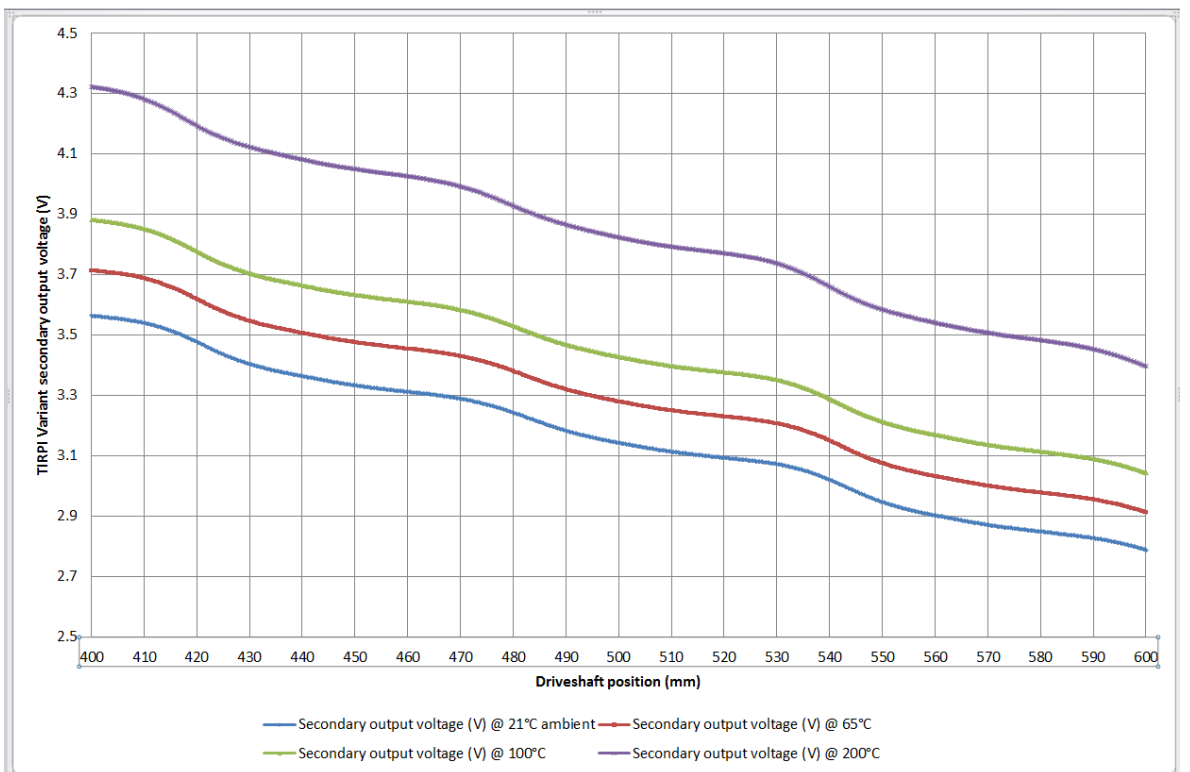


Figure 172 TIRPI Variant secondary output characteristics at 21°C, 65°C, 100°C and 200°C partial sweep

The thermal effects can be shown to be linear by inspecting the test results from the environmental chamber and plotting the change in TIRPI Variant secondary output voltage against the temperature of the environmental chamber as shown in Figure 173.

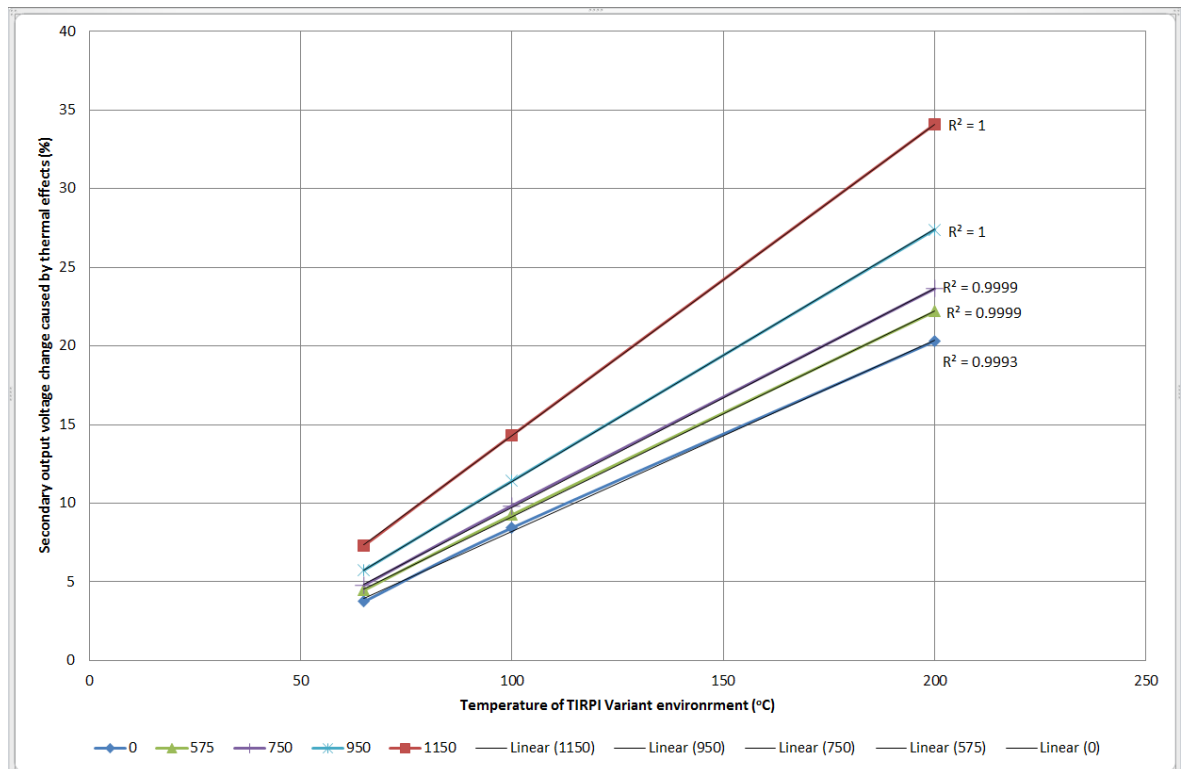


Figure 173 TIRPI Variant secondary output voltage change with respect to environment temperature

Five driveshaft positions were plotted at three temperatures showing the perspective secondary output voltage change relative to the secondary output voltage at ambient (21°C). The results in Figure 173 shows the R^2 values to be either one or very close to one which shows the TIRPI Variant secondary output changes linearly with respect to an environmental thermal change. This analysis suggests not only the copper wire on the TIRPI Variant has a linear thermal coefficient but more importantly the core material 17.4 PH H1100 has a similar effect. This enables the instrumentation card compensation to be more easily implemented and thus reducing the probability of calculation error.

15 References

- [1] Nyce, David S., *Linear position sensors: theory and application*, Wiley-interscience ISBN:978-0-471-23326-8, 2004.

- [2] Karmijit Sidhu, "*Understanding Linear Sensing Technologies*", www.sensormag.com/position-presence-proximity/understanding-linear-position-sensing-technologies-10139, July 1, 2012

- [3] A, S. and T. D, *A position indicator employing magnetic circuits to monitor the position of a magnetically permeable member movable along an axis having one degree of freedom*, US Patent. No.:3,852,661, Dec. 03, 1974.

- [4] Auchterlonic, R.C, *Inductive position sensor having plural phase windings on a support and a displaceable phase sensing element returning a phase indication signal by electromagnetic induction to eliminate wire connections*, US Patent. No.:5,003,260, Mar. 26, 1991.

- [5] M. R. Barrault, "*Electromagnetic Delay Line Incorporated in a Position Detector for a Movable Nuclear Reactor Control Rod*", US Patent. No.:4,604,576, Aug. 5, 1986.

- [6] E. J. Beltz, "*Method and System for Indicating the Position of Control Rods of a Nuclear Reactor*", US Patent. No.:5,563,922, Oct. 8, 1996

- [7] Frederick J. Young, Francis T. Thompson, Dirk J. Boomgaard, "*Position Indication System*", US Patent. No.:3,864,771, Nov 5, 1974

- [8] Dean C. Santis, Andre Wavre, Andras I. Szabo, "*Magnetic Position Sensor*", US Patent. No.:3,742,409, June 26, 1973

- [9] Andrew N. Dames, David T. Ely, Andrew R. L. Howe, "*Position Encoder*", US Patent. No.:5,812,091, Sep 29, 1998
- [10] Michal M. Feilchenfeld, Grant R. Connors, "*Position Indicating Device*", US Patent. No.:4,711,757, Dec 08, 1987
- [11] Jason A. Adler, David R. Barlett, "*Magnetic Position Indicator*", US Patent. No.:3,857,089, Dec 24, 1974
- [12] Yves Pelenc, Jean Ambier, Roger Lavergne, "*Electromagnetic Position Indicator*", US Patent. No.:3,890,607, June 17, 1975
- [13] Joseph E. Knowles, David A. Story, "*Nuclear Control Rod Position Indication System*", US Patent. No.:US 2012/0155596 A1, June 21, 2012
- [14] Vladimir P. Nikolaev, Leopold I. Chaika, Ivan V. Ivanov, "*Position Sensor of Linearity Moving Bodies*", US Patent. No.:4,210,865, July 1, 1980
- [15] Donald R. Barton, "*Control Rod Position Indication System*", US Patent. No.:3,649,450, March 14, 1972
- [16] Charles C. Ripley, "*Nuclear Reactor Control Rod Drive with Rod Position Indicating Means*", US Patent. No.:3,734,824, May 22, 1973
- [17] Johannes J. Schmitz, Theodore M. Heinrich, "*Phase Encoded Digital Position Probe Assembly*", US Patent. No.:4,170,754, Oct 09, 1979
- [18] John C. Singleton, John R. Thayer, Frederick C. Seelenbinder, "*Position Indicator*", US Patent. No.:3,492,616, Jan 27, 1970

- [19] Raymond J. Krisst, "*Magnetostrictive Position Indicator*", US Patent. No.:4,071,818, Jan317, 1978
- [20] William G. Osmer, Robert Rainey, "*Linear Position Sensor Using a Strain Gauge*", US Patent. No.:6,369,689, Apr 09, 2002
- [21] David E. Tanner, "*Position Indicator*", US Patent. No.:4,304,630, Dec 08, 1981
- [22] Kenneth H. Beck, William I. Shepley, Skillman, N.J, "*Ultrasonic Position Indicator System*", US Patent. No.:3,237,150, Feb 22, 1966
- [23] Rajkumar Roy, Srichand Hinduja, Roberto Teti, "*Recent advances in engineering design optimisation:Challenges and future trends*" CIRP Annals – Manufacturing Technology 57 (2008) 697-715

16 Appendix A TIRPI variant

Figure 174, Figure 175 and Figure 176 shows the TIRPI Variant computer Aided Design (CAD) schematic and the manufactured product.

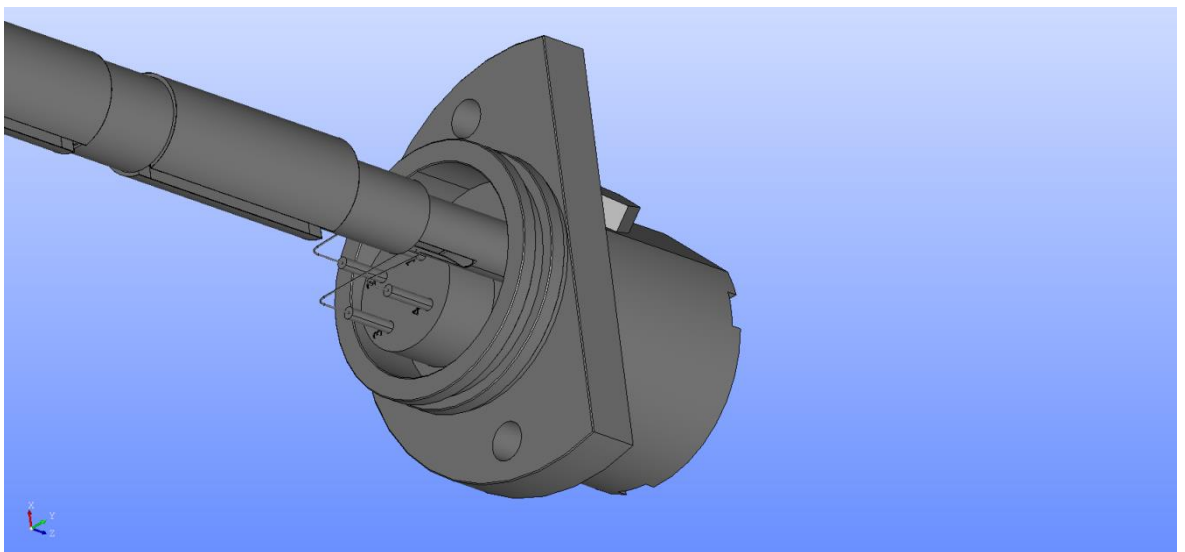
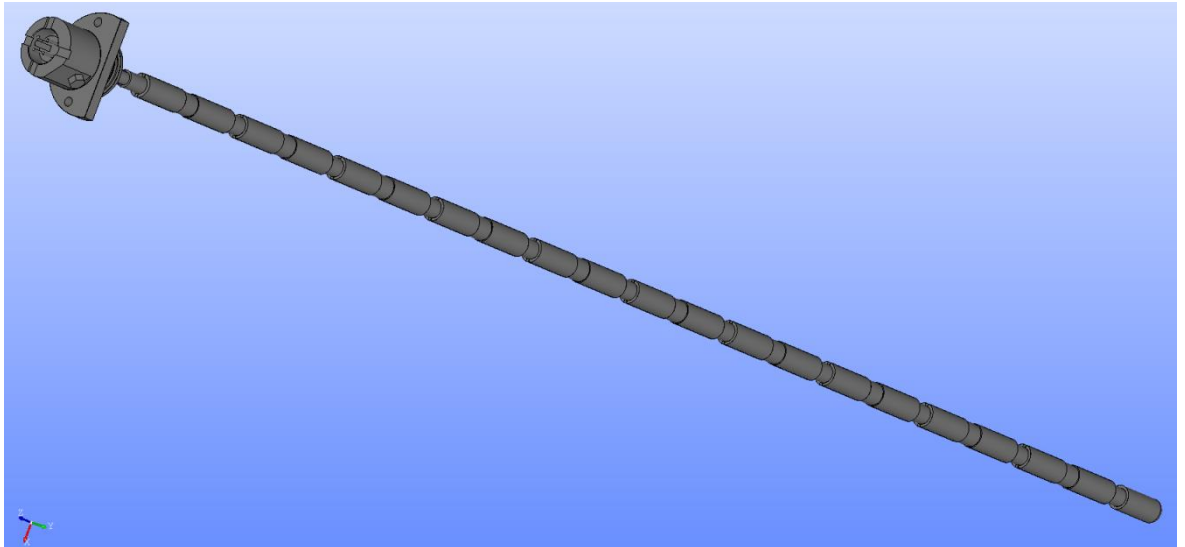


Figure 174 TIRPI variant CAD (Centronics Ltd)

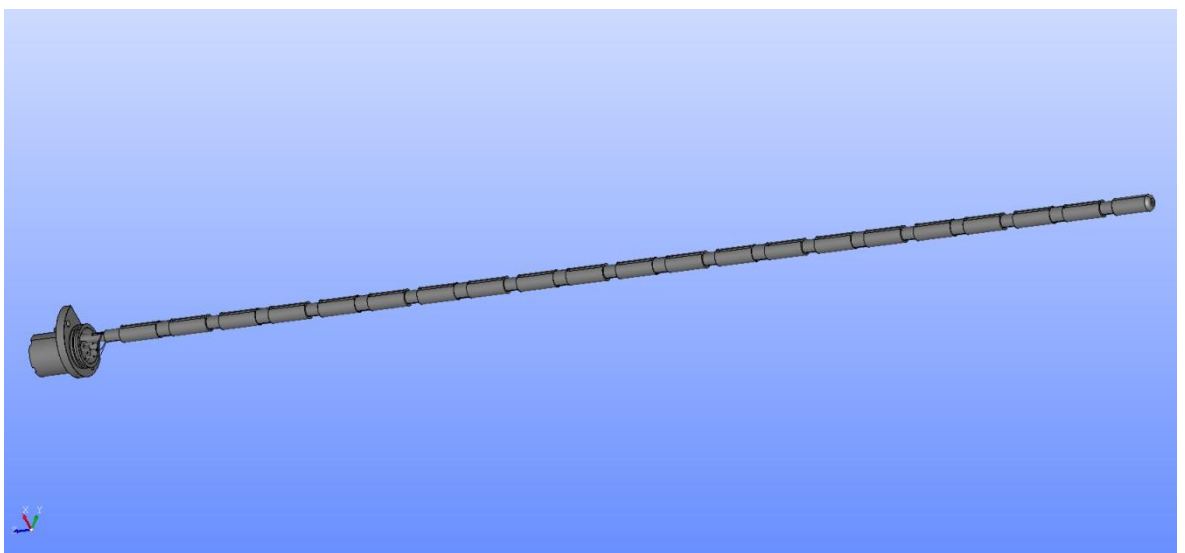
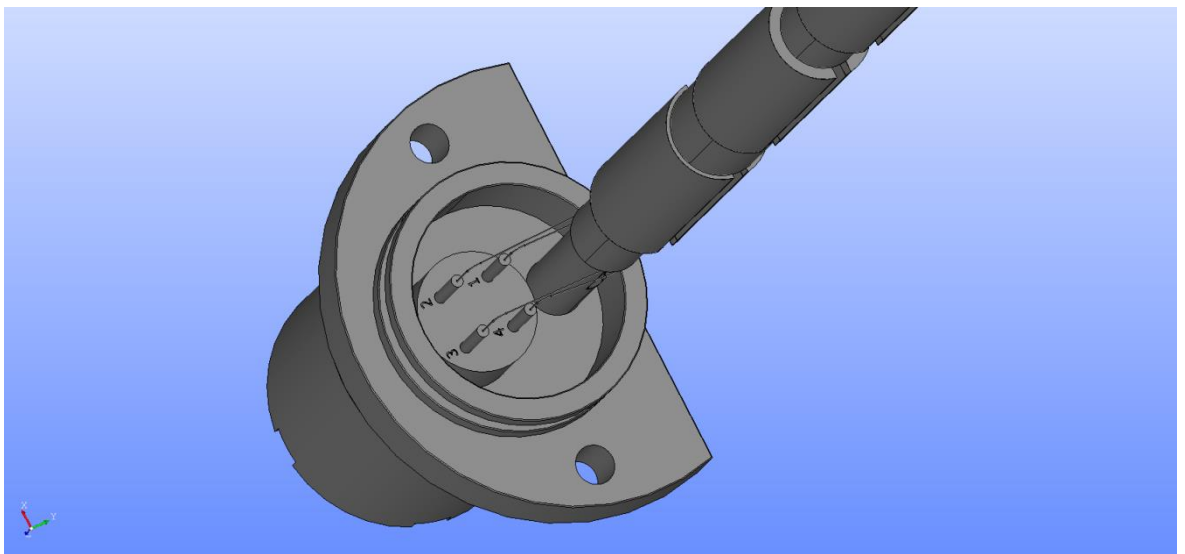
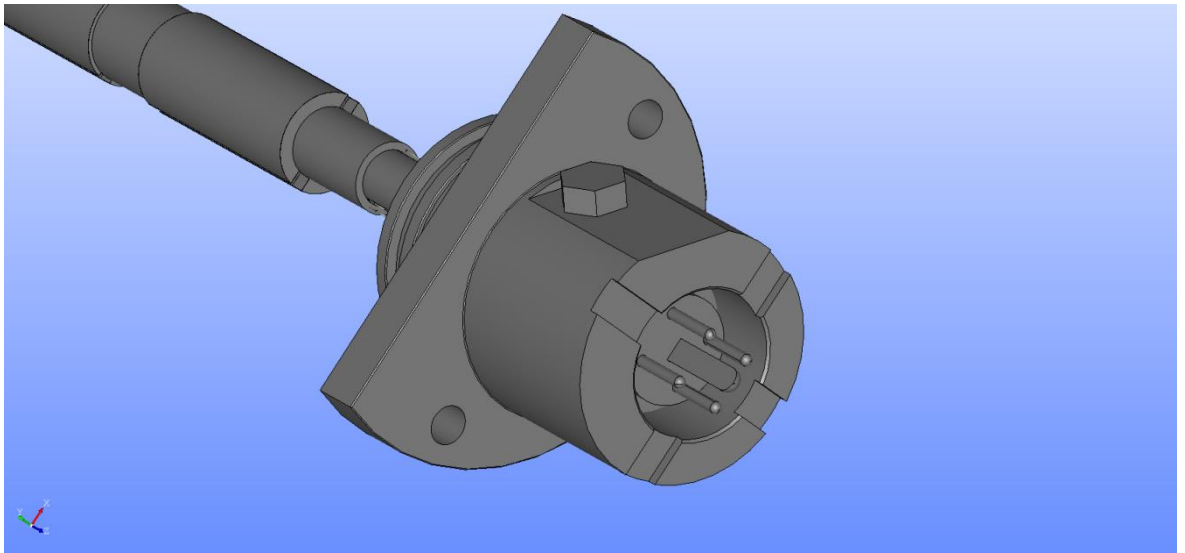


Figure 175 TIRPI variant CAD (Centronics Ltd)

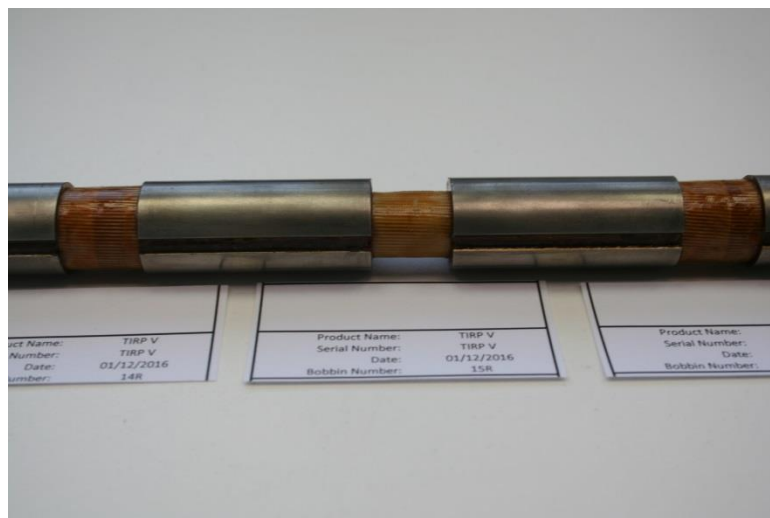



Figure 176 TIRPI variant (Centronics Ltd)


17 Appendix B – DFMEA

		Project No. / Purchase Order.....NG TIRP 12/8/2014..... Page1..... of1.....		Design FMEA														
Operation	Design Feature	Function	Potential Failure Mode	Potential effect of Failure	Severity	Potential Cause Of Failure	Occurrence	Current Process Control To Prevent Failure Mode	Current Process Control To Detect Failure Mode	Detection	RPN	Recommended actions	Responsibility & Deadlines	Action Taken	Severity	Occurrence	Detection	RPN
1			Would not align to probe tube	Difficult to assemble	9	Incorrect geometrical tolerance specified	3	Tolerance calculations based on customer design calculations	3D CAD Model and pre-production manufacture	1	27							0
					9	Interface tolerances between TIRP housing and TIRP	3	Tolerance calculations based on customer design calculations	3D CAD Model and pre-production manufacture	1	27							0
3			Would not align to probe tube connector seating	Potential for O ring seal not to function	9	Interface tolerances between TIRP housing and TIRP	3	Tolerance calculations based on customer design calculations	3D CAD Model and pre-production manufacture	1	27							0
					9	Incorrect pressure direction on O ring	3	Review of customer design	Model calculations	3	81							0
4				Unable to remove the TIRP in service	9	Interface tolerances between TIRP housing and TIRP	3	Tolerance calculations based on customer design calculations	3D CAD Model and pre-production manufacture	1	27							0
5			Potential Jam	Probe tube damage.	9	Interface tolerances between TIRP housing and TIRP	3	Tolerance calculations based on customer design calculations	3D CAD Model and pre-production manufacture	1	27							0
				Catastrophic failure to reactor	9	Interface tolerances between TIRP housing and TIRP	3	Tolerance calculations based on customer design calculations	3D CAD Model and pre-production manufacture	1	27							0
6				Total or intermittent Failure to the TIRP	9	Interface tolerances between TIRP housing and TIRP	3	Tolerance calculations based on customer design calculations	3D CAD Model and pre-production manufacture	1	27							0
7			Probe tube inner scoring (FOD)	Unable or difficult to remove the TIRP during maintenance	9	Interface tolerances between TIRP housing and TIRP	3	Tolerance calculations based on customer design calculations	3D CAD Model and pre-production manufacture	1	27							0
8					9	Interface tolerances between TIRP housing and TIRP	3	Tolerance calculations based on customer design calculations	3D CAD Model and pre-production manufacture	1	27							0

24	O Ring Seal	Produce a moisture and pressure seal	O Ring leakage	Potential for O ring seal not to function	7	Incorrect material selection or shore hardness	3	To be specified on all relevant production documentation.	Documentation review.	3	63									0
25	Lead out wire connection insulation	Insulate the lead out wire connections	Insulation breakdown	Electrical functional failure	7	Incorrect material or method defined	3	To be specified on all relevant production documentation.	Documentation review.	3	63									0
26	Lead out wire staking	Secure in place the loose lead out wires	Loose lead out wires	Electrical function failure due to wire abrasion	7	Insufficient number of stacking point defined	3	To be specified on all relevant production documentation.	Documentation review.	3	63									0
27			Would not align with TIRP Rod	Difficult to assemble	9	Interface tolerances between TIRP connector and TIRP	3	Tolerance calculations based on customer design calculations	3D CAD Model and pre-production manufacture	1	27									0
28			Would not align to probe tube	Difficult to assemble	9	Interface tolerances between TIRP housing and TIRP	3	Tolerance calculations based on customer design calculations	3D CAD Model and pre-production manufacture	1	27									0
29				Difficult to assemble	9	Interface tolerances between TIRP housing and TIRP	3	Tolerance calculations based on customer design calculations	3D CAD Model and pre-production manufacture	1	27									0
30			Would not align to probe tube connector seating	Potential for O ring seal not to function	9	Interface tolerances between TIRP housing and TIRP	3	Tolerance calculations based on customer design calculations	3D CAD Model and pre-production manufacture	1	27									0
31				Potential for O ring seal not to function	9	Incorrect pressure direction on O ring	3	Tolerance calculations based on customer design calculations	3D CAD Model and pre-production manufacture	1	27									0
32				Unable to remove the TIRP in service	9	Interface tolerances between TIRP housing and TIRP	3	Tolerance calculations based on customer design calculations	3D CAD Model and pre-production manufacture	1	27									0
33		Alignment of the TIRP Assembly	Potential Jam	Probe tube damage.	9	Interface tolerances between TIRP housing and TIRP	3	Tolerance calculations based on customer design calculations	3D CAD Model and pre-production manufacture	1	27									0
34				Catastrophic failure to reactor	9	Interface tolerances between TIRP housing and TIRP	3	Tolerance calculations based on customer design calculations	3D CAD Model and pre-production manufacture	1	27									0

39				Moisture seal IP68.	signal integrity impaired	9	Supplier design compromised.	7	Supplier to furnish a drawing package and DFMEA		3	189	Connector design similar to current class	Initial design agreed	Design review before DR5 November 2014 Completed.	5	5	3	75
	TIRP Connector Receptacle.	Internal connector to receptacle seal.	Seal to meet the requirements of the non metallic database	Signal integrity impaired	9	Design colabration to meet the material selection.	7				3	189	Connector design similar to current class	Initial design agreed	Design review before DR5 November 2014 Completed.	5	5	3	75
			Obtaining the correct information on design requirements from Rolis Royce	Unkown design parrameters.	9	Lack of design data requirements	7	Rolis Royce to furnish the correct design			3	189	Connector design similar to current class	Initial design agreed	Design review before DR5 November 2014 Completed.	5	5	3	75
40	Receptacle Backshell.	Cable to backshell termination.	Obtaining the correct information on design requirements from Rolis Royce	Unkown design parrameters.	9	Lack of design data requirements	7				3	189	Connector design similar to current class	Initial design agreed	Design review before DR5 November 2014 Completed.	5	5	3	75
41	Winding Wire	Transformer coil windings	Insulation breakdown (minimum life at 240°C is 20,000 hours)	signal integrity impaired	9	Incorrect material selection	3	Material specification review to match requirement.			3	81							0

18 Appendix C – PFMEA

		Project No./purchase Order: 5200083327 DEV3799999002 and SUB3700031512 TIRP Core Assembly				Process FMEA						Issue: B Date: 10/03/16					
Operation	Process Step	Function	Potential Failure Mode	Potential effect of Failure	Severity	Potential Cause Of Failure	Occurrence	Current Process Control To Prevent Failure Mode	Detection	RPN	Recommended actions	Responsibility & Deadlines	Action Taken	Severity	Occurrence	Detection	RPN
1	Degrease & inspection	Remove traces of oil/dirt & inspection for removal	Contamination not totally removed	Core insulation failure	5	Insulation failure due to oil / dirt contamination.	3	SQEP Operator and cleaning instructions PR1581.	7	105	The cleaning procedure PR1581 is Rolis Royce approved.	In place for preproduction in assembly	Centronic incorporated cleaning process. Completed.	5	3	75	75
2	Removal of burrs / sharp edge inspection.	Inspection of burrs and sharp edge removal	Burrs or sharp edges not totally removed	Winding wire insulation failure	5	Potential of insulation failure due to puncturing.	5	SQEP Operator and operation instructions	7	175	Workmanship standards to be defined before preproduction.	In place for preproduction in assembly	QA to compile controlling documentation.	5	3	75	75
3	Insulation of the core/rod	Insulate the windings from the core	Incomplete insulation not complete coverage	Insulation failure	5	Insulation non-adhesion bare material exposed.	3	SQEP Operator and operation instructions	7	105	The colour difference between the core and insulation material allows for excellent detection.	In place for preproduction in assembly	SQEP Operators training in this inspection. Completed.	5	3	75	75
4	Lay the leadout wires into the rod slot	Leadout wires for the termination of the windings	Wire insulation damage	Insulation failure	5	Damage on receipt	3	SQEP Operator	3	45	Electrical test for insulation damage						0
5	Identification of the leadout wires	Identify the primary and secondary leadout wires	Incorrectly identified	Fails test due to incorrect wire connection	5	Damage during assembly Electrical failure caused by incorrect connection of leadout wires.	3	SQEP Operator and operation instructions	3	45	Electrical test for insulation damage						0
6	Winding machine set up	Ensure the correct location of rod in machine.	Coilet and tailstock set up incorrectly	Rod damage	7	Machine set up incorrectly ensure correct location of rod.	1	SQEP Operator and operation instructions	3	21	Machine set up inspection.						0
		Set the machine counter at zero.	Not set correctly	Incorrect number of windings	5	Machine set up and operation counter is zeroed before start.	1	SQEP Operator and operation instructions	3	15	Machine set up inspection.						0
		Set the machine in the correct rotation.		Wound in the wrong direction.	5	Machine set up ensure correct rotation of winding.	1	SQEP Operator and operation instructions	3	15	Machine set up inspection.						0

CENTRONIC		Project No./purchase Order: 5200033327 DEV3799999002 and SUB3700031512 TIRP Core Assembly				Process FMEA						Issue: B Date: 10/03/16						
Operation	Process Step	Function	Potential Failure Mode	Potential effect of Failure	Severity	Potential Cause Of Failure	Occurrence	Current Process Control To Prevent Failure Mode	Current Process Control To Detect Failure Mode	RPN	Recommended actions	Responsibility & Deadlines	Action Taken	Severity	Occurrence	Detection	RPN	
15	Insulation of windings outside diameters	Tape over the secondary coils for complete coverage.	Incomplete insulation coverage.	Loose insulation tape	5	Tape non adhesion may produce FOD.	3	SOEP Operator and operation instructions	Inspection at x10 magnification at 1000 lux	7	Electrical test for insulation damage. Present inspection process.	In place for preproduction assembly	SOEP Operators training in this inspection.	5	3	3	45	
			Insufficient insulation removed	Poor connection	5	Incorrect solder flow onto joint.	3	SOEP Operator and operation instructions	Inspection at x10 magnification at 1000 lux	7	Electrical test for insulation damage. Present inspection process.	In place for preproduction assembly	SOEP Operators training in this inspection.	5	3	3	45	
			Excessive insulation removed	Insulation failure	7	Damage during assembly	3	SOEP Operator and operation instructions	Inspection at x10 magnification at 1000 lux	7	Electrical test for insulation damage. Present inspection process.	In place for preproduction assembly	SOEP Operators training in this inspection.	5	3	3	45	
16	Primary and secondary windings connection to leadout wires	Wrap the winding wire onto the leadout wire	Insulation damaged	Connection failure	7	Damage during assembly	3	SOEP Operator and operation instructions	Electrical test for identification	3							0	
			Poor wrap insufficient turns		5	Poor connection that may fail in service	3	SOEP Operator and operation instructions	Electrical test for identification	3							0	
		Incorrect solder flow	incorrect solder iron temperature setting	5	Poor connection that may fail in service	3	SOEP Operator and operation instructions	Electrical test for identification	3	45							0	
		Dry solder joint.	Continuity failure	7	Poor connection that may fail in service	3	SOEP Operator and operation instructions	Electrical test for identification	3	63								0
		Incomplete insulation coverage.	Connection failure	5	Poor connection that may fail in service	3	SOEP Operator and operation instructions	Electrical test for identification	3	45								0

19 Appendix D – Bespoke winding machine

A bespoke winding machine was designed to enable prototype units to be manufactured for testing. The results from the prototype were used to ensure the finite element modelling software tool operated as expected. Figure 177 shows the bespoke winding machine.



Figure 177 TIRPI bespoke winding machine

20 Appendix E – TRL Assessment tool

A	B	C	D	E	F	G	H	I	K	M
TRL	Definition	Description	Supporting Evidence	Boundaries	Interpretation (specific, measurable, relevant description)	Test Method Used	Evidence to support Interpretation	Associated Risk	Reference Documentation	
1	Basic principles observed and reported	Lowest level of technology readiness. Blue skies scientific research begins to be translated into applied research and development (R&D). Examples might include paper studies of a technology's basic properties	Published research that identifies the principles that underlie this technology. References to who, where, when. Early lab model of basic concept may be useful for substantiating the TRL level	Recognise specific principles involved. Limited evidence may exist that indicates that observations are repeatable and dependable.	Sensor concept sketched and basic principle identified?					
2					Physical laws and assumptions identified in new technology?					
3					Do paper studies confirm basic principle?					
4					Has Initial scientific research been carried out to identify previous use elsewhere. (eg: journals/conferences/technical reports)?					
5					Has basic scientific principles been observed?					
6					Has idea been proposed to OBU ACDE?					
7					Who will fund technology ?					
8					Research hypothesis formulated?					
9					Know who will perform research and how it will be done?					
10										
11	Technology concept and/or application formulated.	Invention begins. Once basic principles are observed, practical applications can be invented. Applications are speculative, and there may be no proof or detailed analysis to support the assumptions. Examples are limited to analytical studies	Publications or other references that outline the application being considered and that provide analysis to support the concept. Applied research activities, analytical studies, small code units, and papers comparing competing technologies	Emphasis here is still on understanding the science but starting to think about the applications of the specific principles. Analytical studies with possibly some experimental laboratory work to corroborate basic observations. Typical of TRL 1. The step between TRL 1 and 2 consists of realisation that there may be uses for scientific principles, although such uses are not yet well defined.	Is the customer known?					
12					Has component application been identified?					
13					Do paper studies show feasibility of application?					
14					Do you know what program the technology will support?					
15					Is there a theoretical or empirical solution identified?					
16					Are the basic elements of the technology identified?					
17					Is the principle feasible within a desktop environment?					
18					Have the components been partially characterised?					
19					Has performance prediction been made for each element?					
20					Has the customer expressed an interest with the concept and how this is proposed to be applied?					
21					Does the Initial analysis show the major engineering functions which need to be carried out?					
22					Has Modelling/simulation been used to verify physical principles?					
23					Does the system architecture define major functions to be performed?					
24					Is there a requirements tracking system identified?					
25					Rigorous analytical studies confirm basic principles					
26					Do the individual parts of the technology work?					
27					Do you know what output devices are available?					
28					Is there an investment strategy sheet?					
29					Do you know the capabilities of manufacturers?					
30					Have you quantified areas of risk? (cost, project, performance etc)					
31					Do you have a basic idea how to market the technology?					
32	Analytical and experimental critical function and/or characteristic proof-of-concept	Active R&D is initiated. This includes analytical studies and laboratory studies to physically validate the analytical predictions of separate elements of the technology. Examples include components that are not yet integrated or representative	Results of laboratory tests performed to measure parameters of interest and comparison to analytical predictions for critical subsystems. References to who, where, and when these tests and comparisons were performed. What are the plans to address the delta of where the technology is now and that required for ISD – are they viable?	Experimentation with potential elements of systems begins. Performing laboratory work to validate pieces of the technology without trying to integrate components into a system. Modeling and simulation may be used to complement physical experiments. The emphasis is on validating the predictions made during earlier analytical studies so that we are certain the technology concept has a underpinning scientific baseline.	Do you have analytical studies which validate technology capability?					
33					Is there any mathematical or computer modeling/simulation for the concept?					
34					Has the preliminary system performance characteristics been identified?					
35					Laboratory experiments verify feasibility of application					
36					Has the customer representative been identified?					
37					Has the customer participated in the requirements generation?					
38					Has any cross technology identification been carried out?					
39					Have design techniques been identified?					
40					Do paper studies show that the system will work together?					
41					Have experiments been carried out with small representative data sets to prove principle?					
42					Have current manufacturing concepts been assessed?					
43					Have risks areas been identified?					
44					Are there risk mitigation strategies identified?					

4	Technology component and/or basic technology subsystem validation in laboratory environment	Basic technological components are integrated as sub-systems to establish that they will work together. This is relatively low fidelity compared with the eventual system. Examples include integration of ad-hoc hardware in the laboratory.	System concepts that have been considered and results from testing laboratory scale models. References to who did this work and when. Provide an estimate of how hardware and test results differ from the expected system goals and (re)assess the way forward	Represents early laboratory design at less than full system integration but we need to be putting systems together and understand there operation. The components here are not envisioned for the operational system but rather a breadboard mock-up within a laboratory. Simulation can also be used at this stage. Components are a combination of on-hand lab asses and some special purpose devices that may require special handling, calibration or alignment to get them to function.	Have the cross technology issues been identified?			
45					Have the individual components been tested in laboratory environment?			
46					Have you simulated components and interfaces?			
47					Has customer published requirements document?			
48					Do you have the overall requirements for end user?			
49					Have the designs been verified through the formal inspection process?			
50					Does technology demonstrates basic functionality?			
51					Has a scalable technology prototype been produced?			
52					Has a draft conceptual design been produced?			
53					Has the initial cost drivers been identified?			
54					Has key manufacturing process been identified?			
55					Has documentation and diagrams of technology been completed?			
56					Is there a mitigation strategy identified for manufacturing and productivity?			
57					Is there a Integrated Product Team (IPT) formally established?			
58					Is there a formal risk management program			
59					Has a FMEA been considered or performed?			
60					Technology availability dates established			
61					Have trade studies and lab experiments been defined for key manufacturing processes?			
62	Technology component and/or basic technology subsystem validation in relevant environment	Fidelity of technology increases significantly. The basic technological components are integrated with reasonably realistic supporting elements so they can be tested in a simulated environment. Examples include high fidelity laboratory integration of components, and basic field trials to prove capability concepts	Results from testing a laboratory based system are integrated with other supporting elements in a simulated operational environment. How does the 'relevant environment' differ from the expected operational environment? How do the test results compare with expectations? What problems, if any, were encountered?	At TRL 5 the breadboard of TRL 4 becomes a brassboard by improving the fidelity of the individual components and interfaces. This TRL is also distinguished by increases in the accuracy of the controlled environment in which it is tested.	Are interfaces between components realistic or feasible?			
63					Have you created prototypes?			
64					Has the tooling been demonstrated in a lab environment?			
65					High fidelity lab integration completed, ready to test in realistic/simulated environment			
66					Have design techniques been identified sufficiently so that large foreseeable problems are captured?			
67					Has form, fit and function for application been addressed with end user?			
68					Is the fidelity of the system progressed from breadboard to brassboard?			
69					Has the initial assessment of the assembly been performed?			
70					Has integration been considered?			
71					Has the test and validation been considered?			
72					Have mechanical and electrical interfaces been considered?			
73					Has the performance been analysed and translated to the expected final performance?			
74					Has the risk management plan been documented?			
75					Have the individual functions been tested to verify operation?			
76					Have life cycle costs been analysed?			
77								
78	Technology system / subsystem model or prototype demonstration in a relevant environment.	Representative model or prototype system, which is well beyond that of TRL 5, is tested in a relevant environment. Represents a major step up in a technology's demonstrated readiness. Examples include field testing a prototype in a high fidelity laboratory environment or in a simulated operational environment operating under proposed protocols.	Results from field testing of a prototype system that is near the desired configuration in terms of performance, weight, and volume. How did the test environment differ from the operational environment? Who performed the tests? How did the test compare with expectations? What problems, if any, were encountered? What are the plans, options, or actions to resolve problems before moving to the next level?	TRL 6 begins true systems engineering and development as opposed to technology development. The brassboard mock-up of the previous TRL is improved so that it is now representative of the full system in function, but not necessarily in form. The testing environment does not reach the level of an operational environment, although we are moving out of a controlled laboratory environment into something more closely approximating the realities of the technology's intended use.	Has the measurement and performance characteristic validation been completed?			
79					Has the draft design drawings complete or near completion?			
80					Has the collection of actual maintainability, reliability and supportability data been started?			
81					Has the design to cost goals been considered?			
82					Simulation performance in a operational environment			
83					Has the test and evaluation plan been considered?			
84					Has a representative model/prototype been tested in high-fidelity lab/simulated operational environment?			
85					Has a realistic environment outside lab been used but not the eventual operating environment?			
86					Has the inventory of external interfaces been completed?			
87					Has the technology transition agreement been updated and agreed by customer?			
88					Has the analysis of timing constraints been identified?			
89					Has a draft plan been reviewed by the customer?			

89	6					Has a draft plan been reviewed by the customer? Have the critical manufacturing processes been prototyped?			
90	6					Has a prototype been implemented including large scale realistic problems?			
91	6					Have materials, process, design and integration methods been employed?			
92	6					Have production issues been identified and mitigated?			
93	6					Is the process and tooling mature enough for manufacturing?			
94	6					Has a pre-prototype demonstration been completed?			
95	6					Has the engineering feasibility been fully demonstrated?			
96	6					Has the business case been reviewed?			
97	6					Has the formal requirements document been completed?			
98	6								
99	7	Technology prototype demonstration in an operational environment	Prototype near or at planned operational system. Represents a major step up from TRL 6 by requiring demonstration of an actual system prototype in an operational environment (e.g. in an aircraft, in a vehicle, or platform in the field). The operational environment may be defined as that which exposes the technology to the physical, electrical, environmental and security interfaces that will be experienced in service	Results from testing a prototype system in an operational environment. Who performed the tests? How did the test compare with expectations? What problems, if any, were encountered? What are the plans, options, or actions to address the delta of where the technology is now and that required for ISD (the next level)?	Fidelity of the system prototype improves to that of a pre-production prototype that represents a possible system accurately enough to expect only minor design changes. Elements may be modeled/simulated but this will be rare. While the environment may not yet include installations on the boat, the prototype will be exposed to the true operational environment on a surrogate platform or test bed.	Have the materials and manufacturing process been demonstrated? Has a prototype been built? Has process tooling and inspection/test equipment been demonstrated within a production environment? Has the manufacturing machinery and tooling been proven? Are the design changes been fixed/upto date? Has the prototype been tested within a operational environment? (not actual platform) Is the maintainability, reliability and supportability data > 80% of total needed data? Have draft drawing of pre-production component been completed? Have materials, processes, methods and design techniques been moderately developed and Are the prototype components representative of the production components? Have the design to cost goals been validated? Has the production planning been completed? Most functionality available for demonstration in simulated operational environment Is the prototype pre-production quality Are you ready for Initial production?			
100	7								
101	7								
102	7								
103	7								
104	7								
105	7								
106	7								
107	7								
108	7								
109	7								
110	7								
111	7								
112	7								
113	7								
114	8	Actual technology system completed and qualified through test and demonstration	Technology has been proven to work in its final form and under expected conditions. In almost all cases, this TRL represents the end of true technology and integration development. Examples include developmental test and evaluation of the system in its intended platform to determine if it meets design specifications. All functionality tested in simulated and operational	Results of testing the system in its final configuration under the expected range of environmental conditions in which it will be expected to operate. Assessment of whether it will meet its operational requirements. What problems, if any, were encountered? What are/were the plans, options, or actions to resolve	Testing at this level should result in minor changes to form, fit of function, and interfaces rather than changes to system parameters or configuration. Ready to make production decision. Test and developmental data has been accomplished	Do the components conform with form, fit and function within the operational system? Cost estimates <125% cost goals (eg: design to cost goals met) Is machining and tooling demonstrated in a production environment? Is all functionality demonstrated within a operational environment? Are all materials readily available? Is system evaluated through test and evaluation on actual platform? Is maintainability, reliability and supportability data collection completed? Are you ready for full rate production? Has the operational concept been implemented successfully? Are the cost estimates <110% cost goals or meet goals? Is the design stable with few design changes? Is system deployed in platform? Is system fully demonstrated? Is training plan implemented? Has supportability plan been updated? Are all documentations complete?			
115	8								
116	8								
117	8								
118	8								
119	8								
120	8								
121	8								
122	9	Actual technology system qualified through successful mission operations.	Actual application of the technology in its final form and under operational conditions. Technology proven in-service. Successful operational experience.	ISRM reports, User validation. May be linked to FOC.	System is ready for deployment or has been deployed for operation. Any required operational testing and evaluation has been accomplished.				
123	9								
124	9								
125	9								
126	9								
127	9								
128	9								
129	9								

21 Appendix F – Mean time before failure

The following information is provided by Centronics Ltd.

Predicted Failure Rate parameters for Inductive Devices, Transformers:

For the bases of these calculations the classification class for the TIRP is Audio Transformer (15 – 20K Hz).

- a. The TIRP is classed Audio Transformer (15 – 20K Hz). **Base Failure Rate λ_b (F/10⁶ hrs) 0.014**
- b. The Environmental Symbol and Description. Environment - π_E Symbol Naval, Sheltered N_S below deck conditions on surface ships and equipment installed in submarines. **Environment Factor $\pi_E = 5.0$**
- c. **The Temperature Factor - $\pi_T = 6.4$** (calculated on a hot spot temperature of 220°C).
- d. **The Quality Factor – $\pi_Q = 1$** (Military specification build equipment).

3. The Predicated Failure Rate:

The equation for the predicted failure rate: $\lambda_P = \lambda_b \pi_T \pi_Q \pi_E$ Failures / 10⁶ Hours.

Therefore based on these assumptions the calculation for the TIRP MTBF is:

$$\lambda_P = 0.014 \times 5.0 \times 6.4 \times 1 = 0.45/10^6 \text{ Hours.}$$

For a safety margin lower the Quality factor – $\pi_Q = 3$

Therefore based on this safety margin the calculation for the TIRP MTBF is:

$$\lambda_P = 0.014 \times 5.0 \times 6.4 \times 3 = 1.35/10^6 \text{ Hours.}$$

(One failure per 84.5 years if this figure is divided by 2 for additional safety factor then the MTBF for the TIRP would be 42.3 years).

4. Summary.

The predicted MTBF of the TIRP based on the formula in accordance with MIL-HDBK-217F exceeds the requirements of the Rolls Royce Equipment Specification

EDNS37000005814_005. It is noted that the MTBF is a basic calculation on a generic audio transformer with a maximum operation temperature of 220°C. Therefore a substantial safety margin is built into the final calculation.

Rolls Royce TIRP required MTBF = $1/0.26 \times 10^6$ (30 years).

Predicted TIRP MTBF = $1/0.74 \times 10^6$ (84.5 years).

Additional safety margin = Predicted TIRP MTBF/2 = $1/0.37 \times 10^6$ (42.3 years).

22 Appendix G – Octave random optimisation source software

```
%% TIRPI Optimisation Program
%% Angelo Sigona
%% 24/05/2017
diary on;

%% Initial Parameters Definition
clc;
disp('TIRPI Optimisation');
date;
%% Set up initial values
start_primary_turns = 93.97;
start_secondary_turns = 667.555;

start_spacing_length = 43.36;

start_primary_length = 10.91;
start_secondary_length = 11.51;

start_primary_depth = 5.106;
start_secondary_depth = 4.204;

Span_high_value=0;
start_Current_value=0.192785;
start_frequency_set=280.816183;
units='millimeters';
precision=1E-8;
type_set='axi';
depth=0;
minangle=15;
acsolver=0;

%% Set up various parameters internal to the optimization
nmax = 1000;      % Maximum number of iterations in the optimization
nstall = 5;      % Number of iterations before a stall is declared
d = 0.1;        % Starting step size
dmin = 0.01;    % Step size at which it is assumed that we've converged

Current_Span = 1; % Place holder for optimal cost
stall = 0;      % Number of iterations since the last forward progress

for k = 1:nmax
    disp(sprintf('-----
-----'));
    disp(sprintf('Iteration of Optimisation = %i; Multiplying Factor = %3.2f; Span Check
Failure = %i',k,d,stall));

    bOK = 0;
    while (bOK == 0)

        % If first time through the loop, evaluate the initial condition
        % Otherwise, randomly pick a nearby geometry
        if (k == 1)
```

```

        dd = 0;
    else
        dd = d;
    end;

    % Randomly pick a new candidate geometry
    Current_value= start_Current_value* (1 + dd*(2*rand-1));
    frequency_set = start_frequency_set* (1 + dd*(2*rand-1));
    primary_turns = start_primary_turns* (1 + dd*(2*rand-1));      %newrso =
rso* (1 + dd*myrand);    y=2*rand-1;
    secondary_turns = start_secondary_turns* (1 + dd*(2*rand-1));
    spacing_length = start_spacing_length* (1 + dd*(2*rand-1));
    primary_length = start_primary_length* (1 + dd*(2*rand-1));
    secondary_length = start_secondary_length* (1 + dd*(2*rand-1));
    primary_depth = start_primary_depth* (1 + dd*(2*rand-1));
    secondary_depth = start_secondary_depth* (1 + dd*(2*rand-1));

    bOK=1;

    % Validity of Spans from generator
    Total_blk_size=((2*spacing_length)+primary_length+secondary_length);
    Total_blk_number_float = 1300/Total_blk_size;
    Total_blk_number = floor(Total_blk_number_float);

    if ((Current_value) < 0.001) bOK=0; end;
    if ((Current_value) > 0.5) bOK=0; end;
    if ((frequency_set) < 0) bOK=0; end;
    if ((frequency_set) > 400) bOK=0; end;
        if ((Total_blk_number) < 0) bOK=0; end;
    if ((primary_depth) < 4) bOK=0; end;
        if ((secondary_depth) < 4) bOK=0; end;

end;

% Build and analyze candidate geometry -----
-----

fid=fopen('data.txt','wt');
turns_calibration=0;

disp('Build TIRPI');

openfemm;
opendocument('C:\\femm DXF Files\\KTP\\opt.FEM');
%%%%%%%%%%%%%% Opens geometry with leadscrew and probe tube
mi_saveas('C:\\femm DXF Files\\KTP\\opttemp-.fem');

mi_probdef(frequency_set,units,type_set,precision,(depth),(minangle),(acsolver));
mi_modifycircprop('100mA',1,Current_value);

Total_blk_size=((2*spacing_length)+primary_length+secondary_length);
Total_blk_number_float = 1300/Total_blk_size;
Total_blk_number = floor(Total_blk_number_float);

Fit_checker=(Total_blk_number*Total_blk_size)/1300;

```

```

disp(sprintf('Fit_checker = %f',Fit_checker));

if(Fit_checker>0.97)
disp(sprintf(' *** Geometry fit Checker PASSED *** '));

%%%%%%%%%%%%%%%%%%%%%%%%%%%%%%%%%%%%%%%%%%%%%%%%%%%%%%%%%%%%%%%%%%%%%%%%
First block of geometry
mi_clearselected;
mi_drawrectangle(0,0,9.4,(spacing_length)); % First spacing in block
mi_addblocklabel(4.7,(spacing_length/2));
mi_selectlabel(4.7,(spacing_length/2));
mi_setblockprop('17-4 PH',0,1,'None',0,0,0);
%blockname,automesh,meshsize,'incircuit',magdir,group,turns
mi_clearselected;

mi_drawrectangle(primary_depth,(spacing_length),9.4,(spacing_length+primary_length));
%Primary
mi_addblocklabel(((9.4-primary_depth)/2)+primary_depth,spacing_length+primary_length-
(primary_length/2));
mi_selectlabel(((9.4-primary_depth)/2)+primary_depth,spacing_length+primary_length-
(primary_length/2));
mi_setblockprop('Primary',0,1,'100mA',0,1,primary_turns);
%blockname,automesh,meshsize,'incircuit',magdir,group,turns
mi_clearselected;
mi_addblocklabel(1,spacing_length+primary_length-(primary_length/2));
mi_selectlabel(1,spacing_length+primary_length-(primary_length/2));
mi_setblockprop('17-4 PH',0,1,'None',0,0,0);
%blockname,automesh,meshsize,'incircuit',magdir,group,turns
mi_clearselected;

mi_drawrectangle(0,(spacing_length+primary_length),9.4,((2*spacing_length)+primary_le
ngth)); % Second Spacing in block
mi_addblocklabel(4.7,((2*spacing_length+primary_length)-(spacing_length/2)));
mi_selectlabel(4.7,((2*spacing_length+primary_length)-(spacing_length/2)));
mi_setblockprop('17-4 PH',0,1,'None',0,0,0);
%blockname,automesh,meshsize,'incircuit',magdir,group,turns
mi_clearselected;

mi_drawrectangle(secondary_depth,(((2*spacing_length)+primary_length)),9.4,(((2*spacin
g_length)+primary_length+secondary_length))); %Secondary
mi_addblocklabel(((9.4-
secondary_depth)/2)+secondary_depth,(2*spacing_length)+primary_length+secondary_le
ngth-(secondary_length/2));
mi_selectlabel(((9.4-
secondary_depth)/2)+secondary_depth,(2*spacing_length)+primary_length+secondary_le
ngth-(secondary_length/2));
mi_setblockprop('Secondary',0,1,'No Current',0,2,secondary_turns);
%blockname,automesh,meshsize,'incircuit',magdir,group,turns
mi_clearselected;
mi_addblocklabel(1,(2*spacing_length)+primary_length+secondary_length-
(secondary_length/2));
mi_selectlabel(1,(2*spacing_length)+primary_length+secondary_length-
(secondary_length/2));
mi_setblockprop('17-4 PH',0,1,'None',0,0,0);
%blockname,automesh,meshsize,'incircuit',magdir,group,turns
mi_clearselected;

%%%%%%%%%%%%%%%%%%%%%%%%%%%%%%%%%%%%%%%%%%%%%%%%%%%%%%%%%%%%%%%%%%%%%%%%
%%%%%%%%%%%%%%%%%%%%%%%%%%%%%%%%%%%%%%%%%%%%%%%%%%%%%%%%%%%%%%%%%%%%%%%%Repeat block for entire length of geometry

```

```

mi_selectgroup(0);
mi_selectgroup(1);
mi_selectgroup(2);
mi_copytranslate(0,(Total_blk_size),Total_blk_number-1);
mi_drawline(0,-2,0,1300);
mi_drawline(9.4,(Total_blk_number*Total_blk_size),9.4,1300);

%%%%%%%%%%Primary Voltage Setup
mi_clearselected;
mi_createmesh;
primary_cycle=0;

do

    mi_analyze;
    mi_loadsolution;

    circuit=mo_getcircuitproperties('100mA');
    voltage=circuit(1, [2]);

    primary_abs_voltage=abs(voltage);

    disp(sprintf('Primary Voltage Calibration = %fV, primary cycle = %i Primary Turns = %i',primary_abs_voltage,primary_cycle,primary_turns));

    primary_turns=(4.4/primary_abs_voltage)*primary_turns;
    primary_turns=floor(primary_turns);

    mi_selectgroup(1);
    mi_setblockprop('Primary',0,1,'100mA', 0,0,primary_turns);
    primary_cycle=primary_cycle+1;

until(primary_abs_voltage > 4.35 && primary_abs_voltage < 4.45 || primary_cycle>19)

Primary_bobbin_turns_fit_into_area=((primary_length/0.315)*(primary_depth/0.315));

%%%%%%%%%%Secondary Voltage Setup

mi_clearselected;
mi_createmesh;
secondary_cycle=0;
do

    mi_analyze;
    mi_loadsolution;

    circuit=mo_getcircuitproperties('No Current');
    voltage=circuit(1, [2]);

    secondary_abs_voltage=abs(voltage);

    disp(sprintf('Secondary Voltage Calibration = %fV, secondary cycle = %i Secondary Turns = %i',secondary_abs_voltage,secondary_cycle,secondary_turns));

    secondary_turns=(4.15/secondary_abs_voltage)*secondary_turns;
    secondary_turns=floor(secondary_turns);

```

```

mi_selectgroup(2);
mi_setblockprop('Secondary',0,1,'No Current', 0,0,secondary_turns);
secondary_cycle=secondary_cycle+1;

until(secondary_abs_voltage > 4.1 && secondary_abs_voltage < 4.2 ||
secondary_cycle>19)

Secondary_bobbin_turns_fit_into_area=((secondary_length/0.2032)*(secondary_depth/0.
2032));

%%%%%%%%%%%%%%Run Loops

if(primary_cycle>19 || secondary_cycle>19)
turns_calibration=1;
end;

mi_clearselected;

mi_createmesh;

n=1;

x1=zeros(n,1);
y1=zeros(n,1);

x2=zeros(n,1);
y2=zeros(n,1);

circuit=0;
loc=1;

leadscrew_increment=1100;

fprintf(fid,'%i \n', Current_value);
fprintf(fid,'%i \n', frequency_set);
fprintf(fid,'%i \n', spacing_length);
fprintf(fid,'%i \n', primary_turns);
fprintf(fid,'%i \n', secondary_turns);
fprintf(fid,'%i \n', primary_length);
fprintf(fid,'%i \n', primary_depth);
fprintf(fid,'%i \n', secondary_length);
fprintf(fid,'%i \n', secondary_depth);
fprintf(fid,'%i \n', Total_blk_size);
fprintf(fid,'%i \n\n', Total_blk_number);

for leadscrew_position=0:n

    disp(sprintf('iteration %i of %i of leadscrew',leadscrew_position,n));
    mi_analyze;
    mi_loadsolution;

    circuit=mo_getcircuitproperties('No Current');
    voltage=circuit(1, [2]);

    secondary_abs_voltage=abs(voltage);

```

```

if(leadscrew_position==0)
Span_high_value=secondary_abs_voltage;
end;

x1(loc)=(loc*leadscrew_increment)-leadscrew_increment;
y1(loc)=secondary_abs_voltage;

circuit=mo_getcircuitproperties('100mA');
voltage=circuit(1, [2]);

primary_abs_voltage=abs(voltage);

x2(loc)=(loc*leadscrew_increment)-leadscrew_increment;
y2(loc)=primary_abs_voltage;

disp(sprintf('Leadscrew position = %imm Primary = %fV Secondary =
%fV',(leadscrew_position*leadscrew_increment),primary_abs_voltage,secondary_abs_vol
tage));

fprintf(fid,'%i \t', x1(loc));
fprintf(fid,'%f \t', y2(loc));
fprintf(fid,'%f \t', y1(loc));
fprintf(fid,'\n');

mi_selectgroup(5);
mi_movetranslate(0,leadscrew_increment);
mi_clearselected;
mo_close;
loc=loc+1;
leadscrew_position=leadscrew_position+leadscrew_increment;

end
Span_new=Span_high_value-secondary_abs_voltage;

mi_selectgroup(5);
mi_movetranslate(0,-(leadscrew_increment*n),(4));
mi_saveas('C:\femm DXF Files\KTP\PostOptTIRPI.fem');
closefemm;

%-----
-----
-----
% See if this candidate is better than the previous optimum.
% If so, this candidate is the new optimum
stall = stall + 1;

if (Primary_bobbin_turns_fit_into_area < primary_turns)
disp(sprintf(' *** Primary turns bobbin area Check Failure Occurred Simulation
Discarded *** '));
end;

if (Primary_bobbin_turns_fit_into_area > primary_turns)
disp(sprintf(' *** Primary turns bobbin area Check passed *** '));
end;

if (Secondary_bobbin_turns_fit_into_area < secondary_turns)
disp(sprintf(' *** Secondary turns bobbin area Check Failure Occurred Simulation
Discarded *** '));
end;

```



```

if (Secondary_bobbin_turns_fit_into_area > secondary_turns)
disp(sprintf(' *** Secondary turns bobbin area Check passed *** '));
end;

if (Current_value < 0.001 || Current_value > 0.5)
disp(sprintf(' *** Current Check Failure Occurred Simulation Discarded *** '));
end;

if (Current_value > 0.001 || Current_value < 0.5 || Current_value == 0.001||
Current_value == 0.5)
disp(sprintf(' *** Current Check passed *** '));
end;

if (frequency_set < 1 || frequency_set > 400)
disp(sprintf(' *** Frequency Check Failure Occurred Simulation Discarded *** '));
end;

if (frequency_set > 0 || frequency_set < 400 || frequency_set == 400)
disp(sprintf(' *** Frequency Check passed *** '));
end;

if (Span_new < Current_Span)
disp(sprintf(' *** Span Check Failure Occurred Simulation Discarded *** '));
end;

if (Span_new > Current_Span)
disp(sprintf(' *** Span Check passed *** '));
end;

if (turns_calibration == 0)
disp(sprintf(' *** Turns CALIBRATION passed *** '));
end;

if (turns_calibration == 1)
disp(sprintf(' *** Turns CALIBRATION ERROR Check Failure Simulation Discarded
*** '));
end;

if(((Span_new > Current_Span)&&(turns_calibration < 1)&&(frequency_set >
0)&&(frequency_set < 401 || frequency_set == 400)&&(Current_value > 0.001 ||
Current_value == 0.001)&&(Current_value < 0.5 || Current_value ==
0.5)&&(Primary_bobbin_turns_fit_into_area >
primary_turns)&&(Secondary_bobbin_turns_fit_into_area > secondary_turns)) || (k==1))
    stall = 0;
    start_Current_value = Current_value;
    Current_Span = Span_new;
    start_frequency_set=frequency_set;
    start_primary_turns=primary_turns;
    start_secondary_turns=secondary_turns;
    start_spacing_length=spacing_length;
    start_primary_length=primary_length;
    start_secondary_length=secondary_length;
    start_primary_depth=primary_depth;
    start_secondary_depth=secondary_depth;

    disp(sprintf('frequency = %f; Primary Current Value = %f; Current Span =
%f; primary_turns = %f; secondary_turns = %f; spacing_length = %f; primary_length = %f;
secondary_length = %f primary_depth = %f; secondary_depth = %f',frequency_set,

```

```

Current_value, Current_Span, primary_turns, secondary_turns, spacing_length,
primary_length, secondary_length, primary_depth, secondary_depth));
    end;

    % Run through the 'stall logic' to see if the step size should be reduced.
    if (stall > nstall)
        d = d/2;
        stall = 0;
        if (d < dmin) %converged
            break;
        end;
    end;

end;

end;

if(Fit_checker<0.97)
disp(sprintf(' *** Fit check ERROR Check Failure Simulation Discarded *** '));
end;

end;
%% Finished! Report the results
disp(sprintf('Frequency = %f',frequency_set));
disp(sprintf('Primary Current = %f',Current_value));
disp(sprintf('Optimised_Span = %f',Current_Span));
disp(sprintf('primary_turns = %f',primary_turns));
disp(sprintf('secondary_turns = %f',secondary_turns));
disp(sprintf('spacing_length = %f', spacing_length));
disp(sprintf('primary_length = %f', primary_length));
disp(sprintf('secondary_length = %f', secondary_length));
disp(sprintf('primary_depth = %f', primary_depth));
disp(sprintf('secondary_depth = %f', secondary_depth));

diary off;

```

23 Appendix H – Random optimisation output

The command window displays the following data when the random optimisation routine is used. The program converged in 60 iterations. Only the first and the last iteration are shown. The software was used for the TIRPI optimisation and the CRDM optimisation.

First iteration

TIRPI Optimisation

Iteration of Optimisation = 1; Multiplying Factor = 0.10; Parameter Check Failure = 0

Build TIRPI

Primary Voltage Calibration = 3.606738V, primary cycle = 0 Primary Turns = 122

Primary Voltage Calibration = 4.879535V, primary cycle = 1 Primary Turns = 148

Primary Voltage Calibration = 4.121369V, primary cycle = 2 Primary Turns = 133

Primary Voltage Calibration = 4.517575V, primary cycle = 3 Primary Turns = 141

Primary Voltage Calibration = 4.317152V, primary cycle = 4 Primary Turns = 137

Primary Voltage Calibration = 4.416782V, primary cycle = 5 Primary Turns = 139

Secondary Voltage Calibration = 5.004995V, secondary cycle = 0 Secondary Turns = 866

Secondary Voltage Calibration = 4.149638V, secondary cycle = 1 Secondary Turns = 718

iteration 0 of 1 of leadscrew

Leadscrew position = 0mm Primary = 4.366822V Secondary = 4.149638V

iteration 1 of 1 of leadscrew

Leadscrew position = 1100mm Primary = 4.620350V Secondary = 1.100854V

*** Primary turns bobbin area Check passed ***

*** Secondary turns bobbin area Check passed ***

*** Current Check passed ***

*** Frequency Check passed ***

*** Parameter Check passed ***

*** Turns CALIBRATION passed ***

frequency = 200.000000; Primary Current Value = 0.141421; Current Span = 3.048785;
primary_turns = 138.000000; secondary_turns = 718.000000; spacing_length =
42.000000; primary_length = 14.000000; secondary_length = 14.000000 primary_depth =
5.000000; secondary_depth = 5.000000

Final iteration

Iteration of Optimisation = 185; Multiplying Factor = 0.01; Span Check Failure = 5

Build TIRPI

Fit_checker = 0.994340

*** Geometry fit Checker PASSED ***

Primary Voltage Calibration = 4.459695V, primary cycle = 0 Primary Turns = 99

Primary Voltage Calibration = 4.385125V, primary cycle = 1 Primary Turns = 98

Secondary Voltage Calibration = 4.126302V, secondary cycle = 0 Secondary Turns = 985

iteration 0 of 1 of leadscrew

Leadscrew position = 0mm Primary = 4.385125V Secondary = 4.151437V

iteration 1 of 1 of leadscrew

Leadscrew position = 1100mm Primary = 4.737326V Secondary = 0.303344V

*** Primary turns bobbin area Check passed ***

*** Secondary turns bobbin area Check passed ***

*** Current Check passed ***

*** Frequency Check passed ***
*** Span Check Failure Occurred Simulation Discarded ***
*** Turns CALIBRATION passed ***

Output from simulation

Frequency = 398.694807
Primary Current = 0.201649
Optimised_Span = 3.850602
primary_turns = 98.000000
secondary_turns = 991.000000
spacing_length = 61.104511
primary_length = 9.713238
secondary_length = 11.704580
primary_depth = 5.057282
secondary_depth = 6.204279